1-1-2011

Exploring Potential Drug Target Sites In The Ribosome Using Cisplatin And Its Analogues

Keshab Rijal
Wayne State University

EXPLORING POTENTIAL DRUG TARGET SITES IN THE RIBOSOME USING CISPLATIN AND ITS ANALOGUES

by

KESHAB RIJAL

DISSERTATION

Submitted to the Graduate School

of Wayne State University,

Detroit, Michigan

in partial fulfillment of the requirements

for the degree of

DOCTOR OF PHILOSOPHY

2011

MAJOR: CHEMISTRY (BIOCHEMISTRY)

Approved by:

_____

Advisor Date

_____

_____

_____

DEDICATION

In memory of my mother

ACKNOWLEDGMENTS

This dissertation would not have been possible without the support from numerous people and now it is my pleasure to thank everyone who contributed to my work. First and foremost, I am heartily thankful to my advisor Prof. Christine Chow whose encouragement, guidance and support from the initial to the final level enabled me to develop an understanding of the research problem. The creativity, determination and sense of joy with which she responded to research challenges are always inspiring. I am most grateful to my thesis committee members Dr. Andrew Feig, Dr. Philip Cunningham, and Dr. David Rueda for their critical comments, suggestions, and encouragements in every stage of graduate studies. In addition, I would be indebted for allowing me to use their lab equipments and space with same privilege as their group members.

I have been fortunate to work with wonderful group of chow lab members for over five years. I am always grateful to all present and past chow lab members for their help, ideas, and laughter which made these five years enjoyable. I enjoyed working with previous members, Chamila, Pei-Wen, Santosh, Sanjaya, Dinuka, Geethi, Wantanee, Yuqin and current members Sakina, Moninder, Papa Nii, Yogo, Rajesh, Dananjaya, Gayani, Daya, Xun, and Heba. Special thanks to dear friends Tek and Anne-cécile for their help, trouble shooting the problems, and research discussions which always invigorate me to move forward. I would like to acknowledge Christopher, Edna, and Mary, who have worked with me in different projects and made working enjoyable.

I would like to thank Dr. Brian Shay for his help in MALDI and LC-MS experiment and Nestor for his friendship and computer assistance. I am very grateful to office staffs especially Diane Kudla, Sharon Kelly and Melissa Barton for their assistance in solving many paper work issues. I would like to thank Dr. Brock and Dr. Al-Katib for their suggestions and encouragements in a collaborative project. I always appreciate the help

that I got from Cunningham lab, Feig lab, Rueda lab, and Al-Katib lab members; especially I would like to thank Jenna, Sharla, Amanda, and Elvin for their numerous help. I am always thankful to all RNA club members for their critical comments and suggestions.

I will never forget the time that I spent with Rajan, Urmila, Ami, and Vinay with whom I share all aspects of life; tears, laughter's, and excitement for more than five years. I deeply appreciate their support and encouragements for research, and their wisdom of life which always made me feel at home. Rajan, I admire you in a number of ways since we were together. My thanks also extended to dear friends Devi, Jibash, Bhupal, Janardan, and Bishal for their long friendship and support whenever I needed the most.

I am forever grateful to my family members especially, Upendra Rijal and Saraswati Rijal, whose foresight and values paved the way for a privileged education and my sisters for their love and encouragements. I feel lucky to have supportive and encouraging in laws Sandipa and Dhiraj. I am always grateful to my beloved wife Sudipa for her unconditional love and support at each turn of the road.

Lastly, I offer my regards to all of those who supported me in any respect during the completion of this dissertation.

TABLE OF CONTENTS

LIST OF TABLES

LIST OF FIGURES

CHAPTER 1

Introduction

1.1 Introduction to Nucleic Acids

Nucleic acids play a vital role in biological systems. Nucleic acids, more specifically DNA and RNA, are present in all organisms. Though DNA and RNA have very few differences chemically, their three-dimensional structures and biological functions are very different. The presence of a 2'-OH group and uracil, instead of thymine, are the main chemical differences in RNA compared to DNA. In secondary structures, DNA is generally helical and double stranded, whereas RNA contains numerous tertiary structures and is quite diverse (*5-7*). With an increasing number and types of RNAs still being discovered, our understanding of RNA structure and function also has to increase greatly. Traditionally, there are three major classes of RNAs: messenger RNA (mRNA), transfer RNA (tRNA), and ribosomal RNA (rRNA), which are responsible for the conversion of genetic information in DNA to proteins (*8*). In the past, other cellular RNAs were considered as junk or degraded pieces of mRNA. Later, catalytic activities of these RNA molecules were identified (*9-13*). In 1989, Thomas Cech and Sidney Altman were awarded the Nobel Prize in chemistry for the discovery of catalytic properties of RNA. They discovered the catalytic activity of the group I intron (*9*) and ribonuclease P, respectively (*11*). These catalytic RNA, called ribozymes, are found to be involved in a number of cellular processes. In the last decade, the number of newly discovered small RNAs (sRNAs) in bacteria and non-coding RNAs (ncRNAs) in eukaryotes has increased dramatically (*14*). They have been

shown to carry out important regulatory functions such as transcriptional regulation, RNA processing and modification, as well as mRNA stability and translation (*15-16*). Although the overall function of known non-coding RNAs is similar, the mechanism of action and processing of these RNAs is very different (*17-18*). Riboswitches, upon binding to small molecules, refold and control expression (*19-20*), while double-stranded short interfering RNAs (siRNAs) suppress gene expression by cleaving target mRNA at specific sites (*21*). The discovery of RNA interference (RNAi) and its role in defending cells against parasitic genes has significantly increased its application in therapeutics (*22-23*). In addition, RNAi has been used as a genetic tool in molecular biology to suppress gene expression selectively. In 2006, Andrew Z. Fire and Craig C. Mello received the Nobel Prize in physiology or medicine for the discovery of RNA interference. With cutting-edge techniques and genome sequencing, more non-coding RNAs, along with their functions and applications, are expected to be uncovered in the future.

1.2 Introduction to the Ribosome

The ribosome is a large and complex organelle of living organisms, identified as a ribonucleoprotein particle by Palade (*24*). The *E. coli* ribosome is composed of 65% ribosomal RNA and 35% proteins, although the ratio varies a little from organism to organism. In bacteria, the size of the ribosome is about 20 nm and it has a mass of more than 2×10^6 Daltons (*25-26*). The ribosome is an essential component of all living organisms because of its important role in protein synthesis. The cell uses a large amount of energy for its biogenesis.

1.2.1 Composition

The ribosome of all organisms consists of two unequal subunits, each contains one third proteins and two thirds RNA. The unequal subunits of the ribosome are measured in terms of their sedimentation coefficient unit (Svedberg constant) rather than their size. In bacteria, the ribosome (70S) consists of a larger 50S subunit and smaller 30S subunit. The larger 50S subunit is composed of 23S ribosomal RNA with 2900 nucleotides and 5S ribosomal RNA with 120 nucleotides. Along with RNA, the larger subunit also contains 34 different proteins. The smaller 30S subunit consists of 16S ribosomal RNA (1546 nucleotides) and 21 different proteins (**Figure 1.1**). In eukaryotes, the 80S ribosome consists of a larger 60S subunit and a smaller 40S subunit. The large subunit is composed of 28S ribosomal RNA (4700 nucleotides), 5.8S rRNA (160 nucleotides) and 49 proteins. The small subunit contains 18S ribosomal RNA (1800 nucleotides) and 33 proteins. Despite the differences in size and composition, the ribosome has common important functional regions such as the decoding region, peptidyl transferase center, and peptide exit tunnel.

High-resolution X-ray crystal structures of the bacterial ribosome in bacteria reveal that the smaller 30S subunit consists of four distinct structural domains, previously referred to as the head, neck, body and platform based on EM images (**Figure 1.2 A**) (*27*). The 30S subunit of the ribosome is mainly involved in the formation of a pre-initiation complex and the selection of correct aminoacyl tRNAs during protein synthesis.

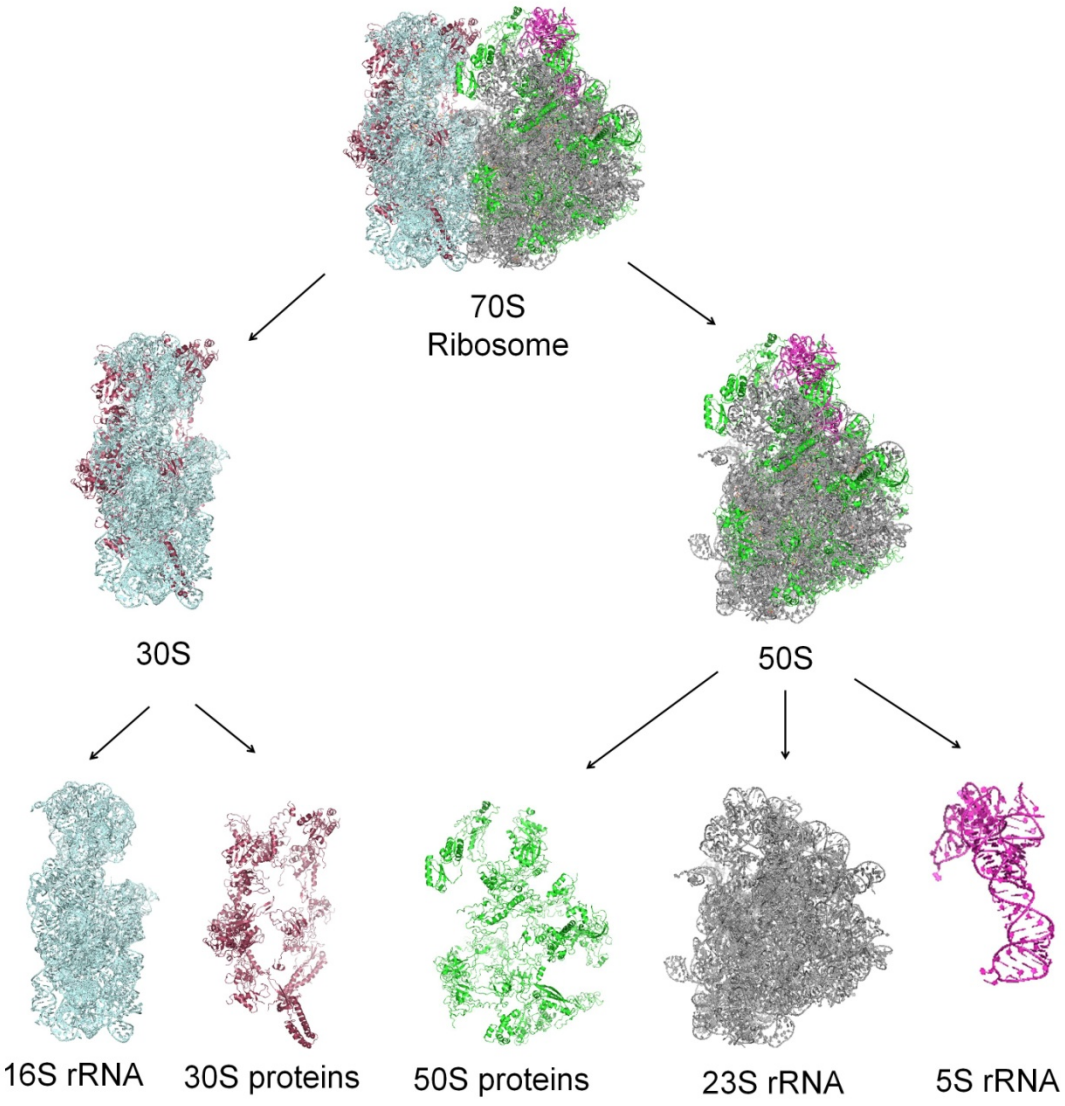

Figure 1.1. The composition of bacterial ribosomes is shown. The bacterial 70S ribosome is composed of 50S and 30S subunits, which are also composed of ribosomal RNA and proteins. This figure was created with Pymol using PDB: 3I1M and 3I1N (*28*).

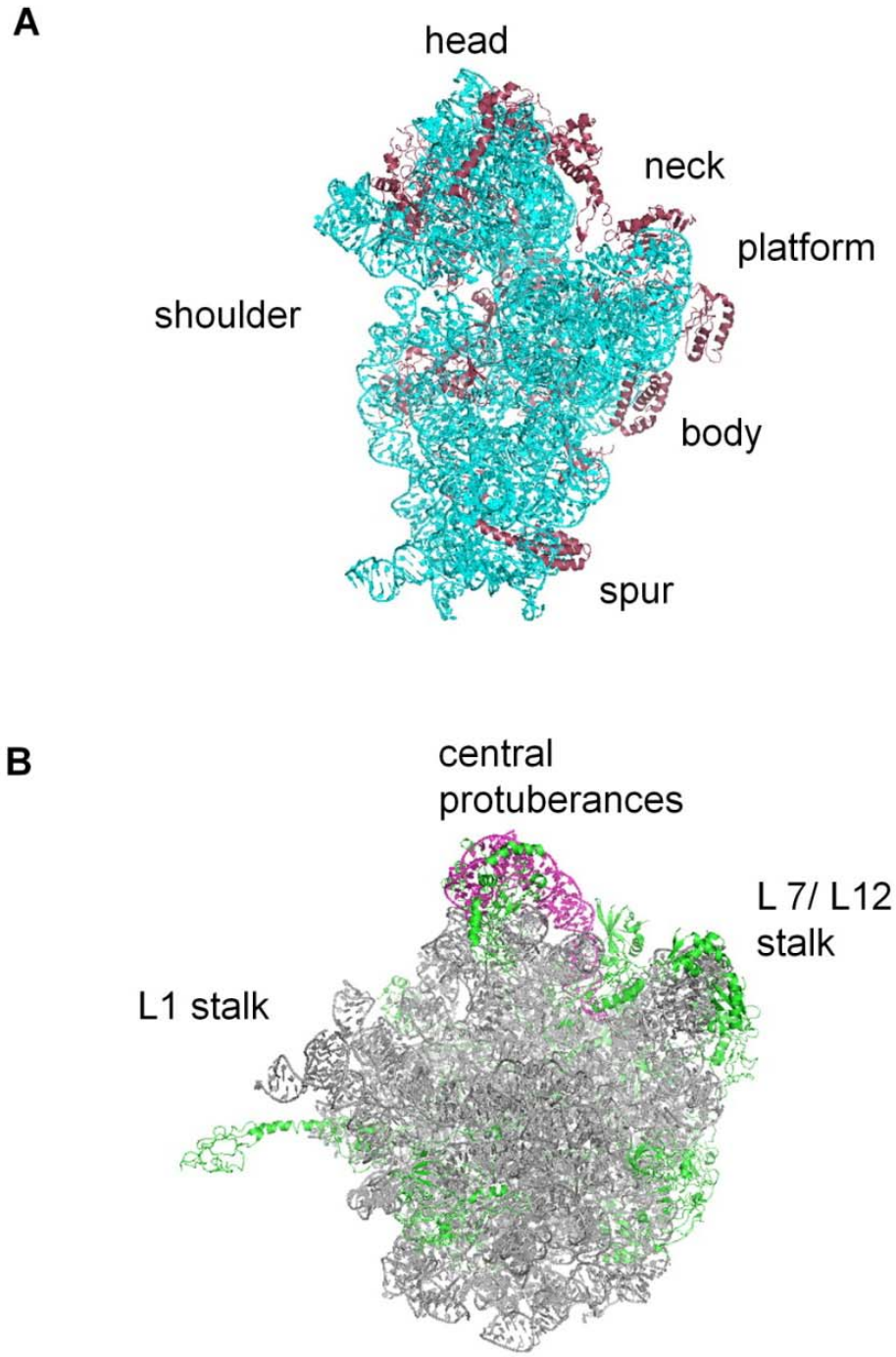

Figure 1.2. Crystal structures of the *E. coli* 30S and 50S subunits as seen from the interface side are shown: (A) 30S crystal structure (PDB: 3I1M) and (B) 50S crystal structure (PDB: 3I1N) (*28*).

The larger 50S subunit consists of a body and three protuberances (**Figure 1.2 B**). The central protuberance consists of 5S rRNA and associated proteins, while the other two arms that extend to the right and left are formed by L1 and L7/L12 proteins. The catalytic center of the ribosome, or peptidyl transferase center (PTC), is located in the 50S subunit and catalyzes peptide-bond formation. Because of this property, the ribosome is also called a ribozyme (*29*). Another important component of the 50S subunit is the peptide exit tunnel, which provides a stable path for the growing polypeptide. The assembly and maturation processes of the ribosomal subunits consist of a complex series of events, including the processing of the ribosomal RNA, modification of nucleotides, binding of ribosomal proteins and metal ions, as well as conformational changes in sequential order (*30-31*).

1.2.2 Structure

The ribosome is organized into distinct three-dimensional structures (*32*). The folded RNA makes the ribosome very diverse in secondary and tertiary structures. The standard Watson-Crick base pairs found in RNA are G-C and A-U; however, G-U and G-A non-canonical base pairs are also observed. Along with these, there are several modified nucleotides and mismatches, which further increase the diversity of the rRNA structure. Some of the common secondary structures found in the ribosomal RNA, such as a hairpin loop, double-stranded region, bulge, internal loop, and junction are shown in **Figure 1.3**. The secondary structure of RNA is mainly composed of single- and double-stranded regions, but when they fold on themselves, they form various complex tertiary structural

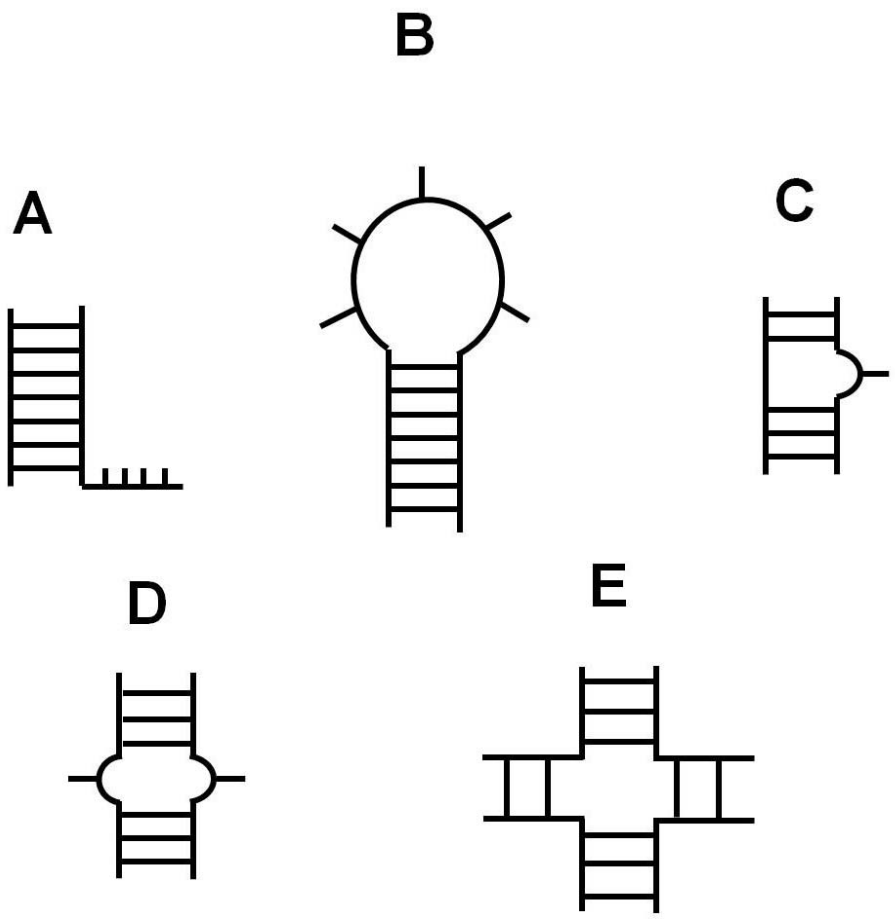

Figure 1.3. Common secondary structures of RNA are shown: (A) single- and double-stranded regions, (B) hairpin, (C) bulge, (D) internal loop, and (E) four-way junction.

motifs, such as the pseudoknot and A-minor motif. These tertiary structural motifs stabilize loop-loop interactions, contact between helices, and conformations of junctions (*32*).

Phylogenetic sequence analysis was initially used to predict the rRNA secondary structure (*33*). Sequence comparison is a robust method to predict the secondary and tertiary structure of RNA. It is based on the principle that homologous RNA molecules, consisting of unique primary sequences, adopt the same secondary and tertiary structures (*34*). It identifies base pairing by finding sites of covariation between sequences in an alignment. Secondary structure predicted by this approach was initially validated by chemical and enzymatic probing. It was further confirmed when the crystal structure of tRNA was solved, and all of the predicted secondary interactions were shown to be accurate. After this, other RNA structures including 5S, 16S and 23S were also predicted based on covariation approach *(35-36)*. With continuous improvements in the covariation algorithms and increase in the diversity of ribosomal RNA sequences, the secondary structure of 16S rRNA and 23S rRNA was further refined. This secondary map was validated initially with chemical probing, and afterwards with the subunit and later complete ribosome crystal structures. Approximately ~98% of the base pairs predicted by sequence comparison in 16S rRNA and 23S rRNA were found to be correct when the crystal structure was solved (*34*). The secondary structure of 16S rRNA is divided into four domains: the 5' domain (nucleotides 1-556), central domain (nucleotides 557-918), 3' major (nucleotides 919-1396), and 3' minor domain (nucleotides1397-1542) (**Figure 1.4**) (*37-38*).

Similarly, the secondary structure of 23S has six domains (domains I-VI) (**Figure1.5**) (*39*).

Secondary and tertiary structures found in the ribosome have very important roles in RNA stability and function. In ribosomal RNA, about 60% of the nucleotides are involved in Watson-Crick base pairing and 62% of adenosines are unpaired, while only about 30% of G, C and U are unpaired (*34*). However, the majority of nucleotides are involved in some kind of interaction within the folded RNA structure, and nucleotides that are not involved in any kind of interaction are very rare (*40*). The secondary structure of rRNA contains short helices that are connected by bulge or internal loops of unequal lengths. They have important roles in initiating RNA folding, stabilizing helical stems, making contacts with proteins, and participating in long-range tertiary interactions (*40-41*). In all domains of life, the functional center of rRNA is highly conserved. Several studies have shown that the key functional part of the ribosome is in fact ribosomal RNA. Noller and coworkers treated 50S subunits of *T. thermophilus* with sodium dodecyl sulfate and proteinase K followed by phenol extraction, and found that 80% activity of the peptidyl transferase reaction was retained (*42-43*). In addition, these structural motifs are important target sites for a number of antibiotics.

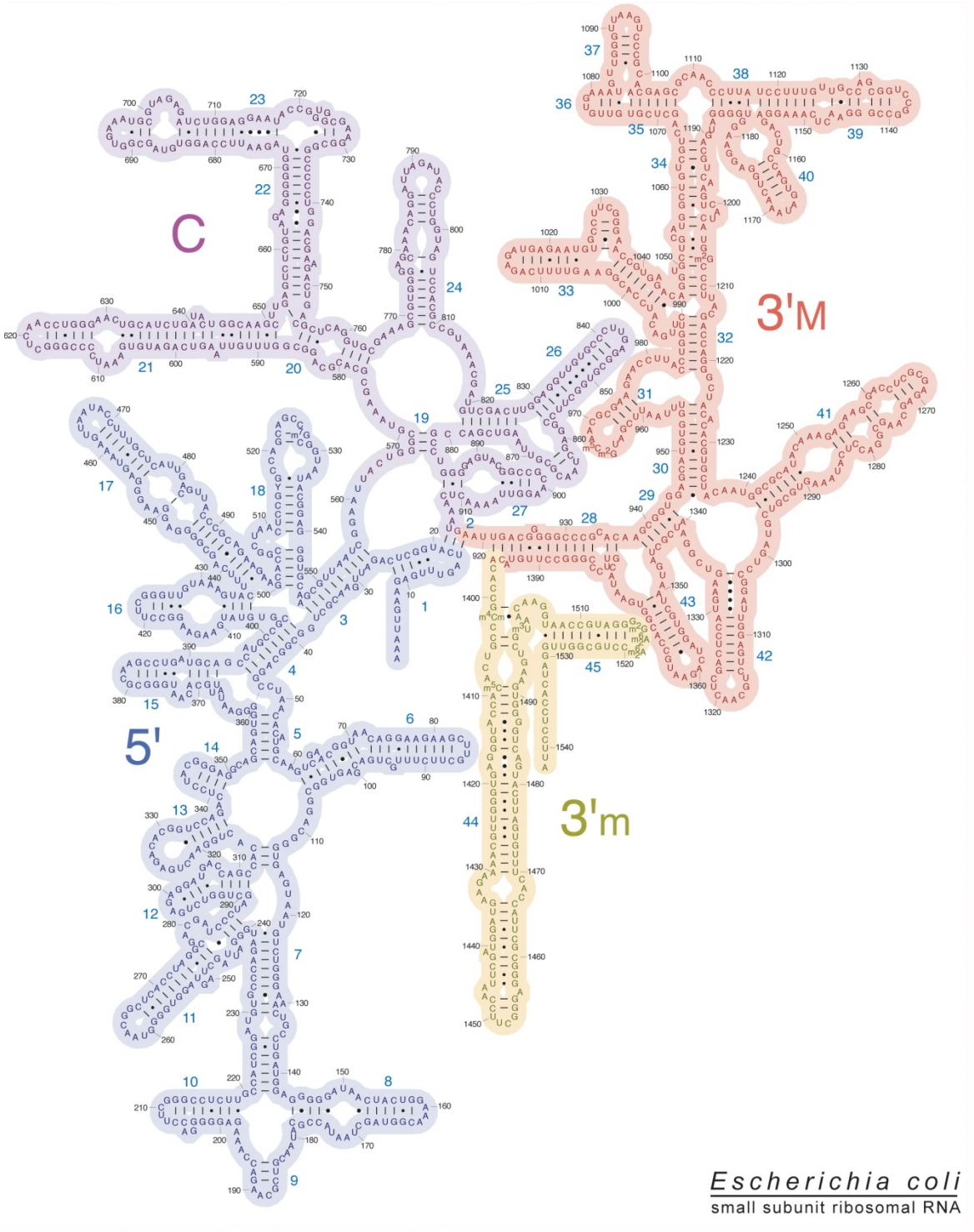

Figure 1.4. The secondary structure of 16S rRNA of *E. coli* is shown (*34*). Domains are indicated and shown in different colors. (Figure taken from: http://rna.ucsc.edu/rnacenter).

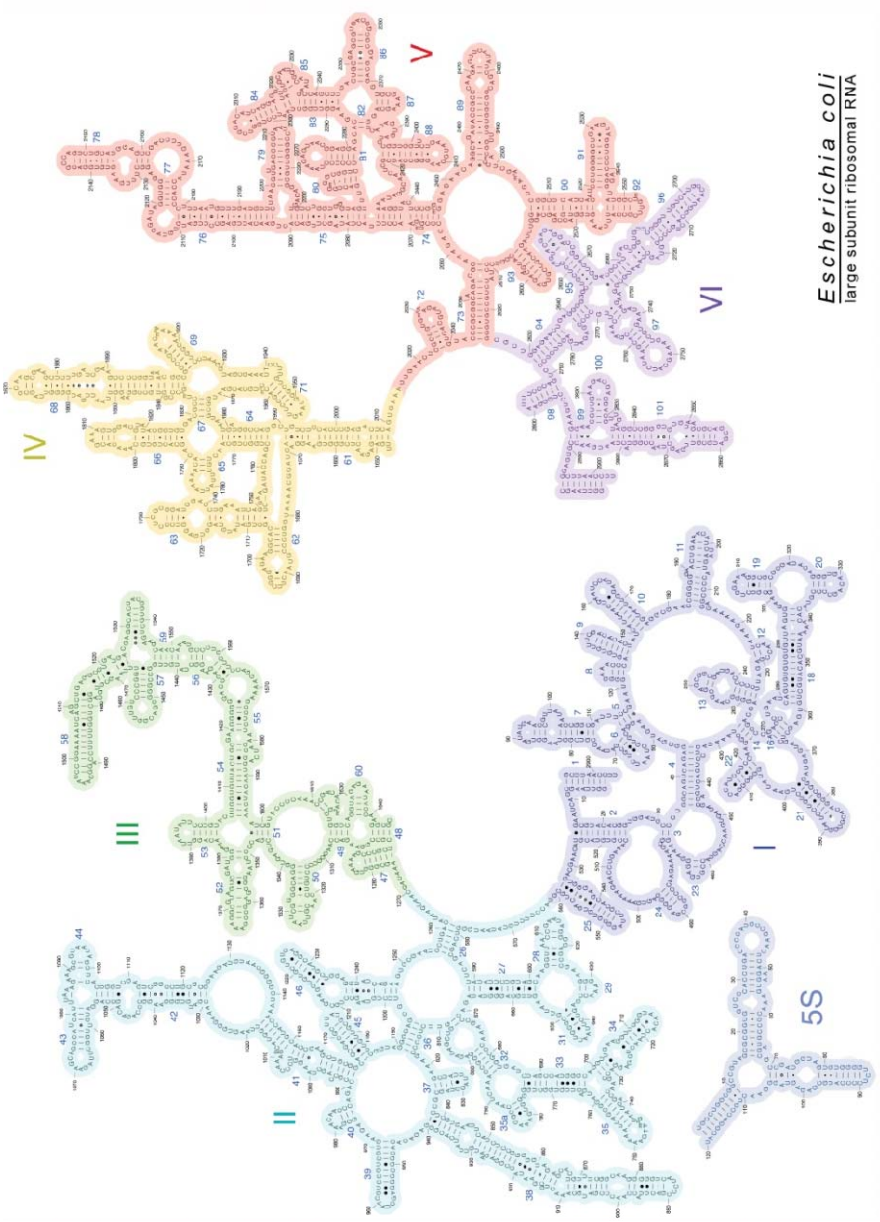

Figure 1.5. The secondary structure of *E. coli* 23S rRNA and 5S rRNA is shown Domains are indicated and shown in different colors. (Figure taken from: http://rna.ucsc.edu/rnacenter).

1.2.3 Function

The main function of the ribosome is protein synthesis. For this process to occur, the DNA sequence is first transcribed into mRNA by an RNA polymerase (*44*). In bacteria, the transcribed mRNA is directly used for translation and does not undergo post-transcriptional modifications. In eukaryotes, the transcribed mRNA from DNA is called the primary transcript and undergoes different maturation steps such as capping and splicing to produce mature mRNA (*45*). The process of capping adds a 7-methyl guanosine to the 5' end, and splicing removes non-coding sequences.

Both ribosomal subunits have three tRNA binding sites: the A site (aminoacyl), which accepts the aminoacylated tRNA; the P site (peptidyl), which catalyzes peptide-bond formation; and the E site (exit), from which deacylated tRNAs leave during elongation. Protein synthesis begins with the binding of mature mRNA to the 30S subunit, guided by the Shine-Dalgarno sequence (*46*). Initiation factor 3 (IF3) prevents binding of the 50S, and initiation factor 1 (IF1) blocks initiator fMet-tRNA binding to the A site of the 30S subunit (*47-48*). After the f-Met-tRNA is correctly positioned, IF3 and IF1 are released and 50S binds to 30S to form the 70S initiation complex. During this process GTP bound to IF2 is hydrolyzed. At this stage, all three initiation factors dissociate from the ribosome. This process leads to the formation of a functional 70S ribosome called the initiation complex (**Figure 1.6**) (*49*).

The next step of protein synthesis is elongation, in which a new aminoacyl tRNA complex with GTP and EF-Tu (elongation factor thermo unstable) binds to

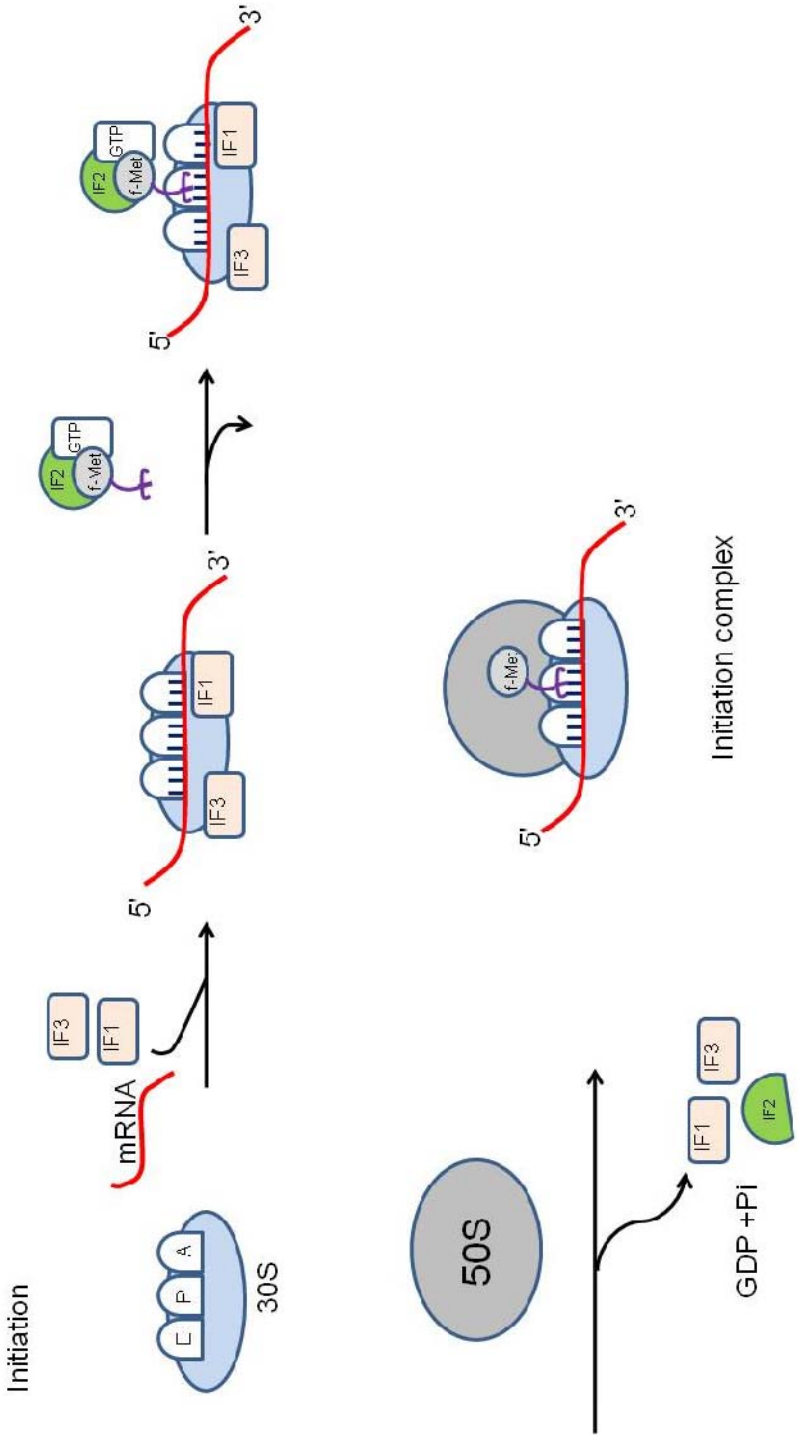

Figure 1.6. An overview of initiation of protein synthesis in bacteria is shown.

the A site (*50*). The decoding region present in the 16S rRNA of the small subunit selects the cognate tRNA according to the mRNA codon (*51-52*). Upon aminoacyl tRNA binding to the A site, GTP is hydrolyzed and EF-TU-GDP is released from the ribosome. After the correct aminoacyl tRNA is placed in the A site, peptide-bond formation occurs at the peptidyltransferase center (PTC) of the 50S (*50, 53*). The amino acid f-Met from the initiator tRNA is then transferred to the aminoacid of the A-site tRNA. In the process of translocation, the deacylated tRNA and A-site tRNA, along with mRNA, move to the E site and P site, respectively. GTP hydrolysis and EF-G (elongation factor G) are the driving forces for this translocation step (*54-55*). This translocation process makes the ribosome ready for the next round of elongation, which continues until the ribosome reaches the stop codon on the mRNA (**Figure 1.7**).

The final step of protein synthesis is termination and recycling of the ribosome. Termination occurs when the mRNA stop codon reaches the A site. The stop codon is recognized by release factors, RF1 and RF2 (*56*). Binding of release factor in the ribosome activates hydrolysis of the peptide chain from tRNA, and RF3 then promotes dissociation of RF1 and RF2. The ribosome is left with mRNA and deacylated tRNA in the P site after the peptide chain is released. This complex is dissociated by RRF (ribosome recycling factor) and EF-G with subsequent hydrolysis of GTP (*57-59*).

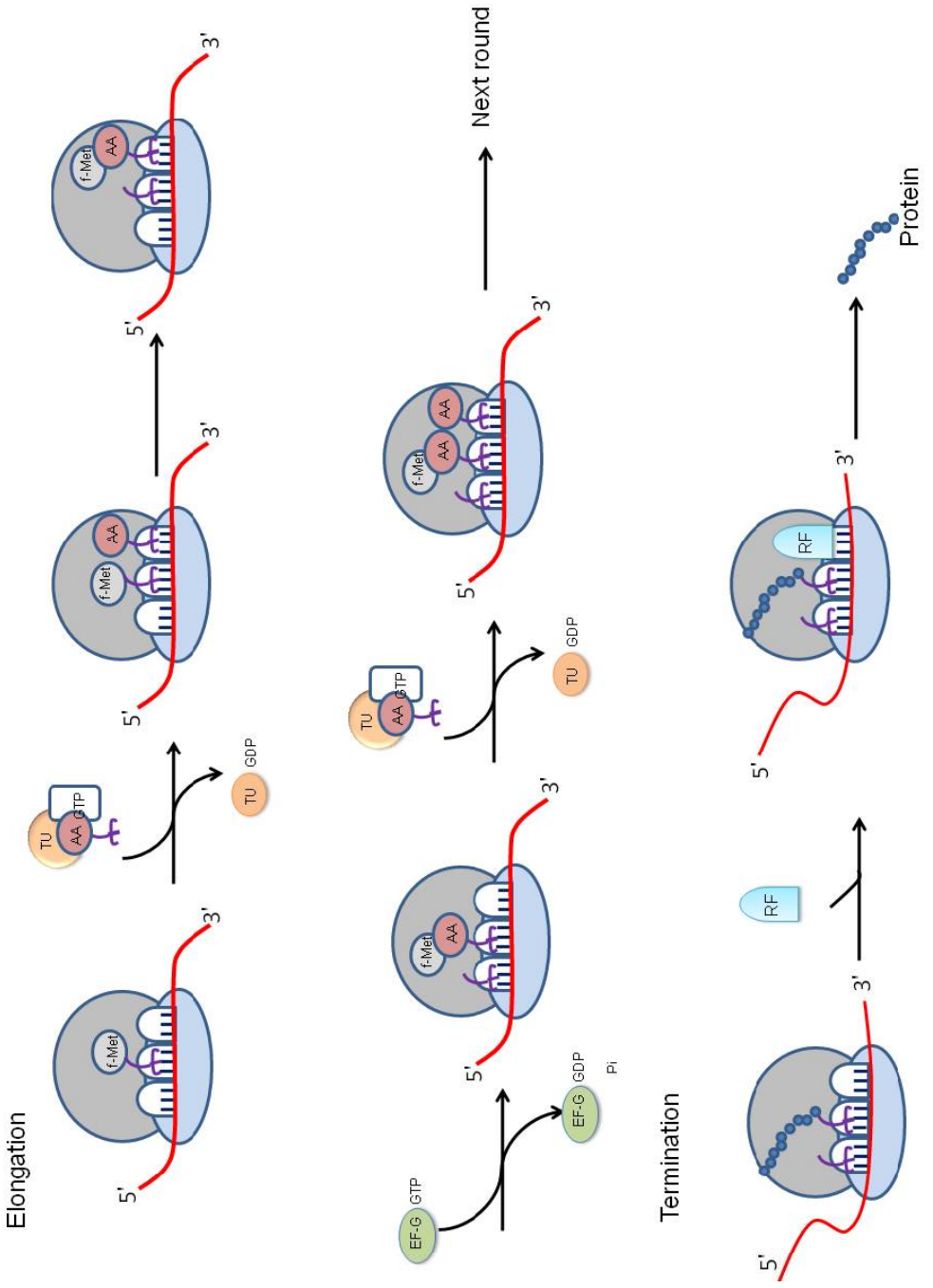

Figure 1.7. An overview of elongation and termination steps of protein synthesis is shown.

It is necessary to accurately match the correct aminoacyled-tRNA with the mRNA codon for protein translation. Before the sequence of 16S rRNA was known, it was observed that the modification of 16S rRNA by kethoxal abolished binding of tRNA to the ribosome (*60*). Afterward, footprinting techniques revealed that binding of the A-site tRNA strongly protected G529, G530, A1492, and A1493 against chemical modification (*3*). In further experiments, it was found that A1492 and A1493 of helix 44, as well as G530 of helix 18, are involved in the decoding process (*48*). This process selects the cognate tRNA and rejects the non-cognate or near-cognate tRNA. The accuracy of translation is 10^{-3} to 10^{-4} per amino acid residue (*61*). Similarly, two residues, A2451 and G2447, of the 50S subunit in the PTC are crucial for peptide-bond formation. It has been shown that peptidyl transferase remains mildly active once many of the ribosomal proteins are removed, indicating this activity is largely catalyzed by rRNA (*42*). In addition, several structural and mutational studies have been carried out to establish the role of nucleotides in peptide-bond formation (*62-64*). To investigate the role of individual nucleotides in various regions of the ribosome, a number of mutational and structural studies have been carried out. From the random mutant library of 30S and 50S subunits, changes at 53 positions in 16S rRNA and 77 positions in 23S rRNA displayed deleterious phenotypes (*2, 65*). In the decoding region, all 15 possible mutations were constructed at conserved nucleotides C1402 and A1500 of helix 44 of 16S rRNA. The results showed that most of the mutations lead to deleterious phenotypes showing the importance of these nucleotides for proper ribosome functioning (*66*).

1.3 Ribosome as a Drug Target and Antibiotic Resistance

The ribosome is a well-validated drug target site because of its accessibility, structural diversity, and lack of known repair enzymes. Various classes of antibiotics bind within the functional centers of the ribosome and inhibit protein synthesis by different mechanisms. About 40% of the known drugs bind to the ribosome (*67-68*). The binding sites are found to be within a limited functional region of the ribosome, such as the decoding region, peptidyltransferase center, peptide exit tunnel, and intersubunit regions. The smaller subunit, 30S, is targeted by many antibiotics, including tetracycline, pactamycin and aminoglycosides (**Figure 1.8 A, Table 1.1**) (*69-71*). Aminoglycosides, such as neomycin, paromomycin, and geneticin, bind to the decoding region and cause bases 1492 and 1493 to flip out (*70, 72*). In addition, binding of these antibiotics to helix 44 of 16S rRNA causes a conformational change, which interferes with translational fidelity by increasing the misincorporation of aminoacylated tRNAs (*73*). Recent crystal structures of 30S complexed with aminoglycosides have greatly increased our understanding of antibiotic sites in the ribosome (*69, 74*). Before the success of crystallography, model systems of RNA were used to map the binding sites and interaction of antibiotics by chemical probing and NMR spectroscopy (*70, 75-77*). This early work in solution allowed researchers to compare and validate the results obtained from crystallography.

Several important regions of the large subunit, 50S, are also targeted by antibiotics (**Figure 1.8 B, Table 1.1**). Several clinically important antibiotics such as macrolides, streptogramins, chloramphenicol, and oxazolidinones, bind to the

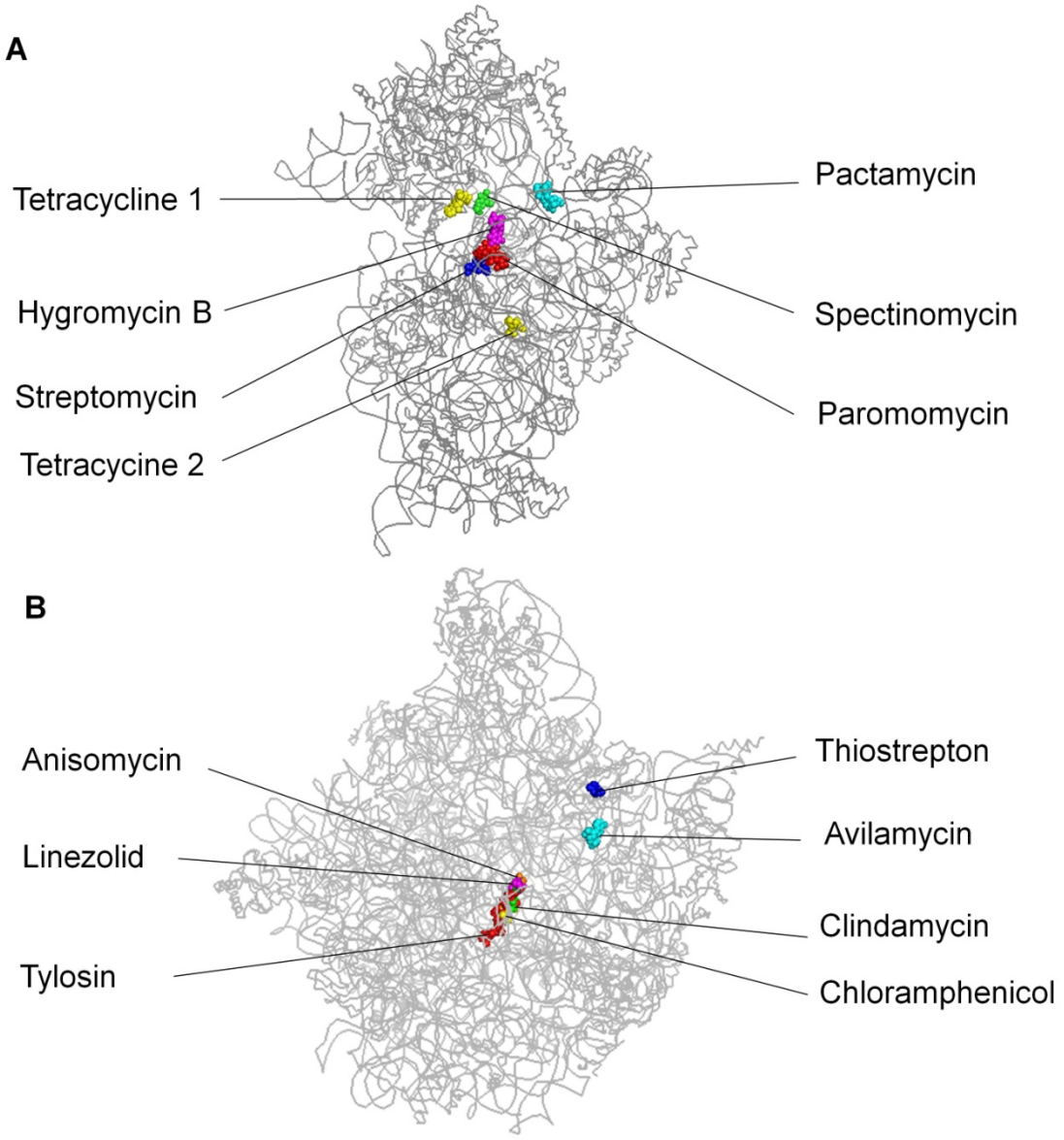

Figure 1.8. Various antibiotics bound to the ribosome are shown. A) Common antibiotics binding to the 30S subunit (PDB: 1FJG, 1HNX, 1HNJ, and 1HNW) are overlaid. B) Common antibiotics binding to the 50S subunit (PDB: 3CC4, 3CPW, 1K9M, 2ZJP 1NJI, and 1YJN) are shown.

Table 1.1. Common antibiotics targeting to the ribosome. Helix number and subunits are indicated.

Antibiotics	Binding sites	Mechanism of action
Aminoglycosides (neomycin, paromomycin, geneticin) (*69, 78-79*)	A site (30S subunits)	Decrease translational accuracy and inhibit ribosomal translocation
Tetracycline (*78, 80*)	helix 34/31 (30S)	Inhibits A-site tRNA binding
Peptides (viomycin, capreomycin, edeine) (*80*)	30S subunits	Inhibit translocation
Spectinomycin (*69*)	helix 34 (30S)	EF-G binding inhibitor
Pactamycin (*78*)	helix 24/P site (30S)	Inhibits initiation factor
Macrolides (erythromycin, azithromycin) (*81-82*)	Peptide exit tunnel near PTC	Block outlet of polypeptide
Lincosamides (lincomycin, clindamycin) (*82*)	Peptide exit tunnel	Interfere with peptide-bond formation
Chloramphenicol (*82-83*)	A site, PTC	Inhibits peptide-bond formation
Oxazolidinones (linezolid) (*84-85*)	P site (50S)	Compete with incoming aminoacyl-tRNA

large subunit near the PTC and inhibit protein synthesis (*86*). The macrolides are one of the important classes of ribosome-targeting antibiotics. Crystal structures of macrolides complexed with the 50S ribosomal subunit revealed that they block the ribosomal exit tunnel for the progress of nascent polypeptide (*81*). Similarly, streptogramins and chloramphenicol bind to the PTC and lock the conformation of the ribosome (*83*). Still, there are several antibiotics for which binding sites and mechanism of action have yet to be determined in detail.

The enormous use of antibiotics and increasing antibiotic resistance of pathogens are the current challenges for scientists. Bacteria may become resistance to antibiotics by various mechanisms, including target site modification, drug modification, and efflux (**Figure 1.9**) (*87*). To keep antibiotic concentrations low, drugs such as tetracyclines or erythromycins are pumped out through efflux mechanisms by bacteria (*88*). Penicillins were found to be destroyed by β-lactamases, while aminoglycosides such as kanamycin are chemically modified, which blocks binding to the recognition site (*89*). Mutations or nucleotide modifications such as methylation of the target residue have also been observed with several antibiotics targeting the ribosome. Modifications or mutations are found in both ribosomal proteins and ribosomal RNA. In spectinomycin resistance, mutation of a serine to proline at position 21 of the S5 protein has been observed (*90*). Similarly, a lysine to arginine change at position 42 of the S12 protein leads to streptomycin resistance (*90*). In RNA, modification of target residues has been found in several antibiotic resistance strains. Methylation of A1408 or G1405 leads to resistance to many aminoglycosides

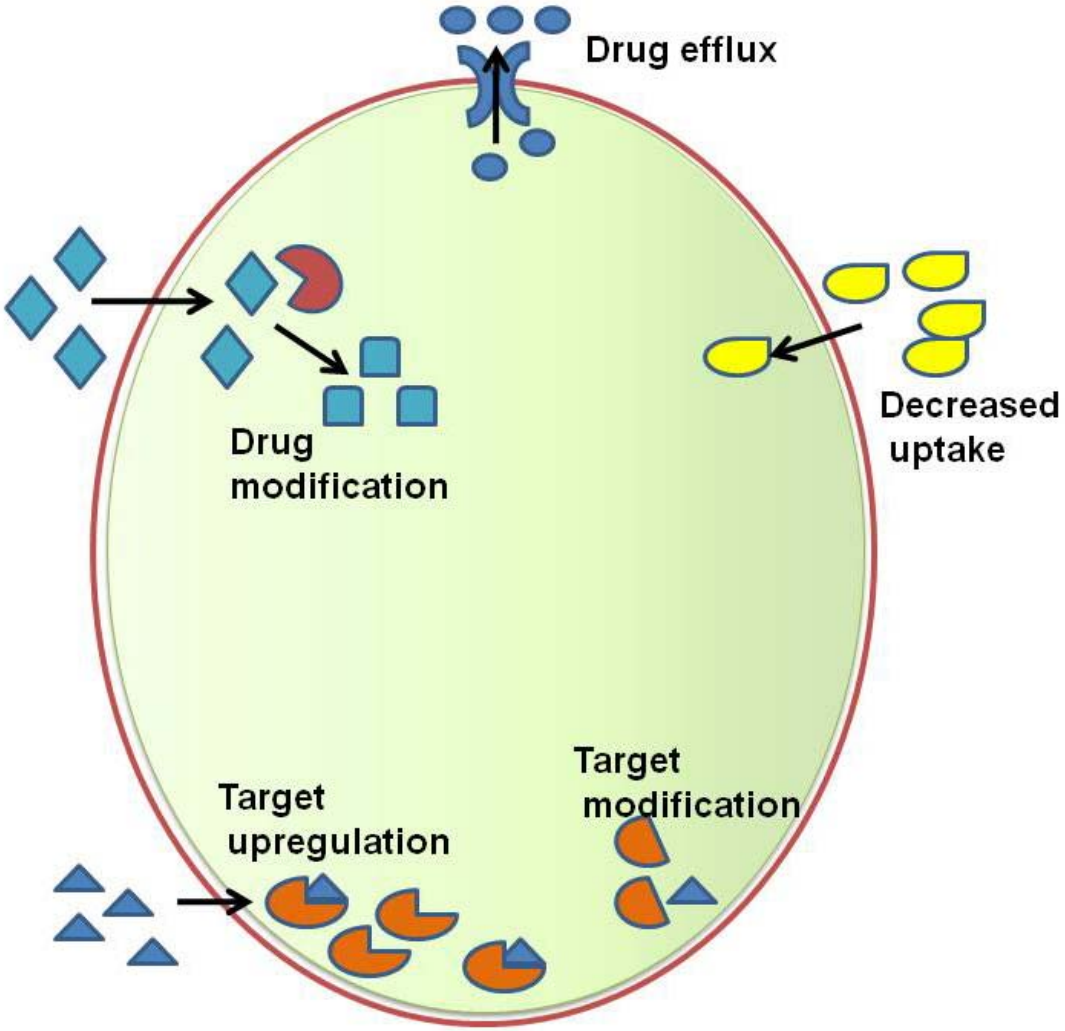

Figure 1.9. Various mechanisms of antibiotic resistance in bacteria are shown.

(*91-92*). Similarly, N7 methylation of G1405 produces resistance to the geneticin class of aminoglycosides (*93*). Mutation of key residues in the decoding region, such as A1408G and C1409G, also causes resistance to most of the aminoglycosides (*94-96*). In the large subunit, methylation of A2058 at N6 leads to resistance of macrolide, clindamycin, lincosamide and spreptogramin, whereas methylation of C1920 makes bacteria resistant to capreomycin (*97-100*). In anisomycin resistance, mutations of U2500A and C2453U have been observed (*101*). Target-site mutation for ribosome-binding drugs is difficult because eubacteria carry multiple copies of ribosomal operons. *E. coli* has seven ribosomal operons, and at least half of them must be in the mutant form to confer antibiotic resistance (*102-103*). In addition, mutations often alter the ribosomal structure, which prevents binding without impairing the biological function. Mutations of certain nucleotides in the ribosome have been found to be lethal and several of them are essential for fidelity of protein synthesis (*103*).

The antibiotic binding sites and resistance mechanisms determined from biochemical and genetic approaches are clarified by the high-resolution crystal structures (*85, 104*). High-resolution crystal structures can now be used to predict novel drug-binding sites as well as modified versions of existing drugs in order to overcome resistance. The binding sites of about half of the known antibiotics are found to be clustered in the central functional regions of the ribosome (*71*). A greater challenge is to identify and target unexploited sites in the ribosome. We do not know whether the known sites are the only ones for effective inhibition, or whether there are more possible target sites on the

ribosome. The ribosome is a complex and dynamic molecule that directs translation in several steps. For the purpose of identifying novel target sites or designing drugs on the basis of structure, a better understanding of the ribosome structure in solution, as well as functional importance of individual nucleotides, is needed.

1.4 RNA Structural Studies

There are a variety of methods for studying RNA structure. Cryo-electron microscopy (cryo-EM) X-ray crystallography and nuclear magnetic resonance (NMR) spectroscopy are the most popular methods for obtaining structural information of biomolecules. X-ray crystallography and cryo-EM are particularly well suited for large macromolecular complexes such as the ribosome. Solution studies such as NMR spectroscopy are typically limited to smaller systems. Other biophysical methods such as circular dichroism (CD) spectroscopy, UV melting, and fluorescence energy transfer (FRET) experiments are also very useful for understanding RNA structure and function (*105-106*). Another method to understand the RNA structure is chemical and enzymatic probing. The available probes are widely used to understand the environment of individual nucleotides at physiological conditions (e.g., solvent exposure, base pairing interactions, etc.) (*107-108*).

1.4.1 Biophysical methods

Cryo-EM in combination with single-particle reconstruction has been utilized by Joachim Frank and coworkers to obtain pictures of the ribosome

during different stages of translation (*109*). In cryo-EM, molecules are rapidly frozen to maintain them in a nearly native state. Unlike crystallography, cryo-EM does not require highly ordered crystals (*110*). A 6.7 Å map of the *E. coli* ribosome was published in association with aminoacyl-tRNA (*111*). By this method, it is possible to analyze the motions and dynamic changes of the ribosome during translation. The resolution, however, is not as high as that obtained by X-ray crystallography.

X-ray crystallography is the most powerful technique for studying larger RNA structures such as the ribosome. The first RNA structure determined by X-ray crystallography was $tRNA^{Phe}$ (*112*). After that, the crystal structures of several small RNA were determined; however, the requirement of highly ordered crystals and solving the phase problem took a much longer time to solve in order to obtain crystal structures of the ribosome. In 1998, Tom Steitz and coworkers published the first crystal structure of the 50S ribosomes from *Haloarcula marismortui* at 9 Å (*113*). In 2000, Yonath's, Steitz's, and Ramakrishnan's groups succeeded in determining the 30S or 50S subunit crystal structures at ~ 3 Å resolutions (*69, 114-116*). A considerable amount of effort has been made to obtain high-resolution structures of the ribosome, and for this groundbreaking work, the 2009 Nobel prize in chemistry was awarded to the three pioneers of ribosome crystallography, Thomas Steitz, Ada Yonath, and Venketash Ramakrishanan. Recent success in obtaining 70S ribosome structures in the presence of various antibiotics and initiation factors at highresolution has greatly increased our understanding of protein translation and the mechanism of

antibiotic action (*104, 117*). It has not only helped to understand ribosome function, but also increased information about antibiotic binding sites in various regions (*118*). For instance, neomycin binding was previously believed to occur only in the A site of the small subunit; however, a recent crystal structure showed that it also binds to helix 69 of 23S ribosomal RNA in the large subunit (*119*). Despite these successes from X-ray crystallography, detailed structural information in solution has not been obtained.

NMR spectroscopy is a powerful tool for studying RNA structure in solution. This method gives high-resolution structural information of RNA in solution. The RNA folding and interactions with various ligands such as peptides, antibiotics, and proteins can also be determined by this method (*120*). However, the structure of a larger RNA structure such as rRNAs cannot be determined by this method. The current size limit is ~100 nucleotides (*121*). Another limitation of this method is the requirement for a large amount of highly pure sample and technical expertise.

Several other biophysical methods are used extensively to obtain RNA structural information. Single-molecule spectroscopy and FRET measurements have been widely used to understand RNA folding, metal ion effects, and ligand binding. Notably, it was used to understand the movement of ribosomes at various stages of translation (*106, 122*). CD spectroscopy and UV melting are also helpful in determining the conformations and stabilities of small RNA constructs (*105, 123*).

1.4.2 Probing RNA Structure

Structure probing carried out in solution is a popular method for RNA structure determination. It is based on the reactivity of RNA molecules with various chemicals or enzymes that target specific regions or nucleotides of the RNA (*124*). These probes can react with RNA in free form or in complex with ligands. Various chemical and enzymatic probes have been used to obtain RNA structural information (**Figure 1.10**). Though there are many advantages of using chemical and enzymatic probes, they also have their limitations. One advantage of this method is being able to test the reactivity of individual nucleotides in near physiological conditions. In addition, the effects of changing pH or salt concentrations can also be monitored (*125*). The RNA does not need to be highly pure, and any size of RNA molecule can be used. Due to their larger size, enzymes are not accessible to all small-molecule binding sites in the RNA. Similarly, chemical probes are limited to *in vitro* studies due to their inability to penetrate the cell due to size and/or charge. Only limited chemical probes such as dimethyl sulfate (DMS), Pb^{2+}, and hydroxyl radicals have been utilized to gain structural information *in vivo* (*108, 124*). More recently, in-line probing (*126*) and selective 2'-hydroxyl acylation analyzed by primer extension (SHAPE) chemistry have been developed to determine RNA structure and to locate the binding sites of small molecules (*127*). For in-line probing, labeled RNA is incubated for extended periods of time (e.g., 40 hours) at higher pH (9.0), and spontaneous cleavage is detected. Small-molecule-binding sites can be observed as protected sites, whereas the other regions undergo strand scission. In SHAPE chemistry, reactivity of the 2'-OH groups with a bulky reagent is determined (*128*). Due to

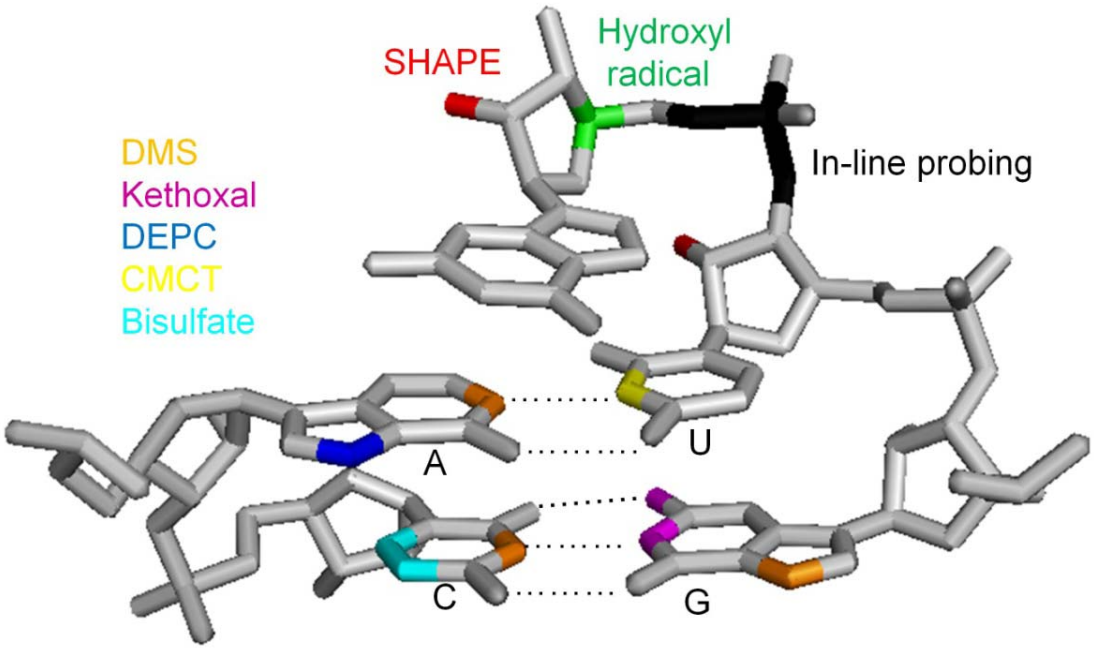

Figure 1.10. Sites of RNA modification by base specific chemical probes and sequence independent probing methods are shown (*129*).

steric hindrance of the bulky group on the reagent, reverse transcriptase stop sites can be detected. The geometrical constraints of the 2'-OH group only allow the reaction to occur in the flexible regions, such as loop or bulges. Hence, this method is independent of the nucleotide type and measures the local dynamics of the nucleotide. This method is also useful for determining small-molecule-binding sites and for acquiring information about secondary structure of RNA (*129*).

1.4.2.1 **Enzymatic probing**

RNases are structure or nucleotide specific and widely used for probing RNA structure (*130*). The commonly used nucleases with their specificity are listed in **Table1.2**. RNase V1 is specific to the double-stranded region (*131*). This ribonuclease cleaves in a sequence-independent manner, but requires at least two residues on either side of the cleavage site to be double stranded or stacked. Nucleotide-specific enzymes cleave after certain nucleotides. RNases A, T1, and T2 are the most common enzymes used to determine single-stranded regions (*132*). RNase T1 cleaves on the 3' side of guanosine, whereas RNase A cuts single-stranded UpN and CpN containing sequences. RNase T2 cleaves all phosphodiester bonds in a single-stranded region, irrespective of the sequences (*124, 132*). RNases are useful for obtaining structural information and ligand binding sites *in vitro*. Unfortunately, RNases are bulky molecules and susceptible to steric hindrance, so in the folded RNA structure, the accessibility information obtained from enzymatic probing is less informative.

Table 1.2. Structure-specific enzymes for RNA structure probing.

Nuclease	Specificity	Detection method	
RNase V1	Paired or stacked nucleotides	A and B	(*131*)
Nuclease S1	Unpaired nucleotides	A and B	(*108*)
RNase T1	Unpaired G	A and B	(*133*)
RNase U2	Unpaired A>G>>C>U	A and B	(*134*)
RNase T2	Unpaired A>C, U, G	A and B	(*135*)
Mung bean nuclease	Single-strand specific	A and B	(*136*)
RNase H	RNA only from DNA-RNA hybrids	A and B	(*137*)

A: detection of cleavage on end-labeled RNA and B: detection by primer extension method.

1.4.2.2 Chemical probing

Chemical reagents are smaller in comparision to enzymes and able to react with nucleotides of the RNA molecule (*125*). Chemical probes can react with nucleotide bases or the backbone of RNA. Their reactivity with nucleotide bases or the backbone is directly influenced by interactions present in the molecule. Base pairing or interactions with ligands strongly reduce reactivity towards the chemical probe. Chemical probes were developed based on specific criteria such as single-hit reactions per molecule of RNA, small size, and easy detection. Depending on the size of the RNA, identification of strand scission or modification sites is achieved by two different methods. For small RNA constructs, the RNA is directly radiolabeled on either the 3' or 5' end, and strand scission can be monitored by gel electrophoresis. This direct detection method works best for short RNAs containing less than 200 nucleotides (*108*). For larger RNAs, the strand scission or modification is detected by using primer extension. Reverse transcriptase shows pauses or stops before the 3' side of modified or cleaved nucleotides. The most commonly used chemical probes with their respective modification or cleavage sites and the methods for their detection are listed in **Table 1.3**.

Chemical probes are basically of two types on the basis of their target sites; base-specific and backbone (ribose-phosphate) specific. The base-specific probes are the most widely used to gain information about the secondary structure of RNA. Dimethyl sulfate (DMS) methylates the N1 position of adenine, and N3 of cytosine, which are not involved in Watson-Crick base pairing. Similarly, kethoxal reacts with N1 and N2 of guanine, while CMCT (1-cyclohexyl

Table 1.3. Structure-specific chemical probes for RNA.

Probing agents		Specificity	Detection method
Nucleotide modifying agents (*107, 124, 138*)	DMS	A (N1), C (N3), G (N7)	A, B, C C
	DEPC	A(N7)	A, B, C
	Kethoxal	G (N1-N2)	B, D
	CMCT	G (N1), U(N3)	B
	Hydrazine	U>>C	A, B. C
Radical generators/ metal complexes (*139-141*)	$Fe(EDTA)^{2-}$	Solvent-exposed backbone (C1', C4')	A, B
	$Cu(phen)_2^{+}$	Accessible SS regions	A, B
	$Rh(DIP)_3^{3+}$	SS solvent exposed G & Ψ, 3' side of GU wobble pairs	A, B
	$CoCl_2$	SS solvent-accessible G	A, B
Synchrotron X-rays (*142*)		Solvent-exposed backbone (C1', C4')	A, B, C
Backbone modifying agent (*124*)	Ethylnitrosourea	Phosphate	A, B

A: detection of cleavage on end-labeled RNA; B: detection by primer extension; C: chemical treatment is necessary for strand scission prior to the detection; D: RNaseT1 hydrolysis can be used after modification; SS: single stranded (*108, 124-125*).

-(2-morpholinoethyl)carbodiimide metho-p-toluene sulfonate) modifies N3 of uridine (*138, 143*). Based on the reactivity of these chemical probes, the folded structure of RNA can be determined. Since the modification occurs in the Watson-Crick base pair regions, these sites of modification can be detected by primer extension directly. However, DMS and diethyl pyrocarbonate (DEPC) can also methylate the N7 position of guanine and adenine, respectively. To detect these modifications, aniline treatment and strand scission are required (*124*). These chemical probes are not only used for smaller RNA structures, but also larger RNA structures such as 16S and 23S rRNA. Danesh Moazad and Harry Noller have mapped nucleotide reactivity in free rRNA, in intact subunits, and 70S ribosomes (*144-145*). They have not only determined the higher-order structure of rRNA, but also explored protected and exposed nucleotides after ribosome assembly (*145-147*).

Another class of probes attacks the ribose-phosphate backbone, resulting in strand scission. This type of chemical probe generates free radicals from a reaction between the reagents, such as the Fe•EDTA complex and H_2O_2 (*148*). The hydroxyl radical generated by the Fe•EDTA attacks the C1' and C4' hydrogens of the ribose sugar, which leads to strand scission. More recently, synchrotron X-ray beams were used to generate hydroxyl radicals in the millisecond range. This time-resolved probing method is very useful in determining the larger RNA folding pathway (*149-150*). Another reagent, ethylnitrosourea, ethylates phosphates, which become unstable and easily cleaved with mild alkaline treatment (*151*).

1.4.2.3 Probing RNA structure *in vivo*

Structural features of RNA are significant for biological function. The use of X-ray crystallography, NMR spectroscopy, and other biochemical and biophysical approaches have enhanced the ability for determining RNA structure. Since the folding of RNA might be different in a more complex environment such as living cells, it is highly important to study RNA structures *in vivo.* Methods and probes that are useful for studying RNA structure *in vivo* are limited. The most commonly used are DMS, kethoxal, and lead (II) (*152-153*). DMS can cross the cell wall and membrane efficiently by diffusion, but other reagents need permeabilization of the cells.

Chemical and enzymatic probes are very useful to test the reactivity of individual nucleotides and predict their accessibility, as well as function in RNA structures. Several chemical and enzymatic probes have been used to probe the RNA structure, but most of them are limited for *in vitro* study. Another limitation is that enzymes can induce conformational rearrangements, which generates possible new target sites and makes the results harder to interpret. In addition, these chemical and enzymatic probes cannot be utilized to monitor the kinetics of the reaction. Hence, a chemical probe that can be used for probing and monitoring kinetics would be very useful. The aquated platinum complex to be discussed is positively charged and can be utilized as a model to understand the kinetics of charged small molecules. Further, it has already been shown to have potential for probing the ribosome structure *in vitro* and *in vivo*. Another advantage of cisplatin is that its size and charge can be altered easily, and hence would be useful to gain more information of RNA structure.

1.5 Cisplatin

Cisplatin, *cis*-diamminedichloridoplatinum (II), is an anticancer drug used to treat various cancers such as testicular, head and neck, and cervical (*154-156*). The cure rate is over 90% in testicular cancer when tumors are diagnosed early (*157*). Despite its success, cisplatin is only active against limited cancers and causes several side effects such as nephrotoxicity, neurotoxicity, and hearing loss (*158-159*). The biological activity of cisplatin was first discovered in the 1960 by Rosenberg and co-workers at Michigan State University (*160*). While testing the effects of electric current in *E. coli*, they observed inhibition of cell growth. They observed that cells were unable to divide and the morphology changed. Cells were elongated 300 times longer than the normal cells (*160*). It was later found that this effect was not caused by the electric current, but rather the production of the cisplatin from platinum electrodes. This result led Rosenberg to test cisplatin in several mice with tumors, and subsequently anticancer activity was observed (*161*). After the successful treatment of several tumors in clinical trials, cisplatin was finally approved by the FDA in 1978.

1.5.1 Biological targets of cisplatin

Cisplatin can enter the cell by passive diffusion or using by copper transporters (*162-163*). The low chloride concentration in the cell facilitates the exchange of a chlorido ligand with water to form the aquated species. The resulting species $[PtCl(NH_3)_2(H_2O)]^+$ is more reactive and subsequently attacks the N7 of purine bases. The primary target of cisplatin is found to be DNA, but it can also attack RNA, proteins, and sulfur-containing biomolecules (*156, 163*).

Cisplatin preferentially binds to G-rich sequences in DNA. The number of platinum molecules bound to these macromolecules has been determined in HeLa cells with a colony forming assay (*164*). This result showed that one DNA contained 22 platinum atoms, while only one platinum atom was found per mRNA. Similarly, one platinum atom was observed per 30 ribosomes and one per 1500 tRNA. Proteins contained a fewer number of platinum atoms; out of 1500 protein molecules, only one equivalent cisplatin was observed. Another study was carried out with 195mPt-radiolabeled cisplatin to determine the number of platinum atoms that would bind to macromolecules in Hela cells (*165*). This study showed similar results, which indicated DNA as the main cellular target. These early studies showed that the most important cellular target of cisplatin was DNA, while its effects on RNA and other macromolecules was mostly overlooked. The binding of cisplatin to DNA has been discussed extensively in the literature (*156, 163, 165-166*), but only a handful of publications focus on RNA as a target.

Recent studies showed that RNA is a competitive target for cisplatin under similar conditions as DNA reactions (*167-169*). When DNA and RNA molecules with similar structures and sizes were compared, RNA was found to be the kinetically preferred target over DNA (*167*). In addition, RNA showed a more pronounced salt dependence, indicating that electrostatic interactions are important (*167*). A similar result was published by DeRose and coworkers, in which the kinetic preference for cisplatin in the U2/U6 RNA compared well to its DNA counterpart (*170*). They have compared cisplatin binding to RNA with an

internal loop, double-stranded RNA, and a corresponding looped DNA. Among these constructs, the RNA with an internal loop had the highest reactivity, while DNA had the lowest. Another study was done with tRNA by Elmorth and coworkers (*168*). Mapping of the binding sites in tRNA and its corresponding microhelix revealed that cisplatin forms cross-links in a common site on the RNAs, despite the difference in their sizes (*168*).

1.5.2 Types of platinum-DNA adducts and their effects

The identification of major cisplatin cross-links formed with DNA was carried out by digestion of cisplatin-treated salmon sperm DNA (*171*). After enzymatic digestion, the products were separated by a chromatographic technique and analyzed by NMR spectroscopy (*172*). The most common cross-links were the 1,2-intrastrand adducts with purine bases, mostly the 1,2-intrastrand d(GpG) and d(ApG) adducts which constitute ~65% and ~25% of all adducts respectively. Less common was the 1,3-intrastrand d(GpXpG) adduct (**Figure 1.11**). Cisplatin also formed a small amount of interstrand and monofunctional adducts with guanine (*171-172*).

The formation of cisplatin DNA cross-links leads to distortion of the DNA structure. Previous studies showed that cisplatin lesions cause bending, unwinding, and destabilization of the DNA double helix (*173-174*). The formation of cisplatin cross-links also inhibits DNA and RNA polymerases for replication and transcription processes (*163*). Bifunctional adducts inhibit polymerases more effectively than monofunctional adducts (*175-177*). In addition, the bending of DNA serves as a recognition site for a number of cellular proteins, such as high

mobility group proteins (HMG), histones, and transcriptional proteins (*178-179*). The binding of these proteins is believed to shield the platinum adducts from repair so that when the DNA repair machinery works to fix the cross-links, failed attempts activate apoptosis and cell death (*166*).

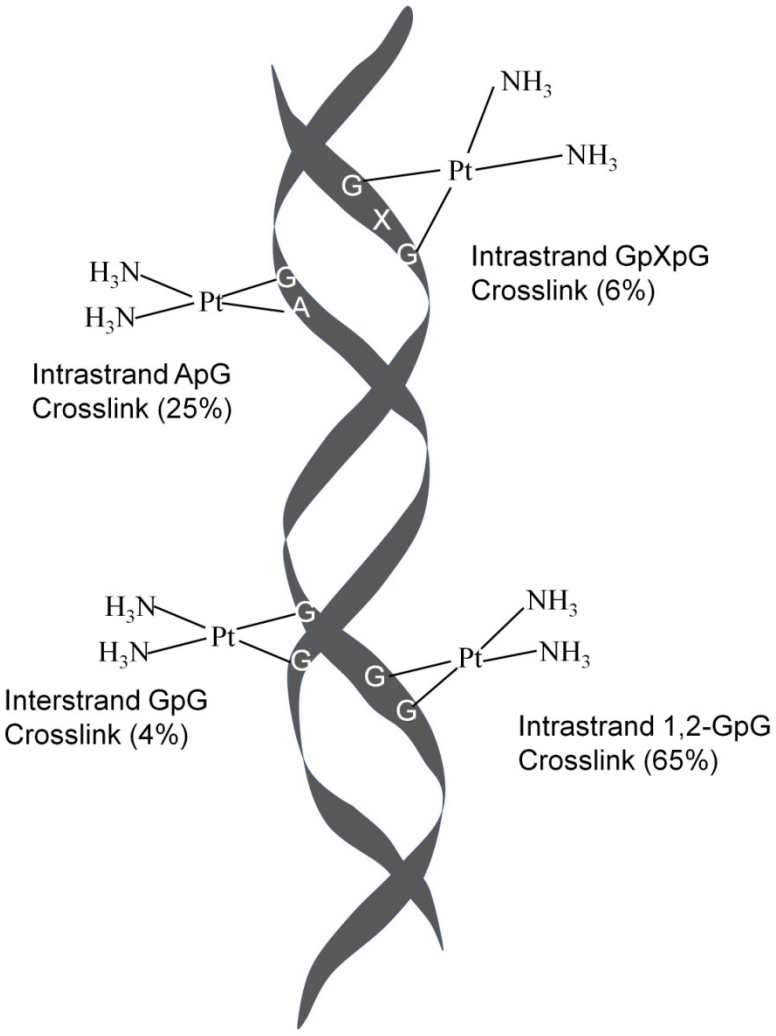

Figure 1.11. The types of cisplatin DNA cross-links and their corresponding ratios are shown.

1.5.3 Cisplatin analogues

Compared to cisplatin, its *trans* isomer, *trans*-DDP, is clinically ineffective. This might be due to its inability to form adducts similar to that of cisplatin. Although both of these isomers form bifunctional adducts through the N7 position of purine bases, *trans*-DDP is unable to form 1,2-intrastrand cross-links due to its stereochemistry. More than 3000 analogues of cisplatin have been synthesized to overcome cisplatin resistance (*180*); however, only less than 30 compounds have entered clinical trials and only one has been approved by the FDA (*166*). Hitherto, only four platinum compounds are listed as marketed drugs, namely, cisplatin, carboplatin, oxaliplatin, and nedaplatin (**Figure 1.12**) (*166, 181*). Among these, carboplatin is less toxic than cisplatin, but has the same spectrum of antitumor activity (*182*). Oxaliplatin is the only platinum compound that shows acitivity against cisplatin-resistant colorectal cancers (*181*). Most of the useful antitumor analogues are mostly associated with the property of labile group. Complexes with highly labile groups are very toxic and cannot be used as drugs. Those types of complexes react with almost all types of nucleophiles available in the cell. In contrast, strongly bound ligands produce kinetically inactive complexes (*183*). The second generation platinum drug, carboplatin, has lower reactivity due to the weaker labile carboxylate group. This effect causes a slower rate of conversion of carboplatin to aquated reactive species. Due to slower reactivity, higher doses can be tolerated and give fewer side effects. Carboplatin has been used for ovarian cancer, but shows cross resistance with cisplatin (*166, 184*). Another analogue, oxaliplatin, is most effective against colon cancer (*163*). In this compound, both the ammine ligands and chlorido groups are altered from

those of cisplatin (*166*). Most recently, water-soluble platinum complexes and complexes that can be used orally, such as JM216, have been synthesized (*166, 185*).

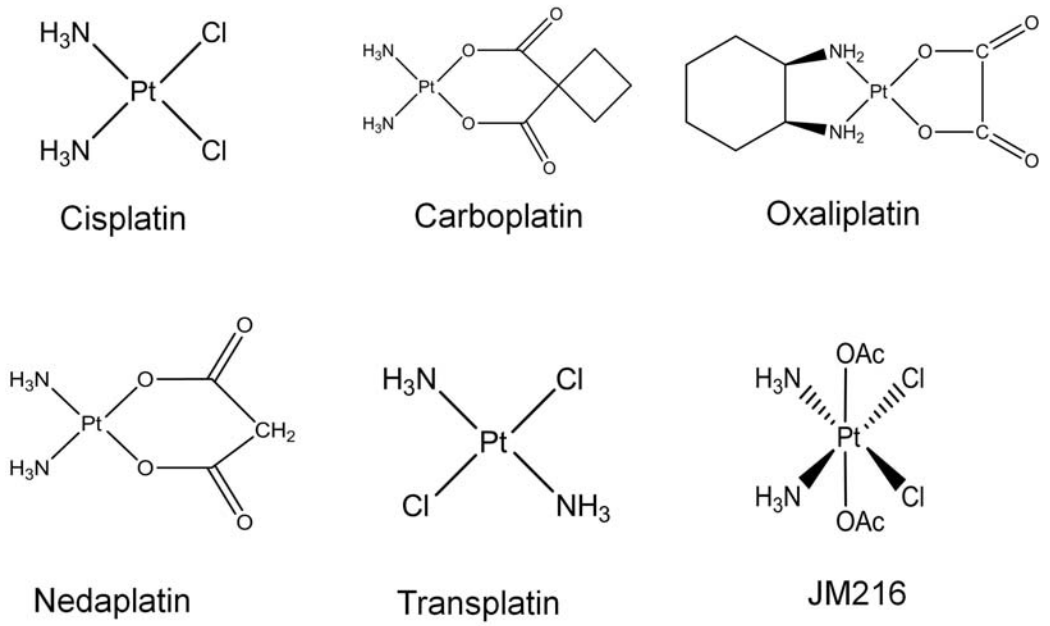

Figure 1.12. Cisplatin and its analogues are shown.

Several amino-acid and peptide-conjugated cisplatin analogues have been synthesized and tested against various tumor cell lines (**Figure 1.13)** (*186-187*). Modifications include platinum complexes with charged, neutral, or hydrophobic amino acids coordinated to the platinum (*188-189*). Those modifications increase the charge or hydrophobicity of the complex, and could potentially alter the binding interactions with the target. Similarly, peptide-tethered platinum conjugates were also synthesized and their interactions with

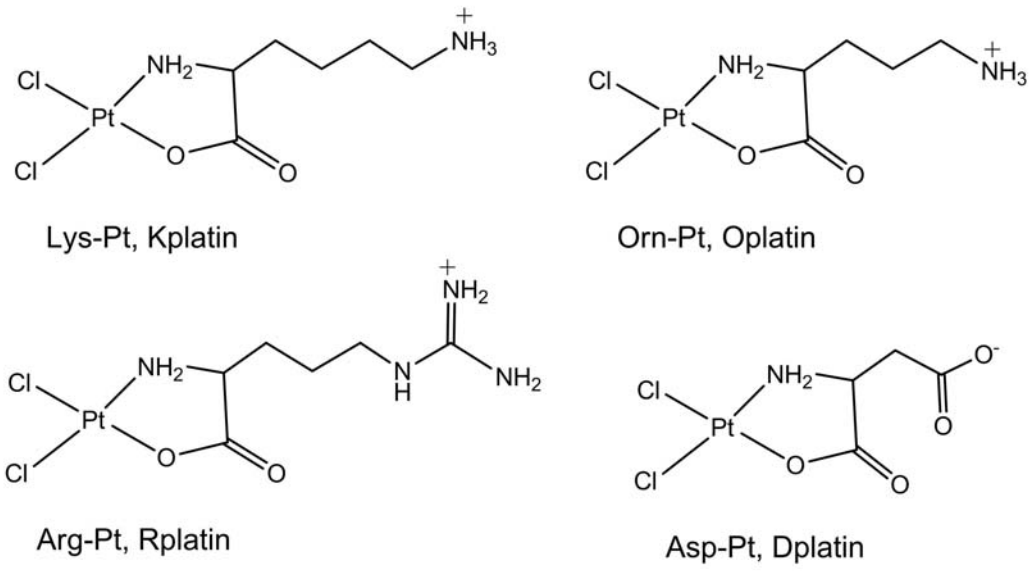

Figure 1.13. Structures of platinum(II) amino acid complexes are shown.

DNA were studied; however, additional functionalities did not increase their reactivity (*186, 190*). The uncharged compounds have lower reactivity compared to cisplatin and positively charged compounds have higher reactivity than the negatively charged compounds, possibly due to electrostatic interactions (*186*). Although the overall reactivity of the amino-acid platinum complexes was lower than cisplatin in DNA, their interactions with RNA have not been discussed in the literature, to the best of my knowledge.

1.6 Objective of Research

With the continually expanding antibiotic resistance of pathogens it has been a challenge for researchers to design and develop new antibiotics. Out of the various drug target sites, the ribosome is an important target to which different classes of antibiotics bind at its key functional regions, such as the

decoding center, peptidyltransferase center, and peptide exit tunnel. Recent crystal structures have revealed a number of antibiotic-binding sites in the ribosome, and it is interesting to note that many of these sites are overlapping. Now, it is important to develop novel target sites and to design new drugs that can help to solve the ever-growing problem of resistance. To achieve this goal, the ideal target sites should not only be functionally important, but also accessible to various small molecules. A number of chemical and enzymatic probes have been used to gain structural information and to understand solvent accessibility of the ribosome, but most of them are limited to *in vitro* studies or they are difficult to detect in solution. Cisplatin has advantages due to its stable coordination chemistry, which makes its detection easier; thus, more information about structural accessibility can be gained. Further, the platinum complexes can be modified with various ligands to alter the charge and size. A number of antibiotics bind to the ribosome by electrostatic interactions and it is difficult to monitor the kinetics. Cisplatin and its charged analogues can be utilized as a model to understand how charged small molecules such as neomycin find their target sites out of the numerous possible sites on the ribosome.

CHAPTER 2

Binding Studies and Adduct Characterization of Cisplatin in 16S Ribosomal RNA

2.1 Abstract

DNA is a well-validated target of cisplatin and various mechanisms leading to the anticancer activity have been extensively studied. In comparison to DNA, much less is known regarding the extent to which cisplatin interacts with cellular RNAs and whether that influences the activity and toxicity of the drug. Recently, cisplatin binding to small RNA constructs and tRNA has been studied. In this chapter, the binding sites of cisplatin on 16S rRNA, which were mapped by the primer extension method, are discussed. Most of the consecutive guanosines in free 16S rRNA were found to be reactive with cisplatin. In addition, the number, as well as types, of adducts formed with cisplatin on 16S rRNA were also characterized.

2.2 Introduction

Cis-diamminodichloridoplatinum(II), or cisplatin, is an antitumor drug that has been utilized effectively in the treatment of several types of cancers, such as testicular, breast, ovarian, lung, and head and neck (*156, 163, 166*). After the discovery of its antitumor activity, much research has focused on understanding the mode of action of this compound (*160-161*). The formation of several types of stable adducts with nucleic acids, such as 1,2-intrastrand and 1,3-intrastrand along with a lower number of interstrand, through coordination to the N7 position

of purines, is believed to contribute to its antitumor activity (*172, 191*). The formation of these adducts with DNA causes structural changes, which block replication and transcription processes (*163*). An X-ray crystal structure revealed that the 1,2-intrastrand adduct induces a bend in a DNA duplex by 35-40º and unwinds the DNA by ~25º; however, solution structures by NMR showed 60-70º bend angles (**Figure 2.1**) (*192-194*). Cellular proteins recognize these DNA lesions and undergo a series of events, eventually leading to cell death (*163, 166, 195*). The reaction of cisplatin with DNA has been studied and discussed extensively in the literature (*163, 166, 172, 191, 196-197*); however, the effects of cisplatin on RNA function are poorly understood. Despite RNA's chemical similarity to DNA and its greatly increased role in various cellular processes (*198-199*), very little is known about cisplatin's effects on cellular processes involving RNA.

Previous reports suggested that the amount of cisplatin reacting with RNA is much less than with DNA (*165, 200*), which might be the reason why RNA has been overlooked as a target of cisplatin. However, there are several pieces of evidence that show RNA is a competitive target for cisplatin. Previously, cisplatin was found to cause disruption of translation and splicing in cell extracts (*201-203*). This fact is further supported by recent *in vitro* studies showing disruptions in the activity of various enzymes (*170, 204*), so it can be expected that the binding of cisplatin to RNA may also contribute to the drug's anticancer effect. In another study, when similar structures and sizes of DNA and RNA hairpins were compared for cisplatin reaction, RNA was found to be the kinetically preferred

target (*167, 205*). A similar result was reported by DeRose and coworkers in U2/U6 RNA; they have shown that platination of the U2/U6 RNA a has higher kinetic preference for RNA than the corresponding DNA construct (*169*).

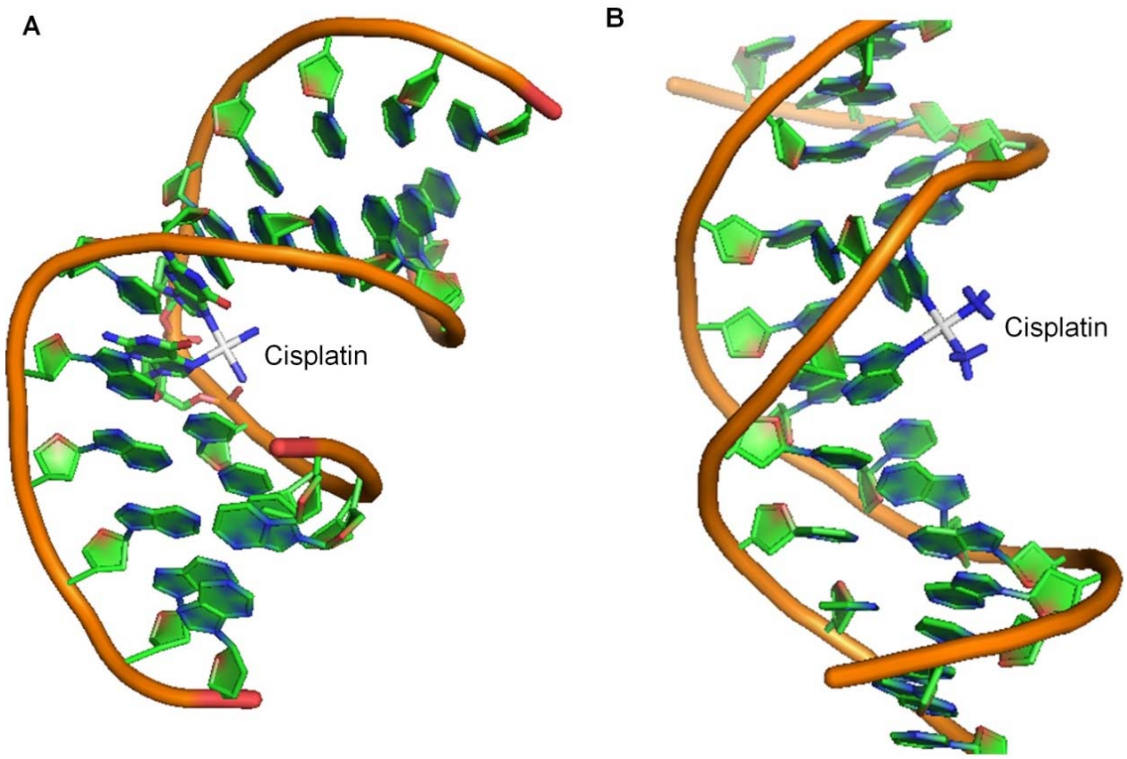

Figure 2.1. X-Ray crystal structures of double-stranded DNA containing the cisplatin adduct are shown: A) cisplatin 1,2-d(GpG) intrastrand cross-link (3LPV) (*193*) and B) cisplatin 1,3-d(GpTpG) intrastrand cross-link (1DA4) (*206*).

Cisplatin binds DNA in a structure specific manner and forms cross-links at specific sites despite the sizes of the nucleic acids (*168, 207*). Elmroth and co-workers studied the rate of platination of 17-nucelotide DNA sequences with guanosines at different locations ((T_nGT_{16-n}) DNA constructs) (*207*). The rate of adduct formation was found to be the highest when guanosine was in the middle of the sequence. In addition, they compared cisplatin reactions with $tRNA^{Ala}$ and a corresponding micro-helix, which revealed similar platination sites at the G○U wobble pair in an acceptor stem of tRNA, despite the different RNA sizes (*168*). Furthermore, cisplatin binding to $tRNA^{Phe}$ observed in a crystal structure showed cross-links at certain GG and AG sites that caused a distortion in the tRNA structure (*208-209*). Hence, targeting RNAs such as tRNA, mRNA, and rRNA may provide another potential pathway for cisplatin and related drugs' mechanism of action (*210*). Cisplatin effects in model RNA systems have been studied to some extent; however, the mechanistic details and binding sites in larger RNA have yet to be discovered.

Although the primary structure of DNA and RNA are very similar, larger RNAs such as ribosomal RNAs have a tendency to fold into complex three-dimensional structures (*40*). The folding of RNA creates local microenvironments with various properties in terms of solvent accessibility and metal coordination. Various metal complexes have been used to identify structural motifs or mismatches in DNA and RNA structure (*139-140, 211-212*). Metal complexes are capable of specific interactions with target sites in nucleic acids. Rhodium complexes such as $Rh(byp)_2(chrysi)^{3+}$ bind with high specificity and affinity to

single base mismatches (*213*). Similarly, $Rh(DIP)_3^{3+}$ induces a strand scission in RNA near the G○U mismatches, as well as exposed Gs (*211*). Cisplatin has been found to react with G-rich sequences in DNA and small RNA constructs. Hence, metal complexes were found to have some specific interaction with nucleic acids. The study of cisplatin binding to the ribosome may increase our understanding of its interactions with much larger RNA structures.

The number and types of cross-links formed with DNA by cisplatin and various analogues have been well characterized (*171-172*). Two research groups, Eastman and Fichtinger-Schepman *et al*., have determined various adducts formed with DNA (*171-172, 191*). Both of these research groups observed intrastrand bifunctional cross-links as the major adducts along with a small amount of monofunctional adducts with guanosine (*171*). In the context of RNA, the number of cisplatin binding sites and possible types of adducts have not been well documented.

The overall goal of this chapter is to find the cisplatin binding sites in 16S rRNA and determine the types of adducts formed by using various methods (**Figure 2.2**). The results from these experiments will be significant to understand the mechanism of cisplatin action on large folded RNA structures. Due to structural differences, it was expected that the binding sites and types of adducts formed with RNA might be different than DNA. In this study, mapping of the cisplatin binding sites in 16S rRNA, as well as characterization of the cisplatin adducts was performed.

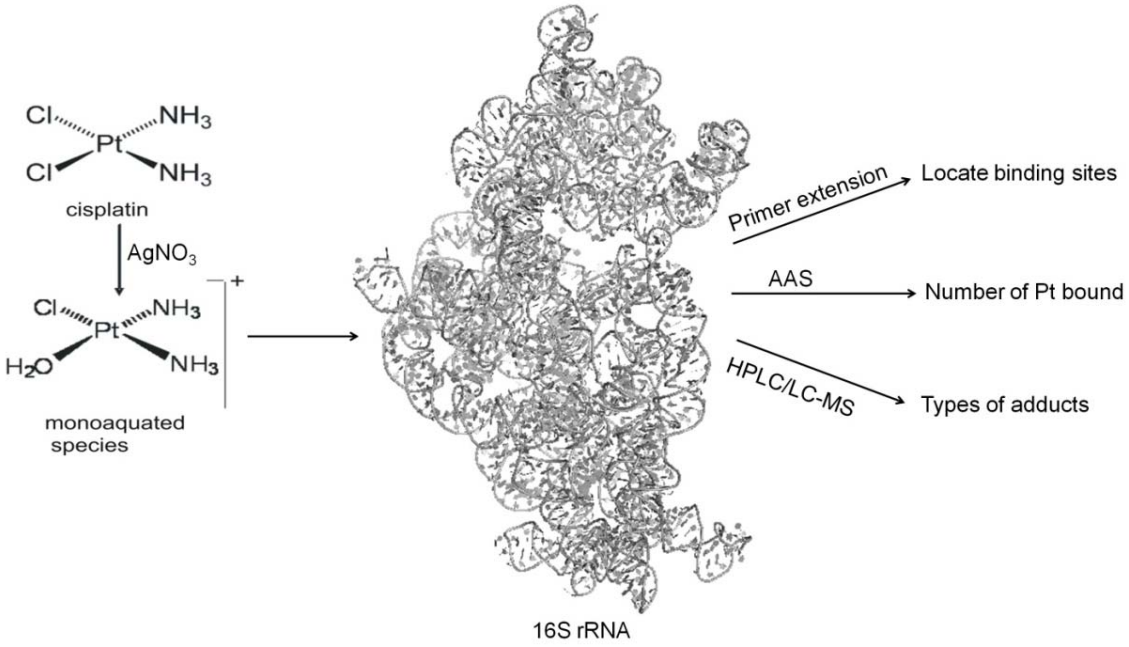

Figure 2.2. An overview of the cisplatin binding study in 16S rRNA is shown. Cisplatin, the corresponding monoaquated species, tertiary structure of 16S rRNA, and various methods used in this study are indicated.

2.3 Materials and Methods

2.3.1 Chemicals, solutions, and DNA

[5'-^{32}P-γ]ATP was purchased from Perkin-Elmer Life Sciences, Inc. (Waltham, MA), and T4 polynucleotide kinase was obtained from New England Biolabs (Ipswich, MA). RNaseT1 and P1 nuclease were purchased from Sigma Chemicals. A reverse transcriptase kit (Improm_II™ Reverse Transcriptase) was purchased from Promega (Madison, WI). The remaining chemicals for buffers, and reagents such as DTT (dithiothreitol), EDTA (ethylenediaminetetraacetic acid), DMF (N, N-dimethyl formamide) were obtained from Sigma Chemicals or Fisher. RNase-free, distilled, deionized water (ddH_2O) was used for all experiments.

Cisplatin, *cis*-diamminedichloridoplatinum(II), was purchased from Alfa Aesar (MA, USA). The complexes *cis*-$[PtCl(NH_3)_2X]^{+/0}$ or *cis*-$[Pt(NH_3)_2X_2]^{2+/0}$, in which X was H_2O, DMF, or NO_3^-, were prepared by addition of 0.98 or 1.96 equivalents of $AgNO_3$ to a DMF solution of *cis*-$[PtCl_2(NH_3)_2]$, respectively. The reaction mixture was vortexed in the dark for 12 hours, the AgCl precipitate was removed by centrifugation, and the supernatant containing platinum complex was recovered. Platinum-DMF complex stock solutions were stored at -20 °C up to 1 week and diluted as required just prior to use.

Single-stranded DNA primers were purchased from Sigma Genosys and purified by using polyacrylamide gel electrophoresis (20%, 19:1 acrylamide:bisacrylamide, 7 M urea) in 1x TBE (90 mM Tris·HCl, 90 mM boric acid, 2.5 mM EDTA, pH 8.3) followed by electroelution in 0.5x TBE in an Amicon Centrilutor™ and desalted. Aqueous solutions of DNA were kept frozen at -20 °C and concentrations were determined spectrophotometrically at 260 nm. Sequences of the DNA primers were named according to the position of the transcribed nucleotides, and are as follows:

1) 5'-CAC TCG TCA GCA AAG AAG-3 (p_86), 2) 5'-GCG ACG TTA TGC GGT AT-3' (p_171), 3) 5'-GTT ACC CCA CCT ACT AGC T-3 (p_245), 4) 5'-AGT CTG GAC CGT GTC TC-3' (p_323), 5) 5'-CCC GCT GAA AGT ACT TT-3 6) (p_431), 5'-GTG CTT CTT CTG CGG GTA-3' (p_485), 7) 5′-CGC TTT AGG CCC AGT AAT-3 (p_561), 8) 5′-GCC AGT ATC AGA TGC AGT-3 (p_631), 9) 5′-CTA CGC ATT TCA CCG CT-3′ (p_686), 10) 5'-CGC ACC TGA GCG TCA GTC T-3' (p_746), 11) 5′-ACC AAG TCG ACA TCG TTT-3′ (p_813), 12) 5′-CCG TCA ATT

CAT TTG AGT TT-3′ (p_906), 13) 5′-GTC AAG ACC AGG TAA GGT-3′ (p_982), 14) 5′ GAG CTG ACG ACA GCC AT-3′ (p_1054)) 15) 5′-GCA ACA AAG GAT AAG GGT-3 (p_1110), 16) 5′-TCG TAA GGG CCA TGA TG -3′(p_1199), 17) 5′-GCG AGG TCG CTT GTC TTT-3′ (p_1251), 18) 5′-CTC CAA TCC GGA CTA CG-3 (p_1296), 19) 5′-GAA CGT ATT CAC CGT GGC-3 (p_1365), 20) 5'-GTT AAGCTA CCT ACT TCT-3′ (P_1430), 21) 5'-TAC CTT GTT ACG ACT TC-3' (p_1490).

The primer hybridization sites on the secondary structure of 16S rRNA are shown in **Figure 2.3**, with primer numbers 1 to 21.

2.3.2 Isolation of 16S rRNA

The 70S ribosomes and 30S subunits were isolated from *E. coli* DH5 strain by the sucrose gradient method (*145, 214*). *E. coli* was grown to 0.6 OD and cooled on ice for 20 min followed by centrifugation at 7,000 rpm for 15 min to pellet the cells. The pellet was resuspended in buffer A (50 mM Tris·HCl, 100 mM ammonium chloride, 10 mM $MgCl_2$ and 1 mM EDTA). The cells were lysed by using a French Press at 1800 psi. In the lysate, 5 U of DNase I was added and incubated on ice for 15min. The lysate was centrifuged at 15,000 rpm for 20 min to remove the cellular debris and about 2/3 of the supernatant was transferred to a new tube. After a second centrifugation, the supernatant was transferred to a new tube and the ammonium chloride concentration was raised to 200 mM. To pellet the ribosome, centrifugation was carried out in an ultracentrifuge at 42,000 rpm for 4 hrs. The supernatant was discarded and the pellet was washed with buffer B (50 mM Tris·HCl, 100 mM ammonium chloride,

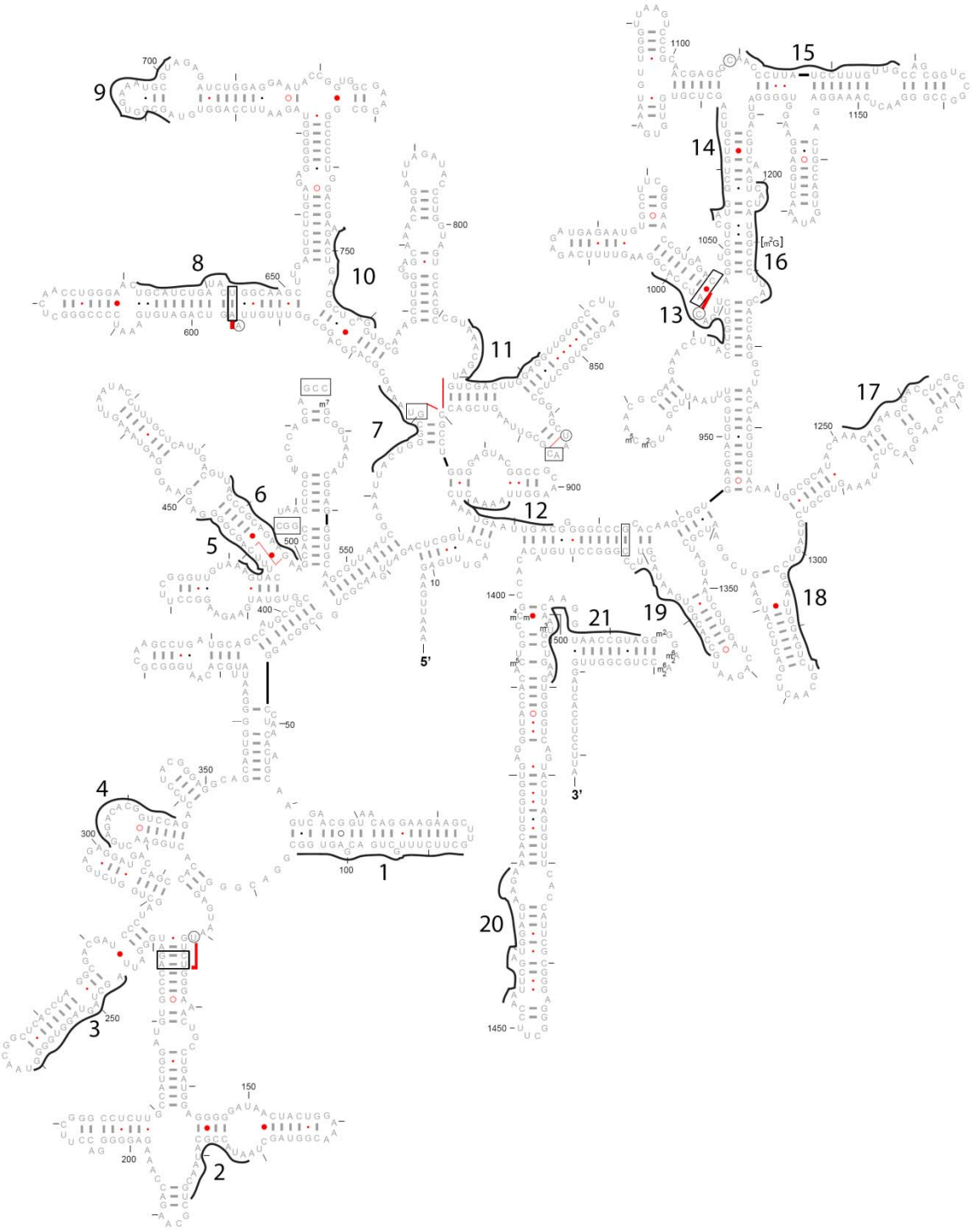

Figure 2.3. Secondary structure map of 16S rRNA with primer hybridization sites with primer numbers (1 to 21) is shown.

10 mM $MgCl_2$). The 70S ribosome pellet was resuspended in buffer B by shaking overnight at 4 ºC. The dissolved ribosome was taken carefully and its concentration was measured spectrophotometrically. To get pure 70S ribosomes, 50S subunits and 30S subunits, the crude ribosomes were layered in a 10% to 30% sucrose gradient in buffer B with 5 mM $MgCl_2$ and centrifuged in a swinging bucket rotor at 18,000 rpm for 16 hrs. Fractions corresponding to the 70S ribosomes, 50S subunits, and 30S subunits were pooled and the Mg^{2+} concentration was again raised to 10 mM. Sucrose was removed by centrifugation in an ultracentrifuge at 42,000 rpm for 18 hrs and the pellet was dissolved in buffer E (10 mM Tris·HCl, 60 mM ammonium chloride, 10 mM $MgCl_2$). Naked 16S rRNA was isolated from 30S subunits by three extractions with phenol and two with chloroform in the presence of 6 mM EDTA. The 16S rRNA was precipitated by addition of 0.1 volumes of 3 M sodium acetate, pH 5.3, and 2.5 volumes of ethanol. The isolated 16S rRNA was renatured in 20 mM Tris·HCl (pH 7.5), 25 mM NaCl, and 10 mM $MgCl_2$ by heating to 90 °C for 2 min and slowly cooling to room temperature.

2.3.3 Platination reactions

The platination reactions with naked 16S rRNA were performed with monoaquated cisplatin. Prior to platination, the 16S rRNA was renatured as stated above. Platination was carried out in 20 mM sodium phosphate buffer, pH 6.5, 10 mM $MgCl_2$ and 10 mM NaCl (buffer P) (*215*). Alternatively, 20 mM HEPES, pH 6.5, 10 mM $MgSO_4$ and 10 mM Na_2SO_4 (buffer H) was used, which had a lower chloride concentration. The 16S rRNA was incubated at 37 °C with

aquated complex in 1:150, 1:75, and 1:30 ratios of metal complex to nucleotides (16S rRNA to metal complex is 1:10, 1:20, and 1:50). The reactions were quenched with 2 M NaCl followed by immediately freezing. A salt dependence study was carried out with the 1:75 ratio of complex to nucleotides in the same buffer (buffer H) with increasing concentration of Na^+ using $NaClO_4$.

2.3.4 Primer labeling and primer extension

Primers were labeled at the 5' end in T4 PNK buffer (50 mM Tris·HCl, pH 7.6, 10 mM $MgCl_2$, 5 mM DTT, 0.1 mM spermidine, 0.1 mM EDTA) with 10 µCi [γ-^{32}P] –ATP and 10 units T4 polynucleotide kinase in a volume of 50 µl at 37 °C. RNA was ethanol precipitated after the reaction. The labeled primer was used for primer extension on the free 16S rRNA (*216*). Primer extension was carried out with 2 pmol of 16S rRNA after reaction with cisplatin. Next, 2 µl of the appropriate 5'-end-labeled primer (200,000 cpm) and 2 µl of 1 pmol/µl 16S rRNA were mixed with 6 µl ddH_2O and heated to 90 °C and then slowly cooled to room temperature for hybridization. The extension mix was prepared by mixing 4 µl of reverse transcriptase buffer (Promega), 2.4 µl of 25 mM $MgCl_2$ and 1 µl of 10 mM dNTPs (10 mM each dATP, dCTP, dGTP, and dTTP), 5.6 µl H_2O and 1 µl reverse transcriptase (Promega). For sequencing, 1 µl of the 10 mM dNTP mix and 1 µl of the appropriate 1 mM ddNTP were used. Unmodified RNA (no cisplatin treatment) was used as a template for sequencing and for control lanes to monitor artifacts of reverse transcriptase. Extension of the primer was carried out at 42 °C for one hour and terminated by heating at 80 °C for 15 minutes. To each sample, 2 µl of loading buffer (80% formamide, 1x TBE, 0.02% bromophenol

blue, and 0.02% xylene cyanol) was added and the products were denatured by heating to 95 °C for 2 min followed by rapid cooling on ice. To the sequencing gel (0.4 mm thick, 8% polyacrylamide, acrylamide:bisacrylamide 19:1, 1X TBE, 7 M urea), 60,000 cpm per sample was loaded. The gel was run at 1500 volts for approximately 2 hours until the bromophenol blue migrated off the gel. The products were identified by imaging on a Molecular Dynamics Phosphorimager and Image Quant™ Software.

The gels were quantified using Image Quant software. The intensity was normalized by calculating the percentage intensity at the corresponding stop with respect to intensity of the whole lane. More than 1% intensity at the corresponding stops were considered as strong hits, 0.5 to 1.0% were moderate hits, and less than 0.5% were considered as weak stops. The reaction ratio cisplatin:nucleotide (1:75) and control were used for quantification.

2.3.5 High performance liquid charomatography

HPLC was carried out with a Waters system equipped with a C18 Discovery column (250 x 4.6 mm, 0.5 µm). Separation was carried out by using buffer A (40 mM ammonium acetate) and B (40% acetonitrile) with a linear gradient in which the ratio of A to B changed from 95:5 to 70:30 over 30 minutes at a constant flow of 1 ml/min. The retention times of the standard nucleosides were confirmed by injection of known standard nucleosides. Control and platinated 16S rRNAs were digested with nuclease P1 to convert to nucleotides, and calf intestinal phosphatase (CIP) was used to remove phosphates and give free nucleosides. Nuclease P1 digestion was carried out in 50 µl of digestion

buffer (1 mM $ZnCl_2$, 20 mM sodium acetate, pH 5.3), for both the control and the platinated 16S rRNAs with 10 µl (10 U) of nuclease P1 at 37 ºC overnight. The enzyme was then deactivated by heating at 75 ºC for 15 min. Five µl of 1.5 M Tris·HCl, pH 8.8, and 1 µl (10 U) of CIP was added to each sample, which were incubated for 4 hrs at 37 ºC. After 4 hrs of incubation, samples were again heated at 75 ºC for 15 min, vortexed, and centrifuged at 12,000 rpm for 5 min. Finally, samples were filtered through YM-3 microcon filters before injection into the HPLC or LC-MS.

Samples were analyzed by HPLC and peaks areas were normalized to account for the differences in extinction coefficients at 260 nm (C = 9,100 M^{-1} cm^{-1}, U= 10,100 M^{-1} cm^{-1}, G= 13,600 M^{-1} cm^{-1}, A= 14,900 M^{-1} cm^{-1}) (*217*) and then peak ratios were calculated relative to the cytidine peak.

2.3.6 Liquid chromatography mass sectrometry

LC-MS (Liquid Chromatography Mass Spectrometry) is a powerful technique to separate and analyze complex mixtures with high sensitivity. LC-MS was carried out on an AQUITY Ultra Performance LC chromatography (UPLC) system (Waters Corporation, MA USA) equipped with an HSST3 C18 column (2.1 x 100 mm 1.8 µm). The column was maintained at 50 ºC and elution was carried out with a linear gradient of acetonitrile and 100 mM ammonium acetate, pH 6.0. The gradient was run for 3 min with a flow rate 700 µl/min, starting at 100% ammonium acetate and decreasing to 60% over the course of the gradient. The column eluent was analyzed by directing it to the mass spectrometer. Mass spectra were collected in the positive ion mode. The percentage of adducts were

calculated by normalizing the area with extinction coefficients followed by relative ratios of adduct present in sum of adducts.

2.4 Results

2.4.1 Mapping platination sites in 16S rRNA

Cisplatin, after aquation, was used to probe 16S rRNA. The monoaquated complex was employed because it is cationic and has ideal reaction kinetics compared to the slowly reacting cisplatin. The binding sites of monoaquated cisplatin were mapped on free 16S rRNA by primer extension. In order to map the binding sites, 16S rRNA was first isolated from *E. coli,* renatured, and then incubated with monoaquated cisplatin (1:10, 1:20 and 1:50 molar ratios of 16S rRNA:cisplatin; or 1:150, 1:75, and 1:30 molar ratios of cisplatin:nucleotides) in 20 mM HEPES buffer, pH 6.5, at 37 °C in the dark for 5 hrs. The binding sites of cisplatin were observed by reverse transcriptase pauses or stop one nucleotide prior to the coordination site. A set of 20 DNA primers were used, covering from nucleotides 1 to 1513 of the 16S rRNA. The 5'-^{32}P-end-labeled primers were hybridized with the RNA and extended with reverse transcriptase in the presence of dNTPs. The transcripts were separated by 8% denaturing polyacrylamide gels. Coordination sites of cisplatin were then determined by comparing with dideoxy sequencing lanes on the same gel. Bands on the gel arising due to nicks in the RNA or strong secondary structures were distinguished from the cisplatin binding sites by comparing with a control treated in a similar manner, but lacking cisplatin.

The magnitudes of the reactivity were classified by the intensities of the bands on the autoradiograms. The intensities of bands could be measured up to approximately 100 nucleotides from the transcription start site. The reactive nucleotides were mostly found to be consecutive Gs, mismatched or present in loop regions. Since cisplatin was known to prefer Gs in DNA targets, it was not surprising that major hits on the 16S rRNA were consecutive Gs. There are 488 guanosines in 16S rRNA and 103 sites with consecutive Gs, some of which include two or more guanosines (consecutive Gs are considered as one reactive site). Out of these 103 sites, strong reactivity was observed in 56 sites, 29 were moderate hits, and 3 showed very weak hits. In addition, several nonconsecutive Gs also showed strong or moderate reactivity. There were 11 consecutive Gs that were not reactive with cisplatin (excluding 4 sites with consecutive Gs in helix 45, which were not probed). **Figures 2.4** to **2.6** show representative autoradiograms of the cisplatin probing experiments with free 16S rRNA. Additional gels are shown in the **Appendix**. The overall summary of results of cisplatin binding to naked 16S rRNA in **Figure 2.7** show a secondary structure model of 16S rRNA with reactive sites in red (strong hits) and green (moderate hits).

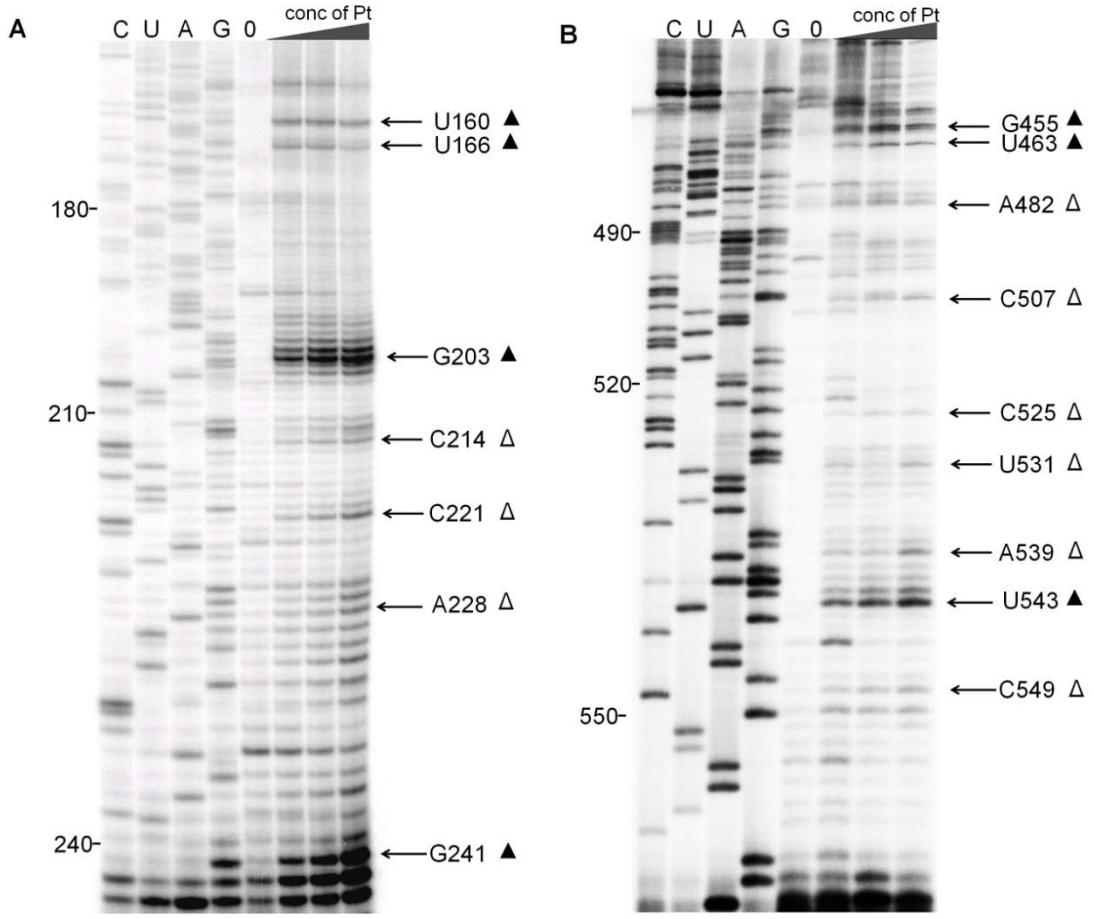

Figure 2.4. Probing results of 16S rRNA at the 5' domain with primers 245 and 561 are shown. (A) The autoradiogram shows the reverse transcriptase pauses or stops by using primer 245. (B) The autoradiogram shows the reverse transcriptase pauses or stops by using primer 561. In both gels, C, U, A, G represent the sequencing lanes, 0 represents the control, and remaining 3 lanes are 16S rRNA treated with increasing concentrations of monoaquated cisplatin (cisplatin:nucleotide is 1:150, 1:75, and 1:30). The strong and moderate hits are indicated with arrows and corresponding nucleotides numbers (▲ (strong hits) and Δ (moderate hits)).

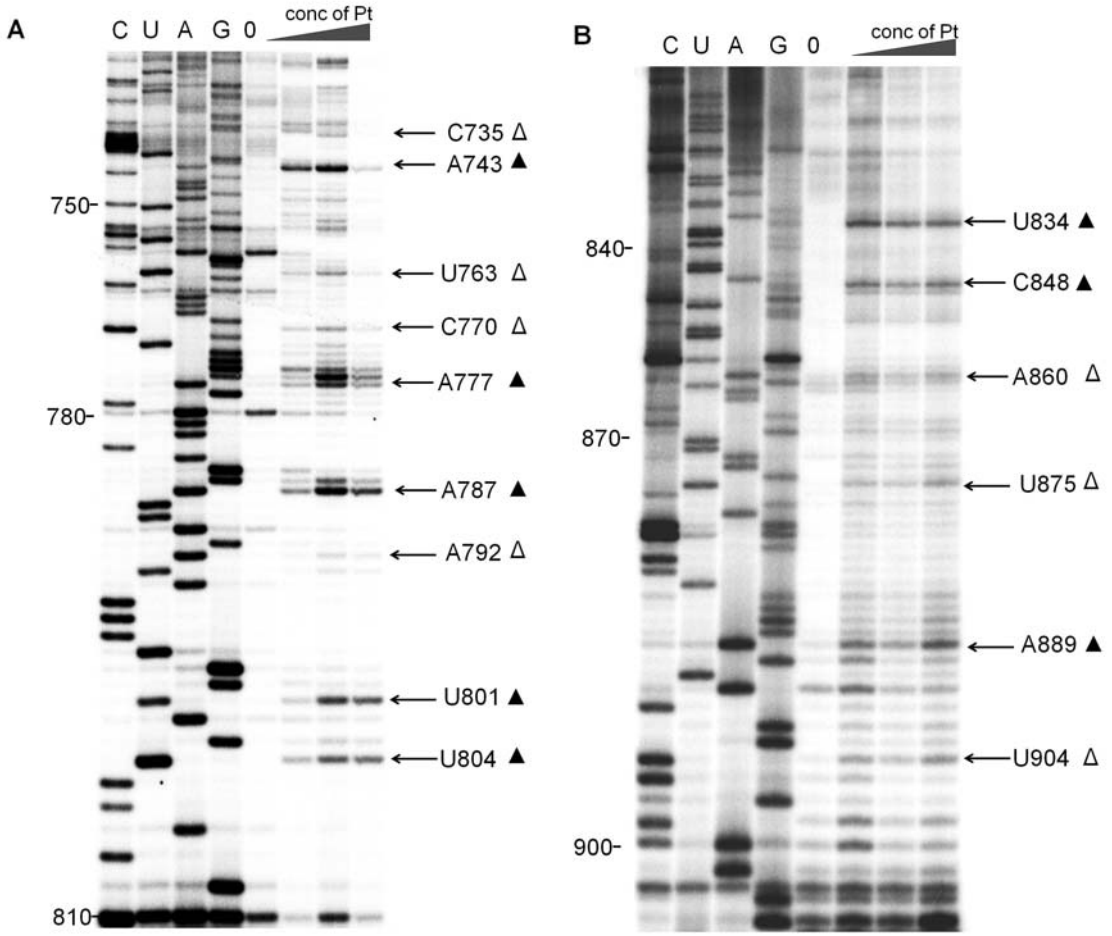

Figure 2.5. Probing results of 16S rRNA at the central domain with primers 825 and 910 are shown. (A) The autoradiogram shows the reverse transcriptase pauses or stops by using primer 825. (B) The autoradiogram shows the reverse transcriptase pauses or stops by using primer 910. In both gels, C, U, A, G represent the sequencing lanes, 0 represents the control, and remaining 3 lanes are 16S rRNA treated with increasing concentrations of monoaquated cisplatin (cisplatin:nucleotide is 1:150, 1:75, and 1:30). The strong and moderate hits are indicated with arrows and corresponding nucleotides numbers (▲ (strong hits) and Δ (moderate hits)).

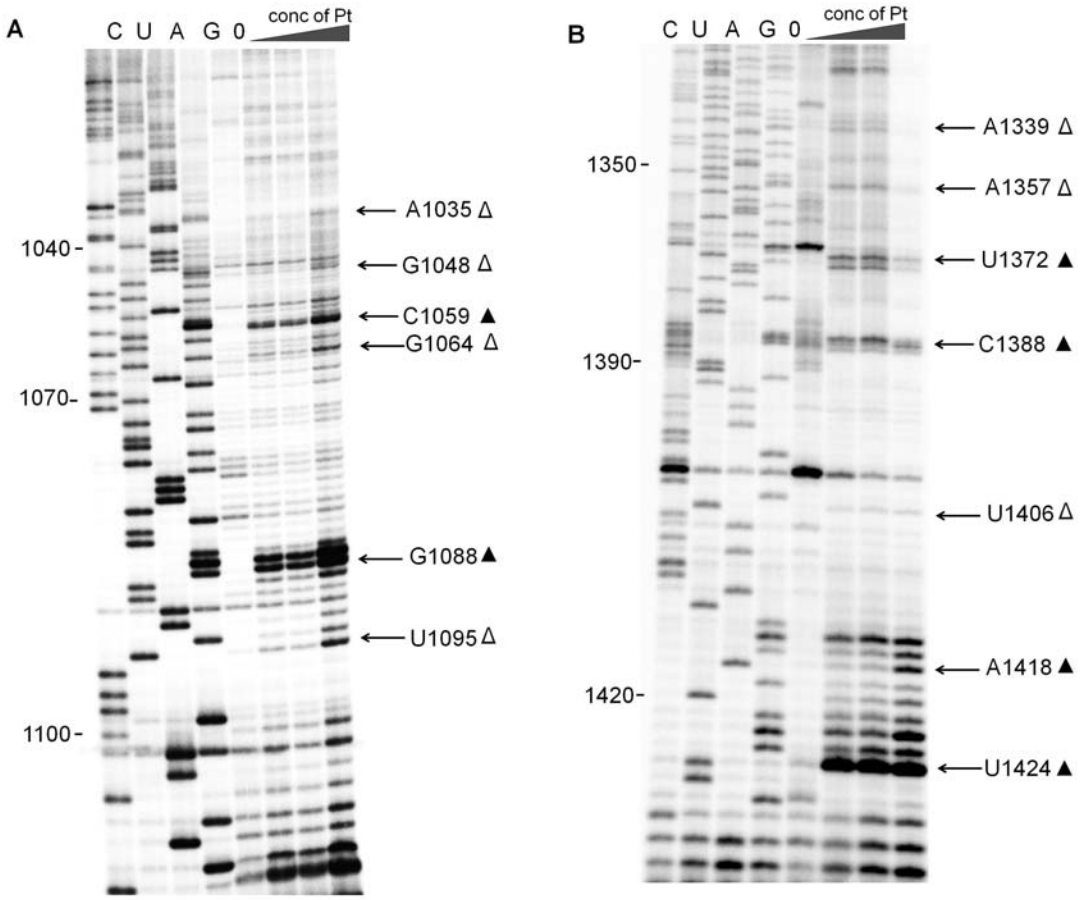

Figure 2.6. Probing results of 16S rRNA at the 3' domain with primers 1110 and 1435 are shown. (A) The autoradiogram shows the reverse transcriptase pauses or stops by using primer 1110. (B) The autoradiogram shows the reverse transcriptase pauses or stops by using primer 1435. In both gels, C, U, A, G represent the sequencing lanes, 0 represents the control, and remaining 3 lanes are 16S rRNA treated with increasing concentrations of monoaquated cisplatin (cisplatin:nucleotide is 1:150, 1:75, and 1:30). The strong and moderate hits are indicated with arrows and corresponding nucleotides numbers (▲ (strong hits) and Δ (moderate hits)).

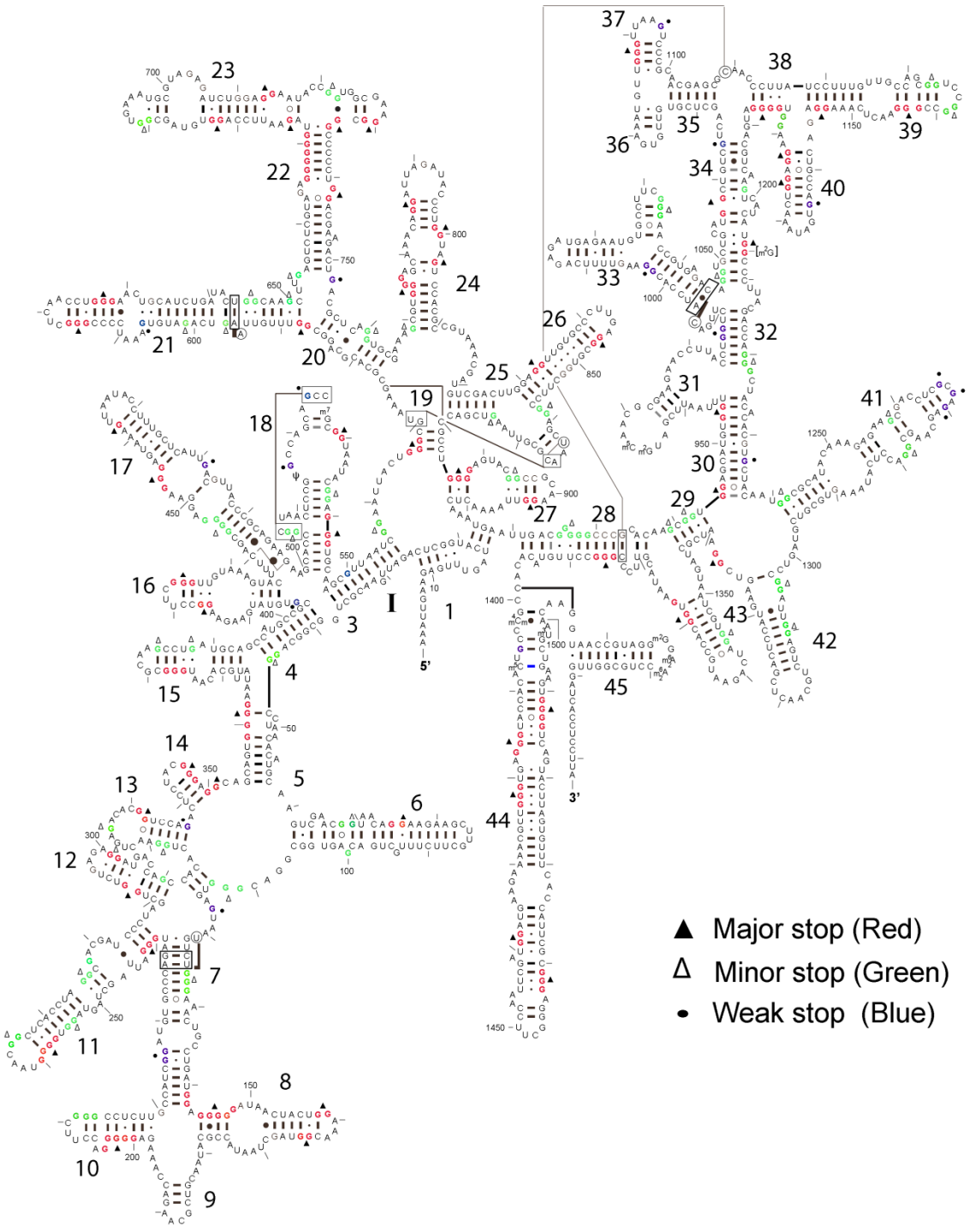

Figure 2.7. Secondary structure map of 16S rRNA (*34*) with probing results is shown. Strong hits (reactive nucleotides) are colored red (shown with ▲), moderate hits are colored green (shown with Δ), and very weak stops are colored blue (shown with •). The helix numbers are also indicated (1-45).

The cisplatin binding sites are distributed throughout the bacterial 16S rRNA. Inspection of **Figure 2.7** shows that in 16S rRNA, more than 50% Gs are reactive towards cisplatin (286/476), excluding helix 45. In the 5' domain (nucleotides 1-566), a number of prominent strong stops were observed, such as at G147, A160, U166, G203, G242, G260, and C352 (**Figures 2.4 A**, **2.8** and **Appendix**). All of these stops are on the 3' side of consecutive guanosines that contained at least one G○U pair or a mismatch, or resided next to a loop region. One of the very strong stops observed at G203 contain a G-C-rich sequence and G○U mismatch, similar to the binding sites observed previously in the tRNA acceptor stem (*168*). In addition to these sites, a number of minor and weak stops were also observed in this region, such as A129, C214, and A319, which were also before consecutive guanosines (**Figures 2.4** and **Appendix**). Most of these weaker sites contain repeating G-C pairs without a mismatch. None of the single guanosines in this region showed strong stops, and not all of the consecutive Gs were targeted. Only moderate or weak stops were observed on the 3' side of non-consecutive guanosines or with guanosines adjacent to adenosines.

In the upper part of the 5' domain, the stops at C379, C418, U426, A456, U463, and U543 (**Figures 2.4 B**, **2.8** and **Appendix**) were the strongest hits observed with cisplatin. Most of the strongest hits in this region were before consecutive guanosines, except for U463 which is on the 3' side of a single guanosine. In this region, several of the strong reactive sites contain either a mismatch, unpaired

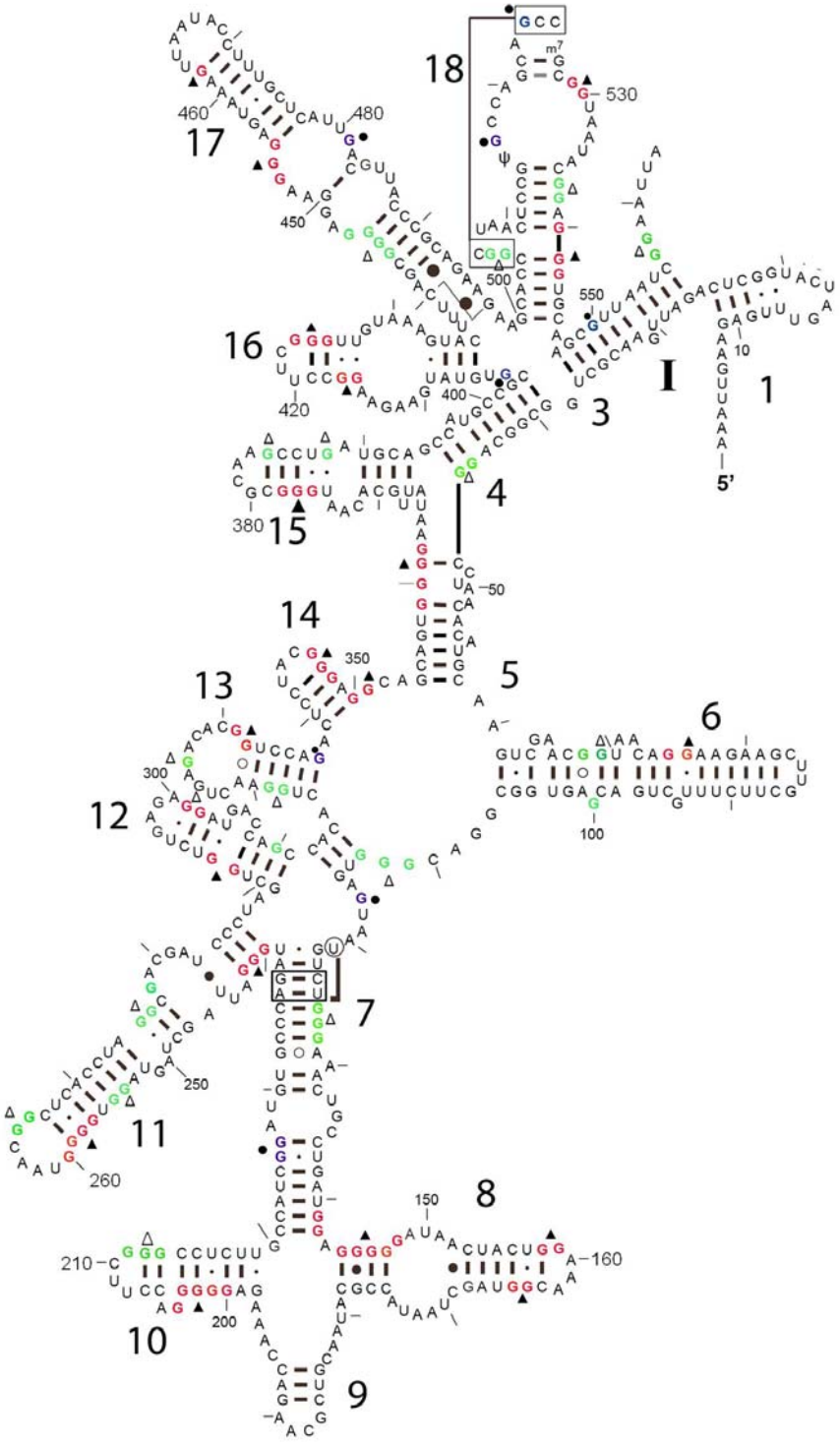

Figure 2.8. The 5' domain secondary structure map of 16S rRNA with probing results is shown. Strong hits (reactive nucleotides) are colored red (shown with ▲), moderate hits are colored green (shown with ∆), and very weak stops are colored blue(shown with ●). The helix numbers are also indicated.

bases in loop regions, or G○U wobble base pairs, indicating that cisplatin binding preferences are not simply limited to GG sites as was observed with DNA.

In the central domain (nucleotides 567-915), which includes helices 19 to 27, also showed a number of strong as well as moderate hits by cisplatin. The majority of the strong hits were observed in helices 22 and 24, such as at A743, A777, A792, U801, and U804 (**Figure 2.5 A**). These strong stops also appeared on the 3' side of the consecutive guanosines, except for U804, which occurred before the closing base-pair of the internal loop of helix 24. Most (22/28) consecutive guanosines in other helices with 16S rRNA also showed reactivity towards cisplatin. Strong stops occurred at C618 and A629 in helix 21 at two sets of GGG sites. Similarly, strong stops at U683 and A715 were observed on helix 23. The functionally important helix 27 also contains a strong stop at A889 (**Figure 2.5 B**) before a cluster of four consecutive Gs containing a G○U pair. In addition to these, several moderate and weak stops were observed, as shown in **Figures 2.5** and **2.9**.

The 3' side of 16S rRNA contains two domains: 3' major (nucleotide 916-1396) and 3' minor (nucleotide 1397-1542). Nucleotides in helix 45 of the 3' minor domain could not be mapped due to lack of appropriate nucleotides needed for primer hybridization. In the 3' major domain, C1059, G1187, C1208, and A1339 (**Figures 2.6**, **2.10** and **Appendix**) were a few of the very strong stops observed. The 3' minor domain contains two important helices: helix 44 and 45. Helix 44 contains the decoding region, which has a key role in protein

synthesis. Several consecutive Gs in this helix are targeted by cisplatin and strong stops were observed at G1416, U1424, U1440, C1460, and G1488 (**Figures 2.6 B** and **Appendix**), which are all located adjacent to consecutive guanosines.

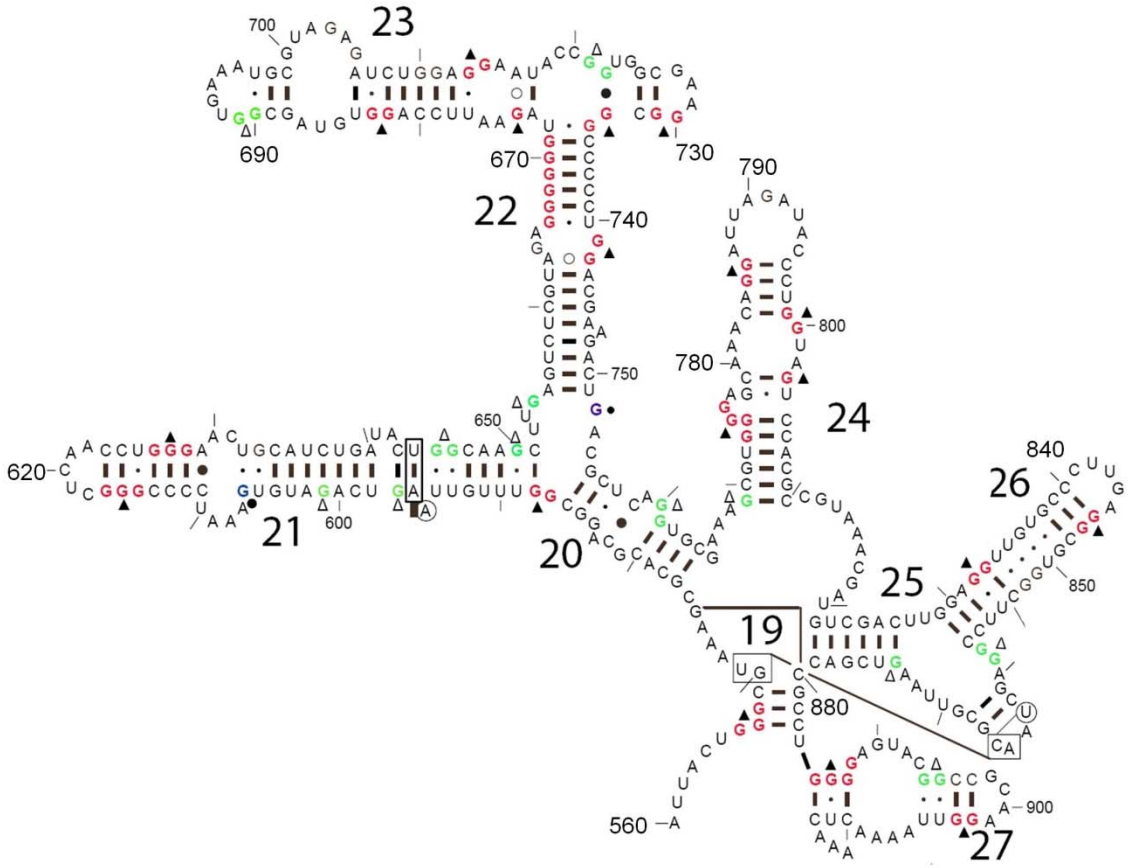

Figure 2.9. The central domain secondary structure map of 16S rRNA with probing results is shown. Strong hits (reactive nucleotides) are colored red (shown with ▲), moderate hits are colored green (shown with ∆), and very weak stops are colored blue(shown with ●). The helix numbers are also indicated.

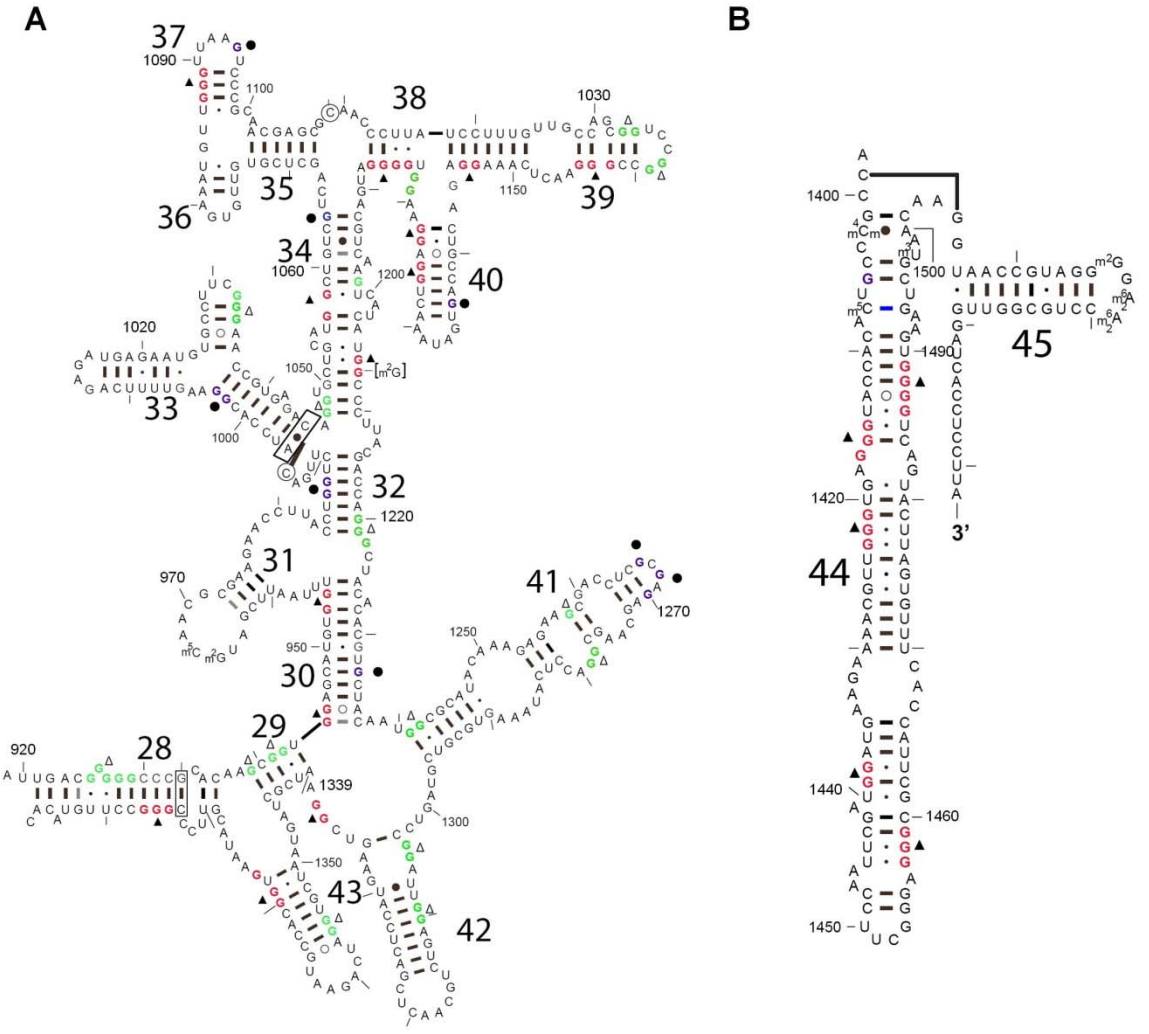

Figure 2.10. The 3' domain secondary structure map of 16S rRNA with probing results is shown. Strong hits (reactive nucleotides) are colored red (shown with ▲), moderate hits are colored green (shown with ∆), and very weak stops are colored blue (shown with o). A) 3' Major and B) 3' minor domains with helix numbers are represented.

2.4.2 Salt dependence binding study

The interaction of charged metal complexes with oligomers is known to be strongly influenced by salt concentration (*218*). The salt dependence of the cisplatin reaction with 16S rRNA under various Na^+ concentrations (10 to 300 mM) was carried out. First, reactivity increased in the presence of 20 mM Na^+, and then further increases of the salt concentration resulted in decreased platination (**Figure 2.11**), which suggests that electrostatic interactions play an important role in cisplatin binding to RNA.

2.4.3 Quantification of the platinum adducts on 16S rRNA

The number of platinum atoms bound per molecule of 16S rRNA was determined by using atomic absorption spectrometry (AAS). Free 16S rRNA and monoaquated cisplatin were reacted at various ratios to determine the total number of possible adducts. After the reaction, excess platinum was removed by ethanol precipitation followed by dialysis for 12 hrs at 4 ºC. The 16S rRNA was then hydrolyzed with NaOH to obtain individual nucleotides. The absorbance of 16S rRNA was measured spectrophotometrically in triplicate by using a NanoDrop UV visible spectrometer and the concentration was calculated by using the extinction coefficient of hydrolyzed 16S rRNA (ε = 17,588,970 M^{-1} cm^{-1}). The concentration of platinum was measured by AAS with a graphite furnace and hollow cathode platinum lamp. At lower reaction ratios, all of the platinum atoms were bound to the 16S rRNA. More specifically, at reaction ratios of 1:50 and 1:100 (16S rRNA:Pt) the number of platinum atoms per rRNA molecule was

52±3 and 101±8, respectively (**Figure 2.12**), suggesting that all Pt complexes reacted with 16S rRNA.

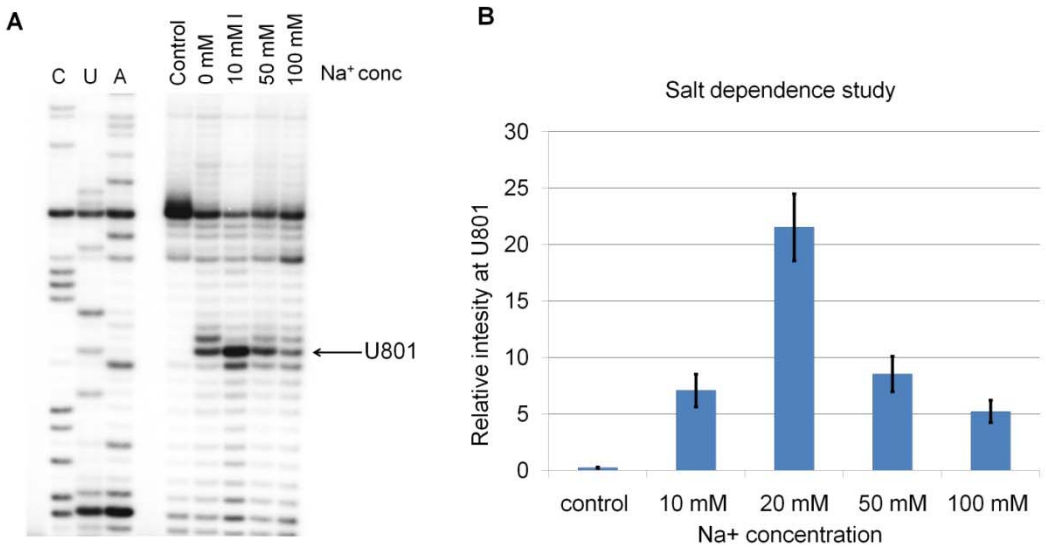

Figure 2.11. An autoradiogram illustrating salt dependence of the cisplatin reaction with 16S rRNA and quantification of the gel is given. A) The autoradiogram shows a strong cisplatin stop site at U801 at various Na^+ concentrations. B) Quantification of the reverse transctiptase stop site at U801 after cisplatin reaction is given. Quantification was performed using ImageQuant software. The gel data were normalized over the entire lane to account for loading differences and then compared at the level of intensity at U801. The relative intensity at U801 was calculated by percentage intensity at U801 with respect to the total intensity of that lane. The data represents an average of two independent experiments.

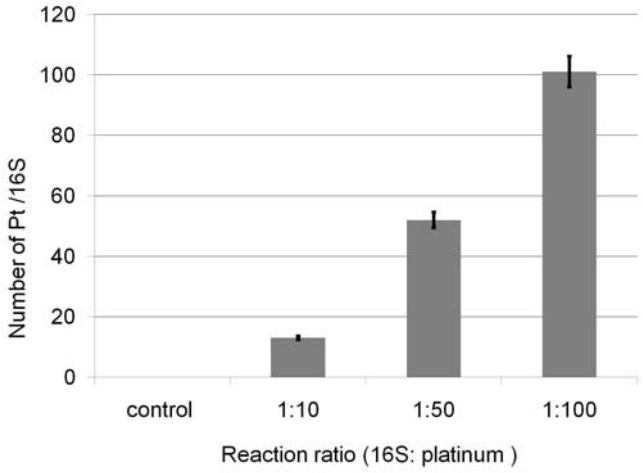

Figure 2.12. The number of platinum atoms bound on each molecule of 16S rRNA at different reaction ratios determined by AAS is shown. The data represents an average of three independent experiments.

2.4.4 Identification of the platinum adducts on 16S rRNA

In DNA, cisplatin forms various types of adducts, such as 1,2-intrastrand and interstrand crosslinks; however, the types of adducts formed with RNA have not been well characterized previously. For this purpose, control 16S rRNA and RNA treated with cisplatin were digested with P1 nuclease and calf intestinal phosphatase (CIP) to generate free nucleosides or possibly dinucleotides. The products were separated and identified by HPLC and high-resolution LC-MS.

In HPLC, four unknown peaks along with four standard nucleoside peaks were observed (**Figure 2.13 A**). The retention times of standard nucleosides were confirmed by injection of standard nucleosides separately. Quantification was carried out by Empower HPLC software and the peak areas were divided by the corresponding extinction coefficients to account for the differences in absorbance at 260 nm. Then, peak ratios were calculated relative to the cytidine peak. Quantification of the nucleosides revealed that free guanosine and adenosine levels decreased with increasing cisplatin concentrations (**Figure 2.13 B** and **C**). To identify other unknown peaks, LC-MS was carried out with an Acquity UPLC system equipped with an HSST3 (2.1 × 100 mm, 1.8 µm) C18 column. The chromatogram and mass of the corresponding peaks are shown in **Figure 2.14.** The observed and calculated masses with retention times are shown in **Table 2.1**. The major peak at retention time 0.96 min is assigned as the bifunctional adduct, GpGPt$(NH_3)_2$, with a molecular mass of 856.14 Da. Similarly, the peak at 1.61 min with mass 840.14 Da corresponds to ApGPt$(NH_3)_2$, and the peak at 1.69 min with mass 795.19 Da is assigned as GGPt$(NH_3)_2$. The peak at

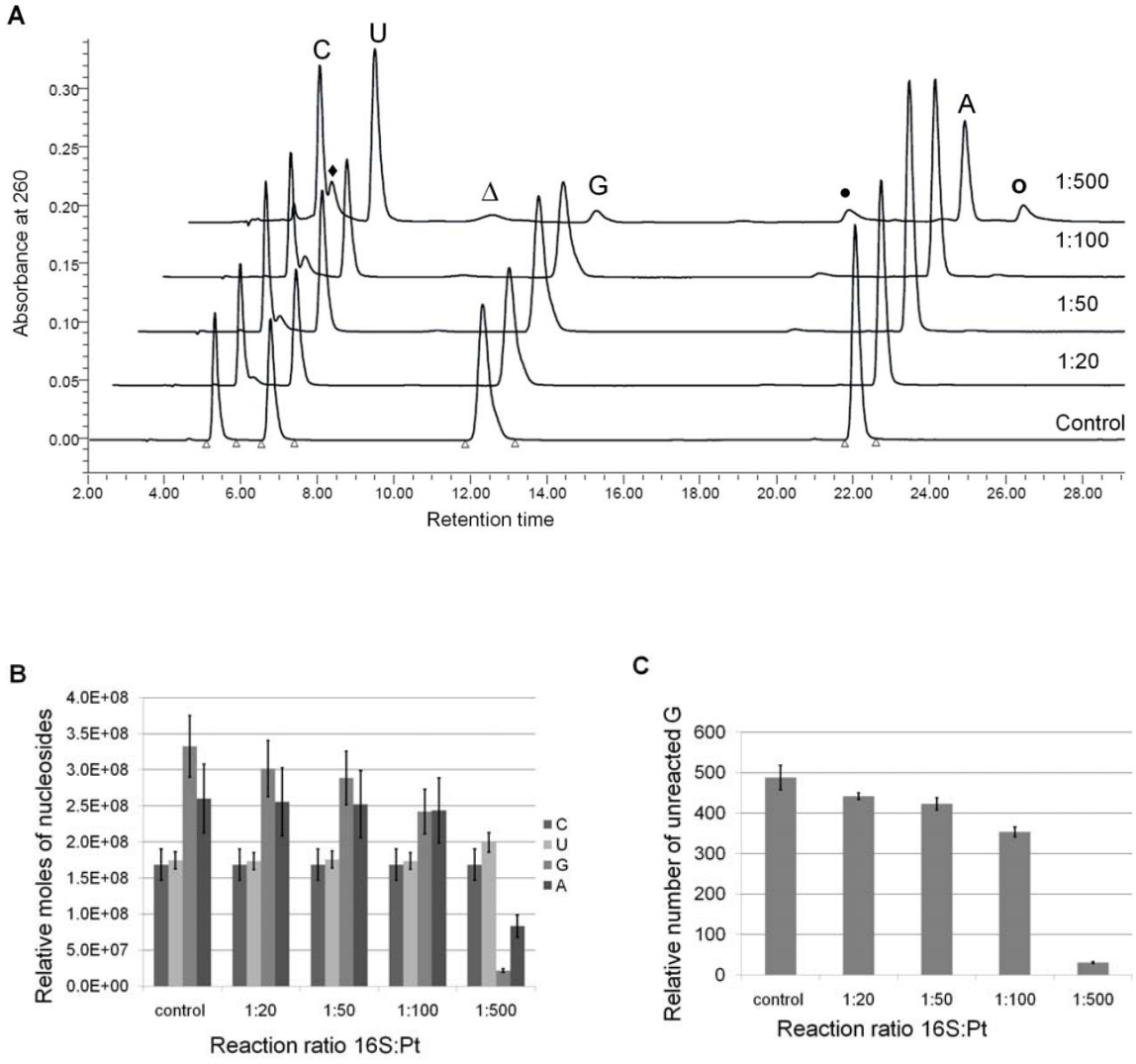

Figure 2.13. HPLC chromatogram and the quantification of digested 16S after reaction with aquated cisplatin are shown. A) An overlay of HPLC chromatograms of control (digested 16S rRNA) and platinated 16S rRNA after digestion is given. New peaks following platination of 16S rRNA are indicated by symbols (♦Δ●o). B) The relative molar concentration of unreacted nucleosides vs. reaction ratios of 16S:cisplatin is plotted. C) The relative number of unreacted guanosines after the reaction in various ratios is shown graphically. The data represents an average of two independent experiments.

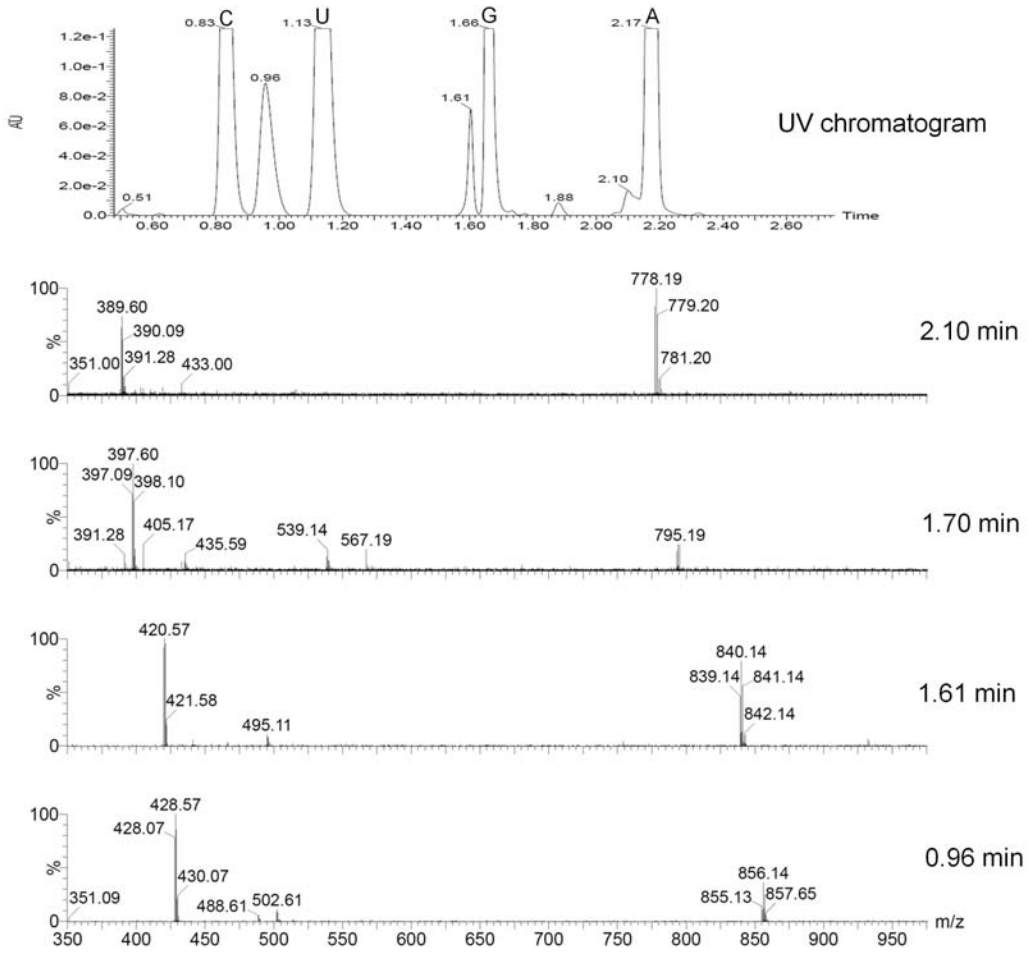

Figure 2.14. LC-MS data of digested 16S rRNA after reaction with cisplatin are shown. The chromatogram with retention times (upper) and mass spectra of the corresponding peaks (lower) are shown.

Table 2.1. Masses, rentention time and % of various adducts of cisplatin with 16S rRNA.

Types of adducts	+1 charged state (Da)		+2 charged state (Da)		Retention time	Relative %
	Calculated	Observed	Calculated	Observed		
GpG[Pt(NH_3)$_2$]	857.13	856.14	428.56	428.57	0.96 min	63 ± 5
ApG or GpA[Pt(NH_3)$_2$]	841.15	840.14	420.57	420.57	1.61 min	20 ± 3
GG[Pt(NH_3)$_2$]	796.20	795.19	398.1	397.60	1.70 min	6 ± 2
AG or GA[Pt(NH_3)$_2$]	780.21	778.19	390.1	389.60	2.10 min	11 ± 2

2.12 min with mass 778.19 Da is assigned as AGPt(NH_3)$_2$. The above assigned adducts are shown in **Figure 2.15**. These results show that cisplatin preferentially reacts with guanosine, forming bifunctional adducts as the major products. The coordination site is presumed to be N7 of the purine, but this has not been confirmed.

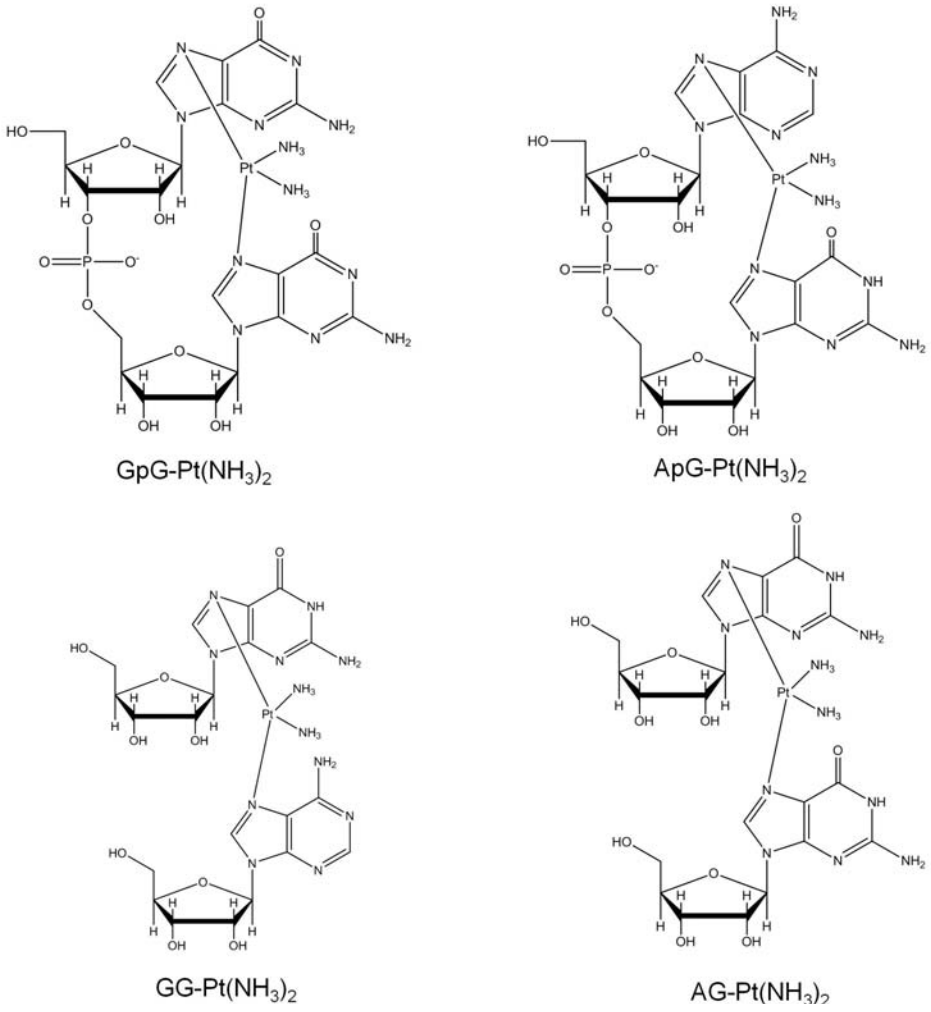

Figure 2.15. Proposed structures of adducts obtained after digestion of 16S rRNA are shown.

2.5 Discussion

Probing data reveal strong and weak stops of reverse transcriptase due to cisplatin cross-links with RNA. Similar to DNA, a majority of the adducts formed

with RNA are observed at consecutive guanosines. On DNA, cisplatin prefers G-rich regions and forms the major bifunctional adducts with purines (*191*). Therefore, it is not surprising that the preference for RNA reactivity is at GG sites. Most of the consecutive Gs that showed strong reactivity with cisplatin contained G-C-rich sequences with a G○U wobble pair. The structural distortion at this base pairing type in RNA might enhance the accessibility for reaction with platinum complex. There are several G-C-rich regions that do not contain G○U pairs or mismatches, and these showed relatively weaker reactivity towards cisplatin. The G○U pair has very important functional roles. For example, in *E. coli* $tRNA^{Ala,}$ it serves as a recognition element for cognate synthetase (*219-220*). In addition, the G○U pair is also important for ribosomal protein recognition (*221*). Thus, the cisplatin complex may reveal preferred sites for protein binding on RNA that have ideal accessibility, electrostatics, and/or structural compatibility. Furthermore, it is possible that such RNA reactivity might be an alternate pathway leading to cisplatin toxicity.

Upon examination of the crystal structure of the bacterial ribosome, the strong and weak cisplatin coordination sites do not display major structural differences. The distances between the N7 position of two consecutive Gs N7 are 3-4 Å when they are stacked (**Figure 2.16**); however, several single guanosines that showed strong reactivity were observed to have their neighboring nucleotide flipped out. This conformational change may provide more space for cisplatin to form monofunctional adducts.

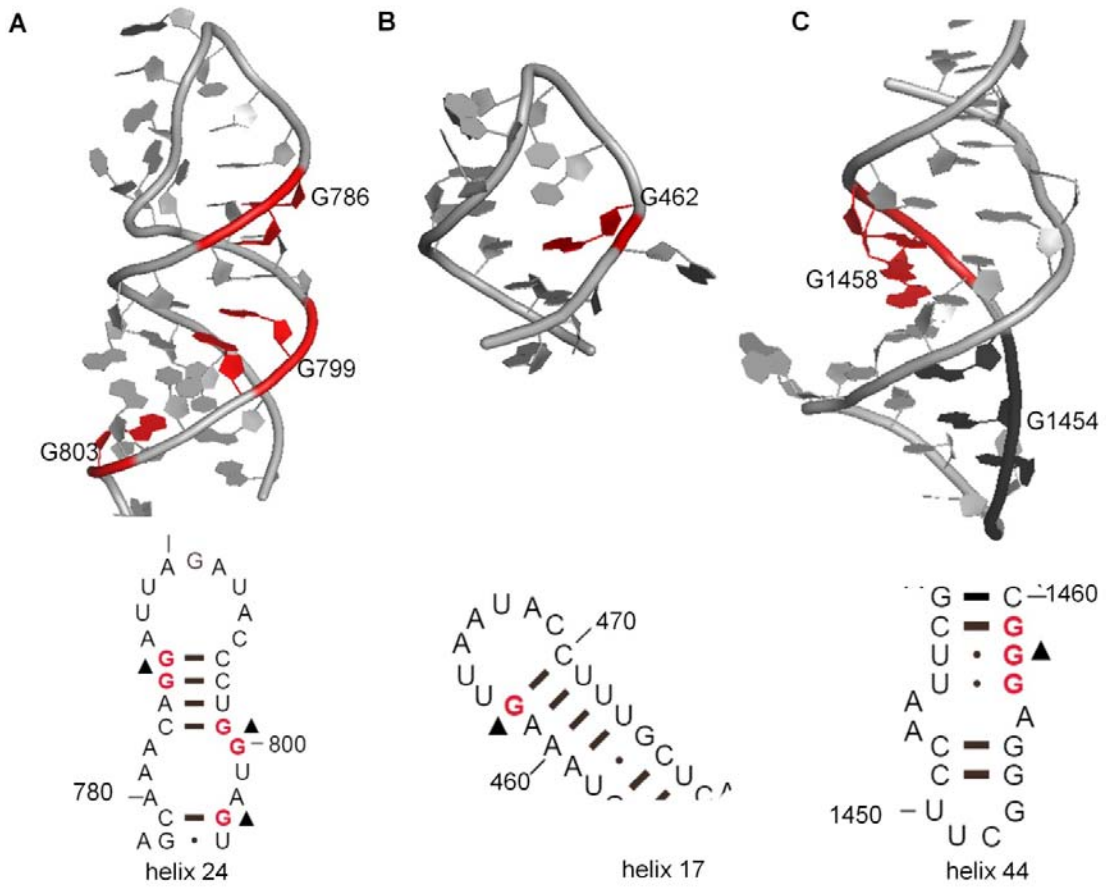

Figure 2.16. Structural features of cisplatin binding sites in 16S rRNA with nucleotide numbering are shown: A) strong binding sites observed in helix 24 with consecutive guanosines; B) strong binding sites observed in helix 17 with single guanosines; C) strong and no hits with consecutive guanosines in helix 44. Secondary structures of the corresponding helices are shown in the lower panel. Nucleotides with strong hits (red) and no hits (black) are represented. This figure is created with Pymol (2AVY) (*222*).

The reactivity of monoaquated platinum species showed differences in reactivity with each of the guanosines in 16S rRNA. This result might be primarily due to the folding and tertiary interactions which change accessibility of the nucleotides within the RNA structure. In addition, RNA may contain preferred ligand-binding pockets that serve as unique recognition sites for small molecules (*223*). The negatively charged phosphodiester groups on the RNA could attract the positively charged platinum complexes, which increases the local

concentration of complex in the RNA environment. Hence, due to preassociation of the complexes, adduct formation at certain sites might be kinetically favored. Similarly, the binding of ligands in the reactive sites might alter the RNA structures, which makes other sites more or less accessible for the reaction.

Cisplatin reactions with RNA can be greatly influenced by cation concentrations and reaction times (*167-168*). Reactivity of cisplatin can be based on oligonucleotide length, electronegativity, target site geometry, as well as secondary and tertiary structures (*197, 224-225*). An increase in cation concentration decreases cisplatin binding due to altered electrostatic interactions (*167*). Hence, it can be expected that larger RNA structures might have charged pockets that are preferable for metal coordination (*226*). The positively charged aquated cisplatin complex is known to associate with nucleic acid surfaces by an electrostatic-driven process prior to formation of the final adduct (*218*). It has been observed that the reactivity of platinum at G-N7 is influenced by the presence of Na^+ concentration. The maximum reactivity was obtained at the middle of an oligonucleotide (17 mer DNA) at 34.5 mM Na^+ concentration (*218*). With the increase in reactivity at the middle of the sequence, the reactivity towards 5' and 3' ends was decreased. Similar results were observed in this work with 16S rRNA, in which reactivity increased at U801 with increasing Na^+, then decreased with higher salt concentrations. In this study, only helix 24 was monitored and changes in reactivity at other sites are not known.

On DNA, adduct formation is more specific (at lower platinum concentrations); however, at higher concentrations adduct formation with

adenosines also increases (*227*). The monoaquated cisplatin derivative readily coordinated with the N7 position of purines to form a monofunctional adduct ($t_{1/2}$ = 0.1 hr) (**Figure 2.17**) (*156, 228-229*). The second chlorido ligand was aquated with a half-life of ~2 hr and finally a bifunctional adduct was formed (*166, 229*). Hence, the monoaquated species used for the reaction can ultimately result in formation of a stable bifunctional adducts.

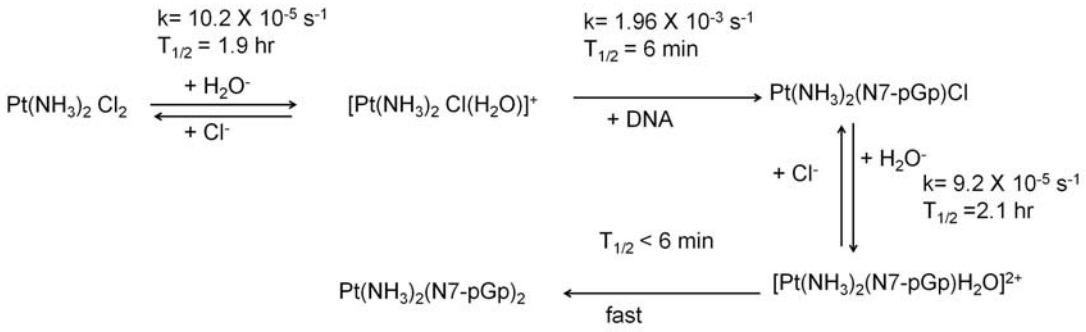

Figure 2.17. Schematic representation of proposed mechanism (*229*) for the binding of cisplatin to double-stranded DNA is shown.

The types of adducts formed with RNA are similar to those found with DNA. The major peak observed in HPLC following cisplatin reaction and rRNA digestion was assigned as a 1,2-intrastrand bifunctional adduct with two neighboring guanosines. The molecular mass corresponding to GpG-$Pt(NH_3)_2$ indicates a product that is not susceptible towards hydrolysis by P1 nuclease at the phosphodiester linkage between adjacent Gs, suggesting protection by the cisplatin coordination. In contrast, the product with a molecular mass corresponding to GG-$Pt(NH_3)_2$ could be either a 1,2-intrastrand, 1,3-intrastrand, or interstrand bifunctional adduct, since these nucleosides were linked by

cisplatin, but not by a phosphodiester bond. Along with these bifunctional adducts, adducts with adenosine and guanosine were also observed (*i.e.,* $AG(PtNH_3)_2$ or $GA(Pt(NH_3)_2)$. The higher reactivity with non-consecutive guanosines and formation of ApG adducts in RNA are unique compared to DNA. This result is likely because of structural difference between RNA and DNA. In RNA, the structure is more diverse and with a large number of unique secondary and tertiary structural motifs, which leads to different reactivity than DNA.

If indeed cisplatin has a kinetic preference for RNA over DNA, then once it enters the cell, it could react with various cellular RNAs, including the ribosome. Previous studies have shown that modification of 16S rRNA by kethoxal greatly affected ribosome assembly (*60*); similar results might be expected with cisplatin. The binding of cisplatin to the spliceosome greatly inhibits its assembly and function (*202*). Several of the functionally important helices such as 18, 24, 28 and 44 showed reactivity with cisplatin. In helix 18, G530 is a universally conserved residue and plays an important role in decoding (*3*). Similarly, helix 24 is present in the subunit interface and has contact with tRNA and initiation factors (*230-231*). Helix 28 and 44 also contain several conserved nucleotides that are involved in decoding (*232*). A number of nucleotides that are universally conserved, such as G530 and G926, showed reactivity with cisplatin. The binding of cisplatin at these functionally important regions could impair its function of protein synthesis.

The repair machinery for the ribosome is largely unknown; hence, the cell may be unable to remove cisplatin adducts from the ribosome. From the

abundance and lifetimes of RNAs, it is suggested that platinum binding may affect RNA function. The transport of cisplatin in the cell and possible intermediate binding with RNA and proteins is still largely unknown. With the increasing number of roles of cellular RNAs that are being identified, detailed binding studies of cisplatin and its effects *in vivo* will determine possible complementary modes of cisplatin action.

CHAPTER 3

Exploring Novel Drug Target Sites in the Ribosome by Using Cisplatin as a Chemical Probe

3.1 Abstract

Knowledge of RNA structure and its relationship to function is fundamental to understanding the biological mechanisms of RNA. Large RNA molecules, such as those in the ribosome, have complex three-dimensional structures. Due to its diverse structure, the ribosome is an ideal target for antibiotics. A number of biophysical and biochemical methods have been utilized to understand its structure-function relationship. In this study, to gain knowledge about small-molecule accessibility on the ribosome, cisplatin has been utilized as a chemical probe. Cisplatin forms stable adducts through coordination to the N7 position of purines and can be detected by primer extension. A number of guanosines in the structurally and functionally important helices are found to be accessible to cisplatin.

3.2 Introduction

The ribosome, the molecular machine for protein synthesis, is a large, folded RNA assembled with proteins (*27, 48, 222*). The folded rRNA can form a number of different secondary and tertiary structural motifs and microenvironments that are solvent accessible (*233*). Due to its structural diversity, solvent accessibility, and general lack of repair enzymes, the bacterial ribosome has been a well-known target of antibiotics (*71, 104*). Various classes of antibiotics such as aminoglycosides and macrolides bind within the ribosome and inhibit protein synthesis (*234-235*). Unfortunately, many strains of bacteria have become resistant to antibiotics, and it is therefore important to design new drugs, as well as explore potential new target sites. Much of the current research is focused on the development of new antibiotics; however, fewer attempts have been made to explore new target sites (*2, 103, 236*).

The first step towards the development of novel therapeutics or target sites is to carry out structure studies. In addition to high-resolution techniques, such as X-ray crystallography and NMR spectroscopy, there are several methods to elucidate the solution structure of nucleic acids, such as chemical or enzymatic probing (*124, 130*). Among these methods, RNA modification or cleavage, induced by a variety of structure-specific enzymes or chemicals, followed by various detection systems, such as reverse transcription or mass spectrometry have been widely used to gain structural information (*108, 129-130*). High-resolution structural analyses of the 70S ribosomes and the 30S subunits have greatly expanded our understanding of the overall folding of the ribosomal RNA when assembled with proteins (*237-238*); however, cooperative interactions

between nucleotides and the formation of charged pockets might occur during the process of ribosome assembly, which have yet to be determined in detail. In addition, RNA structures might differ under various buffer concentrations, temperature, or levels of protein binding.

Several probes have been used to obtain structural information of nucleic acids, but most of them are limited to *in vitro* studies because of their inability to penetrate the cell wall due to their size, structure, and/or charge (*124*). Only a few compounds have been used to probe RNA structure *in vivo,* such as DMS (*152*), kethoxal (*239*), and lead(II) (*240*); however, some of these compounds are toxic to the cell and the detection of their cleavage or reactive sites is also challenging. The various structural features of RNA will be important for biological function *in vivo*. The RNA structures obtained by various *in vitro* methods might be different than the corresponding RNAs present in the complex environment found in living cells; thus, methods to compare the *in vitro* and *in vivo* structures would be useful.

Recent crystal structures have revealed a number of antibiotic binding sites in the ribosome, and it is interesting to know that many of these sites are overlapping (*117*). Now, it is important to develop novel target sites to design new drugs that can help to overcome the ever-growing problem of resistance. In this context, a chemical probe able to work both *in vitro* and *in vivo* can be utilized to explore structure accessibility in RNA. The accessible sites of the RNA can be compared with their functional importance, which might be useful to develop as a new drug target sites. Previously, we have shown that cisplatin can

be used to probe larger RNA structure, the ribosome, *in vitro* and *in vivo (204)*. Cisplatin has several advantages, such as the formation of stable adducts and an easy detection system. Further extended studies to map the accessible regions in the 30S subunits and the 70S ribosomes with cisplatin *in vitro* and *in vivo* were carried out.

3.3 Materials and Methods

3.3.1 Chemicals, solutions, and DNA

[5'-^{32}P-γ]ATP was purchased from Perkin-Elmer Life Sciences, Inc. and T4 polynucleotide kinase was obtained from New England Biolabs. A reverse transcriptase kit (Improm_II^{TM} Reverse Transcriptase) was purchased from Promega. The remaining chemicals for buffers and reagents were obtained from Sigma Chemicals or Fisher. RNase-free, distilled, deionized water (ddH_2O) was used for all experiments.

Cisplatin, *cis*-diamminedichloridoplatinum(II), was purchased from Alfa Aesar. The complexes *cis*-$[PtCl(NH_3)_2X]^{+/0}$ or *cis*-$[Pt(NH_3)_2X_2]^{2+/0}$, in which X was H_2O, DMF, or NO_3^-, were prepared as described in Chapter 2. Platinum-DMF complex stock solutions were stored at -20 °C for up to 1 week and diluted as required just prior to use.

Single-stranded DNA primers that were used to probe the free 16S rRNA were also used to probe the 30S subunits and the 70S ribosomes. Purification of primers was carried out as described in Chapter 2. Sequences of the DNA primers were named according to the beginning position of the transcribed nucleotides, and are same as those in Chapter 2.

3.3.2 Isolation of the 30S subunits and the 70S ribosomes

The 70S ribosomes and 30S subunits were isolated from *E. coli* MRE600 strain by the sucrose gradient method (*145, 241*) as described in Chapter 2.

3.3.3 Platination reactions

The platination reactions with the 30S subunits and the 70S ribosomes were performed with monoaquated cisplatin. Prior to platination, the 30S subunits and the 70S ribosomes, were activated by incubating in ribosome buffer (20 mM HEPES, pH 7.2, 50 mM KCl, and 10 mM $MgCl_2$) at 40 ºC for 30 min (*241*). Platination was carried out in 20 mM HEPES, pH 6.5, 20 mM potassium acetate, and 10 mM $MgSO_4$ (buffer H). The 30S subunits and the 70S ribosomes were incubated at 37 °C with aquated complex in 1:150 and 1:75 ratios of metal complex to nucleotides. After the reactions, samples were quenched with NaCl by raising the concentration to 200 mM, followed by immediate freezing.

3.3.4 Primer extension

Samples for primer extension were prepared by three times extraction with an equal volume of phenol (phenol:chloroform:isoamyl alcohol; 25:24:1) followed by two times with chloroform in the presence of 6 mM EDTA. Finally, samples were ethanol precipitated with 0.1 volumes of 3.0 M sodium acetate, pH 5.3, and 2.5 volumes of ethanol. Samples were dried in a speed vacuum and dissolved in ddH_2O. The concentrations were measured spectrophotometrically at 260 nm using a Nano Drop spectrometer in triplicate. For primer extension, 1 µg

equivalent of 16S rRNA was used. Primer labeling and primer extension was carried out as described in Chapter 2.

3.3.5 *In vivo* probing

E. coli cells MRE600 were streaked from a glycerol storage culture on Luria–Bertani (LB) agar and incubated at 37 °C overnight. A single colony was picked to inoculate a starter culture, which was grown at 37 °C overnight. The starter culture was used to seed 3 ml medium (1/100–1/250 dilution), which was grown with shaking to 0.2–0.3 OD_{600}. Cisplatin dissolved in DMSO was added to 0 to 200 µg/ ml and the cells were further incubated in a shaker at 37 °C for 2 hrs to an OD_{600} of 0.6 to 0.8. Cells were then chilled on an ice bath for 30 min and harvested in pre-chilled 15 ml tubes at 5,000 r.p.m. for 10 min at 4 °C. Cells pellet were washed 3 times with buffer A (50 mM Tris•HCl, pH 7.5 and 10 mM $MgCl_2$ and 100 mM NH_4Cl) and resuspended in 100 µl buffer A. Cell lysis was carried out with lysozyme (0.1 mg/ml) by freezing and thawing (*242*), and then 1 unit of RNase-free DNase I (Promega) was added, and the mixture was incubated in ice for 15 min. The cell lysate was centrifuged at 5,000 r.p.m. for 10 min at 4 °C. The supernatant was transferred to a new tube and extracted with an equal volume of phenol:chloroform:isoamyl alcohol (25:24:1).The aqueous phase was separated by centrifugation at 12,000 r.p.m. for 15 min at 4 °C and was extracted one more time with phenol:chloroform:isoamyl alcohol followed by 3 times extraction with chloroform to remove all proteins. RNA was precipitated from the final aqueous phase with 3 M sodium acetate (pH 5.3) and 2.5 volumes of ethanol. The RNA was collected by centrifugation for 15 min at 12,000 g (4

°C), washed with 70% ethanol and resuspended in 20 µl RNase-free water. The RNA (2 µl) was analyzed on a 1.0% agarose gel prepared in 50 mM Tris–acetate and 1 mM EDTA. Primer extension was carried out as described for the *in vitro* method after isolation of RNA.

3.4 Results

3.4.1 Probing the 30S subunits and the 70S ribosomes *in vitro*

The 30S subunits and the 70S ribosomes were isolated from *E. coli* MRE 600 by the sucrose gradient method (*145*). The platination reaction was carried out similar to that with free 16S rRNA, as described in Chapter 2. Concentrations of the 30S subunits (1 A_{260} unit is equivalent to 69 pmol) and the 70S ribosomes (1 A_{260} unit is equivalent to 23 pmol) (*241, 243*) were determined spectrophotometrically. The reaction was carried out in 1:75 and 1:150 ratios of monoaquated species to nucleotides. Before the reaction, both the 30S subunits and the 70S ribosomes were activated by incubating in ribosome buffer at 42 ºC for 30 min. The reaction with monoaquated metal complex was carried out at 37 ºC for 5 hours and quenched with NaCl, followed by freezing. Samples for the primer extension were prepared by removing proteins with phenol-chloroform extraction followed by ethanol precipitation.

Primer extension was carried out as described in Chapter 2 with free 16S rRNA. The same primers that were used for free 16S rRNA was used to map the cisplatin coordination sites on 16S rRNA of the 30S subunits and the 70S ribosomes. Cisplatin coordination sites were then determined by pauses or stops of reverse transcriptase compare to a corresponding control in the same

gel. Bands on the gel arising due to nicks in the RNA or strong secondary structures were distinguished from the cisplatin binding sites by comparing with a control treated in a similar manner, but lacking aquated complex. The magnitudes of the reactivity were classified based by the intensities of the bands on the autoradiograms. Representative autoradiograms of the cisplatin probing experiments with the 30S subunit and the 70S ribosomes are shown in **Figures 3.1** to **3.3**. Additional gels are shown in the Appendix. The gels were quantified by using 'Image Quant' software as described in Chapter 2. Similar to the free 16S, the intensities of bands could be measured up to approximately 100 nucleotides from the transcription start site. The reactive nucleotides were mostly found to be consecutive Gs, predominantly near mismatches or loop regions. Since cisplatin was known to prefer Gs in the DNA targets, it was not surprising that the major hits on the 16S rRNA from the 30S subunits, as well as 70S ribosomes, were also consecutive Gs. Out of 103 sites with consecutive Gs (two or more Gs present are counted as one site), strong reactivity was observed in 38 sites, and 36 were moderate hits. In addition, several nonconsecutive Gs also showed strong or moderate reactivity. The overall results of cisplatin binding to 16S rRNA in the 30S subunits and the 70S ribosomes are shown in **Figure 3.4** on a secondary structure model of 16S rRNA with reactive sites in red (strong hits) and green (moderate hits).

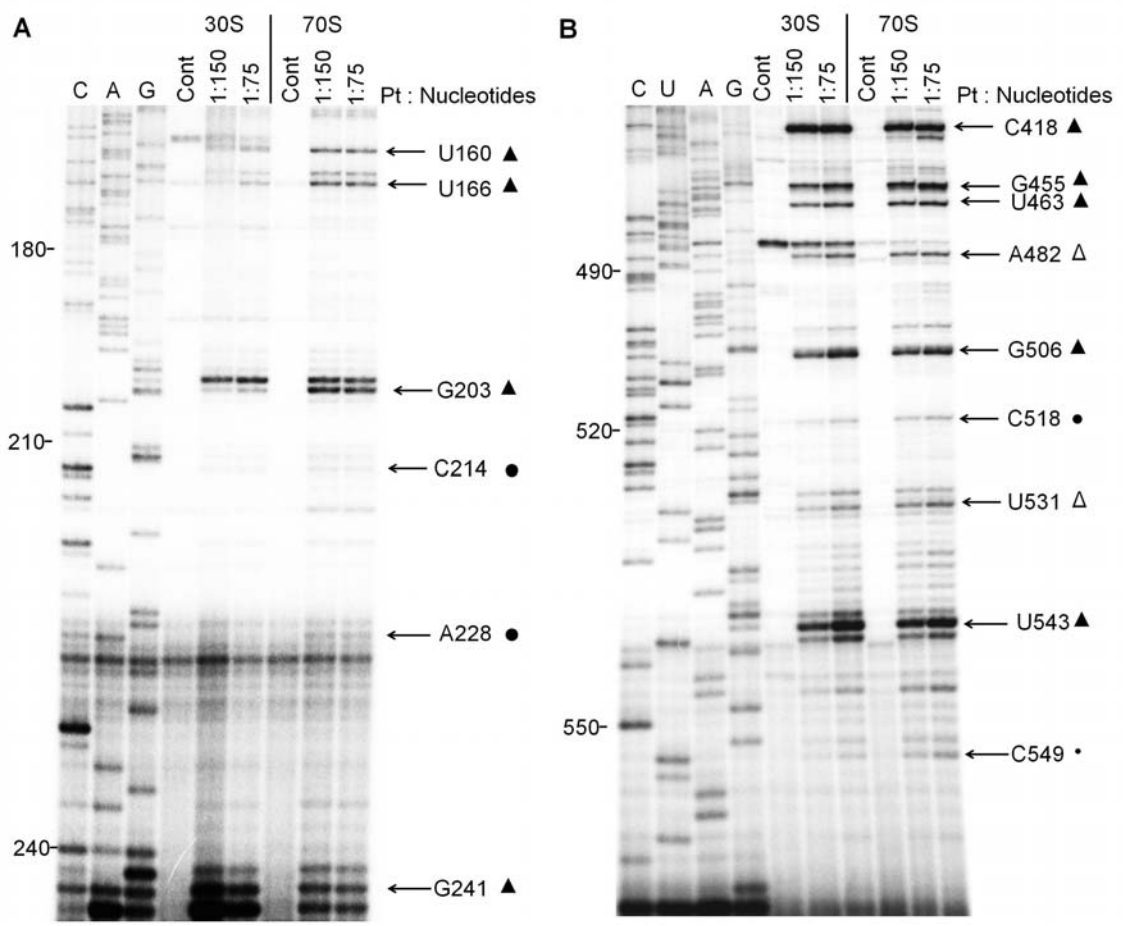

Figure 3.1. Probing results of 16S rRNA of the 30S subunits and the 70S ribosomes at the 5' domain with primers 245 and 561 are shown. (A) The autoradiogram shows the reverse transcriptase pauses or stops by using primer 245. (B) The autoradiogram shows the reverse transcriptase pauses or stops by using primer 561. In both gels, C, U, A, G represent the sequencing lanes, 0 represents the control, and other lanes are 30S subunits and 70S ribosomes treated with increasing concentrations of monoaquated cisplatin (cisplatin:nucleotide is 1:150 and 1:75). The strong and moderate hits are indicated with arrows and corresponding nucleotides numbers (▲ (strong hits), Δ (moderate hits), and ● (minor hits)).

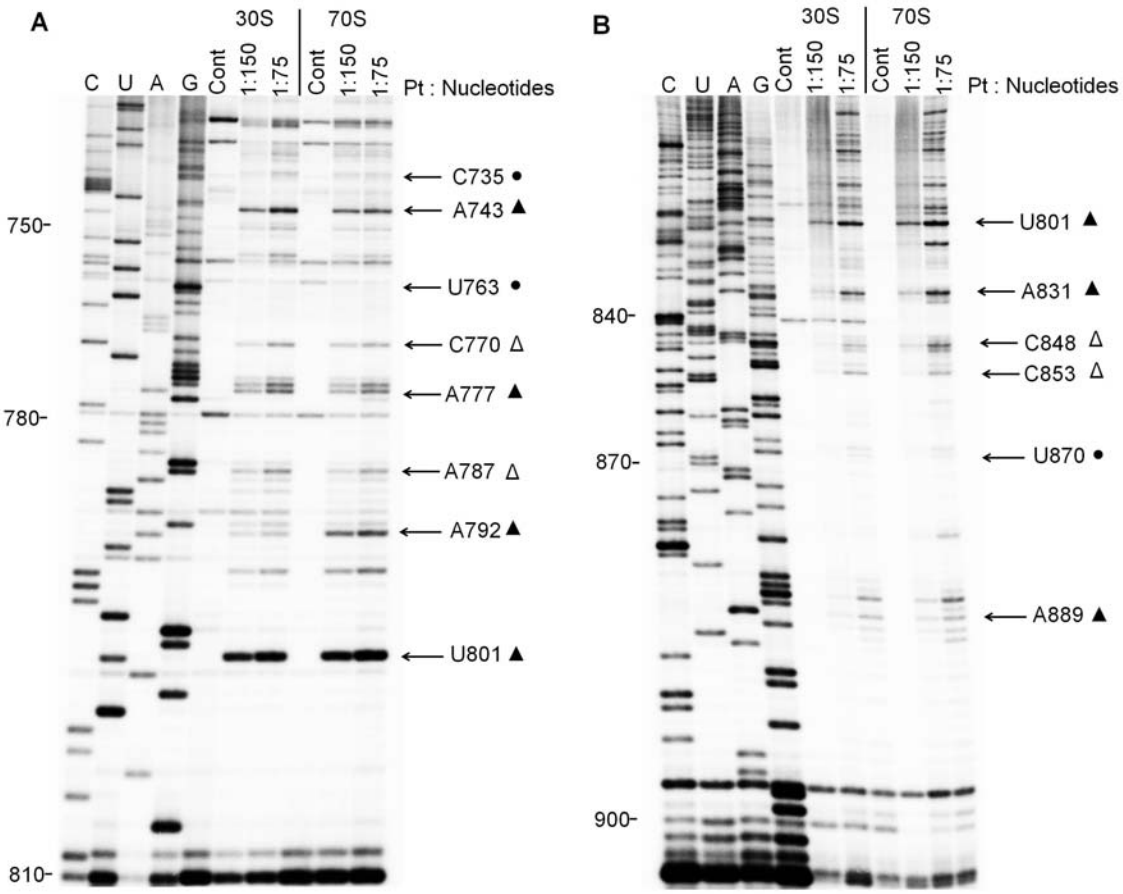

Figure 3.2. Probing results of 16S rRNA of the 30S subunits and the 70S ribosomes at the central domain with primers 831 and 906 are shown. (A) The autoradiogram shows the reverse transcriptase pauses or stops by using primer 831. (B) The autoradiogram shows the reverse transcriptase pauses or stops by using primer 906. In both gels, C, U, A, G represent the sequencing lanes, 0 represents the control, and other lanes are 30S subunits and 70S ribosomes treated with increasing concentrations of monoaquated cisplatin (cisplatin:nucleotide is 1:150 and 1:75). The strong and moderate hits are indicated with arrows and corresponding nucleotides numbers (▲ (strong hits), Δ (moderate hits), and • (minor hits)).

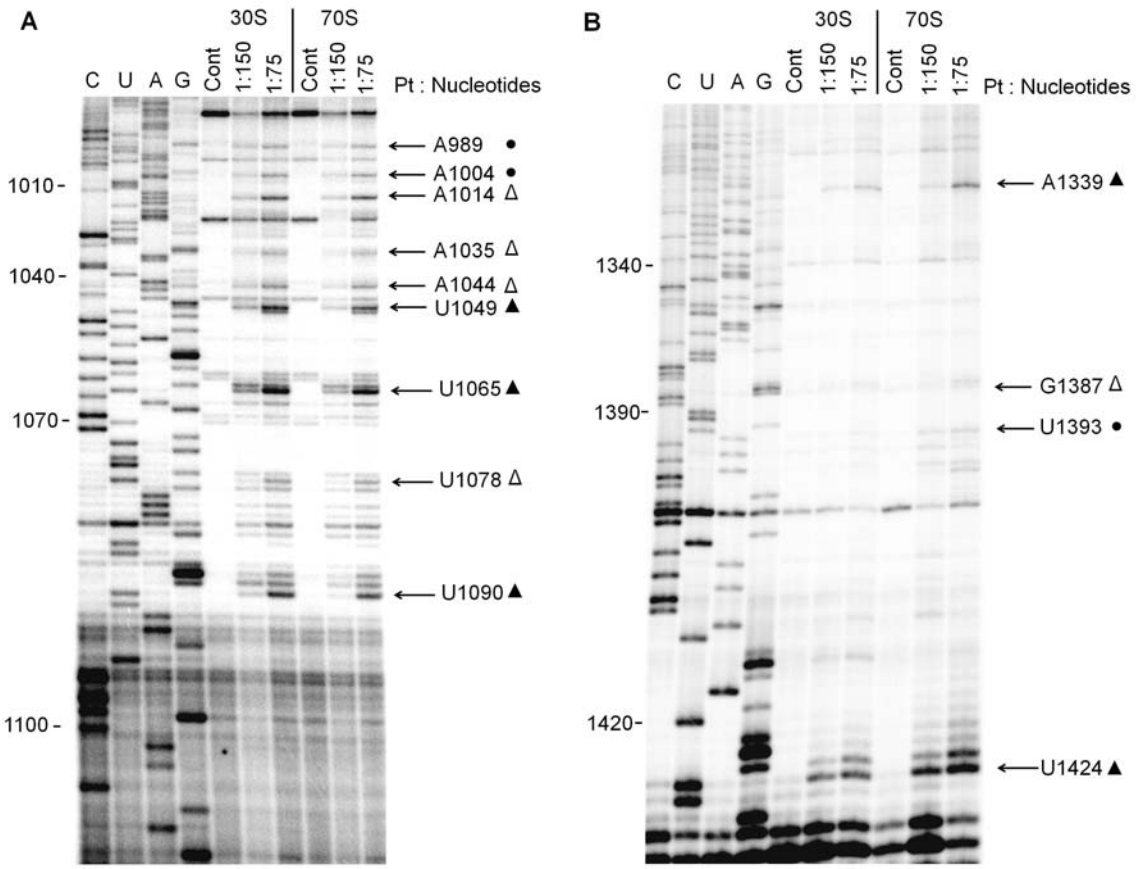

Figure 3.3. Probing results of 16S rRNA of the 30S subunits and the 70S ribosomes at the 3' domain with primers 1110 and 1435 are shown. (A) The autoradiogram shows the reverse transcriptase pauses or stops by using primer 1110. (B) The autoradiogram shows the reverse transcriptase pauses or stops by using primer 1435. In both gels, C, U, A, G represent the sequencing lanes, 0 represents the control, and other lanes are 30S subunits and 70S ribosomes treated with increasing concentrations of monoaquated cisplatin (cisplatin:nucleotide is 1:150 and 1:75). The strong and moderate hits are indicated with arrows and corresponding nucleotides numbers (▲ (strong hits), Δ (moderate hits), and • (minor hits)).

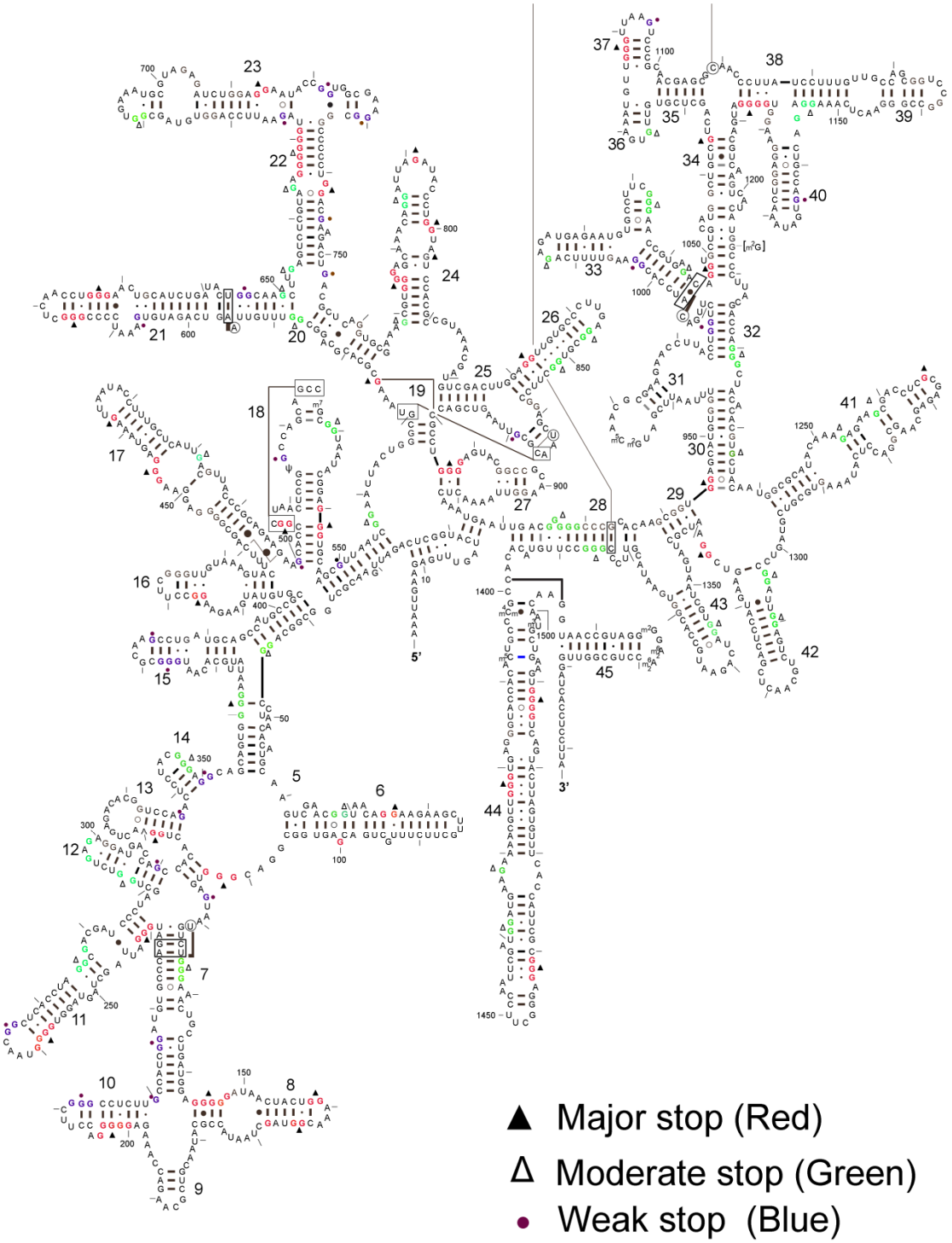

Figure 3.4. Secondary structure map of 16S rRNA (*244*) with probing results from the 30S subunits and the 70S ribosomes is shown. Strong hits (reactive nucleotides) are colored red (shown with▲), moderate hits are colored green (shown with Δ), and weak hits are colored blue (shown with •). The helix numbers are also indicated (1 to 45).

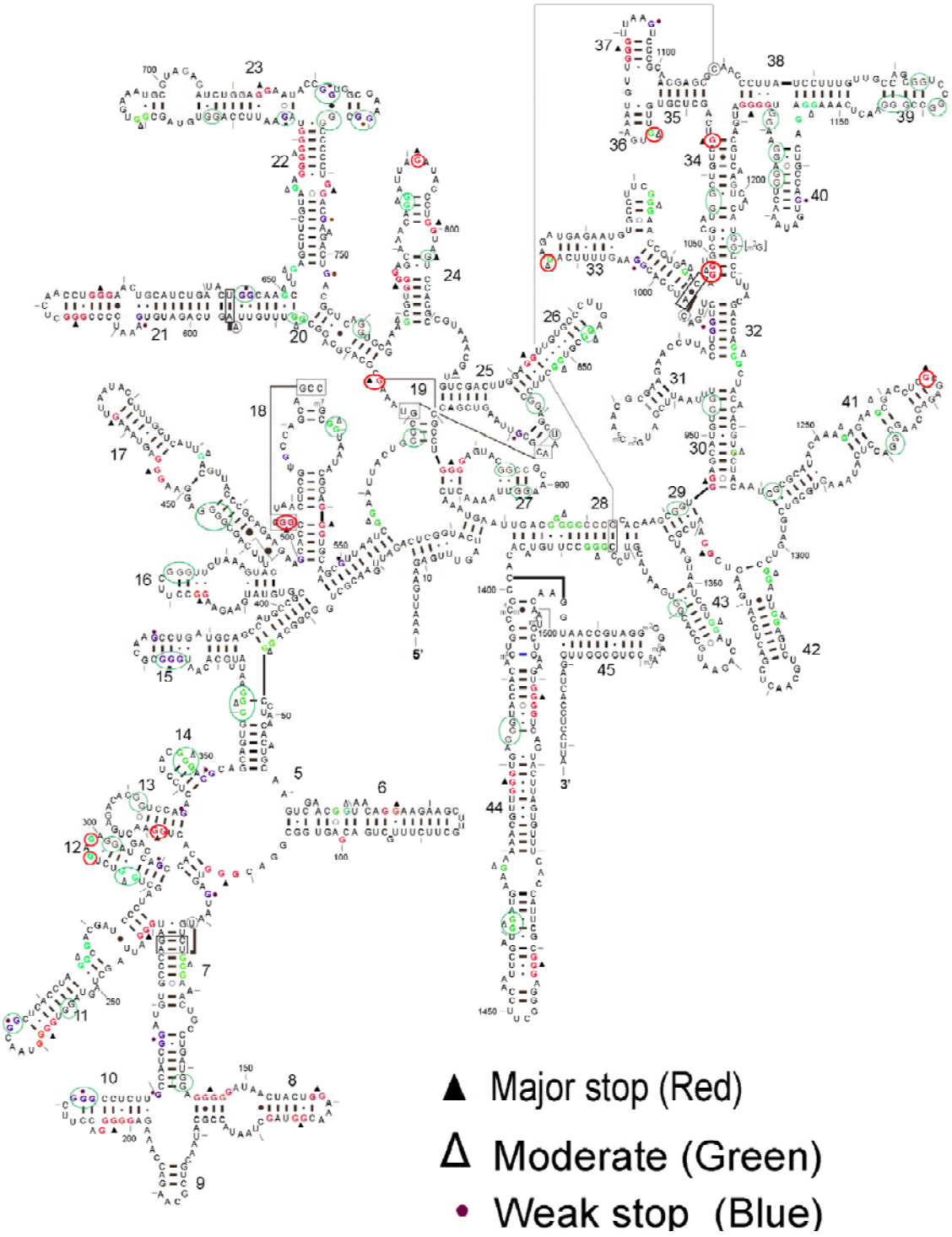

Figure 3.5. Secondary structure map of 16S rRNA (*244*) with probing results from the 30S subunits and the 70S ribosomes is shown. Strong hits (reactive nucleotides) are colored red (shown with▲), moderate hits are colored green (shown with Δ), and very weak hits are colored blue (shown with •). Nucleotides with lower reactivity in 30S/70S compared to free 16S rRNA are indicated with green circles and with higher reactivity with red circles. The helix numbers are also indicated (1 to 45).

The 5' domain of 16S rRNA (nucleotides 1-566), which includes helices 1 to 18, is the main body of the 30S subunit. This domain is mainly stabilized by RNA-RNA interactions (*115, 222*). Culver and coworkers found that modification of five nucleotides (G301, G302, G529, G530, and G558) in this domain of the ribosome were critical for the ribosome assembly (*1*). Previously, Moazed and Noller have shown that, upon A-site tRNA binding, G529 and G530 were strongly protected (*3*). Furthermore, Mankin and coworkers showed that mutations of several nucleotides in helix 18 were deleterious, including G529 and G530 (*2*). In cisplatin probing, moderate stops were observed before these consecutive Gs in the 30S subunits and the 70S ribosomes (**Figure 3.1 B**). Furthermore, G529 and G530 reacted strongly in free 16S, but were more protected in 30S/70S. Many of the sites in 5' domain of 16S rRNA were less reactive within the context of ribosomes. The significance of the result is that critical residues that are protected are also functionally important; therefore targeting of these sites might be feasible.

Mutation of G299A (helix 12) was found to increase both missense and nonsense errors during translation (*4*). Structure studies showed that in helix 12, G299 forms a Hoogsteen pair with G566 in helix 19, and the pair was found to involve Mg^{+2} coordination (*245*). This functionally important nucleotide G299 also showed a moderate reactivity with cisplatin, in which a reactivity difference was observed between free 16S and 30S/70S. In addition to these sites, a number of prominent stops were observed at G147, A160, U166, G201, G260, and G319 (**Figures 3.1 A** and **3.6**). All of these stops are on the 3' side of consecutive Gs.

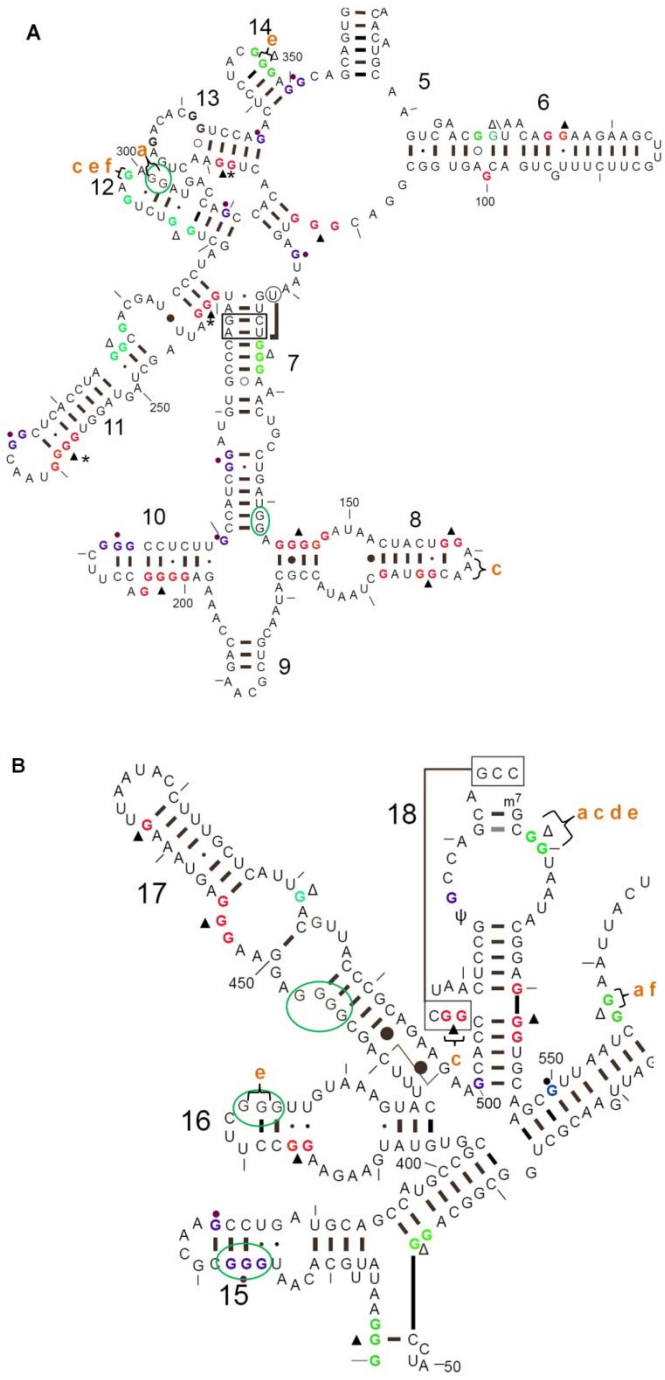

Figure 3.6. Secondary structure map at the 5' domain of 16S rRNA with probing results from the 30S subunits and the 70S ribosomes is shown. Strong hits (reactive nucleotides) are colored red (shown with ▲), moderate hits are colored green (shown with Δ), and very weak hits are colored blue (shown with ●). A) The lower part of the 5' domain and B) the upper part of the 5' domain with probing results are given. Green circles represent nucleotides that showed strong hits on the free 16S rRNA, but are absent or very weak in the 30S subunits and the 70S ribosomes. The (*) indicates the difference in reactivity between 30S subunits and 70S ribosomes.

In the upper part of the 5' domain, strong stops were observed at C418, G454, U462, C507, and U543 (**Figure 3.1 B**). Among these strong stops, all were before consecutive guanosines, except for U463, which is on the 3' side of a single guanosine. In addition to these, several other consecutive and single guanosines showed moderate to weak stops in this region (**Figure 3.6**).

A majority of the nucleotides that showed reactivity with cisplatin in free 16S rRNA also showed reactivity in the 30S subunits and the 70S ribosomes. However, numerous differences in reactivity were also observed, such as the strong stop observed at U426 in free 16S rRNA, which is not present in the 30S subunits and the 70S ribosomes. Helix 16 forms a contact with protein S4, which might protect these nucleotides from cisplatin reaction in the 30S subunits and the 70S ribosomes (*246*). In addition, the reactive nucleotides (G416-417) contain a G○U pair compared to unreactive G-C pairs (G423-425); this cisplatin binding preference was observed on the free 16S rRNA as well. Similarly, a moderate hit at G446 was observed in 16S rRNA, but is not present in 30S or 70S ribosome. In contrast, the stop at C507 is comparatively stronger in the 30S subunits and the 70S ribosomes (**Figures 3.1** and **3.6**). Helix 18 was shown previously to be dynamic in nature and several of its nucleotides are in contact with ribosomal protein S12 (*246*). Hence, in the 30S subunit and the 70S ribosome, the conformation and accessibility of nucleotides might be different than the naked 16S rRNA, which results in different reactivity with cisplatin.

The central domain of 16S rRNA (nucleotides 567-915), which includes helices 19 to 27, folds to form the platform of the small subunit (*115*). Culver and

coworkers found six nucleotides in this region that are functionally important, and assembly was impaired when they were modified (*1*). Out of these six nucleotides, three are guanosines; G575, G791, and G818. Mankin and coworkers found clustering of moderately deleterious mutations in helix 24, and Cunningham and coworkers observed that none of the functional mutants in the 790 loop of helix 24 involved G791 or U793 (*2, 247*). In addition, G791 is located on the functionally important 790 loop, which makes contact with initiation factor (IF3) and the P-site tRNA (*248-249*). In cisplatin probing, G575 in the 30S subunits and the 70S ribosomes showed strong reactivity. In contrast, G791 in the 30S subunit was a weak hit, but in the 70S ribosomes was a strong hit (**Figures 3.2 A** and **3.7**), indicating that cisplatin reactivity is different in the 30S subunits and the 70S ribosomes.

Several other strong cisplatin hits were observed on the 3' side of G799-800, G773-776, and G741-742 (**Figure 3.2 A** and **B**). All of these consecutive Gs showed strong reactivity with the naked 16S rRNA, the 30S subunits and the 70S ribosomes. However, compared to the free 16S rRNA, reactivity at G799-G800 is stronger in the 30S subunits and the 70S ribosomes. G803 showed reactivity only in the naked 16S rRNA. Previously, G791 was found to be protected from kethoxal modification; however, this residue becomes more accessible when 30S subunits were converted from the active to inactive conformation (*144*).

Similarly, in helices 22 and 23, several nucleotides showed differences in reactivity, such as G721-722, G730-731, and G733-734, which were not reactive in the 30S subunits and the 70S ribosomes but were in free 16S rRNA.

Previously, protection of G733, G734, and the 720 to 730 regions from kethoxal reactions has been observed due to S15 binding (*145, 250*), which is consistent these cisplatin probing results in which reactivity was reduced from free 16S rRNA to ribosome.

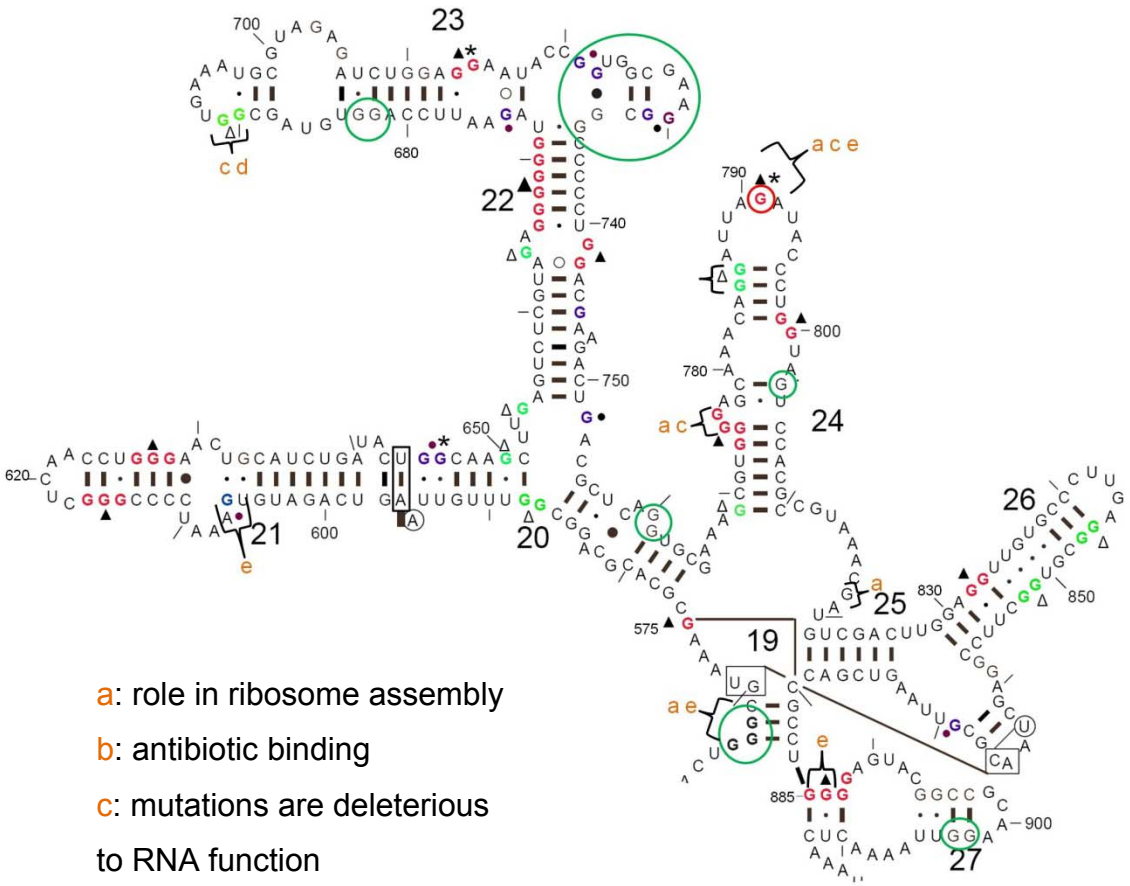

Figure 3.7. Secondary structure map at the central domain of 16S rRNA with probing results from the 30S subunits and the 70S ribosomes is shown. Strong hits (reactive nucleotides) are colored red (shown with ▲), moderate hits are colored green (shown with ∆), and weak hits are colored blue (shown with ●). Red circles represent strong reactivity in the 70S ribosome compared to 30S and free 16S and green circles represent nucleotides that showed strong hits on the free 16S rRNA but are absent or weak in the 30S/70S ribosomes. The (*) indicates the difference in reactivity between 30S subunits and 70S ribosomes.

The 3' region of 16S rRNA, contains the 3' major (nucleotides 916-1396) and 3' minor (nucleotides 1397-1542) domains. The 3' major domain includes helices 28 to 43, and mainly constitutes the head of the small subunit, whereas the 3' minor domain extends from the body to head of the 30S subunit, which includes helices 44 and 45 (*115*). Modifications of 30 nucleotides in the 3' major domain were found to affect ribosome assembly (*1*). Mutational studies showed a cluster of deleterious mutations in helices 34 to 37, which are located far from the known functional centers (*2*). G1058A and G1068A lead to a strong deleterious phenotype. In cisplatin probing, the consecutive Gs, G1057-G1058, showed strong reactivity only in free 16S rRNA, whereas in 30S subunits and 70S ribosomes, a strong stop appeared just before a single guanosine G1064 (**Figure 3.3 A** and **3.8**). In crystal structures of the ribosome, these consecutive Gs (G1057-1058) are in contact with ribosomal protein S3, which might protect them from cisplatin reactivity in 30S/70S ribosomes (*246*). Some other strong cisplatin stops were observed at G1185, C1267, and A1339. All of these stops are on the 3' side of either single or consecutive guanosines.

Modifications of 13 nucleotides on the 3’ minor domain were found to disrupt the assembly of the small subunit,t and a number of deleterious mutations were also located in this domain (*1-2*). However, due to limitations of cisplatin reactivity with guanosines, the accessibility of most of these functionally important nucleotides could not be monitored. The strong and moderate stops observed with cisplatin were at U1424, U1440, C1460, and U1490, which are all on the 3' side of the consecutive Gs (**Figure 3.3 B**). Due to the lack of

appropriate primer hybridization sites, a number of guanosines in the helix 45 also could not be probed.

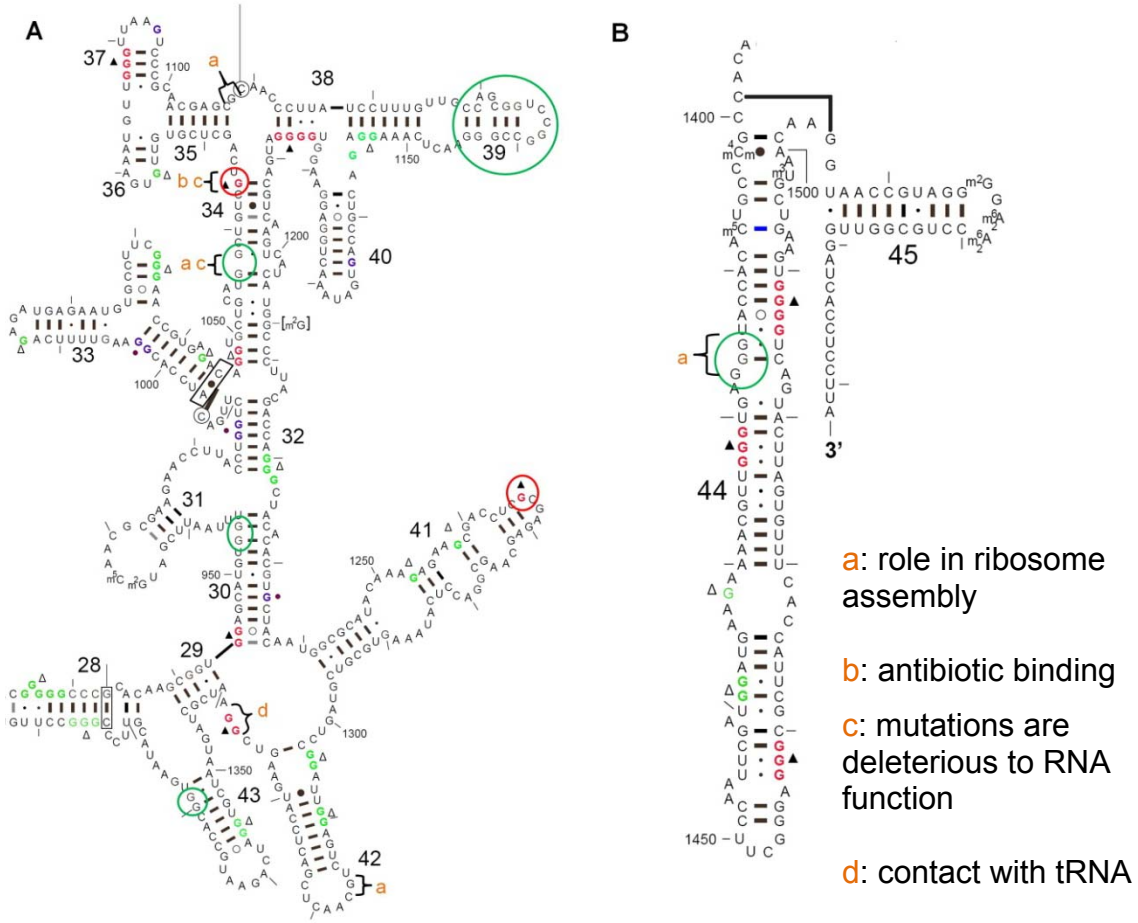

Figure 3.8. Secondary structure map at the 3' domain of 16S rRNA with probing results from the 30S subunits and the 70S ribosomes is shown. Strong hits (reactive nucleotides) are colored red (shown with▲), moderate hits are colored green (shown with Δ), and very weak hits are colored blue (shown with ●). A) The 3' major domain, and B) the 3' minor domain are shown. Red circles represent strong reactivity in the 70S ribosome compared to 30S and free 16S and green circles represent nucleotides that showed strong hits on the free 16S rRNA but are absent or weak in the 30S/70S ribosomes. The (*) indicates the difference in reactivity between 30S subunits and 70S ribosomes.

3.4.2 *In vivo* probing

Cisplatin is believed to enter cells by passive diffusion and undergoes hydration to form the aquated species due to low chloride concentration inside the cell (*163*). Therefore, it is hypothesized that cisplatin can be used to probe the bacterial ribosome *in vivo*. Cisplatin coordination sites can be mapped in a manner similar to *in vitro* studies by using reverse transcription. This type of probing could reveal new target sites for antibacterials on the ribosome. To probe the ribosome *in vivo* using cisplatin, *E.coli* DH5α was grown to ~ 0.2 to 0.3 OD_{600}, 100 to 200 µg/ml of cisplatin was added, and the cells were further incubated for two hours. After cooling on ice for 15 min, the cells were pelleted by centrifugation. The cells were washed three times with buffer (50 mM Tris·HCl, 100 mM NH_4Cl and 10 mM $MgCl_2$) and total RNA was isolated. To carry out the primer extension analysis, total RNA was isolated by phenol-chloroform extraction followed by ethanol precipitation. A primer complementary to positions 831 through 814 of 16S rRNA, as used for *in vitro* probing, was annealed, and then reverse transcription was carried out.

Primer extension of 16S rRNA showed a prominent stop at U801, one nucleotide prior to the consecutive guanines G799 and G800 (**Figure 3.9**). This result is consistent with the strong stop observed with *in vitro* probing. Along with this, a minor stop also appeared before G791, which was seen only in the 70S ribosomes. This result demonstrates that cisplatin can be used to probe accessible guanosine residues *in vitro* and *in vivo*. Furthermore, the differences in nucleotide accessibility in free 16S rRNA vs. that in the ribosomes can be determined. It should be noted, however, that the *in vivo* results shown here

represent an average of all the ribosomes at various stages of protein synthesis in the cell.

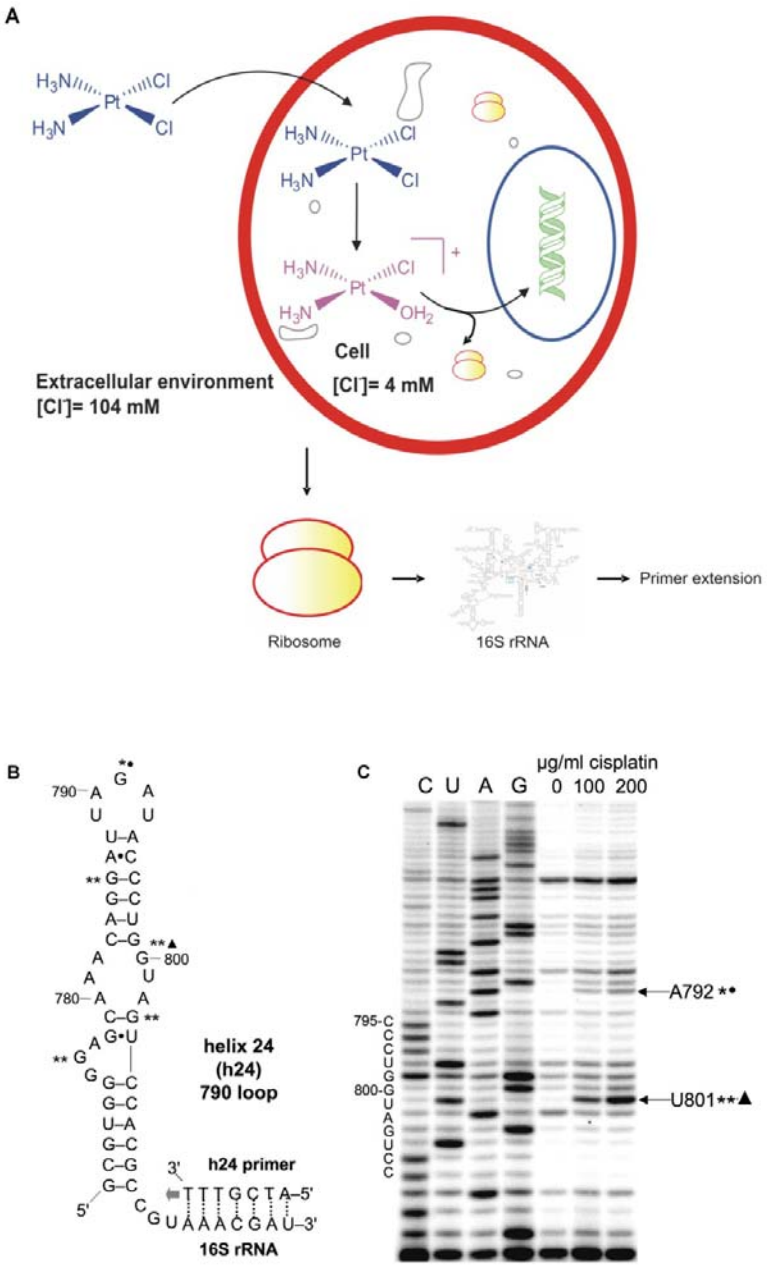

Figure 3.9. Probing results in 16S rRNA from *in vivo* studies are shown. A) An overview of the *in vivo* probing method, B) a partial secondary structure map of 16S rRNA h24 (residues 769–820) with the primer-binding site, and C) an autoradiogram showing reverse transcription mapping of *in vivo* reactive sites (indicated by arrows; **major, *minor) of cisplatin on 16S rRNA/70S ribosomes (the concentrations of cisplatin are given for each lane, 0–200 µg/ml of cells) are shown. Dideoxy sequencing lanes are labeled as C, U, A, and G. Sites that are identical in the *in vitro* and *in vivo* probing experiments are indicated with symbols (▲,•).

3.4.3 Active and inactive conformations

Opposite reactivity of purines at the N1 and N7 positions has been observed previously in activated and inactivated ribosomes by chemical probing (*249*). Cisplatin showed similar reactivity as DMS in the 30S subunits and the 70S ribosomes when used to probe the active form of the 30S subunit. For example, in helix 44, G1415-G1417 showed enhanced reactivity with DMS in the inactive form, and G1422-G1423 showed enhanced reactivity in the active conformation. Probing results with cisplatin showed similar reactivity with the activated 30S subunit, more specifically enhanced reactivity at G1422-G1423 and no reactivity at G1415-G1417 in the 30S subunits and the 70S ribosomes. However, all of these Gs showed reactivity with naked 16S rRNA (**Figure 3.10**). These results demonstrate that cisplatin can be used to identify functionally important nucleotide and distinguish accessible nucleotide under active biological states. These results can be compared to accessible residues in inactive RNAs in the absence of protein factors.

Another similarity of our probing results with DMS studies is observed at G926 and G1401. These nucleotides showed opposite reactivity at the N1 and N7 positions of guanosine when probed with DMS. In the active form, the reactivity of G926 at N1 was higher and there was no reactivity at N7. This result was opposite in an inactive ribosomal conformation (*144*). Cisplatin probing results showed reactivity of these nucleotides in free 16S rRNA and comparatively weaker reactivity in the 30S subunits or the 70S ribosomes; suggesting similar reactivity at the N7 of Gs. Since, both the 30S subunits and the 70S ribosomes were activated before the incubation with cisplatin, these

results indicate that the ribosome was in an active conformation during probing experiments.

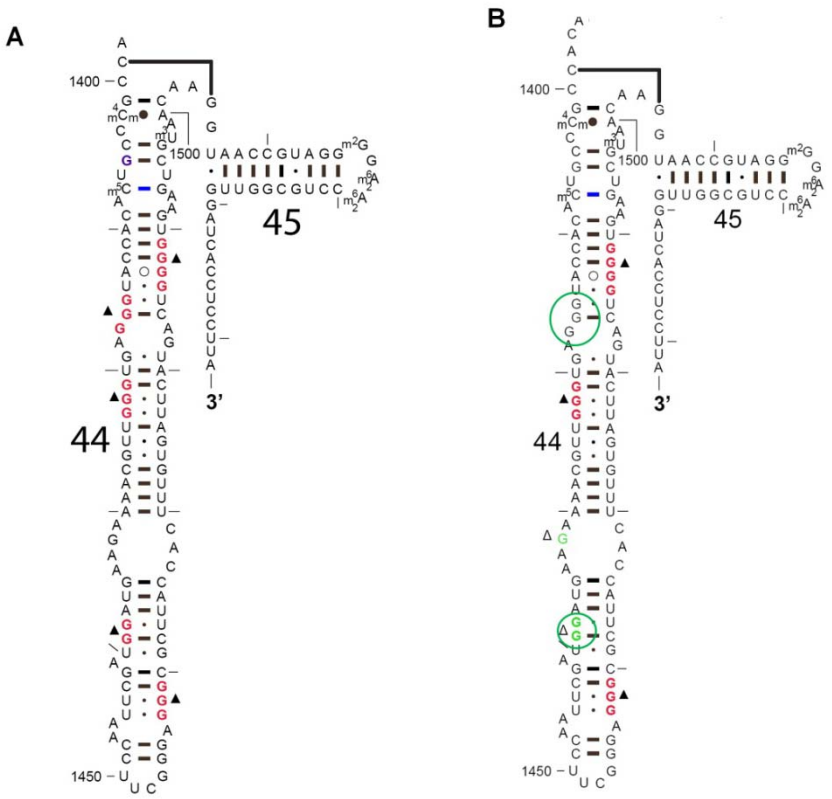

Figure 3.10. Secondary structure map at the 3' minor domain of 16S rRNA with probing results from free 16S rRNA and the 30S subunits and the 70S ribosomes are shown. Strong hits (reactive nucleotides) are colored red (shown with▲), moderate hits are colored green (shown with Δ), and weak hits are colored blue (shown with ●). A) Probing results from free 16S rRNA and B) results from 30S/70S are compared.

3.5 Discussion

Although a number of chemical and enzymatic probes have been utilized to explore the accessibility of nucleotides in the ribosome, very little information is available regarding the reactivity of the N7 position of guanosines. Although DMS can react with the N7 position of guanosine, efficient strand scission is required for detection, which may be difficult to achieve. Cisplatin is believed to react with

the N7 position of guanosines and form a stable coordination complex; hence, it will be useful to provide information about the nucleotide accessibility and reactivity of the N7 position.

The ribosome is a potential target for a number of antibiotics, and half of the known antibiotics already target the ribosome (*104*). However, pathogens become resistant to the common drugs by more than one mechanism. To overcome the problem of resistance, significant efforts have been made, mostly by modifying the existing antibiotics (*251-252*). Despite being a validated target, only a few attempts have been made to explore novel target sites in the ribosome (*2, 103, 236*). Cunningham and coworkers have carried out instant evolution experiments to investigate the nucleotides that do not undergo mutation, and if mutated are lethal. These nucleotides are found to be involved in interactions with tRNA, mRNA, or initiation factors, and are therefore functionally important. In the 790 and 690 loops of the small subunit, nucleotides such as G791, U793, and G691 were not mutated (*247, 253*). Previous probing experiments and now high-resolution crystal structures revealed that the 790 loop is in contact with tRNA and initiation factor 3 (*238, 249*). By targeting these functionally important nucleotides that cannot be mutated, we can be one step ahead of bacterial resistance involving target modification.

To explore the potential drug target sites, in a similar manner, Mankin and coworkers carried out random mutagenesis in the small and the large subunits of the ribosome (*2, 65*). They observed 53 mutations in the small subunits and 54 in the larger subunits that were deleterious. These mutations either affect the

function of the ribosome or disrupt its structure leading to a deleterious phenotype. Deleterious mutations were clustered in certain functional regions that show >98% conservation in 16S rRNA (*65*). Hence, it can be expected that these nucleotides may be functionally important in other bacteria as well. Despite this information, more knowledge about the accessibility of these nucleotides will be needed to target these sites. Probing the 30S subunits and the 70S ribosomes with cisplatin revealed a number of strong and moderate hits. The binding sites of cisplatin in the ribosome are found to be distributed throughout the ribosome and a number of functionally important sites showed reactivity. The functionally important sites that are reactive towards cisplatin should be accessible to small molecules and, hence, could be exploited as novel target sites.

Helix 17 and 18 are promising drug target sites in the ribosome because of their structural and functional importance. Helix 17 is structurally different in bacteria and eukaryotes (*103*). The internal loop is conserved in bacteria and absent in eukaryotes. Helix 18 is located on the surface of the small subunit at the interface that contacts the large subunit, and the 530 loop (nucleotides 515-536) is highly conserved (*244*). The 530 loop is an essential component of ribosomal decoding and controls the accuracy of aminoacyl-tRNA selection (*79*). The lack of functional mutants in the 530 loop further indicates its functional importance (*103*). Another study showed that mutations of nine nucleotides in this loop are deleterious including G506, G521, and G527 (*2*). Cisplatin showed reactivity with several nucleotides in this region, including consecutive Gs in the

internal loop of helix 17 (G453-455), the pseudoknot region of helix 18 (G506-507), and conserved nucleotides G529-530. These nucleotides are accessible to cisplatin and, hence, could be accessible to small molecules. Due to structural differences and the functional importance, these sites could be utilized as a novel target for antibiotics. Recently, a model system of helix 18 has been used as a target to find ligands by phase display (*254*).

Helix 24 of 16S rRNA is very important because of its location near the decoding region, interactions with initiation factor (*230, 248, 255*), and key contacts with 50S subunit (*231, 247, 249*). In addition, the 790 loop in the small-subunit platform and the nucleotides ridge **(**G1338-U1341 (helix 42)**)** in the head form a 13 Å gap, which separates the anticodon stem-loop of the P-site tRNA from the E site (**Figure 3.11 A**) (*222*). The universally conserved residues G1338 and A1339 also play a role in discrimination of initiator $tRNA^{f\text{-}met}$ by initiation factor (IF3) (*256*). Furthermore, helix 24 is located at the interface between the large and small subunits and is known to be exposed to solvent (*231, 257*). The antibiotic pactamycin is already known to bind to this helix (*258*). Hence, nucleotides in this helix need to be accessible to assist these numerous functional interactions, and blocking them could be an effective antibiotic strategy.

All of the consecutive Gs present in helix 24 are accessible for cisplatin reactivity in free 16S, 30S subunits, and 70S ribosomes. However, specific residues such as G803 and G791 show different reactivity. G803 showed reactivity only with the naked 16S and G791 showed higher reactivity in the 70S

ribosomes. Instant evolution experiments with the 790 loop by Cunningham and coworkers showed that positions G791 and U789 do not allow for any viable mutations (*103*), indicating their functional importance. Nucleotides G773-776 are involved in forming bridge 7b and the mutation G775A is found to be lethal (*2*).

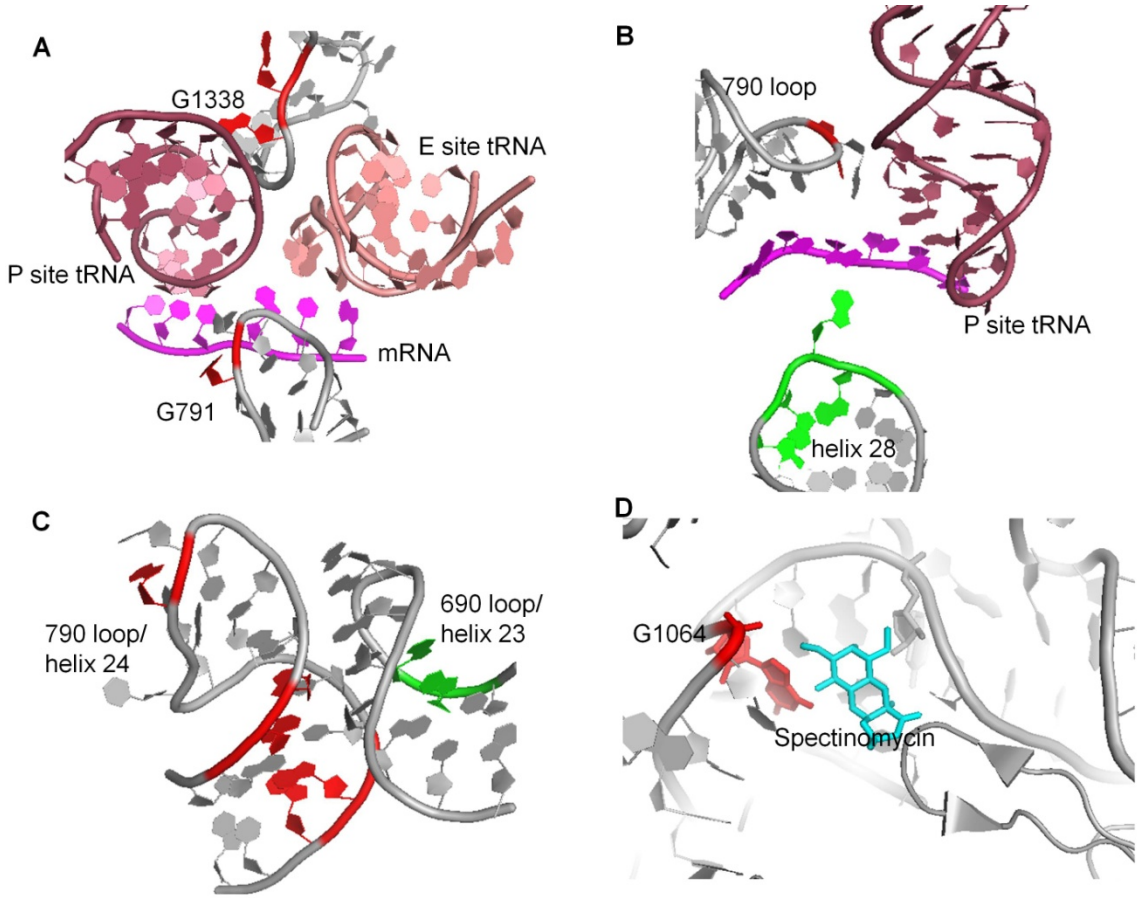

Figure 3.11. Various functionally important helices of 16S rRNA in 70S ribosome crystal structures are shown. A) Helix 24 (790 loop) and helix 42 are in contact with tRNA and mRNA, B) the 790 loop and helix 28 are in close contact with tRNA and mRNA, C) the 790 loop is in contact with functionally important 690 loop (helix 23), and D) helix 34 is in association with the antibiotic spectinomycin. Nucleotides that showed strong hits in cisplatin probing are shown in red color and moderate are shown in green color. This figure was created with Pymol using PDB: 2I2P and 2QOU (*27, 74*).

In addition, in the crystal structures, the 790 loop makes contacts with the 690 loop through N1 and N6 of A696 and the 2'-OH of C797 (**Figure 3.11 C**) (*78, 253*). The 690 loop is also found to be functionally important and involved in tRNA binding at the P site (*3, 232, 249*), initiation factor binding (*230*), and subunit association (*147, 259*). Further, mutational studies carried out on this loop also indicate its functional importance (*253*). Thus, due to its functional importance and extensive contacts with other helices, tRNA, and initiation factor, helix 24 is one of the most promising new drug target sites. All consecutive guanosines in this helix showed reactivity with cisplatin; it is therefore expected that they will be accessible to other small molecules. Binding of small molecules even in the stem regions can disrupt the conformation or contacts of this helix with other helices, tRNA, and the initiation factor.

Similarly, helix 34 can also be exploited as a target site in the ribosome. This helix lies in the head region of the small subunit, and in the folded structure it is very close to the decoding region (*74*). Hence, it has been expected that it has an important role in the selection of the correct aminoacyl tRNA. The reactivity of nucleotides in this helix are different in free 16S rRNA, the 30S subunit, and the 70S ribosome. The consecutive Gs at positions 1058-1059 showed strong reactivity within the free 16S rRNA and no reactivity in the 30S subunits, suggesting that these nucleotides become protected after the ribosome is assembled with proteins. The crystal structure of *E. coli* 70S revealed that ribosomal protein S3 binds to this helix and it contacts several nucleotides in this region (**Figure 3.12**) (*246*). Interestingly, a neighboring nucleotide, G1064, shows

higher reactivity towards cisplatin in 30S subunits and 70S ribosomes, but very weak reactivity in free 16S rRNA. Helix 34 is also a known binding site for the antibiotic spectinomycin, which contacts G1064 along with other nucleotides (**Figure 3.11 D**) (*74*). The lack of cisplatin reaction at the consecutive Gs may be due to protection or conformational changes that occur upon binding of protein S3, which conversely makes the neighboring G1064 accessible for small-molecule interactions.

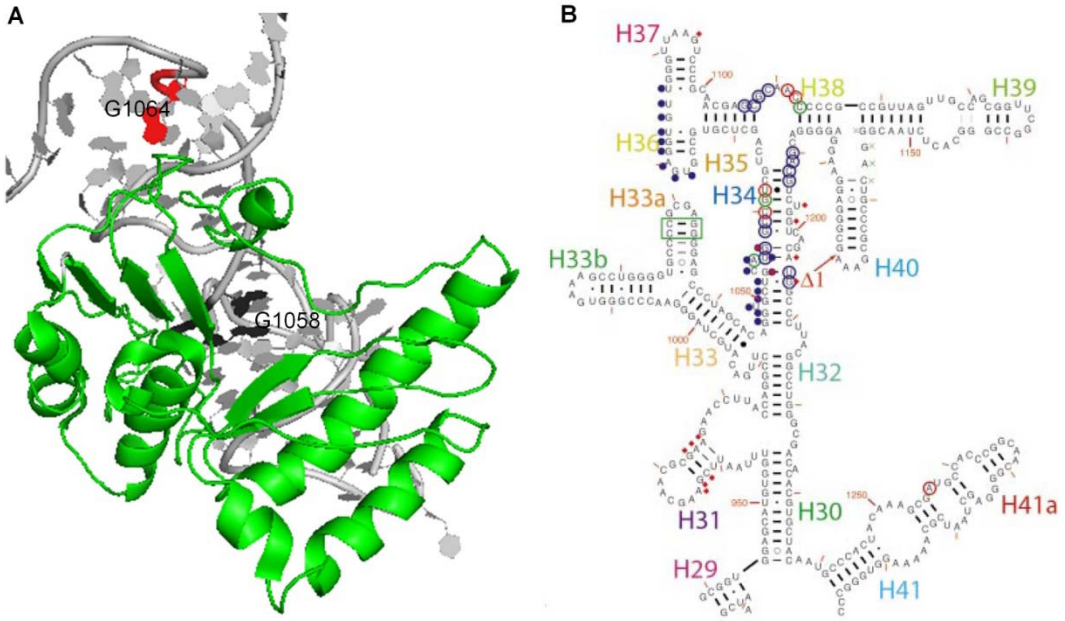

Figure 3.12. Ribosomal protein S3 and part of 16S rRNA secondary structure corresponding to helix 34 are shown. A) The ribosomal protein S3 and helix 34 with cisplatin probing results are compared; nucleotides with strong hits on free 16S and protected in 30S/70S are shown in black, strong hits observed in 30S/70S are shown in red. B) The secondary structure of 16S rRNA shows the contacts of ribosomal protein S3. The nucleotides in contact with S3 are circled with: blue (backbone only), red (base only), and green (both backbone and base). Figure A was created with Pymol (PDB: 2AVY) and B was reprinted with permission (Brodersen *et al.*) (*246*).

Thus, these results demonstrate the ability to discover potential antibiotic sites of both structure accessibility and functional importance. The platinum complex is sensitive to variations in the ribosome structure, and thus could be

employed to examine ribosomes at various stages of protein synthesis, or complexed with various factors, mRNA, or tRNAs. Most importantly, it is revealed that a positively charged platinum complex is useful for targeting rRNA, and has the ability to provide key information about helix or loop accessibility in the ribosomes. Sites that differ in platinum reactivity between 30S subunits and the 70S ribosomes could reveal compelling regions for mechanism-based drug design. Furthermore, the fact that the platinum complex generates stable adducts is significant because the kinetics of the reaction can be monitored, which will allow the determination of how positively charged compounds such as aminoglycosides identify target sites with favorable electrostatic contributions from a number of possible reactive sites on the ribosome (*204*).

CHAPTER 4

Study of Cisplatin Binding to a Small RNA Construct Representing the 790 Loop of 16S Ribosomal RNA

4.1 Abstract

DNA has been considered to be the major target of cisplatin, while RNA has been essentially overlooked. Previous studies in our laboratory demonstrated that RNA is the kinetically preferred target over DNA when similar sizes and structures of nucleic acids are compared. In the present study, we are extending our understanding of cisplatin binding to the 790 loop of *E. coli* 16S ribosomal RNA (rRNA). On the model RNA constructs, the number of platinum adducts were determined by using enzymatic digestion in conjunction with HPLC and atomic absorption spectroscopy. In addition, the binding sites, number, and types of adducts formed with RNA constructs were identified by using MALDI-TOF mass spectrometry and LC-MS spectroscopy. The aquated platinum complex formed a variety of adducts with the 790 RNA hairpins. This information may be helpful towards understanding the usefulness of cisplatin as a probe of RNA structure and function, or to consider rRNA as a potential target of the antitumor drug.

4.2 Introduction

The ribosome is composed of rRNA and proteins, which are organized into the large and small subunits (*48, 222*). For the 70S ribosome of *E. coli*, the large subunit (50S subunit) is composed of 5S and 23S rRNAs and 34 ribosomal

proteins and the small subunit (30S subunit) is composed of 16S rRNA and 21 proteins (*222, 260*). The ribosome is important because it catalyzes protein synthesis in all forms of life. The majority of ribosomal functions rely on the rRNA structure (*222*).

This dependence of ribosome function on RNA is only possible because of the large variety of secondary and tertiary structures formed by RNA (*34*). Single-stranded RNAs fold upon themselves to form well-defined structures that are of great functional importance (*35*). An example of this, which is found in, but not exclusive to, the ribosome is the structural motif called the stem-loop or hairpin (*41, 244*). Although most hairpins rely heavily on hydrogen bonding in the so-called stem region, mismatch base pairing can also occur.

Aside from studying RNA structural regions to understand their functions, such work may also lead to the discovery of new antibiotic binding sites (*119, 261*). It has been reported that human pathogens from infections in patients from various sources have been growing more resistant to commonly used antibiotics (*262*). Since nearly half of the currently used antibiotics target the ribosome, it is important to find new regions for novel antibiotics to bind (*86*). Combined with genetic approaches, biophysical methods and chemical probing may be used as a discovery tools for new antibiotic binding sites (*2, 103, 236*).

The work reported here focuses on a model structure of the 790 loop of *E. coli* 16S rRNA. This loop contains residues 783 to 799 and has been shown to be important for ribosomal function, due to its presence in the inter-subunit region (*231*) and its binding to protein IF3 (*230*). The 790 loop is exposed to solvent in

the small subunit, and it is present in the small subunit rRNAs of all organisms. It has also been shown to have decreased ribosomal function following mutations (*247*). So, not only is it accessible, but information pertaining to molecular binding to the 790 loop is useful for other organisms.

While cisplatin is commonly used as a chemotherapeutic drug for several forms of cancer (*163, 166*), it has also been reported to be a probe for accessible residues of ribosomal RNA (*204*). In DNA, the aquated cisplatin coordinates to the N7 positions of adjacent purine bases to form primarily 1,2-intrastrand crosslinks, but the formation of interstrand and monofunctional adducts is known as well (*172, 197, 263*). The types of adducts formed with RNA have not yet been verified, but are presumed to be the same as DNA. The advantages that cisplatin probing has over other chemical probes is its ability for active or passive cellular uptake, activation within the cell, and stability of the adduct formation with nucleic acids (*163, 264*). Following passive diffusion, this square-planar complex is activated by the replacement of one chlorido ligand by hydrolysis in an aqueous environment because of the decreased chloride ion concentration in the cell (*156*). This reaction produces the mono-aquated form of cisplatin $[Pt(NH_3)_2ClH_2O]^+$ and following coordination, the remaining chlorido ligand is displaced by hydrolysis to produce the bis-aquated form of cisplatin, thus allowing the platinum to more easily coordinate to a second purine base (*229*). *In vitro*, hydrolysis products of cisplatin can be generated by using silver nitrate in order to precipitate the chloride ions out of solution as silver chloride.

Probing the RNA structure with cisplatin provides information concerning the environment of individual nucleotides that can be compared to RNA structural models and hypotheses about RNA function. This is important because a limited number of studies have revealed further details concerning interactions of cisplatin with RNA (*169*). In order to determine the location of cisplatin binding on the 790 RNA hairpin constructs and quantify the number of adducts, matrix-assisted laser desorption/ionization time-of-flight (MALDI-TOF) mass spectrometry, atomic absorption spectroscopy (AAS), high-performance liquid chromatography (HPLC), and liquid chromatography-mass spectrometry (LC-MS) were employed (**Figure 4.1**).

4.3 Materials and Methods

4.3.1 General

Cisplatin (*cis*-diamminedichloridoplatinum (II)) was obtained from Alfa Aesar (Ward Hill, MA). Silver nitrate and ammonium acetate were obtained from Fisher Scientific. DMF (dimethylformamide) from Acros Organics was used for the preparation of the monoaquated and bioaquated cisplatin species. TBAF (tetrabutylammonium fluoride) was obtained from Aldrich, CIP (calf intestinal alkaline phosphatase) was obtained from Promega Corp (Madison, WI). P1 nuclease was purchased from Sigma Chemicals. The remaining chemicals for buffers and reagents were obtained from Sigma Chemicals or Fisher. RNase-free, distilled, deionized (ddH_2O) was used for all experiments.

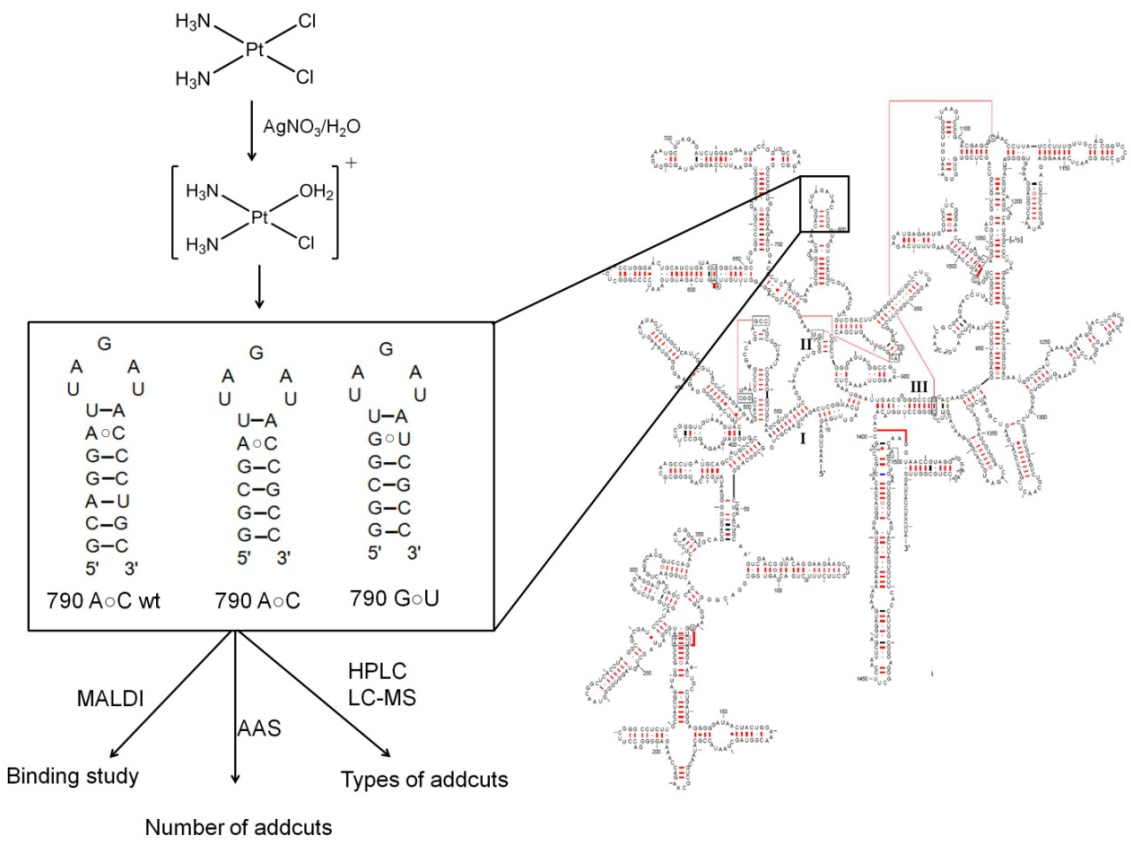

Figure 4.1. The basic outline of cisplatin activation, secondary structure of 16S rRNA, close-up to show 790 RNA constructs, and summary of various techniques used for study of cisplatin binding in RNA model system are shown. Three different RNA constructs used in this study (790 A○C wt, 790 A○C and 790 G○U hairpins) are indicated in the box.

4.3.2 Preparation of aquated complexes

For monoaquated cisplatin, molar equivalents (116 μmol) of cisplatin (35 mg) and silver nitrate (18 mg) were added to 1 ml dH_2O or DMF and dissolved by agitation in the dark overnight. Silver nitrate was introduced in order to precipitate out chloride ions. The solution was centrifuged at 12,000 RPM for 15 minutes to remove the silver chloride precipitate, and the monoaquated cisplatin supernatant was removed. An additional 5 minutes of centrifugation at 12,000 RPM ensured that all of the silver chloride had been removed. The supernatant

was transferred to a new tube. The aquated samples of cisplatin in DMF were stored at -20 °C and kept no longer than one week.

4.3.3 RNA preparation and purification

Three RNA constructs 5'-GGCGAUUAGAUACCGCC-3' (790 A○C) 5'-GGCGGUUAGAUAUCGCC-3' (790 G○U), and 5'-GCAGGAUUAGAUACCC UGC-3' (790 A○C wt) were chemically synthesized at the Keck Foundation, School of Medicine, Yale University. These RNAs were received as the 2'-protected species and deprotected by dissolving in TBAF, followed by incubation at 35 ºC overnight. The RNA was then desalted with a Sep-Pak Light C18 cartridge (Waters), dried in a speed-vac evaporator, and reconstituted in ddH_2O. The RNA then underwent HPLC purification. Solvents were as follows: buffer A was 25 mM triethyl ammonium acetate, pH 6.5; buffer B was 40% acetonitrile in water. The column was pre-equilibrated with 80% buffer A and 20% buffer B with a flow rate 1 ml/min. RNA purification was achieved using the following elution gradient: 80% A and 20% of B to 50% A and 50% of B over 30 min at room temperature. The RNA fractions were detected at 260 nm and collected manually. Following HPLC purification, RNA were ethanol precipitated with sodium acetate and renatured in 20 mM Tris·HCl and 50 mM NaCl by heating to 90 °C for 2 min followed by slow cooling.

4.3.4 Cisplatin reaction with 790 RNA

All cisplatin reactions were carried out with monoaquated complexes in 1:1 or 1:20 ratios of RNA:complex. Prior to platination, RNA was renatured as

stated above. Platination was carried out in 20 mM sodium phosphate buffer, pH 6.5, 10 mM $MgCl_2$ and 10 mM NaCl (buffer P) at 37 °C for 5 hours. The reactions were quenched with 2 M NaCl followed by immediate freezing.

4.3.5 MALDI-TOF mass spectrometry

MALDI-TOF (Matrix Assisted Laser Desorption Ionisation Time of Flight) mass spectrometry analyses were carried out with a Bruker Daltonics TOF-300 MALDI Ultraflex. After platination reaction, RNA oligos were separated by 20% polyacrylamide gel electrophoresis in order to separate bound and unbound RNA samples. The bands were cut out of the gel and electro-eluted. Following desalting with the Sep-Pak Light C18 cartridge, the samples were prepared for MALDI-TOF by mixing 1 µl (25 pmol) of platinated or unplatinated RNA with 3 µl of freshly prepared matrix solution (3-hydroxypicolinic acid in 50% acetonitrile). One µl of this mixture was placed on the MALDI plate and allowed to dry at room temperature. For RNase T1 digestion, 1 µl (1 unit) of RNase T1 was added to the sample and it was incubated at room temperature for 15 min. Then, one µl was spotted on the MALDI plate and allowed to dry at room temperature. The spectra of intact RNA molecules were acquired in positive-ion reflector mode using method RP-3147.par.

4.3.6 Atomic absorption spectroscopy

Atomic absorption spectroscopy (AAS) was used to analyze the amount of platinum bound to the 790 RNA constructs. The instrument used for this study was equipped with a graphite furnace with hollow cathode platinum lamp (Perkin-

Elmer AAnalyst 700). The AAS has adjustable slit width wavelength and direct concentration readout capabilities. All 790 samples underwent 30 hours of dialysis with Spectra/Por 7 dialysis tubing, 3.5 KDa molecular weight cut off membrane to remove any excess platinum present in the reaction. The AAS was optimized and calibrated using calibration standards prior to each analysis. The platinum calibration standards were prepared from commercial standards of platinum (High-Purity Standards, Charleston, SC) in 5% HCl. The data were obtained by using the instrument protocol and the previously described methods in the literature (*265-266*).

4.3.7 High performance liquid chromatography

HPLC was carried out with a Waters system equipped with a C18 Discovery column (250 x 4.6 mm, 0.5 µm). Separation was carried out by using buffer A (40 mM ammonium acetate) and B (40% acetonitrile) with a linear gradient in which the ratio of A to B changed from 95:5 to 70:30 over 30 minutes at a constant flow of 1 ml/min. The retention times of the standard nucleosides were confirmed by injection of known standard nucleosides. Control and platinated RNAs were digested with nuclease P1 to convert to nucleotides, and the CIP was used to remove phosphates and give free nucleosides. Nuclease P1 digestion was carried out in 50 µl of digestion buffer (1 mM $ZnCl_2$, 20 mM sodium acetate, pH 5.3), for both the control and the platinated RNAs with 10 µl (10 U) of nuclease P1 at 37 ºC overnight. The enzyme was then deactivated by heating at 75 ºC for 15 min. Five µl of 1.5 M Tris·HCl, pH 8.8, and 1 µl (10 U) of calf intestinal phosphatase (CIP) was added to each sample and incubated for 4 hrs

at 37 ºC. After 4 hrs of incubation, samples were again heated at 75 ºC for 15 min, vortexed, and centrifuged at 12,000 rpm for 5 min. Finally, samples were filtered through YM-3 microcon filters before injection into the HPLC or LC-MS.

Samples were analyzed by HPLC and peaks areas were normalized to account for the differences in extinction coefficients at 260 nm, (C = 9,100 M^{-1} cm^{-1}, U= 10,100 M^{-1} cm^{-1}, G= 13,600 M^{-1} cm^{-1}, A= 14,900 M^{-1} cm^{-1}) (*217*) and then peak ratios were calculated relative to the cytidine peak.

4.3.8 Liquid chromatography mass spectrometry

LC-MS (Liquid Chromatography Mass Spectrometry) is a powerful technique to separate and analyze complex mixtures with high sensitivity. LC-MS was carried out on an AQUITY Ultra Performance LC chromatography (UPLC) system (Waters Corporation, MA USA) equipped with an HSST3 C18 column (2.1 x 100 mm 1.8 µm). The column was maintained at 50 ºC and elution was carried out with a linear gradient of acetonitrile and 100 mM ammonium acetate, pH 6.0. The gradient was run for 3 min with a flow rate 700 µl/min, starting at 100% ammonium acetate and decreasing to 60% over the course of the gradient. The column eluent was analyzed by directing it to the mass spectrometer. Mass spectra were collected in the positive ion mode. The percentage of adducts were calculated by normalizing the area with extinction coefficients followed by relative ratios of adduct present in sum of adducts.

4.4 Results

4.4.1 Cisplatin binding studies in 790 RNA constructs

Initially, two model systems of the 790 hairpin, 790 A○C and 790 G○U (mutant) were selected to study cisplatin binding (**Figure 4.1**). This 790 loop is part of helix 24 of 16S rRNA and is functionally important (*249*). In addition, extensive mutational and structural studies have been carried out previously in this helix (*247, 258*). MALDI mass spectrometry was used to check adduct formation with small RNA constructs. RNAs were reacted with one equivalent of monoaquated cisplatin for 5 hrs at 37 °C. The products were separated on 15% denaturing gels and visualized by UV shadowing. For the 790 A○C model, two bands were observed with cisplatin, whereas three bands were observed in the case of the G○U variant.

The product bands A○C1, with higher mobility, and A○C2, with slower mobility, were isolated by electro-elution and subjected to MALDI-TOF mass spectrometry (**Figure 4.2**). The higher mobility product, A○C1, has a mass of 5426.53 Da, which corresponds to free RNA. The slower mobility product, A○C2, has a mass 5653.2 Da, which is increased by 227 mass units [$Pt(NH_3)_2$] relative to the free RNA, and corresponds to the formation of a bifunctional adduct. Similarly, three products from the 790 G○U variant; G○U1 (higher mobility), G○U2 (intermediate mobility), and G○U3 (slowest mobility) were also isolated and analyzed by MALDI-TOF (**Figure 4.2**). In 790 G○U, the slower mobility product, G○U1, corresponds to unmodified 790 G○U with a mass 5443.2 Da. The other two products, G○U2 and G○U3, correspond to masses 5670.7 Da and

5670.2 Da, respectively, increased by of 227 mass units relative to the free RNA, equivalent to [(Pt(NH_3)$_2$] (**Table 4.1**). This result also indicates formation of bifunctional adducts.

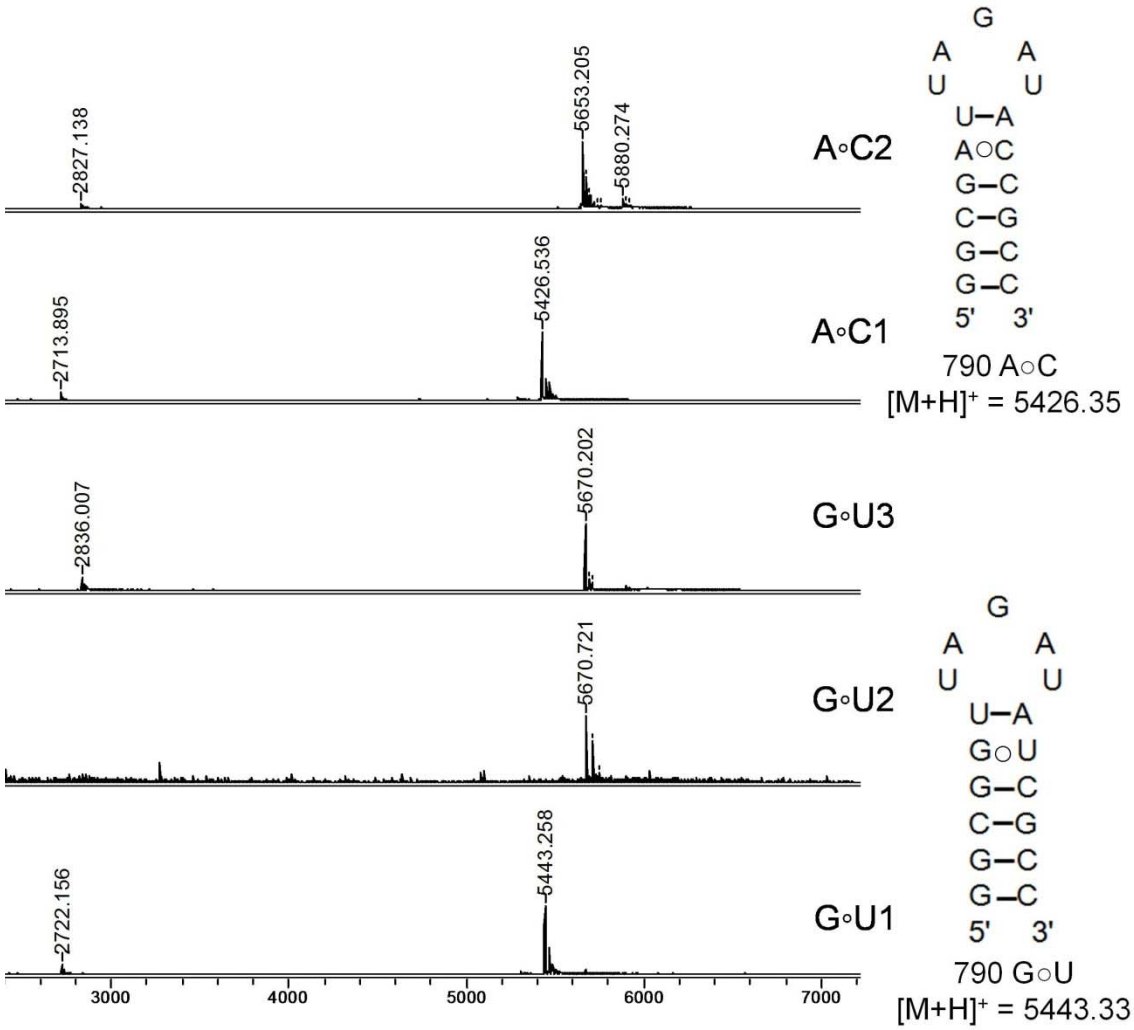

Figure 4.2. MALDI-mass spectrometry data show the masses of various products formed with 790 hairpin loops after the reaction with monoaquated cisplatin. 790 model constructs A○C and G○U with their sequence and calculated mass are also shown.

Table 4.1. Observed molecular mass and predicted species of various cisplatin adducts with 790 RNA model system.

Molecular Ion	Observed mass (Da) $(M+H)^+$		Predicted species
790 A○C1	5426.53		790 A○C (RNA only)
790 A○C2	5653.20	(+227)	790 A○C + $Pt(NH_3)_2$
790 A○C2	5880.27	(+2*227)	790 A○C + 2[$Pt(NH_3)_2$]
790 G○U1	5443.25		790 G○U (RNA only)
790 G○U2	5670.72	(+227)	790 G○U + $Pt(NH_3)_2$
790 G○U3	5670.20	(+227)	790 G○U + $Pt(NH_3)_2$

4.4.2 Mapping binding sites by RNase T1 cleavage

For further confirmation and mapping of the exact cisplatin-binding sites in these model systems, the products were partially digested with RNase T1, and the fragments were analyzed by MALDI-TOF mass spectrometry (**Figure 4.3**). RNase T1 fragments show that A○C1 has no platination in any fragments of RNase T1; however, in A○C2, the fragments corresponding to 3185.1 Da, [$GGCGAUUAG_{>}p+Pt(NH_3)_2$], and 1568.2 Da, [$GGCG_{>}p+Pt(NH_3)_2$], suggested platination at the 5' consecutive guanines (**Figure 4.3** and **Table 4.2**). In the case of 790 G○U, the highest mobility band has no platination in any fragments of RNase T1 digestion; whereas, the other two slower mobility products, G○U2 and G○U3, had fragments corresponding to formation of bifunctional adducts (**Figure 4.4** and **Table 4.3**). The fragment corresponding to 1568.9 Da, [$GGCG_{>}p+Pt(NH_3)_2$], in G○U2, suggested a bifunctional adduct at the 5' consecutive

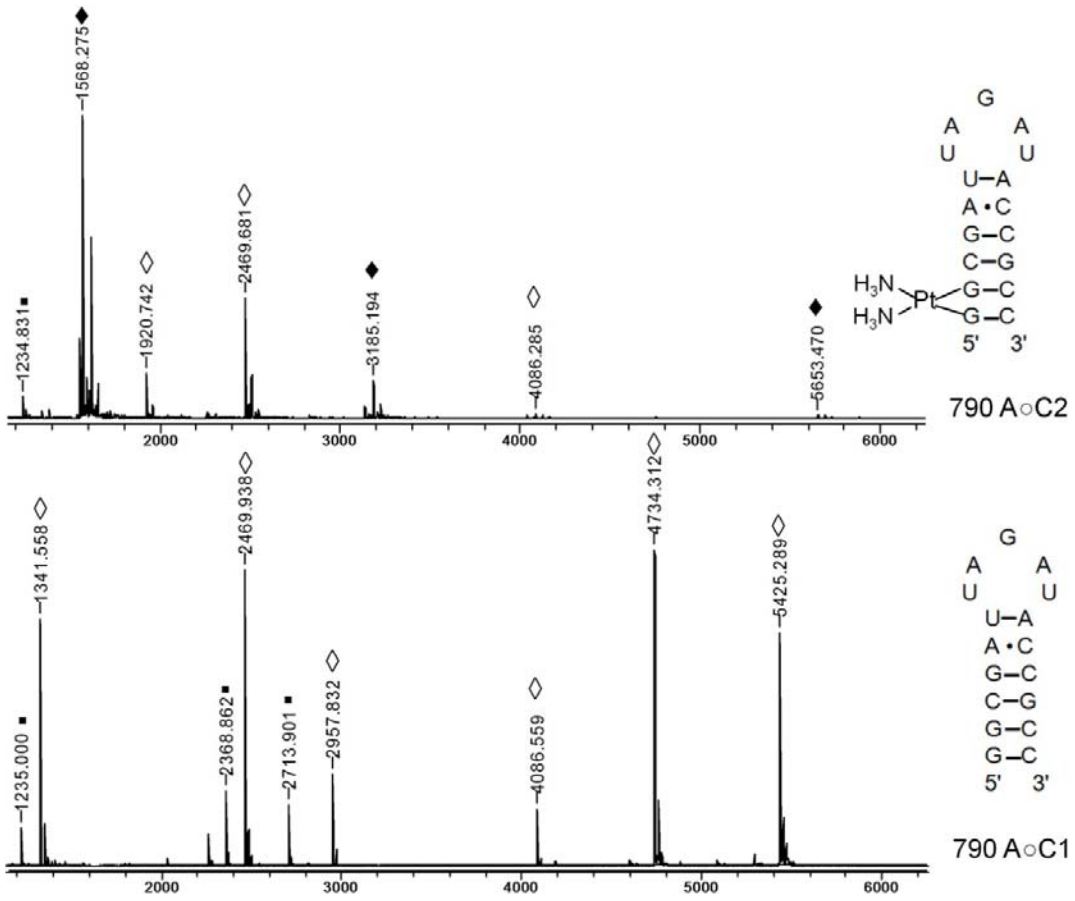

Figure 4.3. MALDI-mass spectrometry data after digestion of 790 A•C construct with RNase T1 are shown. RNA hairpin, platinated (♦) and corresponding unplatinated (◊) fragments, and +2 charge states (▪) are also indicated. The platinated site is shown on A○C2 at positions G1 and G2, which is consistant with the mass data.

Table 4.2. RNase T1 fragments of 790 A○C1 and A○C2 with calculated and observed mass.

RNA fragments (5' to 3')	Calculated mass (Da) $[M+H]^+$	Observed mass A○C1 (Da) $[M+H]^+$	Observed mass A○C2 (Da) $[M+H]^+$
GGCGp	1341.81	1341.55	1568.27 [+ $Pt(NH_3)_2$]
AUACCGp	1921.16	-	1920.74
AUACCGCC	2469.56	2469.93	2469.68
GGCGAUUAGp	2957.77	2957.83	3185.19 [+ $Pt(NH_3)_2$]
AUUAGAUACCGCC	4085.53	4086.55	4086.28
CGAUUAGAUACCGCC	4734.92	4734.31	-
$(M+H)^+$	5425.3	5425.25	5653.27 [+ $Pt(NH_3)_2$]

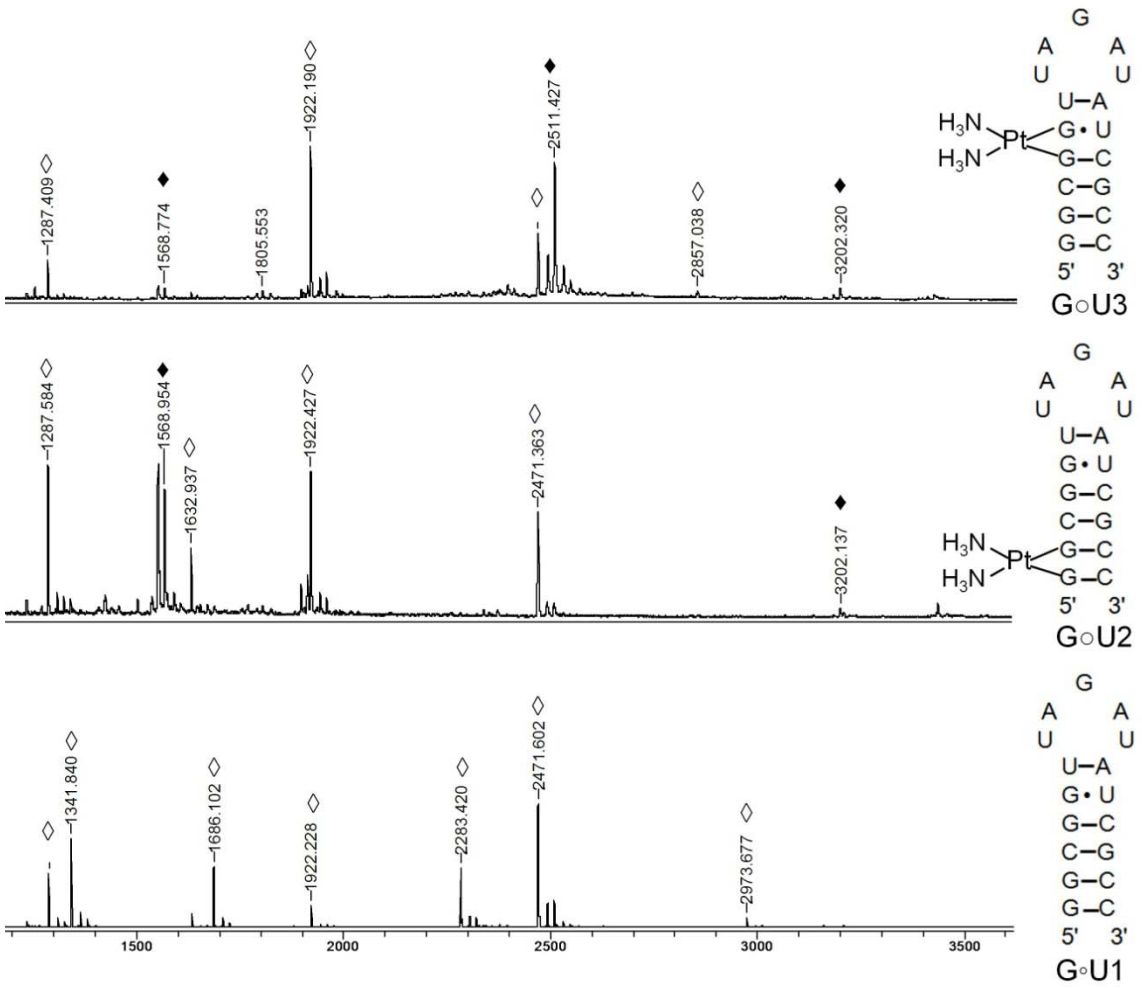

Figure 4.4. MALDI-mass spectrometry data after digestion of 790 G○U construct gel fractions (G○U1, G○U2, and G○U3) with RNase T1 are shown. 790 G○U hairpin, platinated (♦) and corresponding unplatinated (◊) fragments of RNA are also indicated. The platinated site is shown on G○U2 at positions G1 and G2, and on G○U3 at positions G4 and G5, which is consistent with the mass data.

guanines, and fragment with 2511.4 Da, [CGGUUAG$_{>}$p+Pt$(NH_3)_2$], in G○U3 indicated formation of an adduct at the G○U mismatch region. The fragment 1568.9 Da is not significant in G○U3; but compared to G○U2, the mass corresponding to 2511.4 Da had higher intensity. The result is opposite in G○U2, which confirms adduct formation at two different sites.

Since the cisplatin was shown to bind preferably to the 5' consecutive guanosines on the modified construct, which were not the part of wild-type 16S rRNA, we made another construct with an A○C mismatch (wild type), but lacking the 5' consecutive guanosines. The rest of the binding studies in this chapter focus on the 790 A○C wild-type (wt) construct.

Table 4.3. RNase T1 fragments of 790 G○U1, G○U2, and G○U3 with calculated and observed mass.

RNA fragments (5' to 3')	Calculated mass (Da) $[M+H]^+$	Observed with G○U1 (Da) $[M+H]^+$	Observed with G○U2 (Da) $[M+H]^+$	Observed with G○U3 (Da) $[M+H]^+$
UUAGp	1287.75	1287.58	1287.45	1287.40
GGCGp	1341.81	1341.84	1568.95 [+ Pt $(NH_3)_2$]	1568.7 [+ Pt $(NH_3)_2$]
GGCGGp	1687.02	1686.10	-	-
AUAUCGp	1922.14	1922.22	1922.42	1922.19
CGGUUAGp	2283.35	2283.42	-	2511.42 [+ Pt $(NH_3)_2$]
AUAUCGCC	2470.55	2471.60	2471.36	2471.26
GGCGGUUAGp	2973.77	2973.67	3202.13 [+ Pt $(NH_3)_2$]	3202.32 [+ Pt $(NH_3)_2$]

4.4.3 Binding studies in model system 790 A○C wild type

The new 790 model RNA (790 A○C wt) was reacted with monoaquated cisplatin in an equimolar ratio with monoaquated platinum complex similar to the other constructs and the products were separated by gel electrophoresis. Separated products after desalting were examined by Ultraflex MALDI-TOF mass

spectrometry in the positive-ion mode (**Figure 4.5**). The band with the faster mobility was unplatinated RNA and the band with slower mobility contained a mixture of various adducts. The expected and observed mass of the possible adducts are summarized in **Table 4.4**. The reaction of *cis*-$[PtCl(H_2O)(NH_3)_2]^+$ resulted in the formation of what we believe to be a bifunctional adduct, RNA-$Pt(NH_3)_2$, which was identified through an observed molecular mass of 6288.53 Da. Two other products were observed in the MALDI spectrum with less intensity, corresponding to two and three platinum complexes bound to the 790 RNA construct.

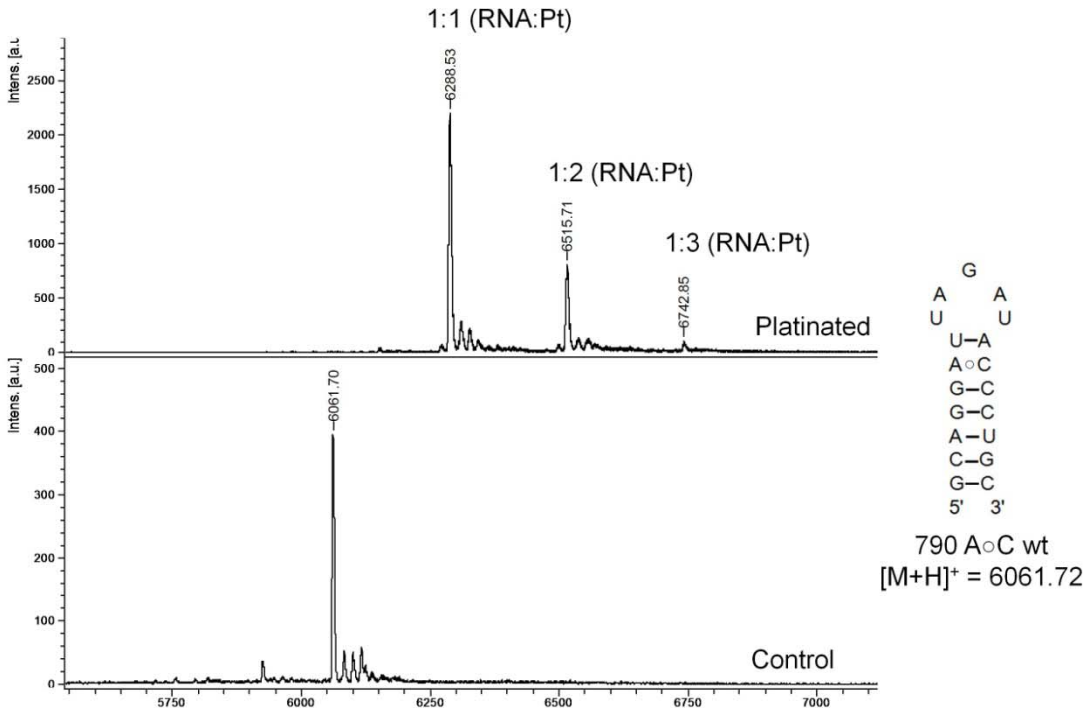

Figure 4.5. MALDI-TOF spectra of undigested control (bottom) and platinated 790 A○C wt model (top) with aquated platinum complexes (stoichiometry of 1:1, 1:2, and 1:3 RNA:Pt adduct) are shown.

Table 4.4. Calculated and observed molecular mass of various cisplatin adducts with 790 RNA model system.

Molecular ion	Calculated mass (Da) $[M+H]^+$	Observed mass (Da) $[M+H]^+$
790 A○C wt control	6061.72	6061.70
790 A○C wt + $Pt(NH_3)_2$	6290.74	6288.53 (+227)
790 A○C wt + 2[$Pt(NH_3)_2$]	6519.76	6515.71 (+(2*227))
790 A○C wt + 3[$Pt(NH_3)_2$]	6748.78	6742.85 (+(3*227))

4.4.4 Mapping the binding site with RNase T1 cleavage

In order to determine the location of the cisplatin-binding sites, both RNA samples (control and platinated) were partially digested with RNase T1. This digestion was performed to produce fragments of various lengths and molecular mass. The location of cisplatin-binding could then be localized to a specific fragment for closer analysis. Following a five-hour incubation at 37 °C of equimolar amounts of 790 RNA (A○C wt) and *cis*-$[PtCl(H_2O)(NH_3)_2]^+$, the products and control were subjected to RNase T1 cleavage. **Figure 4.6** and **Table 4.5** compare the mass spectra for the digested control and platinated 790 loop.

Three major fragments were observed in both samples and a fourth fragment was only observed in the product. The three fragments that are common to both spectra were the result of the RNase T1 digestion. The first fragment, CAGp, was identified with an observed molecular mass of 979.4 Da. whereas the second fragment, corresponding to AUUAGp, was identified with an observed molecular mass of 1615.5 Da, and the third fragment, AUACCCUGp,

contained the observed molecular mass of 2530.7 Da. The fourth fragment was observed only on the platinated sample, which corresponds to CAGGAUUAGp+ $Pt(NH_3)_2$. This is because the RNase T1 cleavage at the 3' end of guanine residues was likely blocked by a bifunctional platinum adduct at consecutive guanosine residues (residues 785 and 786). This is further supported by the fact that there is a mass peak with lower intensity at 1541.92 Da on the platinated sample, which corresponds to formation of bifunctional adduct on CAGGp.

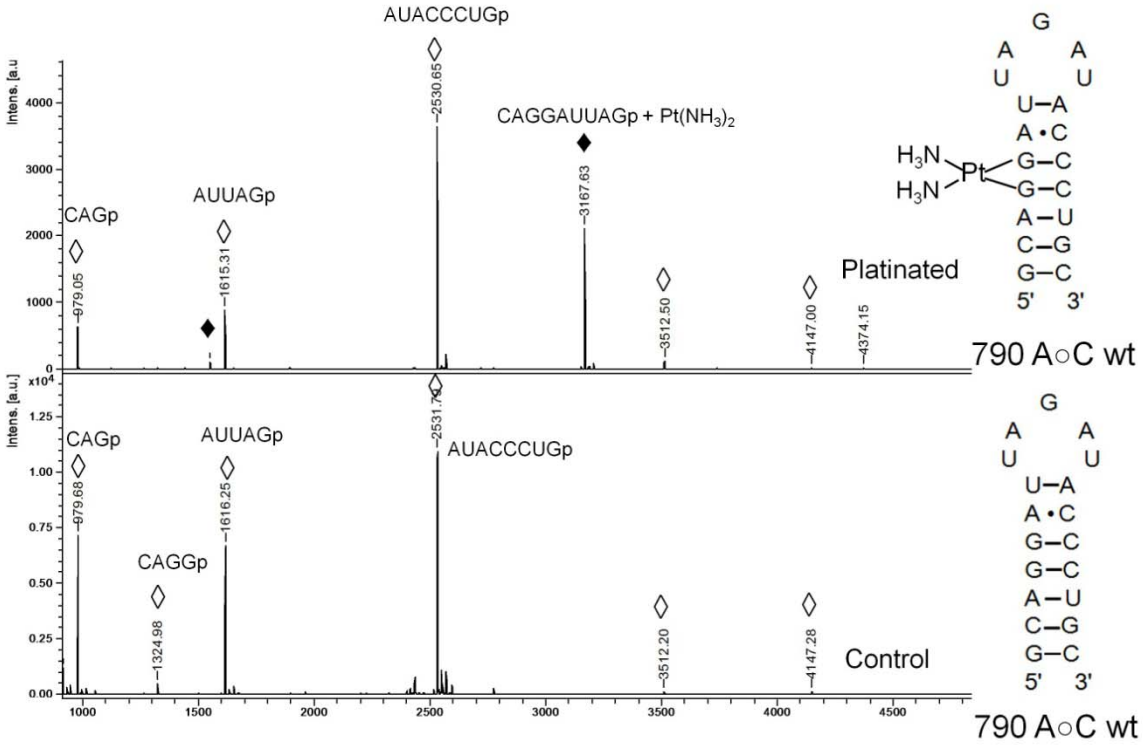

Figure 4.6. MALDI-TOF mass spectra of digested control and platinated 790 loop model (790 A○C wt) are shown. The model RNA construct, platinated (♦) and corresponding unplatinated (◊) fragments with RNA sequence are also indicated. The platinated site is shown on A○C wt (platinated) at positions G4 and G5, which is consistant with the mass data.

Table 4.5. RNA fragments, calculated and observed m/z values of 790 A○C wt are listed for the digested control RNA and platinated RNA.

RNA fragments (5' to 3')	Calculated mass (Da) $[M+H]^+$	Observed mass control RNA (Da) $[M+H]^+$	Observed mass platinated RNA (Da) $[M+H]^+$
CAGp	979.6	979.68	979.05
CAGGp	1324.81	1324.98	1541.42 [+ Pt $(NH_3)_2$]
AUUAGp	1615.96	1616.25	1615.31
AUACCCUGp	2531.51	2531.79	2530.65
CAGGAUUAGp	2940.77	-	3167.63 [+ Pt $(NH_3)_2$]
AUUAGAUACCCUGp	4147.48	4147.28	4147.00

4.4.5 Determination of number of adducts formed with 790 A○C wt hairpin

The 790 RNA (A○C wt) was reacted with a 20x excess amount of monoaquated platinum complex, *cis*-$[PtCl(H_2O)(NH_3)_2]^+$, in 10 mm phosphate buffer at 37 ºC for 5 hours. A control reaction was also prepared with a volume of H_2O equivalent to that of the cisplatin added to the other reactions. After 5 hours, the reactions were quenched with NaCl followed by freezing. Next, all reaction mixtures were dialyzed with a tubing of a MW cut off of 3.5 kDa for 30 hours in order to remove any excess unbound platinum. The concentration of dialyzed RNA samples were measured spectrophotometrically (ε = 188,800 $mol^{-1}cm^{-1}$) and 0.1 OD was used for atomic absorption spectroscopy (AAS) to determine the number of platinum atoms bound to RNA. A calibration curve prepared from known concentrations of platinum was created and platinum concentrations of the sample volumes were determined in triplicate. These values were used to

determine the number of moles of platinum present in the sample and a ratio to the number of moles of 790 RNA in the sample were calculated. When a 20x excess of aquated platinum (80 nmol) was reacted with 790 RNA (4 nmol) nearly three moles of platinum were bound to every mole of 790 model RNA construct (**Figure 4.7A**).

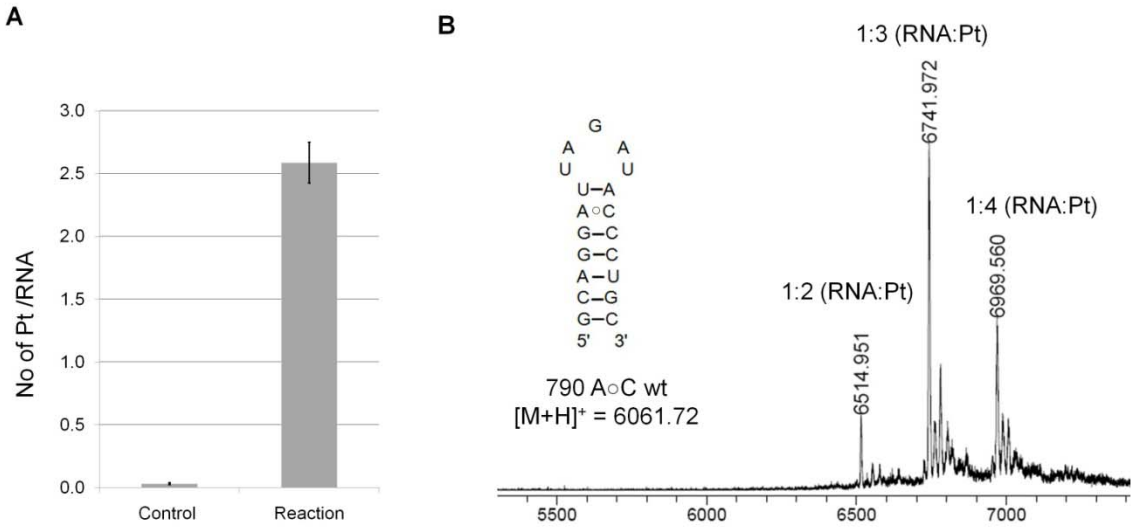

Figure 4.7. The molar ratio of the bound platinum to 790 RNA with 20x excess platinum is shown. A) Number of platinum atoms bound to each molecule of 790 construct (average of triplicate data) and B) MALDI mass spectra showing various adducts formed with excess aquated platinum complex are shown.

Further, MALDI mass spectrometry was employed to elaborate on the findings of the excess platinum reaction previously analyzed with AAS. The MALDI spectrum of the analyzed reaction with 20x excess cisplatin showed three different products as shown in **Figure 4.7B**. The major molecular ion peak at 6741.9 Da corresponds to the three platinum adducts associated with 790 construct, while the other two peaks with lower intensities, 6514.9 Da and 6969.5

Da, correspond to two and four cisplatin adducts bound to the RNA molecule. This data supports the average three platinum complexes present in 790 RNA construct determined from AAS.

4.4.6 Types of adducts

Five reactions of 790 RNA (A○C wt) with different molar amounts (1:1 to 1:5) of *cis*-$[PtCl(H_2O)(NH_3)_2]^+$ in 10 mm phosphate buffer were incubated at 37 ºC. After five hours, reactions were quenched with 2 M NaCl raising the concentration to 200 mM of NaCl and stored in the freezer. For comparison, a control reaction was also treated in a similar manner. All six reactions were treated with P1 nuclease to separate nucleotides and then CIP to remove phosphates. The concentrations of the sample volumes were determined by a UV-vis spectrophotometer and a volume corresponding to 0.1 OD was injected into the HPLC. An overlay of the resulting chromatograms showed that concentration of guanosine is decreased as the reaction ratio increases. The second major change is observed with adenosine, while the other two nucleotide concentrations remain fairly constant (**Figure 4.8A**). Quantification was carried out by Empower HPLC software and the peak areas were divided by the corresponding extinction coefficients to account for the differences in absorbance at 260 nm. The peak ratios were then normalized to the cytidine peak (**Figure 4.8B**).

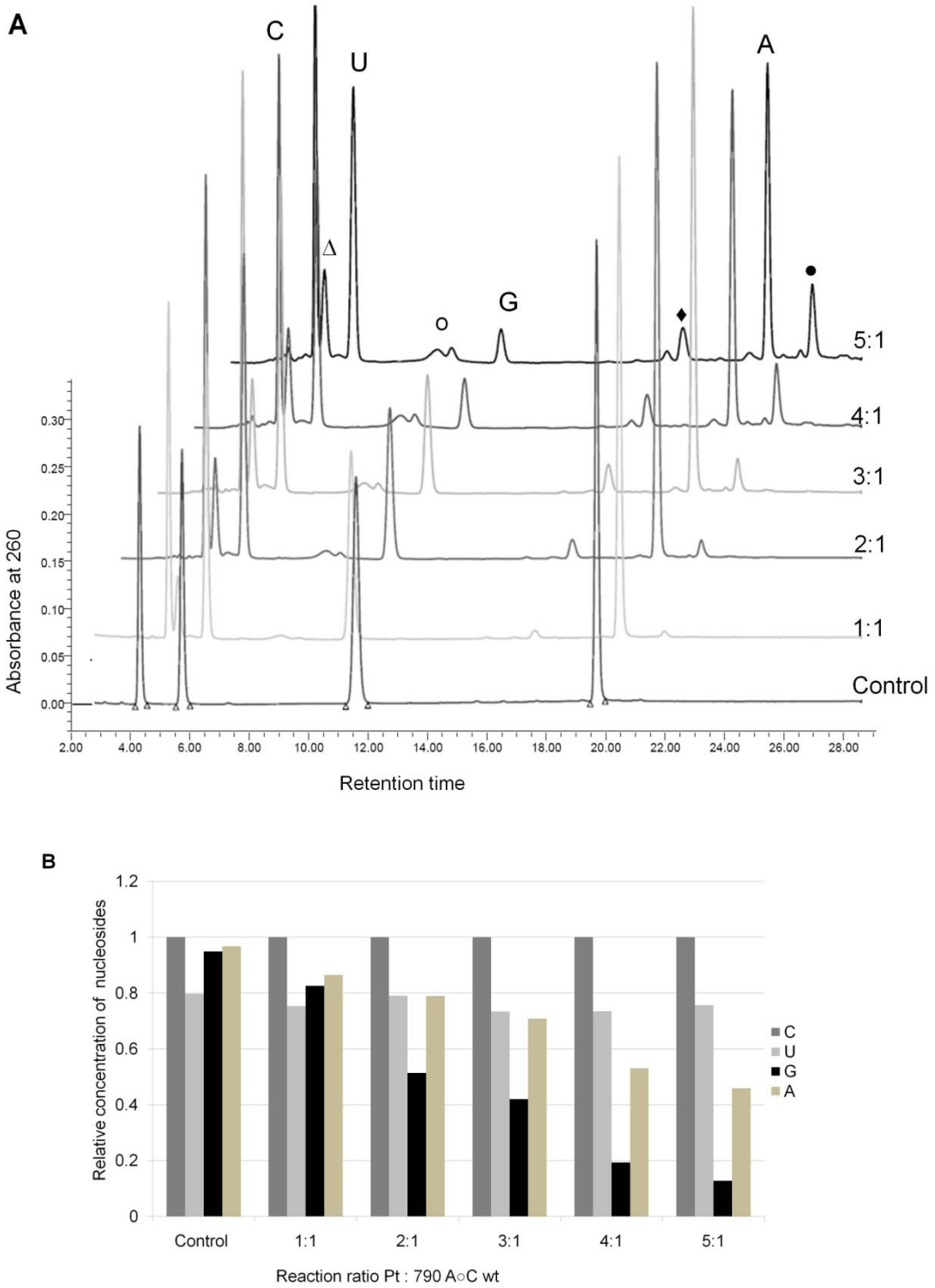

Figure 4.8. HPLC chromatograms (A) and quantification (B) of the digested 790 RNA after reaction with cisplatin is shown. A) An overlay of the HPLC chromatograms of control (digested 790 RNA) and platinated 790 RNA of different reaction ratios is shown. New peaks following platination of 790 RNA are indicated by symbols (Δ o ♦ ●). B) Relative molar concentrations of unreacted nucleosides to reaction ratios vs. relative moles are plotted (this data was collected by Christopher Lajeunesse).

Along with four standard nucleosides, several other peaks were observed in the HPLC traces. These peaks were observed to increase in intensity as the ratio of cisplain was increased in the reaction mixture. To characterize these unknown peaks, LC-MS characterization was carried out.

To identify other unknown peaks, LC-MS was carried out with an Acquity UPLC system equipped with an HSST3 (2.1 × 100 mm, 1.8 µm) C18 column. The chromatogram and mass of the corresponding peaks are shown in **Figure 4.9.** The observed and calculated masses with retention times are shown in **Table 4.6**. The major peak at retention time 0.90 min is assigned as the bifunctional adduct, GpGPt$(NH_3)_2$, with a molecular mass of 856.16 Da. Similarly, the peak at 1.60 min with mass 840.16 Da corresponds to ApGPt$(NH_3)_2$, and the peak at 1.68 min with mass 794.20 Da is assigned as GGPt$(NH_3)_2$. The peak at 2.12 min with mass 778.22 Da is assigned as AGPt$(NH_3)_2$. Along with these, two monofunctional adducts were also assigned. The peak at 1.49 min with mass 547.09 Da is GPt$(NH_3)_2$Cl and at 1.81 min with mass 531.08 Da is GPt$(NH_3)_2H_2O$. These results show that cisplatin preferentially reacts with guanosine, forming both bifunctional and monofunctional adducts.

Further, the ratio of these adduct-formations was calculated and found to be in favor of the GpG platinum adduct. The UV chromatogram from the LC-MS analysis of the 5:1 (Pt:RNA) molar ratio reaction was quantified using Mass Lynx software and **Table 4.6** shows the relative percentage of adducts present in solution. The GpGPt$(NH_3)_2$ adduct was the most prevalent adduct found in the reaction volume accounting for 35% of the total adducts found. The bifunctional

ApGPt(NH_3)$_2$ adduct contributed to the second most preferred product with 24%. This was followed by the GGPt(NH_3)$_2$ and AGPt(NH_3)$_2$ adducts with values 12% and 11%, respectively. The monofunctional adducts were not as prevailing as the bifunctional adducts, but still provided 17% of the products with GPt(NH_3)$_2$Cl accounting for 9% and GPt(NH_3)$_2$$H_2O$, 8%. The formation of the bifunctional adducts was the more preferred product by a factor of almost 4:1 in comparison to the monofunctional adducts.

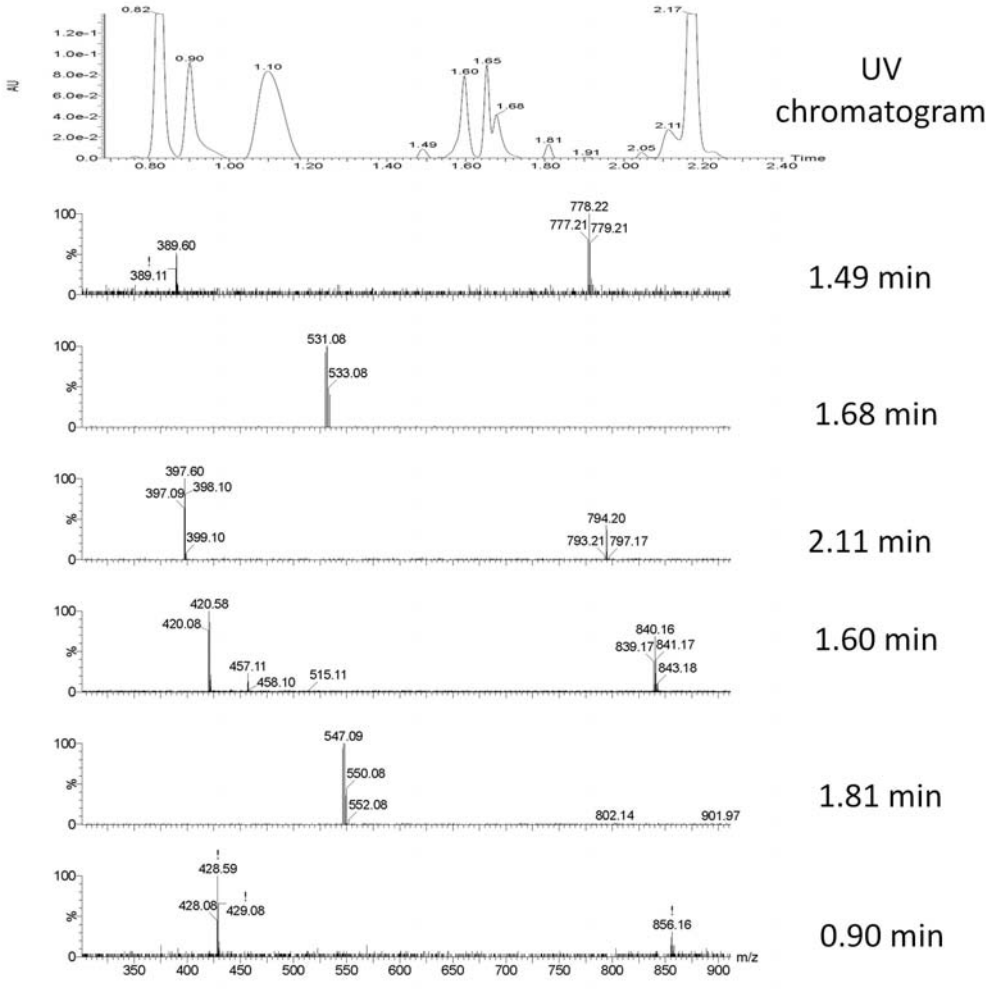

Figure 4.9. LC-MS data of digested 16S rRNA after reaction with cisplatin are shown. The chromatograms with retention times (upper) and mass spectra of the corresponding peaks (lower) are shown.

Table 4.6. Masses, retention times, and % of various adducts of cisplatin with model RNA construct.

Types of adducts	+1 charged state (Da) $[M+H]^+$		+2 charged state (Da) $[M+H]^+$		Retention time	Relative %
	Calculated	Observed	Calculated	Observed		
GpG[$Pt(NH_3)_2$]	857.15	856.14	428.57	428.59	0.96 min	35
G[$Pt(NH_3)_2Cl$]	548.08	547.09	-	-	1.49 min	9
ApG or GpA[$Pt(NH_3)_2$]	841.15	840.14	420.57	420.57	1.60 min	24
GG[$Pt(NH_3)_2$]	796.20	794.20	398.1	397.60	1.68 min	12
G[$Pt(NH_3)_2H_2O$]	531.12	531.08	-	-	1.81	8
AG or GA[$Pt(NH_3)_2$]	780.21	778.19	390.1	389.60	2.11 min	11

4.5 Discussion

The binding study with small RNA constructs has shown that *cis*-$[PtCl(H_2O)(NH_3)_2]^+$ coordinates with the 790 RNA loop preferentially at consecutive guanosines. MALDI and LC-MS data revealed that the aquated complex is capable of forming bifunctional adducts with consecutive guanine residues, as well as mono-functional adducts with single guanine residues. Results from MALDI-TOF and AAS have uncovered that more than three cisplatin molecules can bind to 790 RNA constructs, though there is only one consecutive guanosine. HPLC can be utilized to identify various types of adducts formed with RNA constructs; however, due to lack of authentic platinated standards, LC-MS was used for further confirmation.

Our work has shown that MALDI-TOF, AAS, HPLC, and LC-MS are useful for characterizing and mapping the interactions between cisplatin and the 19-nucleotide 790 RNA loop. Though HPLC has demonstrated to be effective in determining whether a reaction has occurred between cisplatin and the RNA, the information gained from this technique is limited. A high-resolution mass spectrometry technique is needed for product identification. MADLI-TOF allows for the detection of bound complexes, before or after digestion. In addition, the relative number of bound species can be obtained from the mass spectra.

In MALDI-TOF, the platinated RNA showed masses with 227 Da increments compared to the parent RNA, which is two mass units (Hs) less than would be expected from the coordination of $Pt(NH_3)_2$ (229 Da). This is due to the proton necessary to compensate for the charge of Pt^{2+} and still produce singly charged molecular ions (*267*). However, it is still uncertain whether the products are mono- or bifunctional adducts, because of less number of purines and high laser intensity used for ionization. Previously, it has been suggested that the lower mass observed with platinated-RNA complex in MALDI-TOF was the result of possible ligand loss (chlorido) during the ionization process rather than formation of a bifunctional adduct (*170*). Using the relatively soft ionization method (LC-MS), both mono- and bifunctional adducts were detected. The monofunctional adduct includes both the chlorido and aqua ligand. In LC-MS, the monofunctional adduct with one chlorido ligand was detected with a mass one Da less than calculated. In bifunctional adducts, loss of two protons was

observed with GG-Pt$(NH_3)_2$ and AG-Pt$(NH_3)_2$, whereas only one proton loss was observed with the GpG and ApG adducts.

In 16S rRNA and 790 model constructs, the preferable binding sites of aquated platinum complex were similar; mostly targeting the consecutives Gs. The similarity in type of adducts obtained from HPLC and LC-MS indicates that the 790 construct is a good model to understand the mechanism of cisplatin binding and kinetic studies. Due to the larger structure of 16S rRNA and numerous binding sites, kinetics studies are challenging; hence, the information obtained from a model system would be very useful.

The 790 loop is an ideal site for small-molecule binding studies because it is highly conserved, and extensive genetic and NMR information are also available (*247-248*). Mutational studies showed that a number of nucleotides in this loop are functionally important, and cisplatin probing study revealed this loop is accessible for small molecules. Thus, 790 loop is a promising target for antibiotic development. The kinetics and chemical probing studies in 790 model system can help us to understand the mechanism of small-molecule interactions with RNA.

CHAPTER 5

Synthesis of Amino-acid-linked Analogues of Cisplatin for Probing the Ribosome Structure

5.1 Abstract

Cisplatin has several advantages as a chemical probe to determine nucleotide accessibility in RNA structure. One advantage is the ease with which its ligands can be modified. Ammine ligands of cisplatin can be modified with various reagents to alter the size and charge of the complex. Several amino-acid-linked platinum complexes were synthesized and a binding study was carried out with a model RNA system as well as 16S rRNA. Amino-acid-linked complexes alter the reactivity with RNA by increasing the charge, size, and H-bonding potential of the ligand. Lysine- and ornithine-linked platinum complexes showed higher reactivity with AG-rich sequences and the arginine-linked complex showed reactivity mostly in the bulge and loop regions of 16S rRNA.

5.2 Introduction

Cis-diamminedichloridoplatinum (II), cisplatin, is a clinically used antitumor drug that has long been believed to react preferentially with DNA (*156, 163*). The cross-links at GG sequences are considered to be crucial for its biological activity (*156, 175*). The main coordination site of cisplatin with DNA is the N7 of guanine, and the complex forms adducts mainly at runs of consecutive Gs, with less damage at AG or GA sequences (*191, 197*). The acquired and intrinsic resistance of tumor cells to the drug has lead researchers to look for other

platinum complexes that have better chemotherapeutic applications (*268-269*). Various platinum coordination compounds are currently used as clinical anticancer drugs (*166*) and lot of effort has been made to improve the therapeutic effectiveness of platinum compounds (*181, 270*). One of the strategies to improve the effectiveness of the drug is to design complexes that interact with the target DNA in a different manner. For this purpose, numerous cisplatin analogues composed of ligands that have high affinity with DNA, such as intercalators, have been synthesized (*183, 271*). A cisplatin analogue with a tethered 9-aminoacridine-4-carboxamide showed an altered DNA sequence specificity (*272*). This compound has a higher reactivity with purines (GA sequences). The biological activity of this and related compounds was similar compare to cisplatin, and they also exhibited activity against cisplatin-resistant cell lines (*273*).

Several amino-acid-linked platinum complexes were synthesized and their activity was compared with cisplatin in various cell lines (*187-189, 274*). Other modifications include platinum complexes with charged, neutral, or hydrophobic amino acids coordinated to the platinum. These modifications increase the charge or hydrophobicity of the complex and potentially alter the binding interactions with the target. Similarly, peptide-tethered platinum conjugates were also synthesized and their interactions with DNA were studied; however, the additional functionalities in those cases did not lead to increased reactivity (*186, 190*). The uncharged compounds had lower reactivity than cisplatin and the positively charged compounds had higher reactivity than the negatively charged

compounds, which may be due to electrostatic interactions (*186*). The overall reactivity of the amino-acid platinum complexes was lower than the parental compound cisplatin; however, their interactions with RNA were not discussed in the literature, to the best of my knowledge (*186, 189-190*).

One of the advantages of using cisplatin as a probing agent is the ease with which its size and charge can be altered. Cisplatin is relatively small in size and numerous binding sites in 16S rRNA have been observed (Chapters 2 and 3). In order to reduce or alter the number of binding sites to gain more information about accessibility of the RNA structure towards various ligands, the platinum complex can be modified to contain different functionalities. Introducing charged ligands such as lysine, arginine, and aspartic acid alters the net charge of the complex; whereas, the addition of glycine or alanine would change the bulkiness and hydrophobicity of the complex compared to the cationic amino acids. Electrostatic interactions play an important role in ligand binding with RNA (*223*), and it is expected that the introduction of positive charges or hydrophobicity alters the binding site preference and reactivity. Similarly, the presence of bulky groups may reduce the number of binding sites due to inaccessibility of the target nucleotides in the folded RNA structure. Having different functionalities tethered to the platinum complex could be useful in order to probe the ribosome and discover charged pockets and/or accessibility of RNA structural motifs as potential drug target sites. In this chapter, the interaction of amino-acid-linked platinum complexes (**Figure 5.1**) with the model RNA system

and their potential as chemical probes to study the ribosome structure will be explored.

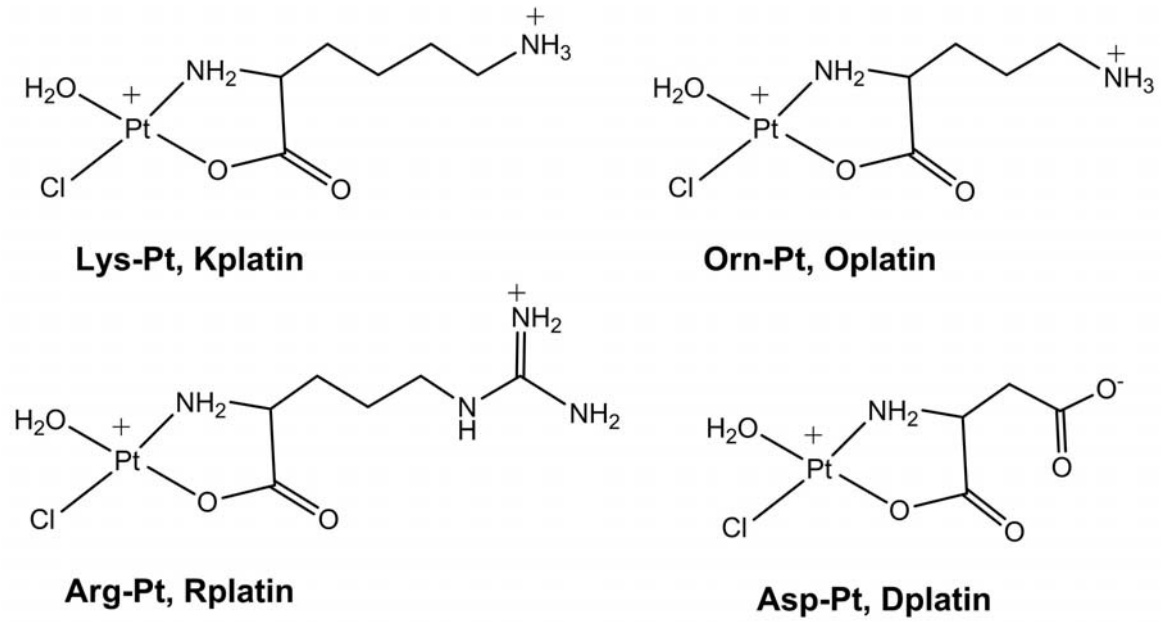

Figure 5.1. Structures of monoaquated amino-acid-linked platinum complexes used in this study are shown. Note that only one possible isomer is shown.

5.3 Materials and Methods

5.3.1 General

Potassium tetrachloroplatinate (K_2PtCl_4) was purchased from Strem Chemicals, Inc. (Newburyport, MA). L-Ornithine hydrochloride, L-lysine, L-arginine and L-aspartic acid were purchased from Alfa-Asear (Ward Hill, MA). All other chemicals and reagents were purchased from Sigma-Aldrich or Fisher, unless otherwise stated. RNase-free, distilled, deionized ddH_2O (Millipore water) was used throughout the experiments.

5.3.2 Synthesis of amino-acid-linked complexes

Amino-acid-linked complexes were synthesized as previously described in the literature (*187, 189*). For the synthesis of [*cis*-$PtCl_2$(*N,O*-Lys)], (Kplatin), K_2PtCl_4 (0.21 g, 0.50 mmol) was dissolved in 500 µl of ddH_2O in a centrifuge tube, and the solution was vortexed until the crystals were completely dissolved. In a separate tube, L-lysine monohydrochloride (0.18 g, 1.0 mmol), was dissolved in 500 µl of ddH_2O and vortexed. The pH of the amino-acid solution was measured to ensure that it was between 5.0 and 6.0. Then, both solutions were combined in a dry 10 ml round bottom flask and stirred, which produced a reddish-colored solution. The flask was attached to a reflux condenser and heated at 80 ºC for two hours, until the solution had turned a yellowish color. The solution was allowed to cool and filtered by using gravity filtration. The filtrate was transferred to a beaker and kept in dark. The crystals started to appear after 12 hours at room temperature. Yellow crystals formed over a period of 1-3 days. The crystals were collected and washed with cold ddH_2O, ethanol, and ether. The yellowish-orange crystals, [*cis*-$PtCl_2$(*N,O*-Lys)] (0.11 g, 46% yield), were dried thoroughly using a pressurized vacuum pump and the final product was confirmed and characterized by mass spectrometry and NMR spectroscopy. Electrospray MS (H_2O/methanol, positive ion): m/z found 433.99 $(M+Na)^+$. ^1H NMR (δ, DMSO): 7.6, 5.6, 4.9, 3.0, 2.5, 1.8, 1.7 ppm.

To synthesize the L-ornithine and L-arginine-linked platinum complexes, the procedure was the same as above, except 0.091 g (0.5 mmol) of L-ornithine and 0.087 g (0.5 mmol) of L-arginine were used instead of L-lysine. Oplation was precipitated as yellow crystals with a yield of 56%. Electrospray MS

(H_2O/methanol, positive ion): m/z found 419.98 $(M+Na)^+$. ^1H NMR (δ, DMSO): 7.67, 5.68, 4.91, 3.0, 2.4, 1.72, 1.6 ppm. Rplatin was obtained as light yellowish crystals with a yield of 38%. Electrospray MS (H_2O/methanol, positive ion): m/z found 462.00 $(M+Na)^+$. ^1H NMR (δ, DMSO): 7.5, 5.6, 4.8, 3.0, 2.4, 1.7, 1.5 ppm.

5.3.3 RNA and DNA

RNA corresponding to the 790 loop (5'-GCAGGAUUAGAUACCCUGC-3') of 16S rRNA was purchaged from the Keck Oligo facility (Yale University). This RNA was received with 2' protection and was deprotected by dissolving in TBAF (tetrabutylammonium fluoride), followed by incubation at 35 ºC overnight. The RNA was then desalted with a Poly-pack cartridge (Glen Research) according to the company protocol, and dried in a speed-vac evaporator. The dried RNA was reconstituted in TE buffer (10 mM Tris·HCl and 1 mM EDTA) and gel purified. DNA primers were purchased from Sigma Genosis, purified, and labelled as described in Chapter 2. The 16S rRNA was isolated from *E. coli* MRE600 and renatured as described in Chapter 2.

5.3.4 Platination reaction and primer extension

All amino-acid-linked complexes were converted to the mono-aquated form by reaction with 1:1 molar ratios of complex:$AgNO_3$, in dimethylformamide (DMF). Platinum-DMF complex stock solutions were stored at -20 °C for up to 1 week and diluted as required just prior to use. The platination reaction with model RNA and 16S rRNA were performed with monoaquated complexes. Prior to platination, model RNA and 16S rRNA was renatured as described before. The

reaction was carried out in 20 mM HEPES, pH 6.5, 20 mM K_2SO_4 and 10 mM $MgSO_4$ (buffer H) and incubated at 37 °C for 5 hours. In the model system, the molar reaction ratio was 1:1 (RNA:metal complex) and in 16S rRNA, the ratio was 1:20 (16S rRNA: complex) or 1:75 (complex: nucleotides). After the reaction, unreacted complex was removed by ethanol precipitation. To map the binding sites in 16S rRNA, primer extension was carried out as described in Chapter 2.

5.3.5 MALDI-mass spectrometry

MALDI-TOF mass spectrometry was carried out on a Bruker Daltonics in the Central Instrument Facility of the Chemistry department. The samples were reacted with cisplatin or amino-acid platinum complexes as described in section 5.3.4 and the unreacted complex was removed by ethanol precipitation. A second ethanol precipitation with ammonium acetate was carried out, and the resulting pellet was washed with 70% ethanol and dried in a speed vaccum. Finally, the samples were resuspened in ddH_2O. The concentration was measured spectrophotometrically and about 2 µl of RNA (20 pmol) was mixed with 3 µl of saturated hydroxypicolinic acid (HPA) matrix in 50% acetonitrile, and 0.5 µl of 100 mM ammonium citrate. On the MALDI plate, 1 µl of the HPA:RNA mixture was spotted. For RNase T1 digestion, 1 unit of RNase T1 was added to the remaining RNA sample and incubated at room temperature for 30 min. One µl of the digested sample was spotted on the MALDI plate. All samples were checked in the positive ion mode using method RP-3147.par.

5.4 Results

5.4.1 Synthesis of amino-acid-linked complexes

Amino-acid-linked platinum complexes were synthesized in order to react and determine the number of binding sites on RNA. Positively charged amino-acids such as ornithine, lysine, and arginine were linked to the platinum to determine the effects of altered electrostatics and bulkiness. Similarly, the platinum complex with the negatively charged amino acid, aspartic acid, was synthesized (the net charge of this complex is neutral). Amino-acid-linked platinum complexes were synthesized from potassium tetrachloroplatinate, and formations of the products were confirmed by NMR spectroscopy and mass spectrometry as described previously in the literature (*188-189*).

5.4.2 Binding studies in small RNA constructs

Amino-acid-linked complexes were converted to the corresponding monoaquated species by reacting them with $AgNO_3$ overnight. Small RNA constructs (790 A○C loop) (**Figure 5.2**) and aquated amino-acid analogues were reacted in a 1:1 molar ratio at 37 °C for 5 hrs. The reaction was quenched with NaCl and followed by freezing. The samples were ethanol precipitated to desalt and adduct formation was checked by MALDI-mass spectrometry. Mass data showed the formation of bifunctional adducts with their corresponding amino-acid-linked complexes (**Figure 5.2** and **Table 5.1**). Oplatin showed a major peak with molecular mass of 6385.1 Da, which corresponds to the +1 adduct (increased in mass of RNA by 325 Da corresponding to the control RNA) and a

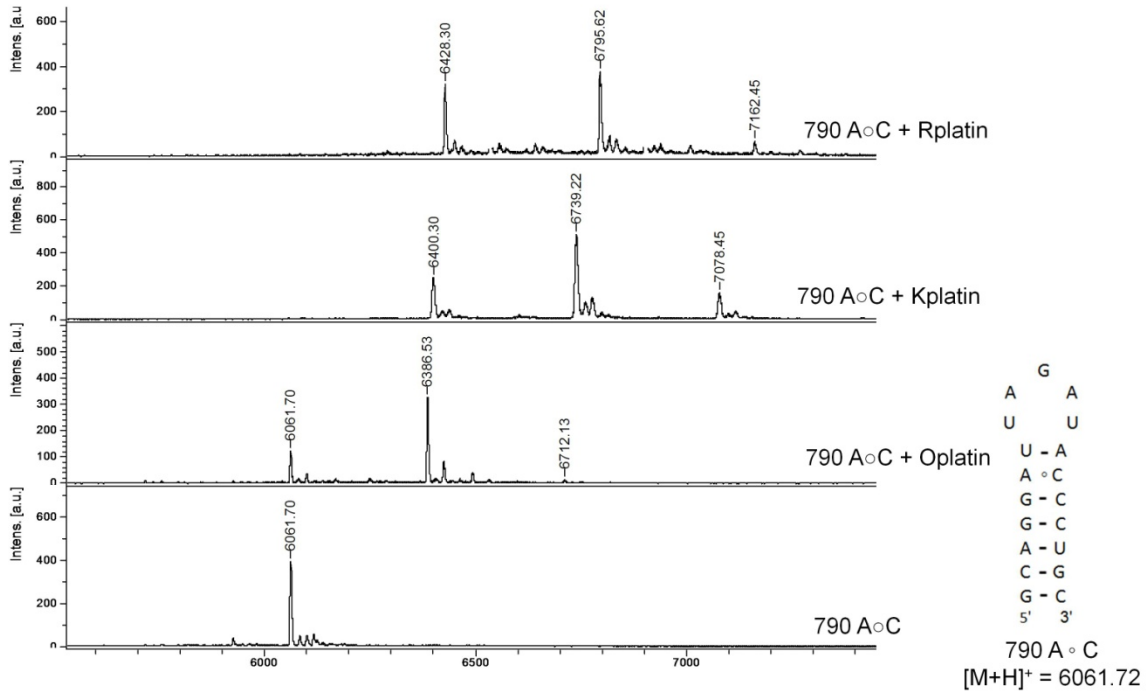

Figure 5.2. Mass spectral data of products after the reaction of amino-acid complexes with 790 A○C construct are shown. Model RNA construct (790 A○C loop) with its molecular mass is also shown.

Table 5.1. M/z values of the various adducts for RNA-Pt complexes are listed.

Complexes	RNA + Pt(amino-acid) $[M+H]^+$		RNA +2 [Pt(amino-acid)] $[M+H]^+$		RNA + 3 [Pt(amino-acid)] $[M+H]^+$	
	Calculated	Observed	Calculated	Observed	Caluclated	Observed
Oplatin	6388.7	6386.5	6715.8	6712.1	7042.8	-
Kplatin	6402.7	6400.3	6743.8	6739.2	7084.9	7078.4
Rplatin	6430.74	6428.3	6799.8	6795.6	7168.8	7162.4

minor peak at 6710.7 Da, which corresponds to the +2 adduct formation (increased in mass by 2 x 325 Da) (**Figure 5.2**). Kplatin and Rplatin showed the formation of +1 adducts with masses corresponding to 6401.6 Da (RNA + 339 Da) and 6428.0 Da (RNA + 367 Da), respectively. These complexes also showed molecular masses corresponding to +2 and +3 adduct formation with RNA (**Figure 5.2** and **Table 5.1**). Although there is only one set of consecutive guanosines in this small RNA construct, more than one bifunctional adduct was detected. Hence, other binding sites such as guanosine and/or adenosine in the loop region had to be considered. This result is consistent with an increase in mass of RNA that is equivalent to the formation of a bifunctional adduct (**Table 5.1**). Monofunctional adducts were not detected by MALDI-mass spectrometry with any of these complexes. In the MALDI spectrum, peaks of RNA showed masses corresponding to the parent RNA plus platinum complexes, with two less H's than would be expected from the attachment of a Pt(amino-acid) fragment for each adduct. This result is due to a proton transfer necessary to counterbalance the binding of a charged complex and still produce singly charged molecular ions (*267*). This result is consistent with other adduct formation such as, 4 Da less in [RNA+2(Pt-amino-acid)] and 6 Da lower in case of [RNA+3(Pt-amino-acid)]. Hence, the observed mass is 2 Da less than the calculated for each adduct formed with 790 RNA construct.

5.4.3 RNase T1 cleavage study in small RNA construct

To locate the binding site of amino-acid-linked complexes in the model RNA system, all reaction samples and controls were partially digested with

RNase T1. The fragments were analyzed by MALDI-TOF mass spectrometry (**Figure 5.3**) and compared to the control. Platinated RNA with Oplatin showed a fragment with a mass of 3266.3 Da, which corresponds to [CAGGAUUAG>p+Pt(ornithine)]. The increase in mass (325 Da) on the platinated fragment corresponds to the formation of a bifunctional adduct with Oplatin. Similarly, Kplatin and Rplatin also showed a fragment of RNA with complexes. The mass peak at 3624.9 Da with Kplatin suggested complex formation with the GCAGGAUUAG>p fragment of RNA (increase in mass by 339 Da). Rplatin also showed RNA-complex formation with a mass of 3653.7 Da (increase in mass by 367 Da) corresponding to the same fragment of RNA. No other fragments of RNA shown in **Table 5.2** contained platinum complexes. This result suggests platination somewhere on the 5' half of the 790 RNA.

The complex-bound RNA fragment contains a pair of Gs and two AG sites; hence, the exact location of the binding sites could not be identified. Several RNA fragments were observed with these complexes; however, they were slightly different than those with the parental compound cisplatin. For example, cleavage occurred at the site of consecutive Gs with RNase T1 after reaction with the Oplatin and Rplatin complexes. This result indicates a possible alternation of sequence preference by the amino-acid-linked complexes compared to cisplatin. For example, with Kplatin and Rplatin, the RNA fragment $GCAGG_{>p}$ does not contain a platinum complex; however, $GCAGGAUUAG_{>p}$ was detected with the complex, which is evidence for adduct formation in the loop region. With cisplatin and Oplatin treated samples, the RNA fragment $AUUAG_{>p}$

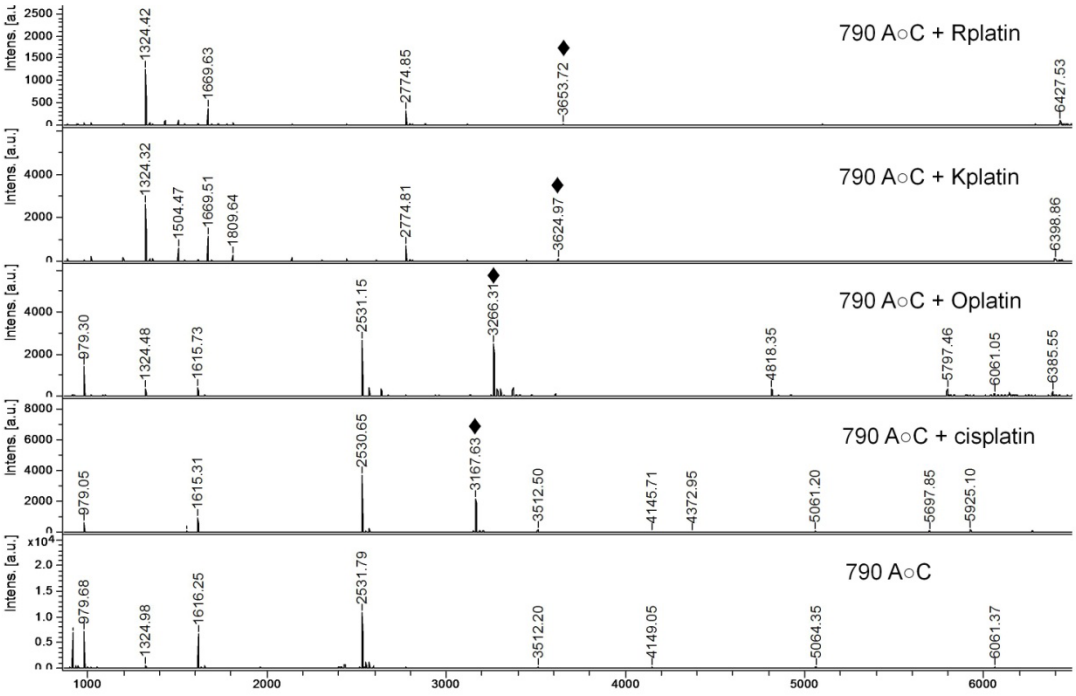

Figure 5.3. MALDI-mass spectrometry data showing the mass after digestion of 790 constructs with RNaseT1. Platinated fragments are indicated with (♦).

Table 5.2.The masses of RNase T1 fragments of 790 RNA after reaction with cisplatin and its analogues.

Fragments	Calculated mass (Da)	Observed mass of RNase T1 fragments of 790 RNA following platination (Da)				
		Control	Cisplatin	Oplatin	Kplatin	Rplatin
$GCAG_{>p}$	1324.81	1324.98	-	1324.48	1324.32	1324.42
$AUUAG_{>p}$	1615.96	1616.25	1615.31	1615.73	-	-
$GCAGG_{>p}$	1670.02	-	-	-	1669.51	1669.63
$AUACCCUG_{>p}$	2531.51	2531.79	2530.65	2531.15	-	-
$CAGGAUUAG_{>p}$	2940.76	-	3167.63 (+227)	3266.31 (+325)	-	-
$GCAGGAUUAG_{>p}$	3285.98	-	-	-	3624.97 (+339)	3653.72 (+367)

did not contain a platinum complex, and the platinated $CAGGAUUAG_{>p}$ was obtained with both complexes, suggesting adduct formation at the consecutive guanosines **(Figure 5.4).**

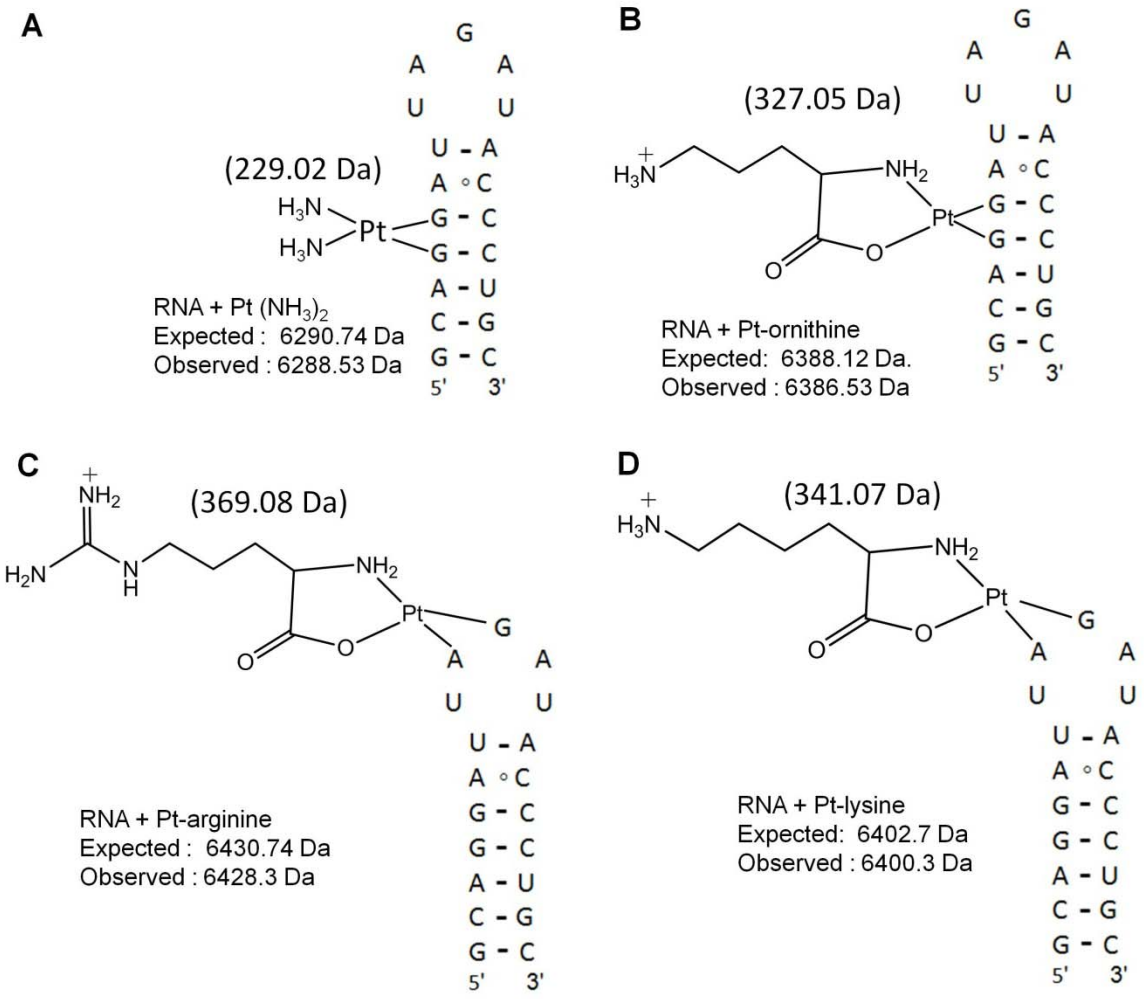

Figure 5.4. Some of the possible adducts with cisplatin and amino-acid-linked complexes with 790 RNA model system are shown. The expected and observed mass of the RNA-Pt complexes are indicated. The observed masses are 2 Da less than the expected for the bifunctional adducts, because proton transfer necessary to compensate for the positive charges.

5.4.4 Mapping binding sites in 16S rRNA by primer extension

Cisplatin and amino-acid-linked platinum complexes, after mono-aquation, were used to probe 16S rRNA. The monoaquated species contain positive charges that are different than the parental compound cisplatin, and hence, a change in reactivity was expected. The binding sites of monoaquated complexes were mapped on free 16S rRNA by using primer extension. The 16S rRNA was isolated from *E. coli* and renatured as described in Chapter 2. The reaction was carried out in 1:20 molar ratios of 16S rRNA:complex (or 1:75 molar ratios of complex:nucleotides) in 20 mM HEPES buffer, pH 6.5, at 37 °C in the dark for 5 hours. The reaction was quenched by increasing the concentration of NaCl to 200 mM, followed by freezing. The unreacted complex was removed by ethanol precipitation or dialysis. To compare the binding sites with the parental compound, several functionally important helices such as h18, h24, h27, and h28 were selected for the probing studies. Primers corresponding to these helices of 16S rRNA were used to map the coordination sites of complexes.

The magnitudes of the reactivity were classified by the intensities of the bands on the autoradiograms. The intensities of bands could be measured up to approximately 100 nucleotides from the transcription start site. Coordination sites of cisplatin and analogues were determined by comparing with a control treated in a similar manner, but lacking metal complex. The positions of the stops due to coordination of the complexes were identified by comparing with dideoxy sequencing lanes on the same gel.

The results showed clear differences in the binding sites of amino-acid-linked complexes and cisplatin (**Figure 5.5**). Cisplatin showed reactivity mostly

with consecutive Gs, or Gs in mismatched or loop regions; however, several of the consecutive Gs that showed strong reactivity with cisplatin were not reactive towards the amino-acid-linked complexes. These complexes showed quite different patterns of reactivity, mostly with the ApG sequences and in the loop regions.

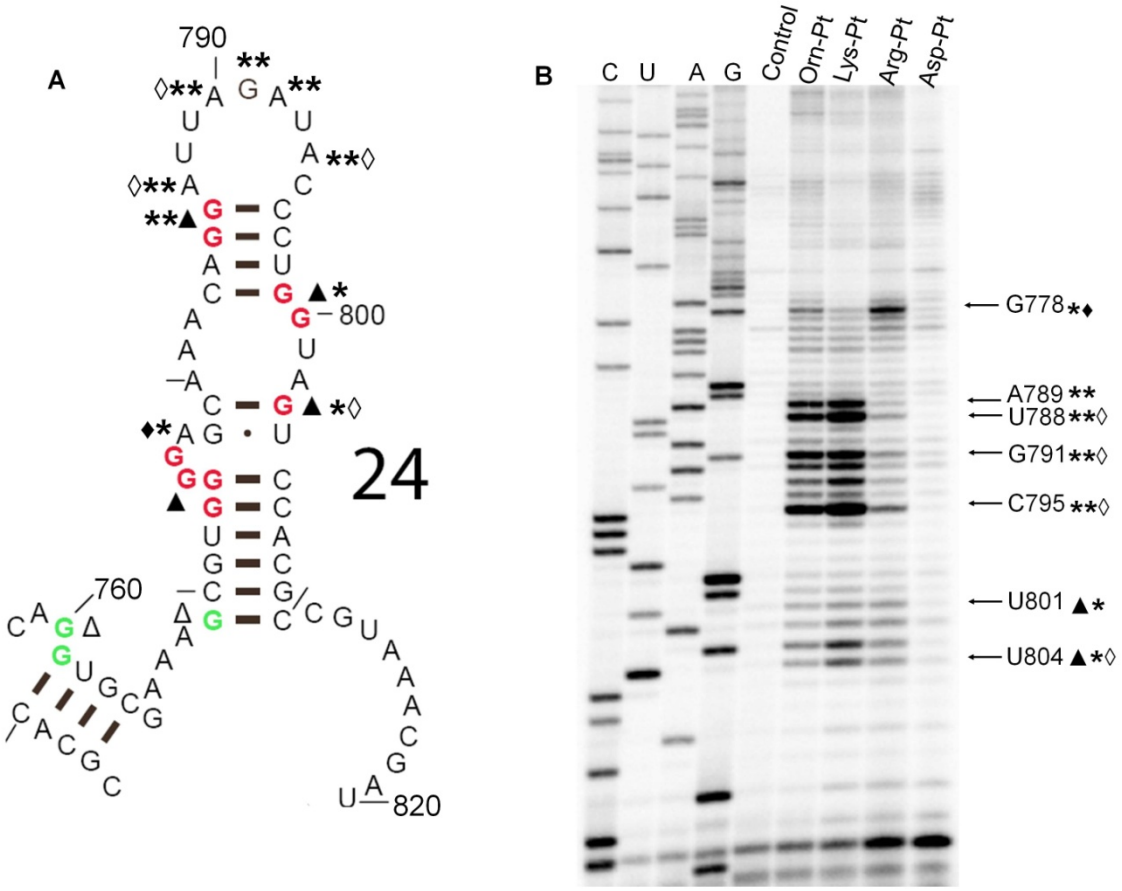

Figure 5.5. Autoradiogram of probing results with amino-acid-linked complexes corresponding to the helix 24 of 16S rRNA is shown. A) The secondary structure of 16S rRNA corresponding to helix 24 is shown. Nucleotides with strong and moderate cisplatin hits are shown with red and green, respectively. B) The autoradiogram showing the reverse transcriptase pauses or stops is presented. In the gel, C, U, A, G represent the sequencing lanes; the control is 16S rRNA lacking treatment with complexes; and other lanes contain 16S rRNA treated with corresponding complexes Orn-Pt, Lys-Pt, Arg-Pt, or Asp-Pt (complex:nucleotide is 1:75). The strong and moderate hits are indicated with arrows and corresponding nucleotide numbers. Strong hits with: cisplatin (▲), Oplatin and Kplatin (**), Rplatin (♦); moderate stops with: cisplatin (Δ), Oplatin and Kplatin (*), and Rplatin (◊).

In helix 24, the strong cisplatin-binding site observed at U801 was not present with any of the amino-acid-linked complexes; however, a number of binding sites were observed in the loop region with Oplatin and Kplatin monoaquated complexes (**Figure 5.5**). The strong stops occurred at C795, G791, and U788, which were all on the 3' side of the adenosines on the loop region. Some additional minor stops were also observed, such as at U804 and G778, which had shown strong reactivity with cisplatin. Rplatin showed strong binding site on the three-nucleotide asymmetric bulge region of helix 24. Only minor reactivity with Rplatin was observed on the sites that showed strong reactivity with Kplatin and Oplatin. The preference for adenosine residues by these complexes is highly unusual, and being explored currently in more depth by another student in the laboratory. There were no such strong stops observed with the Dplatin complex. This result indicates that electrostatics and structure are likely to be important factors for platinum complexes to interact with RNA. The strong stop that appeared at the consecutive Gs on the stem region at A787 with Oplatin and Kplatin might be the structural distortation caused by the A◦C mismatch close to it. Various other bands are observed in all lanes, including the control lane, possibly due to strong secondary structures in the RNA template that block reverse transcriptase.

Helix 18 contains several universally conserved residues and showed reactivity with the parental compound cisplatin, such as consecutive Gs at residues 540-542 and 529-530; however, the amino-acid metal complexes showed different sequence selectivity (**Figure 5.6**). Instead of a strong hit

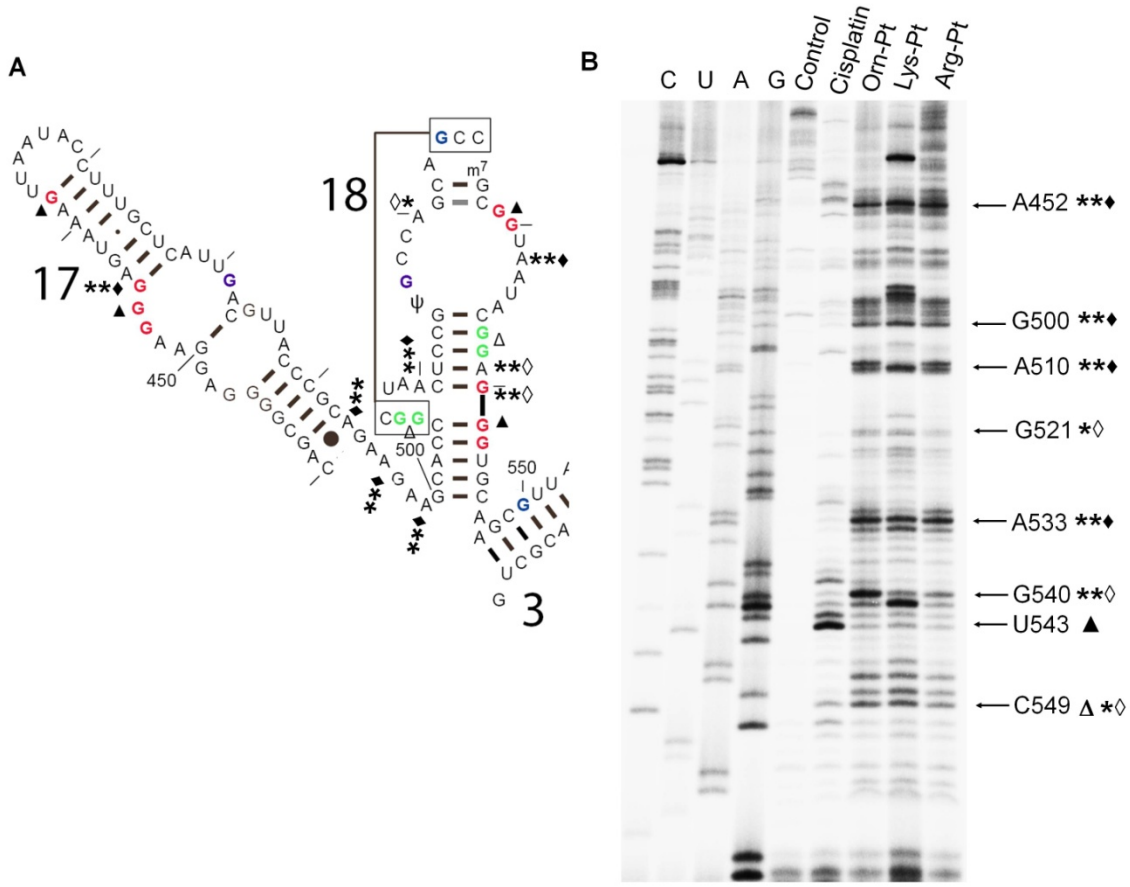

Figure 5.6. Autoradiogram of probing results with amino-acid-linked complexes at helix 17 and 18 of 16S rRNA are shown. A) The secondary structure of 16S rRNA corresponding to helix 17 and 18 is shown. Nucleotides with strong and moderate cisplatin hits are shown with red and green, respectively. B) The autoradiogram showing the reverse transcriptase pauses or stops is presented. In the gel, C, U, A, G represent the sequencing lanes; the control is 16S rRNA lacking treatment with complexes; and other lanes contain 16S rRNA treated with corresponding complexes Orn-Pt, Lys-Pt, Arg-Pt, or Asp-Pt (complex:nucleotide is 1:75). The strong and moderate hits are indicated with arrows and corresponding nucleotide numbers. Strong hits with: cisplatin (▲), Oplatin and Kplatin (**), Rplatin (♦); moderate stops with: cisplatin (Δ), Oplatin and Kplatin (*), and Rplatin (◊).

present at U543 before the consecutive Gs, it appeared on the 3' side of A539, which is present between the two sets of consecutive Gs, indicating possible cross-links at the ApG sequence. Interestingly, this stop was strong with Oplatin and Kplatin, although the intensity was shifted by one nucleotide, and did not show strong reactivity with Rplatin. Another strong stop appeared at A533, which was also found one nucleotide prior to the cisplatin stop site. A number of other strong stops appeared at A510, G500, and A452, which were all different than the stops observed with the parental compound cisplatin. These stops are on the 3' side of an ApG sequence on the RNA. From 490 to 500, there are three pairs of consecutive ApG, which all showed strong reactivity with the cationic amino-acid complexes.

The binding sites of amino-acid platinum complexes were also mapped on helices 27 to 31 (**Figure 5.7**). As observed in other regions, the stop sites were mostly at ApG sequences. A number of sites with consecutive Gs did not show reactivity with the amino-acid complexes, such as G953, G942, G927, and U904 (stops with cisplatin). Residue A946, before the consecutive Gs, showed moderate reactivity with these analogues. One similarity with the parental compound was observed at G885, which was a strong hit on free 16S rRNA, 30S subunits, and the 70S ribosomes. Several sites with consecutive adenosines were also not reactive towards these complexes indicating that a neighboring guanosine is required for the adduct formation at these sites.

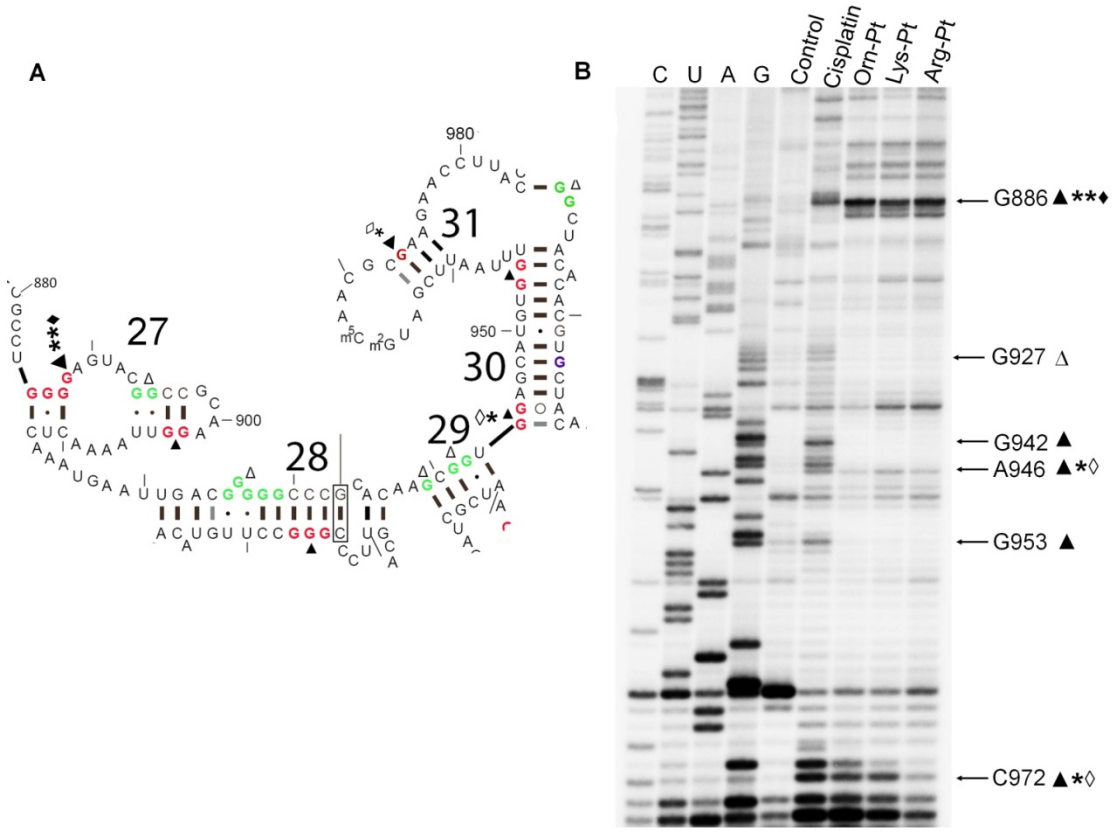

Figure 5.7. Autoradiograms of probing results with amino-acid-linked complexes and helices 27 to 31 of 16S rRNA are shown. A) The secondary structure of 16S rRNA corresponding to helix 27 to 31 is shown. Nucleotides with strong and moderate cisplatin hits are shown with red and green, respectively. B) The autoradiogram showing the reverse transcriptase pauses or stops is presented. In the gel, C, U, A, G represent the sequencing lanes; the control is 16S rRNA lacking treatment with complexes; and other lanes contain 16S rRNA treated with corresponding complexes Orn-Pt, Lys-Pt, Arg-Pt, or Asp-Pt (complex:nucleotide is 1:75). The strong and moderate hits are indicated with arrows and corresponding nucleotide numbers. Strong hits with: cisplatin (▲), Oplatin and Kplatin (**), Rplatin (♦); moderate stops with: cisplatin (Δ), Oplatin and Kplatin (*), and Rplatin (◊).

5.5 Discussion

The amino-acid-linked platinum complexes were synthesized and a binding study was carried out with a short RNA model system, as well as full length 16S rRNA. In both RNAs, differences in reactivity and binding-site preference of these complexes compared to the parent compound cisplatin were observed. The amino-acid-linked complexes in the model RNA system (790

RNA) showed the formation of more than one adduct indicating possible coordination at sites other than Gs. The model RNA contained only one site with consecutive Gs; hence, the strong mass signal with bis-adducts indicates the altered binding preferences of the cationic amino-acid complexes. The RNase T1 cleavage experiments could not be used to locate the exact binding sites, but showed evidence that an adduct might have formed on a sequence containing many Gs. Probing studies on 16S rRNA showed that the binding-site preferences for Oplatin and Kplatin complexes were quite similar, mostly at AG sequence in the loop or bulge regions. This result was not surprising, because these two amino-acid complexes differ only by a CH_2 group and each contains a single positive charge. Rplatin showed differences in reactivity compared to the other two cationic analogues, such as a stronger binding preference for nucleotides in the bulge or loop regions. The presence of the amino-acid ligand on these complexes leads to increased bulkiness of the *cis*-ligand and introduced an additional positive charge to the complex relative to the cisplatin; which, in turn, altered the interactions with the negatively charged RNA. The negatively charged amino-acid complex, Dplatin, did not show any significant reactivity compared to the cationic complexes at the same reaction ratio, leading to the likelihood that electrostatic repulsions prevented a favorable reaction with RNA.

Previously, the binding sites of Kplatin were mapped on an 82-bp DNA fragment by exonuclease (*274*). This mapping study revealed that Kplatin induced a significant stops at all d(ApG) and d(GpG) sites in DNA. It had no apparent preference for d(GpG) over d(ApG)sequences. The authors of that

study also observed stops at other polypurine sequences, which were presumed to be monofunctional adducts. In this study, a similar result was observed with RNA. Most of the ApG sequences showed strong reactivity with Oplatin and Kplatin, whereas a number of GpG sequences did not show any reactivity. In contrast, Rplatin reactivity was different from the other complexes. Rather than being sequence selective, it showed a structural preference for reactivity, such as three nucleotide bulges or in the loop regions. This might be the result of the charge and larger size when compared to Oplatin and Kplatin. The reactivity of Rplatin at the internal bulge on helix 24 is quite similar to the TAR-Tat interaction in which the three-nucleotide bulge of TAR RNA is recognized by the arginine-rich Tat protein (*275*). Arginine is an ideal RNA-binding molecule because of its positive charges, planar hydrogen-bonding patterns, and stacking interactions with the bases (*223*). It has been observed that molecular contacts with RNA occur at the bulge sites because they are more accessible to the ligand (*223, 276*). In crystal structures of the ribosome, it is not as obvious as in the case of TAR RNA, but this interaction might be favorable due to a structural distortion caused by the presence of the asymmetric bulge in 16S rRNA.

Another factor for coordination is the charge present in these complexes. Electrostatic interactions and local accumulation of cationic concentration determines the product formation. The amino-acid-linked complexes might increase the local concentration differently than the parental compound due to charge and hence, the binding sites are also different. The number of binding sites of amino-acid-linked complexes is higher than parental compound cisplatin;

however, Rplatin showed less number of hits in helix 24. In addition, the binding sites are also altered, which indicates that more factors must be involved than just electrostatic interaction. Previous studies showed that cisplatin preference for guanine is due to a strong hydrogen bond between the amine-hydrogen of cisplatin and the O=C6 moiety (**Figure 5.8**) (*196*) . In adenine, comparatively weaker hydrogen bond forms between amine-hydrogen of cisplatin and the H_2N-C6 group. In addition, significantly stronger molecular orbital interaction was also observed for guanine compared to adenine (*196*). The alternation of binding preference for amino-acid-linked complex is not very clear; however, the presence of NH_2 group in adenosine might influence hydrogen bonding in the transition state, which results in preference for coordination with amino-acid-linked complexes over cisplatin.

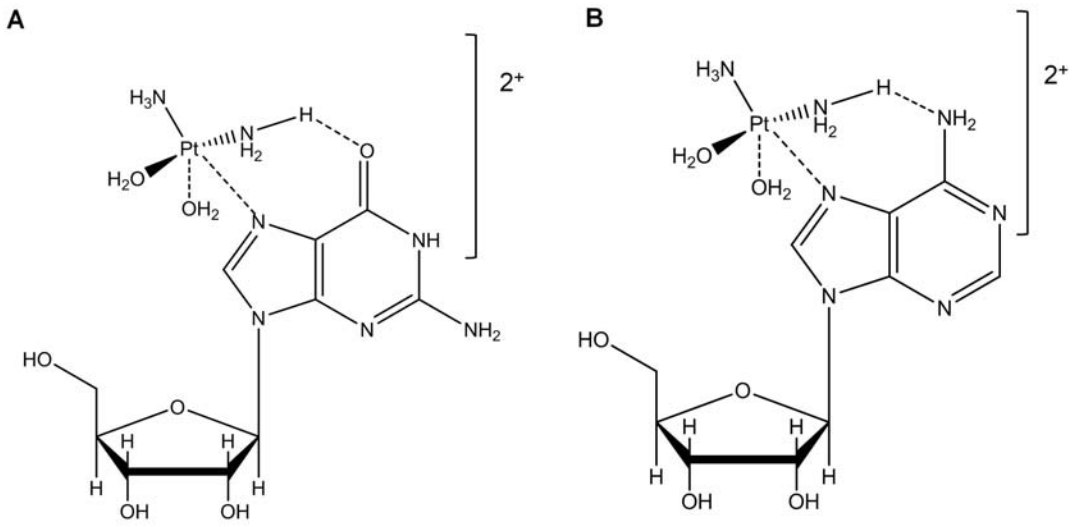

Figure 5.8. Possible transition state for the formation of cisplatin adducts with guanosine and adenosine is shown.

The altered binding preferences of these complexes are highly unusual and further studies will be needed to understand the sites of interaction and types of adducts formed. Previously, several platinum complexes have been made in an attempt to alter the sequence specificity of cisplatin on DNA (*269, 277*). The minor groove binder distamycin was linked with cisplatin with the expectation that it would change the binding mode, but this approach was unsuccessful (*277*). One successful alteration of cisplatin binding sites was made by Bierbach and coworkers with the monofunctional platinum-acridinylthiourea conjugate, or Pt-ACRAMTU, intercalators (*278*). They were able to increase sufficiently the product formation with AT-rich regions in the DNA sequence. However, these complexes were not studied with RNA to the best of my knowledge.

Small molecules that bind to DNA or RNA in a sequence-specific manner have potential applications in cancer chemotherapy. In DNA, purine nitrogens are susceptible to covalent modifications both in the major and minor grooves. In the major groove, the most reactive site is guanine N7, while the N3 positions of adenine and guanine are mainly attacked by nucleophiles in the minor groove (*279*). The sugar edge of RNA is comparatively wider and shallower than the Hoogsteen edge; hence, ligands can interact through the sugar edge in RNA. The amino-acid-linked platinum complexes, due to their larger size compared to the parental compound, may be able to access RNA through the sugar edge, hence the preference would be for adenosine.

In conclusion, amino-acid-linked complexes cross-link to RNA with different sequence specificity than cisplatin, preferably to ApG; therefore, the

accessibility of adenosine in the 16S rRNA could be monitored. The higher reactivity of Rplatin to the bulge or loop can give more information about accessibility to RNA motifs for ligand binding. In addition, the charge present in these complexes would be useful for monitoring the kinetics and interpreting how small charged molecules find their target sites. To understand the mechanism of action, however, further studies will be needed.

CHAPTER 6

Targeting non-Hodgkin's Lymphoma with siRNA Mediated through Liposomes

6.1 Abstract

Non-Hodgkin's lymphoma (NHL) is a cancer of the lymphocytes, which is a significant cause of mortality in the United States. As a treatment for NHL, we propose reducing expression of the associated protooncogene c-myc using siRNAs. We first incorporated siRNAs into liposomes to improve drug delivery. Then, we attempted to purify an antibody fragment (scFv) that specifically recognizes CD20-positive NHL cancer cells. Our preliminary data suggest that this is a promising strategy.

6.2 Introduction

Non-Hodgkin's lymphoma (NHL) is a cancer that starts in lymphocytes and can occur at any age. There are various types of non-Hodgkin lymphomas, but they are mainly divided into two types: aggressive (fast growing) and indolent (slow growing) (*280*). Out of various types of lymphomas, B-cell lymphoma is the most common in the United States (*281*). The National Cancer Institute estimated 65,540 new cases and 20,210 deaths from non-Hodgkin's lymphoma in the United States in 2010 (*282*).

6.2.1 Non-Hodgkin's lymphoma and c-myc

MYC regulates over 15% of all cellular gene expression and is involved in almost every aspect of cell biology (*283*). MYC contributes to the regulation of various genes including those involved in cell-cycle progression, protein biosynthesis, cell growth, and metabolism (*283-284*). The c-myc proto-oncogene is activated in a number of human tumors (*283*). In a normal cell, expression of the c-myc gene is under exquisitely fine control, and translocations in the B cell activate the c-myc gene and promote lymphoid malignancies (*285*). In cells affected by aggressive B-cell lymphomas, known as Burkitt lymphoma (BL), there is an arrangement of the c-myc oncogene, usually associated with a t(8;14) translocation (*286*). In addition, point mutations in the coding sequences of c-myc have been observed (*287*). The consequence of mutations is a negative regulation of c-Myc activity. In composite lymphoma, both the low (not aggressive) and high-grade (aggressive) components have an identical rearrangement of bcl-2; however, only the high-grade component has a c-myc oncogene rearrangement (*288*).

6.2.2 Targeting non-Hodgkin's lymphoma with siRNA

Small-interfering RNAs (siRNA) suppress gene expression by a process called RNA interference (RNAi) (*22, 289*). RNAi is a highly regulated enzyme-mediated process by which sequence-specific siRNA selectively targets and cleaves complementary mRNA (*290*). Long pieces of double-stranded RNA are cleaved by Dicer into small fragments of RNA (21 nucleotides), called siRNAs (*291*). Small-interfering RNAs can be directly introduced into the cell, thus

bypassing the Dicer mechanism (**Figure 6.1**) (*292*). In the cytoplasm, siRNA is incorporated into a protein complex called the RNA-induced silencing complex (RISC) (*293*). Argonaute 2, present in the RISC complex, unwinds the siRNA and cleaves the sense

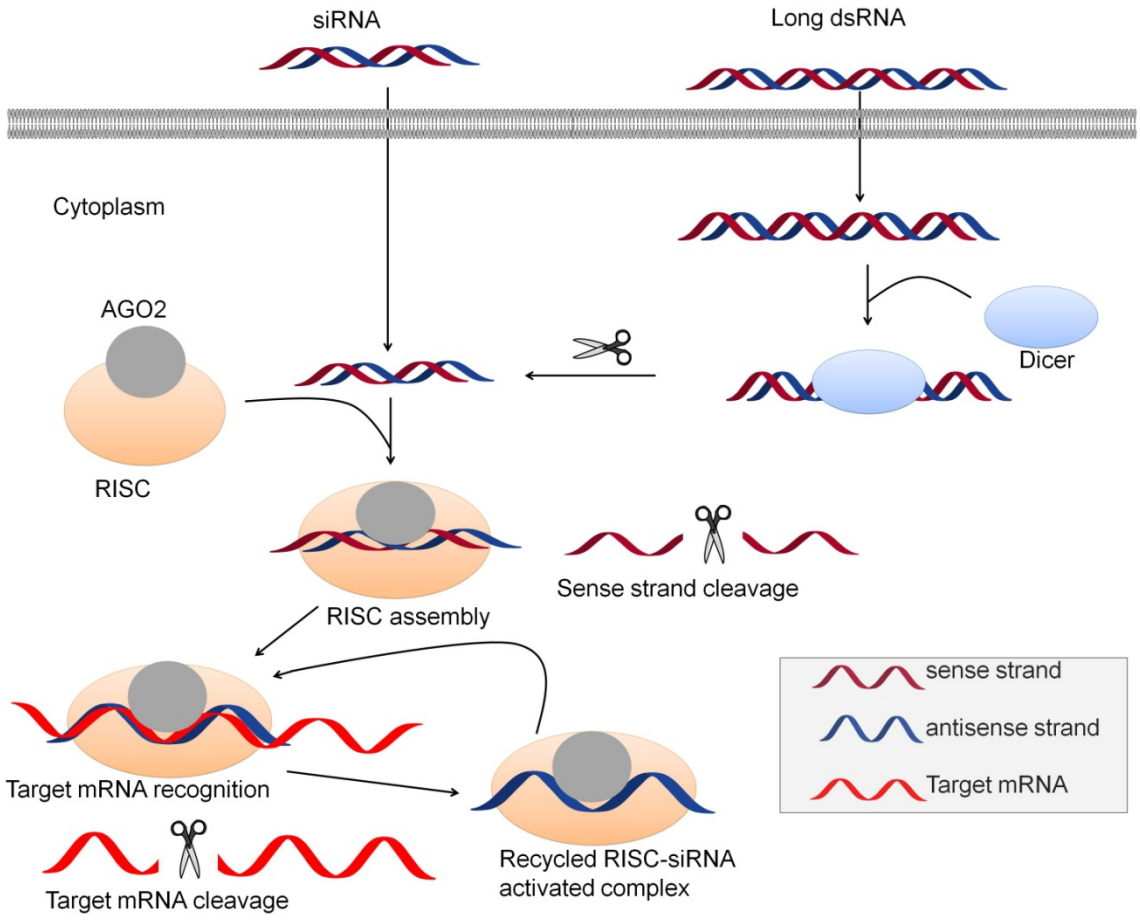

Figure 6.1. The mechanism of RNA interference is shown (*292*). Long double-stranded RNA (dsRNA) is cleaved by the enzyme Dicer into small-interfering RNA (siRNA). siRNA can be directly introduced into the cell by various methods. The siRNA is incorporated into the RNA-induced silencing complex (RISC), which results in cleavage of the sense strand and activation of siRNA-RISC complex. This activated complex binds to the targeted mRNA and degrades it, which causes silencing of the gene and reactivation of the siRNA-RISC complex.

strand (*294*). The activated RISC containing the antisense strand selectively degrades the complementary mRNA (*295*). After cleaving one mRNA strand, the activated RISC complex can then move on to destroy additional mRNA targets until siRNAs are diluted below the threshold concentration or degraded within the cell (*292, 296*). In theory, appropriately designed siRNAs can be used to silence any gene in the body. It has been shown that siRNA can be used to knock down targets in a number of diseases *in vivo,* such as liver cirrhosis (*297*), hepatitis B virus (*298*), human papillomavirus (*299*), ovarian cancer (*300*), and bone cancer (*301*). Since higher expression of c-Myc has been observed in non-Hodgkin's lymphoma, siRNA specifically designed to target c-myc mRNA in NHL cells would be useful. For clinical purposes, however, a safe and effective delivery system is essential.

The major challenge of siRNA therapy is to find an efficient delivery method to the intended target to minimize side effects. This approach is challenging due to off-target effects, aggregation with serum proteins, poor cellular uptake, and enzymatic degradation by nucleases (*292, 302*). To overcome these difficulties, a number of drug-delivery vehicles have been used, including liposomes, nanoparticles, synthetic polymers, carbon nanotubes, dendrimers, and polypeptides (*303-305*). Out of these, liposomes are used quite often because of their low toxicity and efficient cellular uptake.

6.2.3 Drug delivery vehicles

Liposomes are small, spherical, artificially prepared vesicles consisting of a lipid bilayer with an internal aqueous compartment (*304*). When phospholipids

are hydrated, they spontaneously form an internal aqueous environment surrounded by a phospholipid bilayer membrane. Liposomes, which can be prepared from cholesterols, glycolipids, sphingolipids, and long chain fatty acids, are good carriers for a variety of molecules such as drugs, nucleic acids, and proteins (*306*). The work of Bangham and coworkers about 40 years ago revealed that phospholipids can form liposomes in aqueous solution (*307*), and this versatile method has been applied to biology, biochemistry, and medicine. This discovery is very important because liposomes are excellent carriers for delivering specific compounds to targets of interest. Preferred site targeting with liposomes can be achieved by the attachment of an antibody or appropriate fragments that specifically recognize the receptors present on the cells (*308-309*). Liposomal drug delivery has several advantages such as enhanced drug solubilization, protection of sensitive drugs, enhanced uptake, and altered bio-distribution (*309*).

Liposomes are of many different sizes and shapes (*310*). Small-sized liposomes called small unilamellar vesicales (SUVs) are usually 100 nm in diameter. Larger-sized liposomes (200-800 nm) are classified as large unilamellar vesicles (LUVs), and multilamellar (MLVs) range in sizes from 500-5000 nm and consist of several concentric bilayers (*309-310*). There are several methods for synthesizing liposomes including sonication, detergent dialysis, mechanical mixing, freeze-thaw, and solvent evaporation (*309-310*). Unequal vesicle sizes, low yields, uneven size distribution, and inconsistent encapsulation efficiencies are the major problems associated with these methods. It is essential

to generate liposomes with uniform size and distribution for therapeutic applications and to overcome these problems, a high pressure technique was used to prepare them (*311*). Liposome extruders use high pressures, approximately 200-800 lb/in^2, and small-pore-size (~100 nm) membranes to generate relatively uniform vesicles. Membranes with different pore sizes can be utilized to generate liposomes of various sizes (*310-311*). Hence, the extruder can be utilized to generate either SUVs or LUVs. The advantages of this method include relatively rapid liposome preparation and potentially high encapsulation efficiencies.

The application of liposomes has considerably expanded over the years. It is now possible to engineer a wide range of liposomes with various sizes, phospholipid compositions, and surface morphologies for increased therapeutic potential (*304*). In addition, biocompatibility and targeted delivery are important advantages of liposomes (*312*). Liposome encapsulation can also be used to increase delivery of hydrophilic drugs or oligonucleotides that often have difficulty crossing the cellular membrane. After entrapment, the drug does not interact with the lipid bilayer of a cell. In contrast, the liposome interacts favorably with the natural lipid and is embedded into the cellular membrane. A liposome can release the entrapped drug after its integration into the cellular membrane or by the mechanism of endocytosis (*304, 312*). Liposomes constitute an effective carrier of siRNA for *in vivo* delivery; when incorporated into a liposome, they are protected from nuclease degradation, which increases the half life and potency of RNA (*313*).

To increase the target specificity, at least three criteria need to be considered (*313*). First, the drug-delivery vehicle, such as a liposome, should reach and deliver theraupetic agents to the target cells. Second, the targeted mRNA should be preferentially expressed in tumor cells. Third, the carrier and siRNA should both eventually degrade. Targeting and selectively delivering siRNA to tumor cells in liposomes is an attractive therapeutic strategy. Cancer cells can be specifically targeted because many express unique antigens that are not available in normal cells.

To study non-Hodgkin's lymphoma, a human B-cell line (WSU-FSCCL) was used, which was established from peripheral blood of a patient (*314*). B cells express a wide variety of cell-surface antigens, such as CD20, throughout their development. B-cell-specific, cell-surface antigen CD20 is an appropriate target for therapeutic monoclonal antibodies (*315*). It is expressed at most stages of B-cell development. Our collaborators (Ayad Al-Katib and coworkers) have engineered an antibody fragment (scFv) and GPI (glycosylphosphatidylinositol)-tagged scFv by cloning VH and Vn regions from a widely available mouse hybridoma (HB-9645) directed against human CD20 (*308*). Previous studies showed that when this GPI-tagged scFv has been loaded onto the surface of sheep erythrocytes (E^{sh}), it specifically forms rosettes with CD20-bearing tumor cells (*308*). In this study, we are extending this study to target specifically the CD20-positive cancer cells with siRNA.

6.3 Objectives

siRNA has been widely used for silencing the oncogenic genes; however, the major challenge with siRNA is selective delivery to specific target cells (*292*). To achieve this we will use the newly engineered antibody fragment (scFv) to deliver liposome-encapsulated cytocidal agents to specific cancer cells. This antibody fragment can also be utilized for cell imaging using quantum dots or fluorescent tags packed into liposomes. Hence, the main goal is to generate a complex with siRNA, liposome, and antibody that would specifically target c-myc mRNA in NHL cells (**Figure 6.2**).

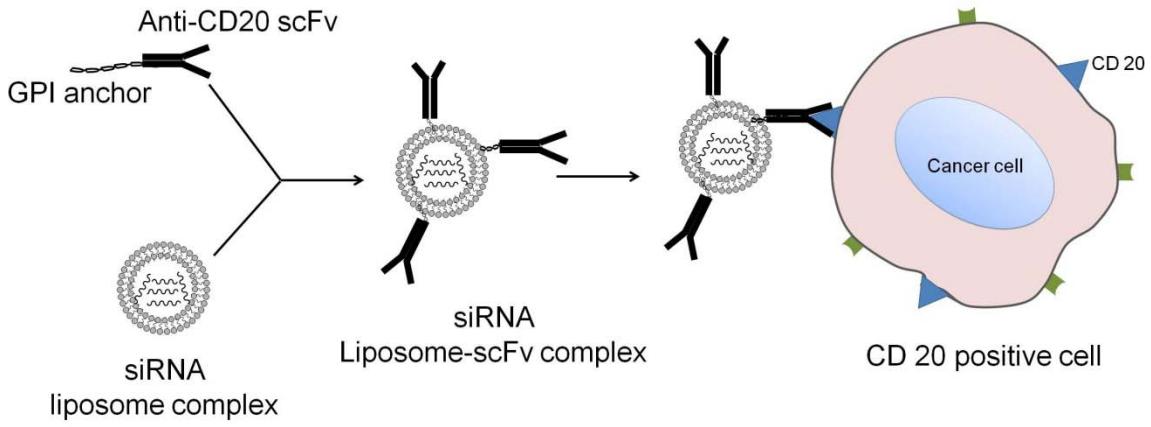

Figure 6.2. Overview of targeting CD20-positive cancer cells by siRNA-GPI-scFv-liposome complex is shown.

6.4 Materials and Methods

6.4.1 General

Lipids were purchased from Avanti Polar Lipids, Alabaster, AL. The extruder was obtained from LipexTM Extruder, Vancouver, BC, Canada.

Polycarbonate filters (0.1 μm) were purchased from Osmonics, Inc., Minnetonka, Minnesota. Sepharose 4B was purchased from Sigma. siRNAs were purchased from the Keck Foundation, School of Medicine, Yale University, CT. γ-^{32}P-CTP was obtained from Perkin Elmer Life Sciences, Inc. Boston, MA. RPMI and Express Five SFM culture media were obtained from Invitrogen Corp. Primary antibody (HA.11 MoAb) was purchased from Covance, Princeton, NJ and seconday antibody (goat anti-mouse HRP conjugate) was obtained from Santa Cruz Biotechnology, Santa Cruz, CA. Other chemicals and buffers were purchased from Sigma Chemical or Fisher. Sterilized ddH_2O was used for all experiments.

6.4.2 RNA purification and labeling

The siRNA obtained from Keck Foundation was deprotected, desalted and purified by polyacrylamide gel electrophoresis. Deprotection was carried out in TBAF (tetrabutylammonium fluoride) at 35 °C overnight. After deprotection, the RNA was desalted using poly pack (II) cartridges using 100 mM TEAA (triethyl amine acetate), pH 7.4. For the labeling and cell growth inhibition study, RNA was purified by polyacrylamide gel electrophoresis followed by ethanol precipitation. The trace amounts of organic reagents that may have been present in RNA were removed by ether extraction. In order to monitor the stability of RNA in buffer and media, the 3' end of the RNA was labeled with γ-^{32}P-CTP. The PAGE-purified siRNA, 2 μl (25 pmol/μl), 5 μl of T4 RNA ligase buffer, and 41 μl of ddH_2O were added to a centrifuge tube. The solution was mixed gently and centrifuged, 1 μl of γ-^{32}P-CTP and 1 μl of T4 RNA ligase (10 units) was added.

The solution was incubated for 4 hours in ice. After the incubation, the contents of the labeling tube was quenched with ammonium acetate, added to a Sephadex G-25 column, and centrifuged for 2 min at 3,000 rpm to remove excess CTP. The radioactivity of the sample was measured using a scintillation counter.

6.4.3 Lipid mixture preparation

Lipids were brought to room temperature in desiccators just prior to weighing. First, 11 mg of cholesterol (294.1 g/mol, 28.4 µmol), 26.2 mg of DPPC (734 g/mol, 35.6 µmol), 10.4 mg of DODAP (684.5 g/mol, 16.2 µmol), and 0.6 mg of DPPE (692 g/mol, 0.8 µmol) were weighed and transferred to a tube. After that, 500 µl of $CHCl_3$ was added to the lipid mixture, and the solution was vortexed to suspend the lipids. Aliquots containing 42 µl (6.5 µmol total lipids) of lipid mixture was transferred to several tubes. These aliquots were dried under reduced pressure and kept in the freezer until further use.

6.4.4 Liposome size determination

Dynamic light scattering (DLS), was performed on a Malvern Zetasizer Nano-ZS instrument. DLS analyzes the particle size by measuring dynamic fluctuations of light scattering caused by the particle. Liposomes were prepared by resuspending the lipid mixture in 500 µl ddH_2O and passed through the extruder ten times by using a 0.1 µm polycarbonate membrane. In a low volume plastic cuvette, the measurements were carried out at a temperature of 25 °C. In order to eliminate dust particles, the samples were filtered through syringe filters

with 0.2 μm pore size membrane. At least three repeat measurements on each sample were taken. The intensity size distributions were obtained from analysis of the correlation functions in the instrument software.

6.4.5 RNA incorporation and stability test

The lipid mixture was hydrated by resuspending a dried sample of 6.5 μmol mixed lipids with 200 μl of 300 mM sodium citrate (pH 4.0) and then vortexed to yield a white suspension. After that, 300 μl of 300 mM sodium citrate was added to approximately ~ 50 μg of unlabeled siRNA and a small amount of ^{32}P-labeled siRNA (~10,000-20,000 cpm) in another tube. Both solutions were vortexed and the lipid-containing solution was heated at 65 °C for five minutes. The clear siRNA solution was added drop-wise to the lipid suspension and the 500 μl mixture was then passed ten times through 0.1 μm polycarbonate filters at 200-300 psi using an extruder. The liposome was collected in a glass container and the extruded solution was dialyzed against 1 L of 25 mM HEPES and 50 mM NaCl buffer (pH 7.4) for 24 hours at 4 °C to raise the pH from 4.0 to 7.4. The unbound RNA from the complexes was separated by gel-exclusion chromatography with Sepharose 4B. The radioactivity present in various fractions was measured with a Beckman scintillation counter.

To test the stability of the RNA, the RNA was labeled at the 3' end and renatured with unlabelled RNA by heating to 90 °C for 2 min followed by a slow cooling. For double-stranded RNA, the sense strand was labeled. Equimolar amount of both strands with trace amounts of labeled strand were annealed by heating to 90 °C for 2 min followed by slow cooling. The renatured RNA was

incubated with RPMI culture media (containing 5% serum) at 37 °C for various time intervals.

6.4.6 Transfection of plasmid to Hi Five cells

Plasmid (GPI-scFv) obtained from the Al-Katib laboratory was transfected in High Five cabbage looper cells using cellfectin according to the manufacturer's protocols (InsectSelect system, Invitrogen). The pIZT/V5-His plasmid was used to clone the engineered scFv containing GFP-Zeocin fused in-frame for selection. The transfected insect cells express the GFP-Zeo and scFv with similar efficiencies; hence, GFP can be used to estimate the transfection efficiencies and Zeocin as a selection marker. Selection of stable transfectants was carried out using 200 µg/ml of Zeocin until the control cells completely died after which the concentration of Zeocin was lowered to 50 µg/ml. Approximately 15 µl of transfected and control High Five cells were spotted on microscope slides for checking GFP expression with an Olympus 1X71 microscope, equipped with a TH4 100 Olympus lamp and an Olympus UCMAD 3 camera. The magnification used was 60X, and images were taken in bright field and fluorescence mode for 200 ms exposure times.

6.4.7 Isolation and purification of protein

For isolation of protein (GPI-scFv), stable transfected cells were grown to confluent in T-75 flasks in serum-free media at 27 °C. The cells were scraped out and spun down to remove the media. Cells were lysed in lysis buffer (300 mM NaCl, 50 mM Tris HCl pH 7.6, 0.5% Triton X-100, 10 mM PMSF, and EDTA free

cocktail protease inhibitor) using a French Press. After lysis, centrifugation was carried out at 13,000 rpm for 15 min at 4 °C to remove cellular debris. The clarified supernatant was transferred into the new tube and protein was purified using a Ni^{+2} affinity column (HisTrap, Amersham Biosciences) according to the manufacturer's protocol.

The crude cell lysate (10 µl) and aliquots from various stages of protein purification (10 µl each) were electrophoresed on a 12% SDS polyacrylamide gel at 170 V until the bromophenol blue migrated off the gel. The gel was transferred to a nitrocellulose membrane (Hybond- C Extra, Amersham Biosciences) at 300 mA for one hour. After the proteins were transferred to the membrane, it was washed two times with TBST buffer for 15 min. The membrane was blocked with 5% skim milk for one hour in TBST buffer and incubated with primary antibody (HA.11 MoAb) overnight at 4 °C. The membrane was again washed twice with TBST buffer for 15 min and incubated with secondary antibody (goat anti-mouse) coupled to horseradish peroxidase for one hour. After washing with TBST, the protein bands were visualized with the ECL Advance Western Blot detection system. The chemiluminescense was scanned by a Typhoon and analyzed by Image Quant™ software.

6.5 Results

Human cancers frequently show altered expression of c-Myc emphasizing the importance of this gene in cancer (*287*). The c-Myc protein or the c-myc gene is overexpressed in a wide variety of human cancers. To check our system, we are specifically targeting expression of c-Myc in lymphoma cells (WSU-FSCCL)

using siRNA. These cells express CD20 antigens that can be specifically recognized by an antibody fragment (scFv) (*308*). CD20 is a highly phosphorylated, non-glycosylated 33-37 kDa membrane protein found on both normal and neoplastic B-cells. CD20 is an excellent target for therapeutic purposes, because it is neither shed from the cell nor internalized upon binding with antibodies (*316*).

6.5.1 Designing siRNA for targeting c-myc mRNA

Humans have evolved a number of mechanisms to fight against viral infections, which also work against siRNA. Hence, siRNA is degraded before reaching the target by several mechanisms (*317*). To increase the stability of siRNA, a number of methods are currently in use such as RNA modification and encapsulation using various carrier molecules (*292*). Several modifications have been used in siRNA to increase its stability and efficiency. 2'-*O*-methyl modifications are resistant to endonucleases and also abolish off-target effects when incorporated into nucleotides 2-8 on the antisense strand (*318*). Similarly, introduction of phosphorothioate backbone linkages at the 3' end of the RNA reduces susceptibility to exonucleases, and a substitution of fluorine at the 2'–position increases resistance to endonucleases (*302*).

Initially, single-stranded RNA 5’-AAG CUA ACG UUG AGG GGC AU-3’, which is complementary to the c-Myc mRNA at positions 1 to 20 from the start codon, and the scrambled version 5’-GAU CGA UCG AGC GAU GAU AG-3’, were used to check the incorporation efficiency, stability, and effect on cell

growth. These RNAs contained 2'–OCH_3 groups on the first three nucleotides at the 5'-end, which is the optimal site of modification.

The second RNA is a double-stranded construct in which all pyrimidines have a 2'-F group and the 3' ends contain phophorothiorates to increase stability. To design this RNA, the following four rules were considered, as described in the literature (*319*) : i) A/U at the 5' end of the antisense strand; ii) G/C at the 5' end of the sense strand; iii) AU-richness on the 5' terminal one-third of the antisense strand; and iv) absence of any GC stretch over nine base-pairs in length. The double-stranded siRNA targeting the c-Myc mRNA and a schematic representation of four rules used to designed siRNA are shown in **Figure 6.3**.

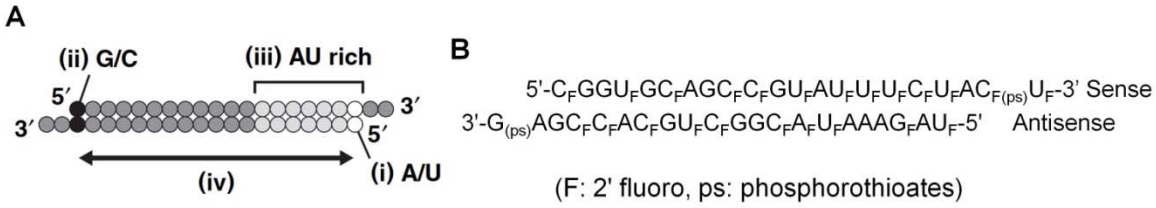

Figure 6.3. An overview of the four rules to design siRNA and siRNA targeting c-Myc mRNA is shown. A) A schematic representation of siRNA with four rules is indicated. B) The siRNA designed according to the rules for targeting c-Myc mRNA in NHL cells is shown.

6.5.2 Encapsulation of siRNA into the liposomes

For efficient encapsulation of oligonucleotides into the liposomes, many variables have to be considered, such as lipid types and buffer pH. Currently, all types of phospholipids are available for liposome preparation: neutral, cationic, and anionic. Among them, cationic lipids are most commonly used to prepare encapsulated oligonucleotides. The positively charged lipids can interact with

negatively charged oligos through electrostatic interactions, which are considered an initial driving force for encapsulation. Previously, it has been shown that cationic liposomes are useful to efficiently encapsulate and deliver nucleic acids to the target. In this study, the protocol for liposome formulation was based on a previous study conducted in our lab (*320*), which was a modified protocol of Zelphati *et al.* (*321*). This composition contains four lipids: 1,2-dioleoyl-3-dimethylammoniumpropane (DODAP), dipalmitoylphosphotidyl choline (DPPC), cholesterol, and dipalmitoylphosphotidyl ethanolamine (DPPE). They were used in the ratio of 20:44:35:1 of DODAP:DPPE:cholesterol:DPPC to prepare liposomes (**Figure 6.4**). DODAP has improved encapsulation efficiencies because of an ionizable aminolipid with a tertiary amine (pK_a 6.6), which becomes positively charged at low pH. Hence, pH 4.0 was used to encapsulate the siRNA into the liposomes. Furthermore, backbone modification with phosphorothiorates and the presence of a methyl group at 2'-positions also increases encapsulation efficiency and stability of the RNA.

To check encapsulation efficiency, single-stranded RNA was labeled at the 3'-end with ^{32}P in order to track the amount of RNA incorporated into the liposomes. A small amount of RNA (50 µg) and a trace amount of labeled RNA (5,000 cpm) was mixed with a hydrated lipid mixture and passed through the extruder at ~ 200 psi. The mixture was prepared in sodium citrate buffer at pH 4.0, and after extrusion, the liposomal mixture was dialyzed against HEPES buffer at pH 7.5 for 12 hrs. Separation of unincorporated RNA from liposome-RNA was done by using a Sepharose 4B column.

The level of encapsulation was determined by measuring the radioactivity of all fractions. The level of RNA encapsulation was found to be more than 30% by using the following equation (**Figure 6.5 A**);

$$\text{Encapsulation effenciency} = \frac{\text{Cpm (liposome fraction)}}{\text{Cpm (liposome fraction + void fraction)}} \times 100\ \%$$

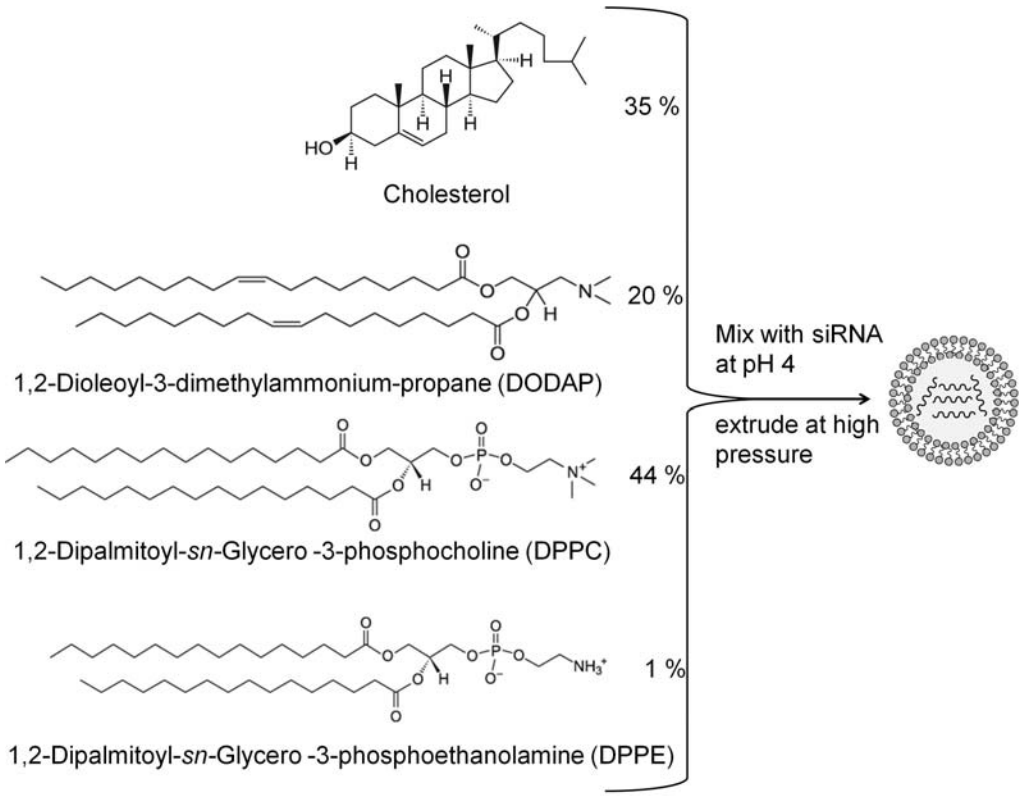

Figure 6.4. A liposome-siRNA complex is shown. Four different lipids; cholesterol, DODAP, DPPC, and DPPE were mixed at low pH with siRNA to generate the complexes.

Particle sizes of liposomes were measured by using a dynamic light scattering (DLS) instrument. From the time-correlation function, the size of the particles were determined by the instrument software. The output can be used to

plot as a number or intensity percentage vs. size of the particles. Larger particles scattered more light compared to small particles and the plot of intensity vs. size may not reflect the actual distribution of the particles size. Thus, a histogram with number percentage vs. size of the liposome particles was plotted. The majority of liposomal particle size was found to be ~100 nm (**Figure 6.5 B**).

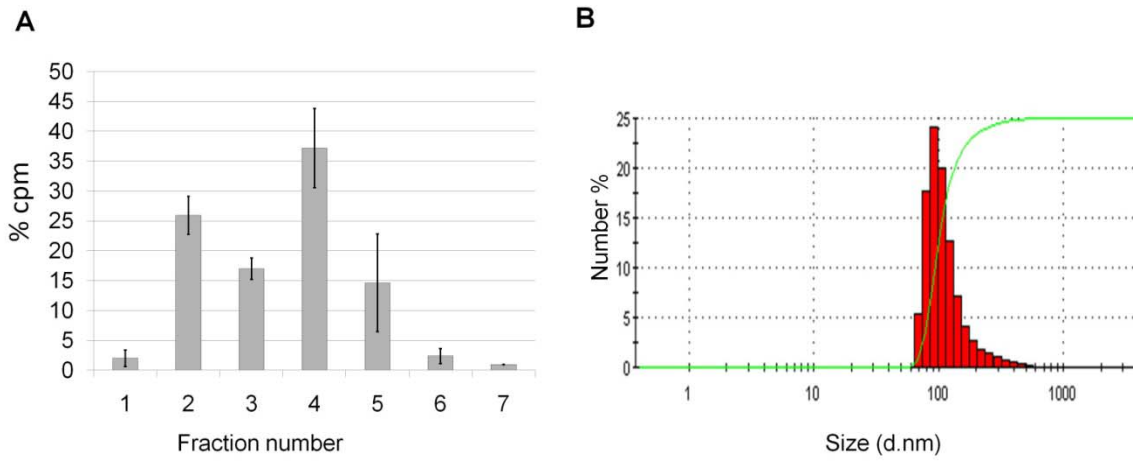

Figure 6.5. Incorporation efficiencies and liposomal particle size are shown A) the % incorporation of single-stranded RNA into the liposomes; fractions 2 and 3 from column contain liposomes with RNA, whereas fractions 4 and 5 show the presence of unincorporated RNA. The data represents an average of three independent experiments. B) Particle size distribution of liposomes measured by DLS is represented.

6.5.3 siRNA stability

The single-stranded RNAs (modified and scrambled) were labeled at the 3' end to test stability. After labeling, trace amounts of labeled RNA and 20 µg of unlabelled RNA were renatured in 25 mM HEPES and 50 mM NaCl. Fifty µl culture media or an equivalent amount of buffer were added to the renatured RNA (50 µl) and incubated at 37 °C for various time intervals. In the presence of media, both the modified and scrambled versions of single-stranded RNA were

degraded in less than 30 min (**Figure 6.6 A**). Similarly, to check the stability of double-stranded RNA, both strands of RNA (20 µg each) were annealed with trace amounts of 3' labeled sense strand. Fifty µl of annealed siRNA and 50 µl of the culture media was combined and incubated at 37 °C for various time intervals. After each time interval, the samples were quenched on dry ice and run on a polyacrylamide gel. The double-stranded RNA with modifications was found to be stable for more than 18 hours in RPMI media with serum (**Figure 6.6 B**). The presence of 2'-F and phosphorothiorate modifications makes the double-stranded RNA less susceptible to the nucleases present in the medium.

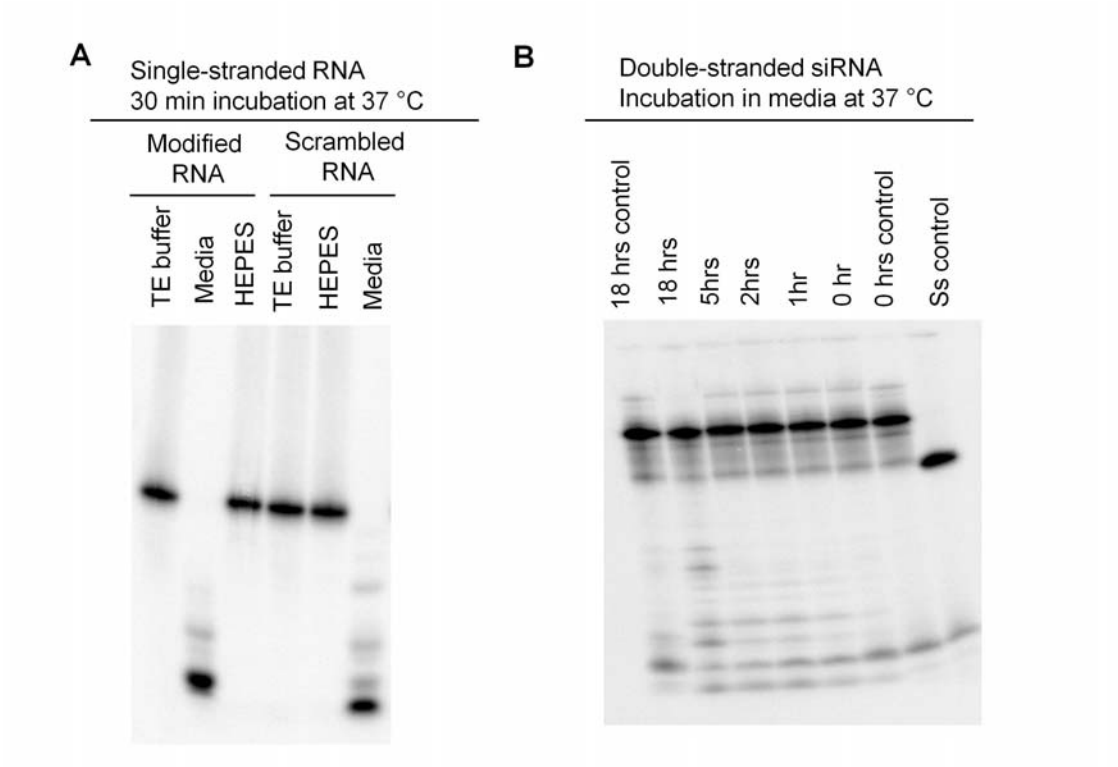

Figure 6.6. Autoradiogram of modified single- and double-stranded siRNA stability test in RPMI culture media at different time intervals is shown. A) Single-stranded RNA and the scrambled version with different buffers and media and B) double-stranded RNA with media at various time intervals are shown (autoradiogram B was done by Gayani Dedduwa Mudalige).

6.5.4 Transfection of GPI-scFv and protein purification

The GPI-scFv expression plasmid (obtained from Al-Katib's lab) (**Figure 6.7**) was stably transfected into High Five™ cells. After 4 rounds of selection with Zeocin (200 µg/ml), control cells died and green fluorescence from GFP was readily visible in transfected cells using fluorescence microscope (**Figure 6.8**). The presence of fluorescence compared to untransfected High Five™ insect cells confirms the generation of stably transfected cells. Plasmid concentration (2-5 µg), number of High Five cells (~ $1*10^6$), and viability (> 90%) are important factors to generate the stable transfection. To avoid the contamination often found with the use petri dishes (as described in protocol), T75 flasks were used.

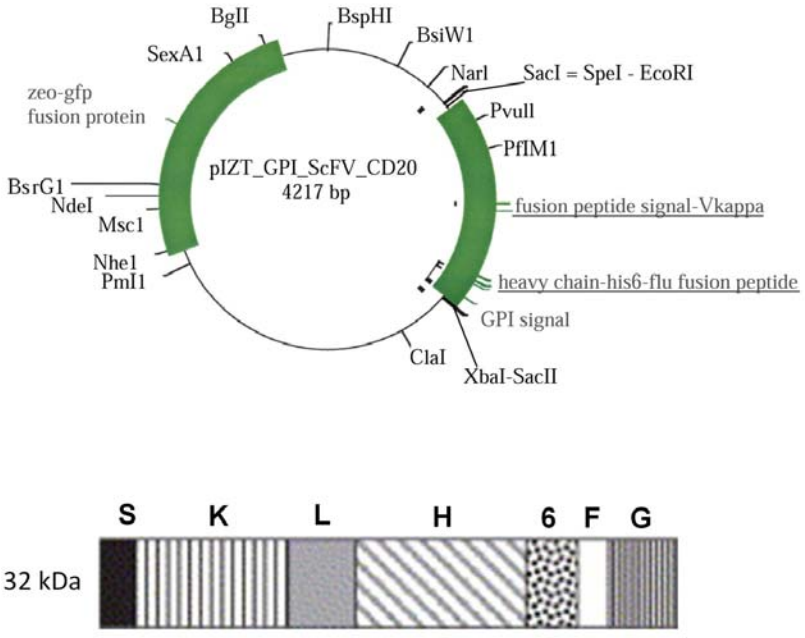

Figure 6.7. A schematic diagram of the pIZT-GPI-anti-CD20 scFv expression construct obtained from Al-Katib laboratory (upper) and GPI-tagged SKLH6FG (lower) cloned in multiple cloning site are shown: The abbreviations are S: secretory signal, K: light chain variable region, L: linker, H: heavy chain variable region, 6: six histidine residues, F: Flu tag HA, and G: GPI (glycosylphosphatidyl inositol) signal. Modified with permission from Hamdy et *al. (308).*

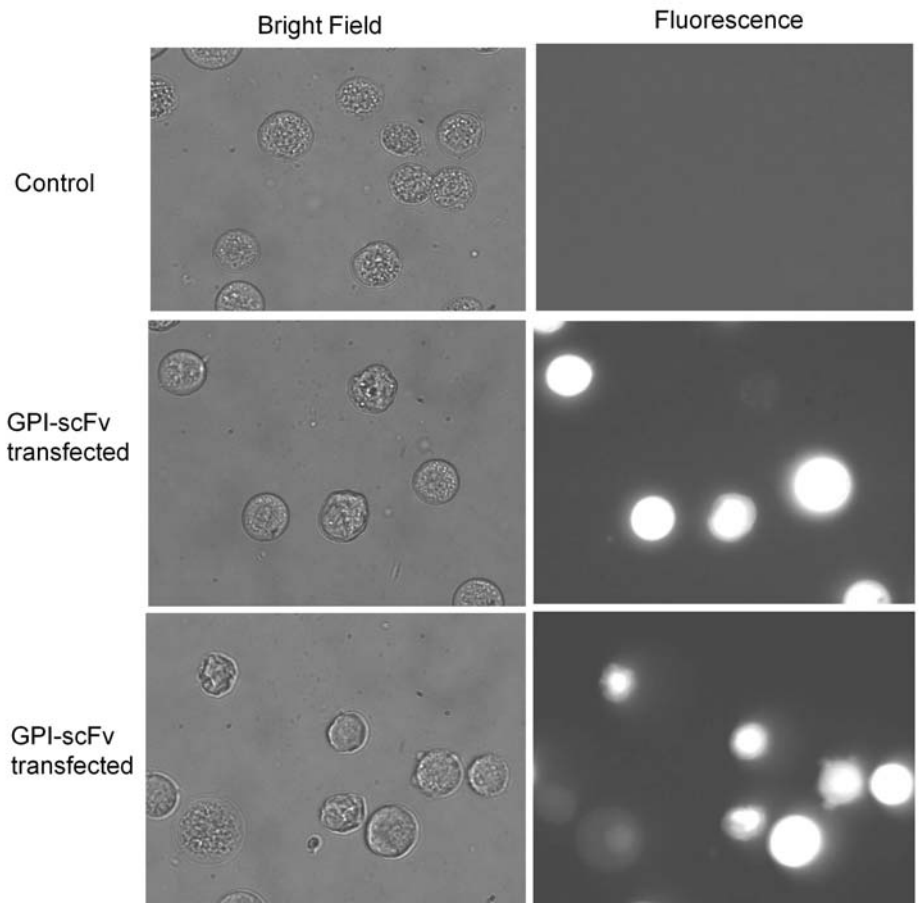

Figure 6.8. GPI anchored scFv after stable transfection to the Hi Five cells are shown. The left panel represents the bright field and right panel represents the corresponding GFP fluorescence at 200 ms exposure time. Control (no transfection) cells do not show any fluorescence and most of the transfected cells showed fluorescence.

GFP fluorescence and Zeocin resistance indicated the formation of stably transfected High Five cells. Protein purification was carried out from stably transfected cells using a Ni^{2+} column, and the presence of protein at various stages was detected by Western blotting. Western blotting showed presence of the desired protein in the crude lysate and in purified fractions of ~32 KDa, corresponding to the protein GPI-scFv (**Figure 6.9**).

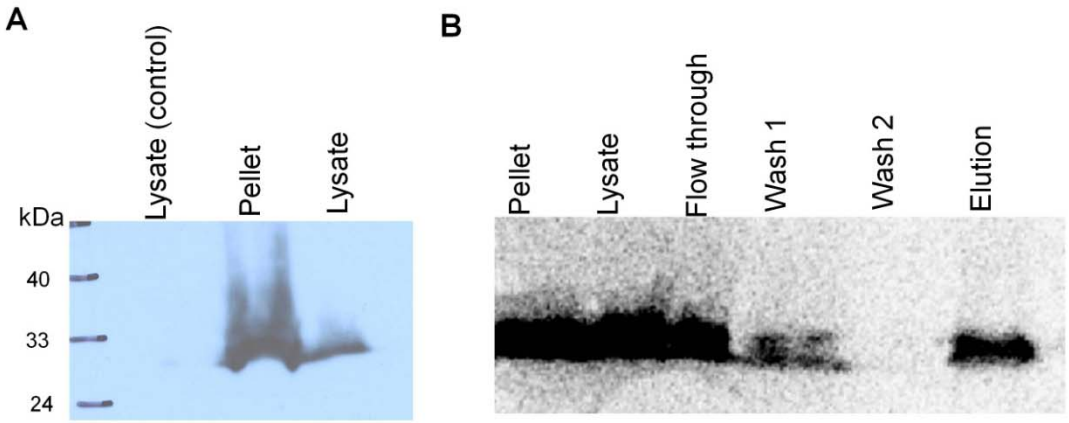

Figure 6.9. A 12% SDS-polyacrylamide gel and immunobloting analysis of GPI-anchored scFv proteins at different stages of purification are shown: A) before protein purification showing lysate (control) from untransfected High Five cells; pellet and lysate from transfected cells; and B) fractions from different stages of protein purification from transfected cells.

6.6 Conclusions and Future Directions

The double-stranded siRNA with specific modifications was found to be stable long periods of time (> 20 h), even in the culture media. We have successfully stably transfected High Five cells with a GPI-scFv expression plasmid and purified small amounts of the expressed protein. The stably transfected cells can be used to purify larger quantities of the GPI-anchored scFv for further experiments. Liposomes, siRNA, and the GPI-scFv complex can be used to deliver siRNA to CD20-positive cells. This can be confirmed by measuring the level of c-Myc expression in CD20-positive WSU-FSCCL cells. Further, instead of siRNA, quantum dots can be used to check the targeted delivery by scFv. Quantum dots can be incorporated into the liposomes and complexes with GPI-scFv can be generated. When this complex is incubated with cells, it is expected that QDs will be delivered to the cells. As QDs are highly

luminescent, they can be detected by fluorescence microscopy. This method will have the advantage of simultaneous cell imaging and targeted delivery of cytocidal agents to cancer cells.

CHAPTER 7

Conclusions and Future Directions

7.1 General Conclusions

The ribosome is the protein synthesis machinery and serves as an ideal target for various classes of antibiotics because of its accessibility and structural diversity (*68, 71*). In the last decade, the growth of multiple-drug-resistance bacterial pathogens is rapidly evolving, while the development of new antibacterials is lagging behind. To overcome the ever-growing problem of resistance, we can either design new drugs for traditional target sites, or explore novel target sites. Despite the existence of validated antibiotic binding sites, very few attempts have been made to explore novel drug target sites in the ribosome (*2, 103*). The ideal target sites should not only be functionally important, but also accessible to various small molecules. In this thesis, a new role for cisplatin as a discovery tool for potential new drug target sites on the ribosome was explored. Cisplatin has several advantages over other chemical probes due easy detection of its target sites and the possibility to use it *in vitro* as well as *in vivo*. In addition, the positive charge in aquated complex and stable adduct formation are useful to monitor binding and kinetics of the reaction.

The first objective of this thesis was to understand the binding interaction of cisplatin with model RNA constructs and 16S rRNA. A number of methods were employed to obtain information about the binding sites, number of adducts, and types of cross-links formed with RNA. The binding studies showed that cisplatin interacts preferably with guanosine-rich RNA sequences. Many of the

consecutives Gs on the 16S rRNA that showed reactivity with cisplatin were involved in G○U wobble base pairs. Since G○U pairs are known to be functionally important for RNA-protein interactions (*219, 221*), the cisplatin complex may reveal preferential sites for protein binding on RNA that have ideal accessibility and structural compatibility. The various adduct profiles obtained from the small RNA construct and 16S rRNA also showed that RNA is a viable target and may be part of an alternate pathway for cisplatin anticancer activity. Cisplatin mainly forms bifunctional adducts with purine bases; however, it showed a unique adduct profile with RNA compared to that of DNA. In DNA, the most common cross-links are the 1,2-intrastrand with purine bases, mainly the 1,2-intrastrand d(GpG) adduct (~65%) and the 1,2-intrastrand d(ApG) (~25%), and less common 1,3-intrastrand d(GpXpG) adducts (*172, 191*). In 16S rRNA, the adduct distribution is 63% GpG, ~20% ApG, 6% GG, and 11% AG. Strong reactivity with nonconsecutive Gs such as G462 and G791 may be the result of structural differences between DNA and RNA. RNA contains several secondary structural motifs, such as hairpins, internal loops and bulges, which cause distortion of the RNA structure and therefore change accessibility of the nucleotides.

The second objective of this thesis was to map on the ribosome accessible binding sites that could possibly be used as a novel target sites for new antibiotics. This study showed that several helices of the ribosome are clearly accessible to platinum complexes, such as helix 18, 24, 27, and 34, and thus could also be accessible to small molecules and serve as targets for novel drug

leads. Several nucleotides in these helices that are functionally important, such as G530-531, G791, and G1058, were found to be highly reactive towards cisplatin. Mutational studies showed that these cisplatin reactive sites when mutated lead to deleterious phenotypic effects (*2*). A number of these mutations has impaired assembly of the ribosome and growth of the bacteria (*1*).

Several sites in the 16S rRNA showed different platinum reactivity between 30S subunits and 70S ribosomes, which could be exploited for structure-based or mechanism-based drug design. Recently, a model system of helix 18 was used as a target to find ligands by phage display (*254*). Hence, phage display or SELEX could be carried out to find the ligands targeting the sites that showed different reactivity in 16S rRNA, 30S subunits and 70S ribosomes.

The fact that the platinum complex generates stable adducts that can be quantified is significant, because the kinetics of the reaction can be monitored. This will allow determination of how positively charged compounds such as aminoglycosides identify their target sites from a number of possible reactive sites on the ribosome. In RNA, we do not know whether the known sites are the only ones for effective inhibition, or whether there are more possible target sites on the ribosome. Hence, it will be important understand the kinetic preference for charged small molecules binding to the functionally important sites on the ribosome.

The third objective of this thesis was to exploit another aspect of cisplatin, namely, the ease with which its charge and size can be altered. Unlike other

probing agents, aquated cisplatin has a positive charge; thus, accessibility and kinetic information can be obtained simultaneously. For this purpose, a number of platinum complexes with various charges and sizes were synthesized by tethering amino acids. The binding studies with amino-acid-linked complexes with 16S rRNA showed a clear alteration of the binding sites compared to cisplatin. The positively charged Kplatin and Oplatin showed a preference for AG over GG sites on 16S rRNA. Similarly, Rplatin showed a preference for loop and bulge regions. The negatively charged amino-acid-linked complex Dplatin did not show any reactivity under similar reaction conditions. These results indicate that an electrostatic interaction is likely a primary driving force for charged small molecules to react with the negatively charged nucleic acids, although H-bonding might also play a role.

In a different aspect of my thesis work, the use of siRNA to target non-Hodgkin's lymphoma was explored. siRNA has great therapeutic applications, including those related to anticancer approaches; however, it has been often difficult to achieve selective targeting, efficient delivery, and appropriate stability of the siRNA, while at the same time minimizing toxic side effects. A newly engineered antibody fragment (scFv) in conjugation with liposomes was proposed for this purpose. An scFv plasmid obtained from Al-Katib's lab was successfully transfected to High Five insect cells to generate stably transfected cell lines. This step of the project presented a number of challenges that were overcome, and now with stably transfected cell lines, sufficient quantities of protein can be generated for future studies. siRNA stability in cell-growth media

and its incorporation into liposomes were also optimized. The siRNA with 2'-F, phopshorothiate, and 2'-OMe modifications were found to be stable in culture media for extended periods of time (24 hours), and gave ~30% incorporation efficiency into the liposome.

7.2 Future Directions

Future experiments include the use of these probing techniques to monitor the accessibility of purines in 23S rRNA, functional ribosomes in the presence of mRNA and tRNA, as well as polysomes. Mapping of cisplatin binding sites in 23S rRNA *in vitro* and *in vivo* will greatly increase accessibility information for various functionally important regions, such as the peptidyl-transferase center, helix 69, and the peptide exit tunnel. In addition, *in vitro* probing of the ribosome in presence of mRNA and/or tRNA can generate information about nucleotide accessibility in fully functional ribosomes. This work could be further expanded to the polysomes. Previous studies showed that a number of nucleotides were protected when mRNA, tRNA or initiation factors were assembled on the ribosome. Thus, cisplatin probing result can be compared with previously obtained results from biophysical and biochemical methods to find novel target site for antibiotics on the ribosome.

The binding studies with amino-acid-linked cisplatin analogues and the 790 region of 16S rRNA revealed an alteration of binding sites relative to the parent cisplatin; thus, the adduct profiles on 16S rRNA are expected to be different. The binding sites of cisplatin analogues on the 30S subunits and 70S ribosomes can be obtained by primer extension and in small constructs by

MALDI (TOP-DOWN sequencing or RNase cleavage) and chemical probing. The types and number of adducts formed with cisplatin analogues with varying ligands will further increase our understanding of RNA-platinum complex interaction. HPLC and LC-MS can be used for this purpose, as described in Chapter 2. In addition, NMR analysis of various products obtained with individual nucleosides or nucleotides could be useful to find the exact coordination site of platinum on the nucleotide base, which has not yet been verified on RNA. As charge and size of cisplatin can be altered easily, various analogues with bulkier groups, higher charge, or varying hydrophobic or H-bonding moieties can be synthesized. These compounds could be exploited to gain information about nucleotide or helix accessibility on the ribosome, as well as map the interaction modes.

Cisplatin and its analogues were demonstrated as probing tools to gain information about nucleotide accessibility in the RNA tertiary or higher-order structure. Probing the ribosome from other organisms will have the great advantage of predicting accessibility and assisting with the design of selective structure-based drug targeting agents for pathogenic bacteria. It has been of great interest to know how charged small molecules such as aminoglycosides find their target sites out of the numerous possible sites in the ribosome. Cisplatin and analogues, due to their stable coordination and charges present in the aquated species, can be used as a model to understand how charged molecules find their target sites. This kinetic interaction combined with thermodynamic preferences will also aid in future drug design.

Small interfering RNAs (siRNA) were designed to specifically target the c-Myc mRNA in non-Hodgkin's lymphoma cells. High Five cells with stable transfection of GPI-scFv have been generated, which showed expression of the desired protein. The stably transfected cells can be used to purify larger quantities of the GPI-anchored scFv for further experiments. Liposome, siRNA, and the GPI-scFv can be combined to generate a complex that can be used to deliver siRNA to CD20-positive cells. This targeting can be confirmed by examining the levels of c-Myc expression in CD20-positive WSU-FSCCL cells or related cancer-cell lines. Further, instead of siRNA, quantum dots can be used to monitor the targeted delivery by scFv. Quantum dots can be incorporated into the liposomes, and complexes with GPI-scFv can be generated. When this complex is incubated with cells, it is expected that QDs will also be delivered to the cells and can be utilized for imaging purposes. As QDs are highly luminescent, they can be detected by fluorescence microscopy. This method will have the advantage of simultaneous cell imaging and targeted delivery of cytocidal agents to cancer cells. These projects taken together provide the basis for new applications directed towards novel drug discovery or selective targeting as antibacterial or anticancer agents.

APPENDIX

Figures in this appendix are additional autoradiograms for Chapters 2 and 3. The primer and RNA used for probing are mentioned in figure captions.

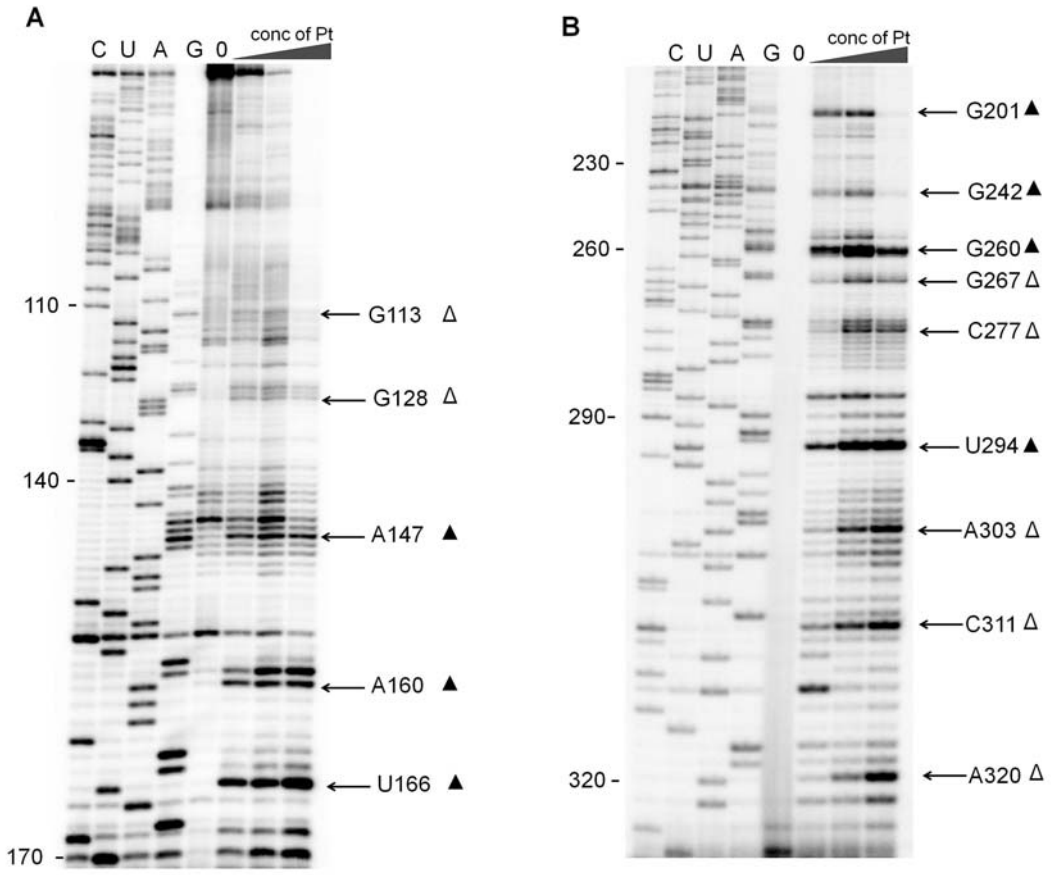

Figure. Probing results of 16S rRNA at the 3' domain with primers 171 and 323 are shown. (A) Autoradiogram showing the reverse transcriptase pauses or stops by using primer 171. (B) Autoradiogram showing the reverse transcriptase pauses or stops by using primer 323. In both gels, C, U, A, G represent the sequencing lanes, 0 represents the control, and other 3 lanes are 16S rRNA treated with increasing concentrations of monoaquated cisplatin (cisplatin:nucleotide is 1:150, 1:75, and 1:30). The strong and moderate hits are indicated with arrows and corresponding nucleotides numbers (▲ (strong hits) and Δ (moderate hits)).

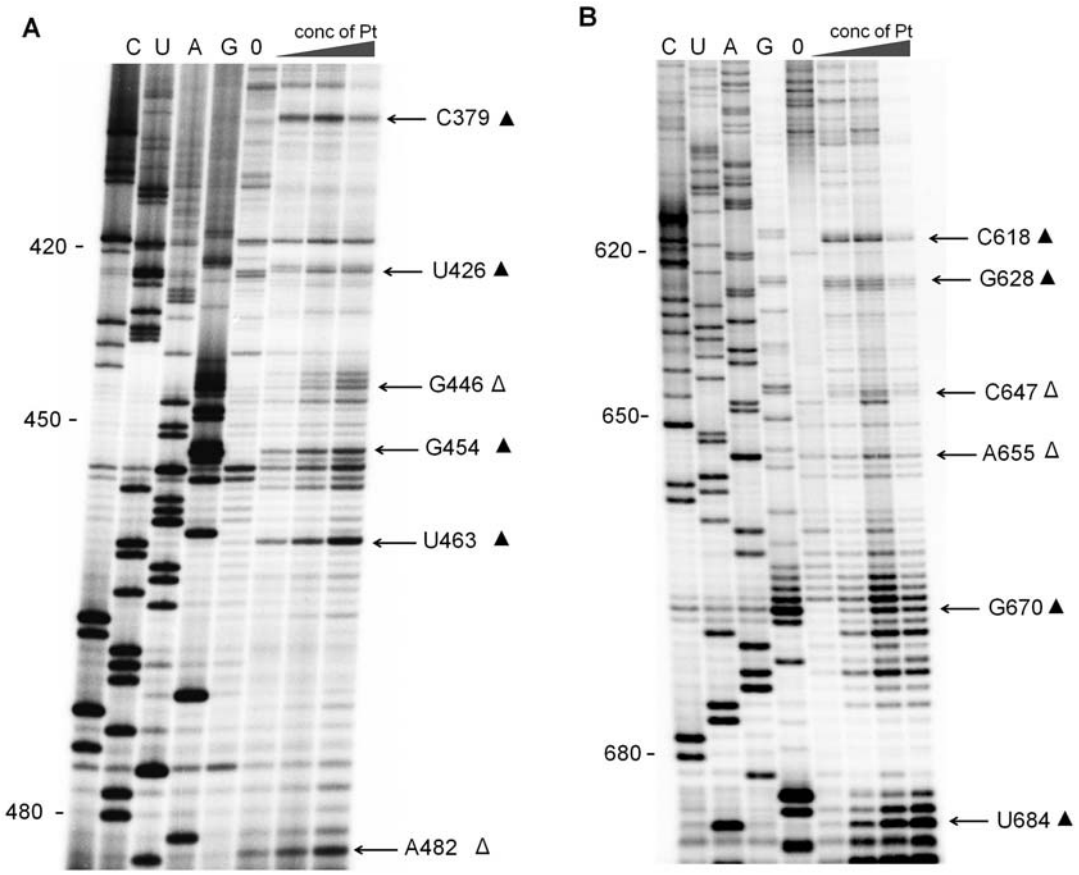

Figure. Probing results of 16S rRNA with primers 485 and 686 are shown. (A) Autoradiogram showing the reverse transcriptase pauses or stops by using primer 485. (B) Autoradiogram showing the reverse transcriptase pauses or stops by using primer 686. In both gels, C, U, A, G represent the sequencing lanes, 0 represents the control, and other 3 lanes are 16S rRNA treated with increasing concentrations of monoaquated cisplatin (cisplatin:nucleotide is 1:150, 1:75, and 1:30). The strong and moderate hits are indicated with arrows and corresponding nucleotides numbers (▲ (strong hits) and Δ (moderate hits)).

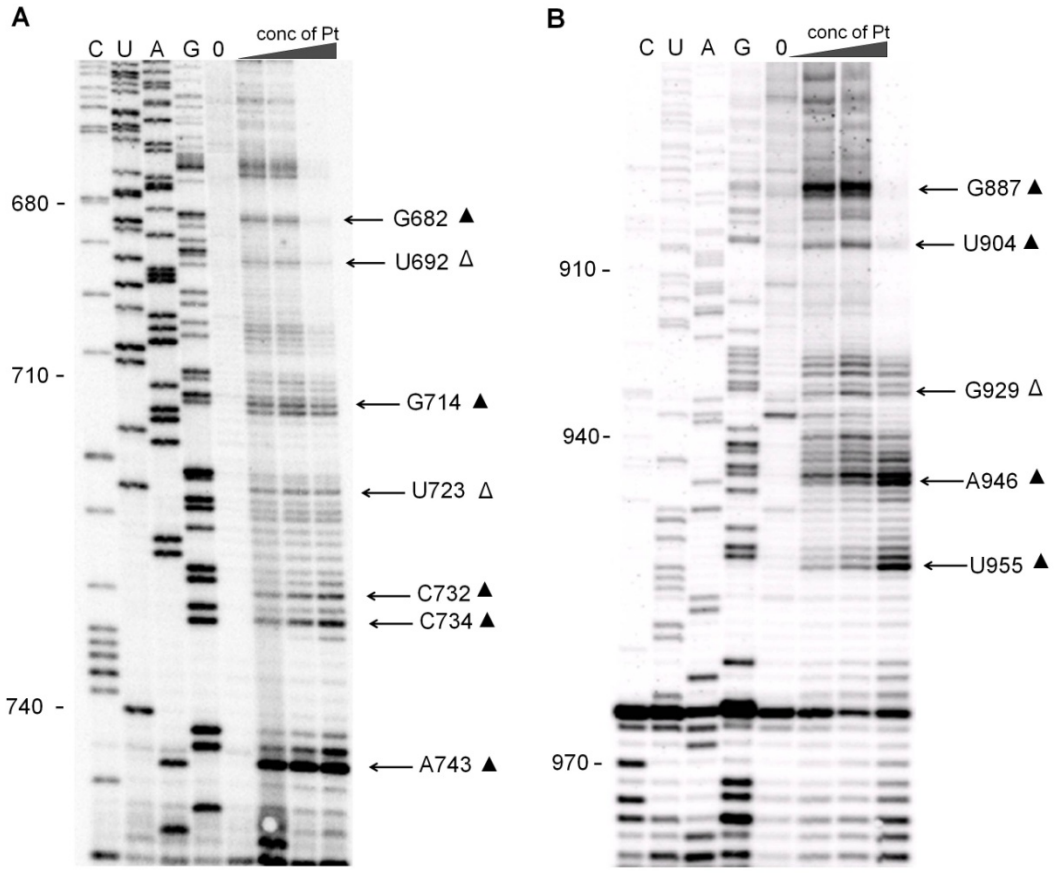

Figure. Probing results of 16S rRNA with primers 746 and 982 are shown. (A) Autoradiogram showing the reverse transcriptase pauses or stops by using primer 746. (B) Autoradiogram showing the reverse transcriptase pauses or stops by using primer 982. In both gels, C, U, A, G represent the sequencing lanes, 0 represents the control, and other 3 lanes are 16S rRNA treated with increasing concentrations of monoaquated cisplatin (cisplatin:nucleotide is 1:150, 1:75, and 1:30). The strong and moderate hits are indicated with arrows and corresponding nucleotides numbers (▲ (strong hits) and Δ (moderate hits)).

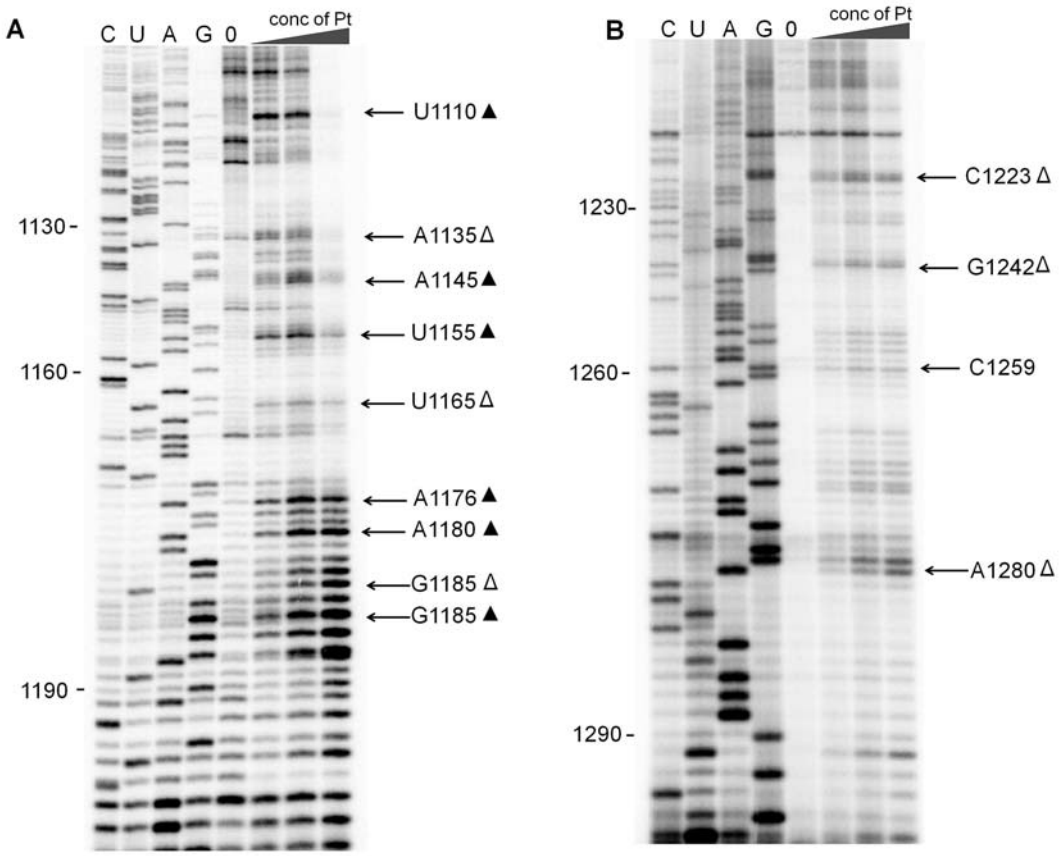

Figure. Probing results of 16S rRNA with primers 1199 and 1296 are shown. (A) Autoradiogram showing the reverse transcriptase pauses or stops by using primer 1199. (B) Autoradiogram showing the reverse transcriptase pauses or stops by using primer 1296. In both gels, C, U, A, G represent the sequencing lanes, 0 represents the control, and other 3 lanes are 16S rRNA treated with increasing concentrations of monoaquated cisplatin (cisplatin:nucleotide is 1:150, 1:75, and 1:30). The strong and moderate hits are indicated with arrows and corresponding nucleotides numbers (▲ (strong hits) and Δ (moderate hits)).

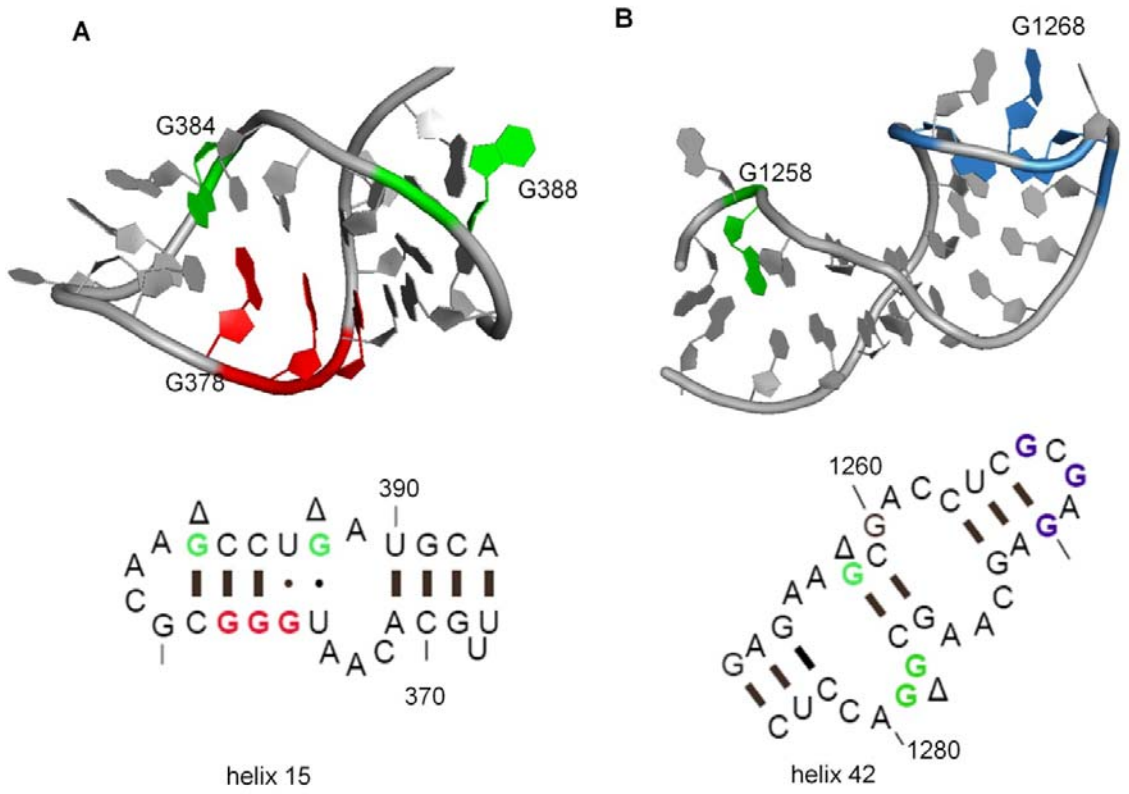

Figure. Crystal structures and secondary structure regions of 16S rRNA corresponding to helix 15 and 42 are shown with reactive nucleotide (colored).

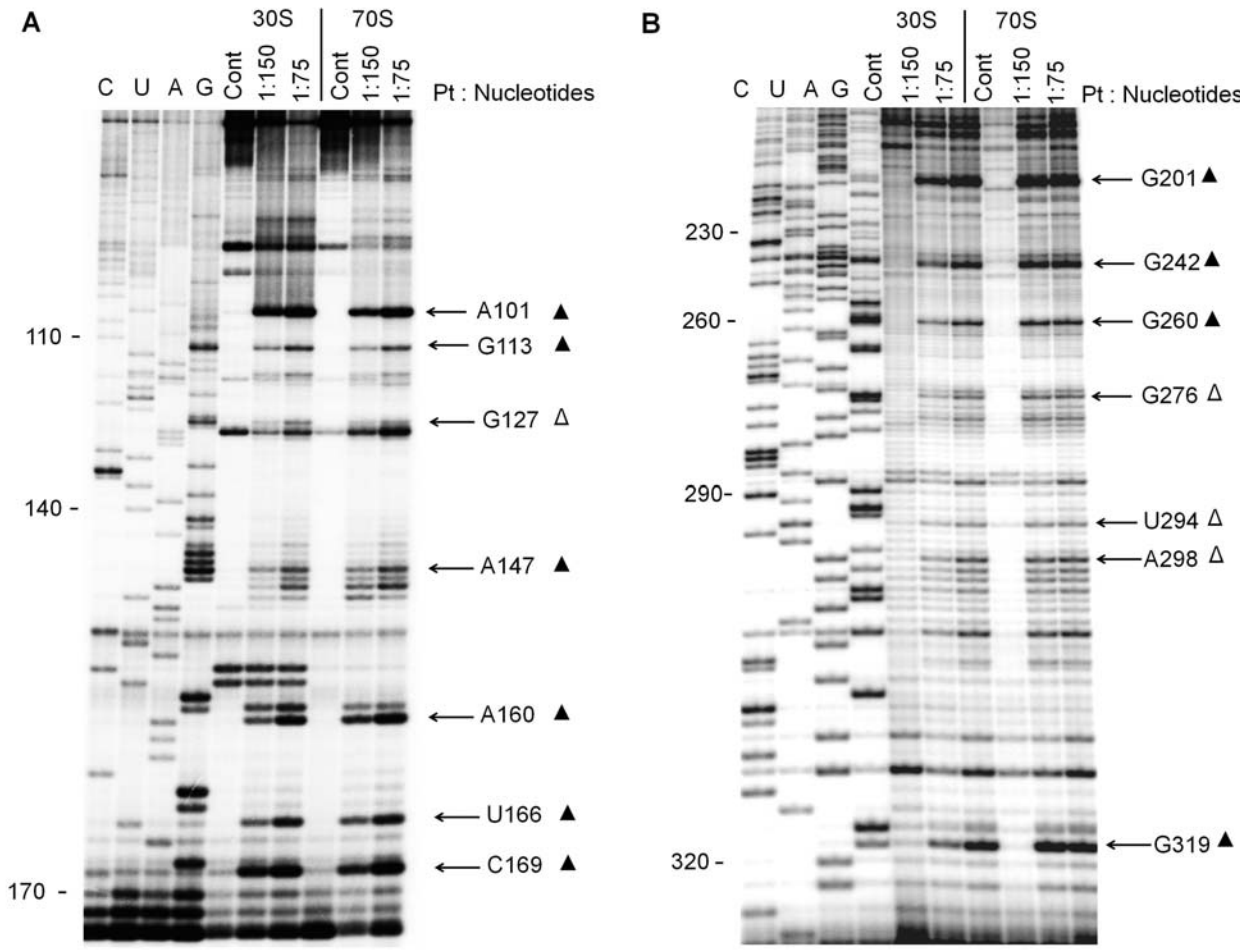

Figure. Probing results of 16S rRNA of the 30S subunits and the 70S ribosomes at the 5' domain with primers 171 and 323 are shown. (A) Autoradiogram showing the reverse transcriptase pauses or stops by using primer 171. (B) Autoradiogram showing the reverse transcriptase pauses or stops by using primer 323. In both gels, C, U, A, G represent the sequencing lanes, 0 represents the control, and other lanes are 30S subunits and 70S ribosomes treated with increasing concentrations of monoaquated cisplatin (cisplatin:nucleotide is 1:150 and 1:75). The strong and moderate hits are indicated with arrows and corresponding nucleotides numbers (▲ (strong hits) and Δ (moderate hits) and ● (minor hits)).

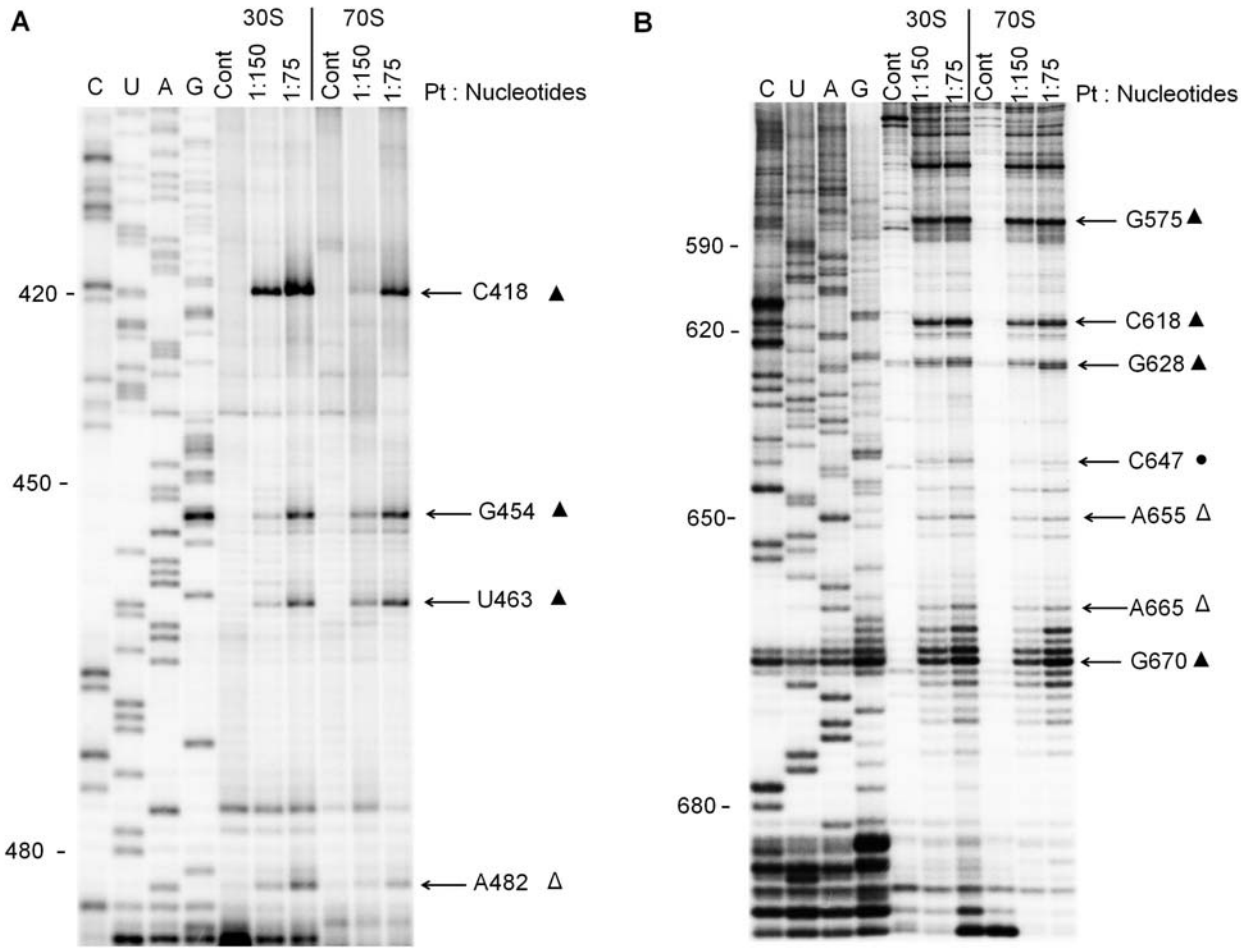

Figure. Probing results of 16S rRNA of the 30S subunits and the 70S ribosomes at the 5' and central domain with primers 485 and 687 are shown. (A) Autoradiogram showing the reverse transcriptase pauses or stops by using primer 485. (B) Autoradiogram showing the reverse transcriptase pauses or stops by using primer 687. In both gels, C, U, A, G represent the sequencing lanes, 0 represents the control, and other lanes are 30S subunits and 70S ribosomes treated with increasing concentrations of monoaquated cisplatin (cisplatin:nucleotide is 1:150 and 1:75). The strong and moderate hits are indicated with arrows and corresponding nucleotides numbers (▲ (strong hits) and Δ (moderate hits) and ● (minor hits)).

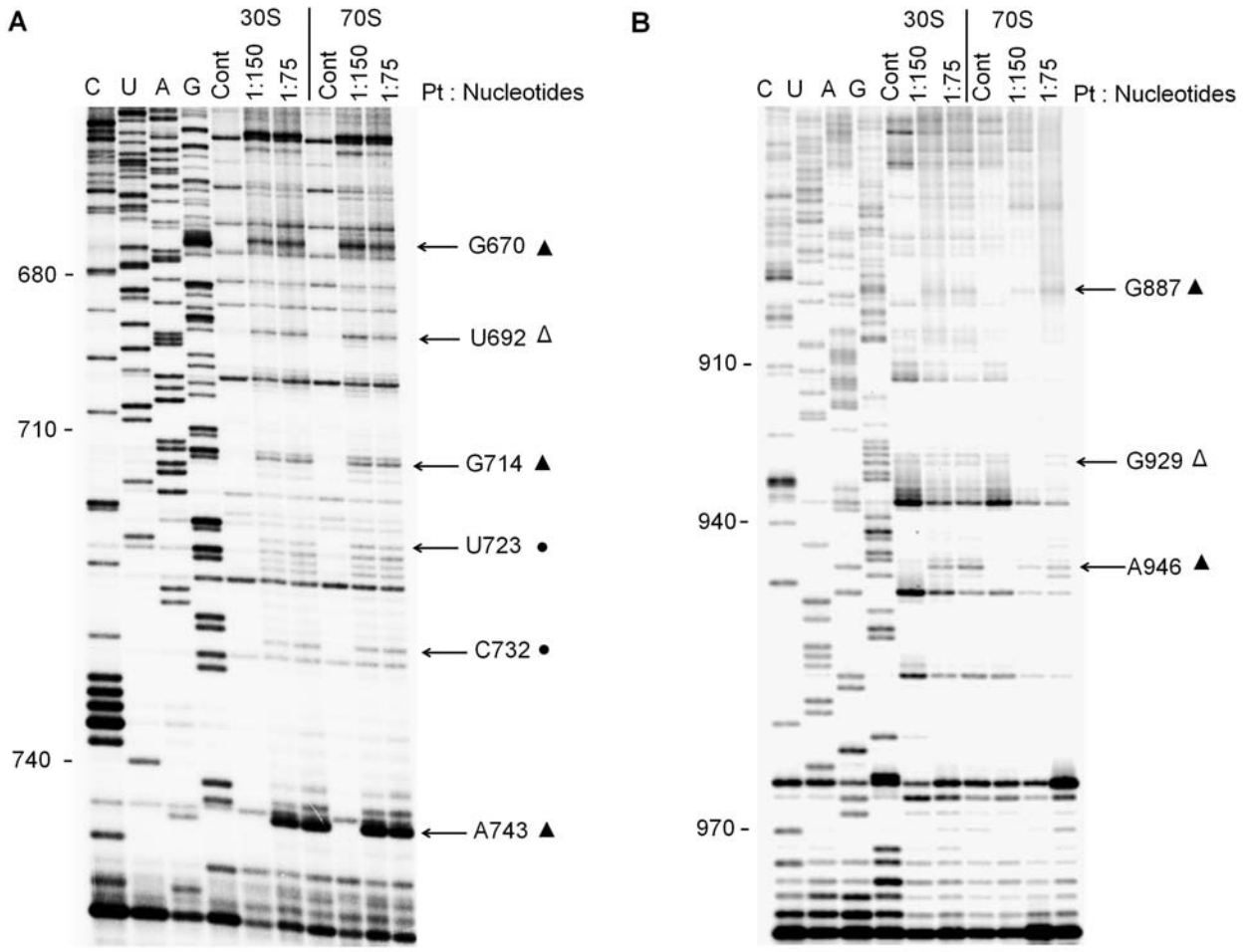

Figure. Probing results of 16S rRNA of the 30S subunits and the 70S ribosomes at the central and 3' major domain with primers 748 and 978 are shown. (A) Autoradiogram showing the reverse transcriptase pauses or stops by using primer 748. (B) Autoradiogram showing the reverse transcriptase pauses or stops by using primer 978. In both gels, C, U, A, G represent the sequencing lanes, 0 represents the control, and other lanes are 30S subunits and 70S ribosomes treated with increasing concentrations of monoaquated cisplatin (cisplatin:nucleotide is 1:150 and 1:75). The strong and moderate hits are indicated with arrows and corresponding nucleotides numbers (▲ (strong hits) and Δ (moderate hits) and • (minor hits)).

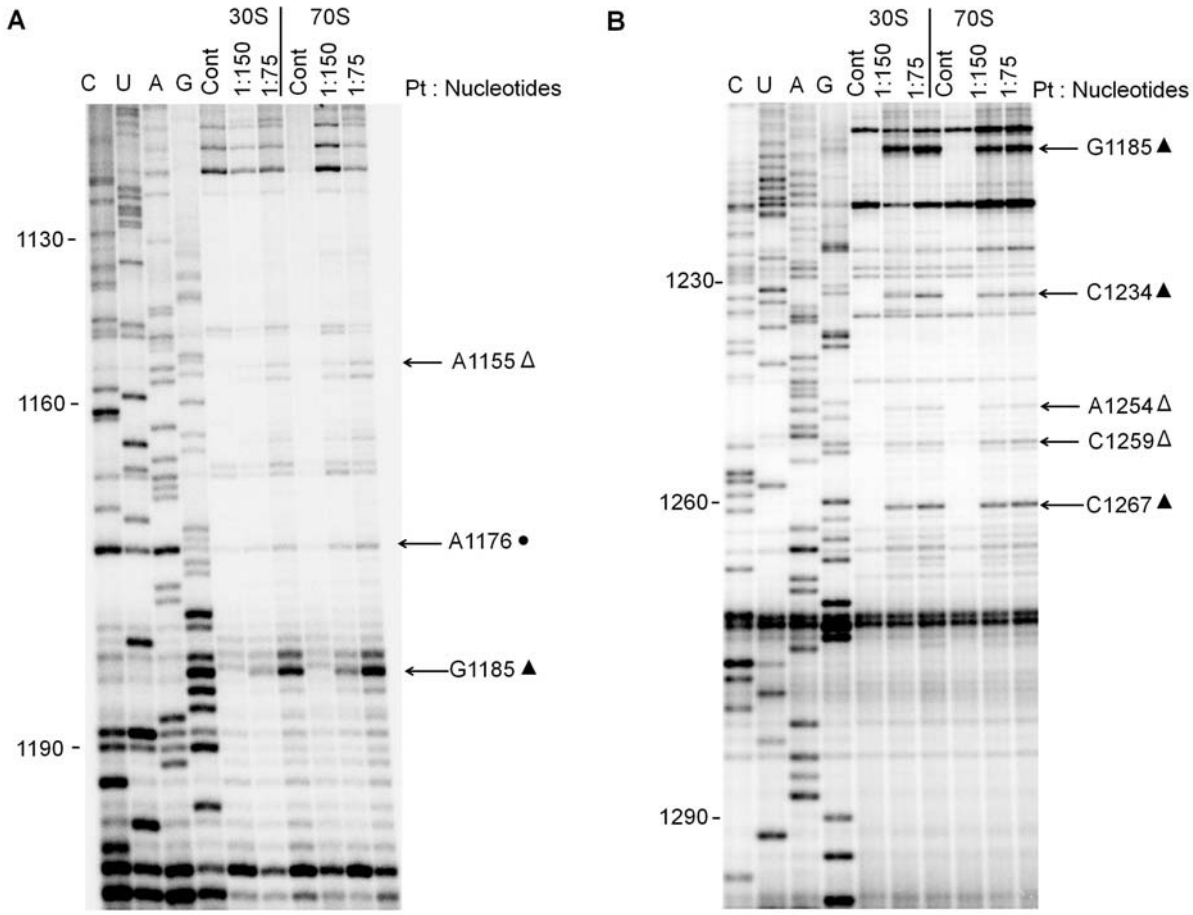

Figure. Probing results of 16S rRNA of the 30S subunits and the 70S ribosomes at the 3' domain with primers 1199 and 1296 are shown. (A) Autoradiogram showing the reverse transcriptase pauses or stops by using primer 1199. (B) Autoradiogram showing the reverse transcriptase pauses or stops by using primer 1296. In both gels, C, U, A, G represent the sequencing lanes, 0 represents the control, and other lanes are 30S subunits and 70S ribosomes treated with increasing concentrations of monoaquated cisplatin (cisplatin:nucleotide is 1:150 and 1:75). The strong and moderate hits are indicated with arrows and corresponding nucleotides numbers (▲ (strong hits) and Δ (moderate hits) and • (minor hits)).

REFERENCES

1. Xu, Z., and Culver, G. M. (2010) Differential assembly of 16S rRNA domains during 30S subunit formation, *RNA 16*, 1990-2001.
2. Yassin, A., Fredrick, K., and Mankin, A. S. (2005) Deleterious mutations in small subunit ribosomal RNA identify functional sites and potential targets for antibiotics, *Proc Natl Acad Sci U S A 102*, 16620-16625.
3. Moazed, D., and Noller, H. F. (1990) Binding of tRNA to the ribosomal A and P sites protects two distinct sets of nucleotides in 16 S rRNA, *J Mol Biol 211*, 135-145.
4. McClory, S. P., Leisring, J. M., Qin, D., and Fredrick, K. (2010) Missense suppressor mutations in 16S rRNA reveal the importance of helices h8 and h14 in aminoacyl-tRNA selection, *RNA 16*, 1925-1934.
5. Woese, C. R., Winker, S., and Gutell, R. R. (1990) Architecture of ribosomal RNA: constraints on the sequence of "tetra-loops", *Proc Natl Acad Sci U S A 87*, 8467-8471.
6. Winker, S., Overbeek, R., Woese, C. R., Olsen, G. J., and Pfluger, N. (1990) Structure detection through automated covariance search, *Comput Appl Biosci 6*, 365-371.
7. Gutell, R. R., and Woese, C. R. (1990) Higher order structural elements in ribosomal RNAs: pseudo-knots and the use of noncanonical pairs, *Proc Natl Acad Sci U S A 87*, 663-667.
8. Crick, F. (1970) Central dogma of molecular biology, *Nature 227*, 561-563.

9. Kruger, K., Grabowski, P. J., Zaug, A. J., Sands, J., Gottschling, D. E., and Cech, T. R. (1982) Self-splicing RNA: autoexcision and autocyclization of the ribosomal RNA intervening sequence of Tetrahymena, *Cell 31*, 147-157.

10. Guerrier-Takada, C., Gardiner, K., Marsh, T., Pace, N., and Altman, S. (1983) The RNA moiety of ribonuclease P is the catalytic subunit of the enzyme, *Cell 35*, 849-857.

11. Guerrier-Takada, C., McClain, W. H., and Altman, S. (1984) Cleavage of tRNA precursors by the RNA subunit of *E. coli* ribonuclease P (M1 RNA) is influenced by 3'-proximal CCA in the substrates, *Cell 38*, 219-224.

12. Guerrier-Takada, C., and Altman, S. (1984) Catalytic activity of an RNA molecule prepared by transcription in vitro, *Science 223*, 285-286.

13. Zieve, G. W. (1981) Two groups of small stable RNAs, *Cell 25*, 296-297.

14. Szymanski, M., Erdmann, V. A., and Barciszewski, J. (2007) Noncoding RNAs database (ncRNAdb), *Nucleic Acids Res 35*, D162-164.

15. Storz, G. (2002) An expanding universe of noncoding RNAs, *Science 296*, 1260-1263.

16. Eddy, S. R. (2001) Non-coding RNA genes and the modern RNA world, *Nat Rev Genet 2*, 919-929.

17. Vazquez, F., Vaucheret, H., Rajagopalan, R., Lepers, C., Gasciolli, V., Mallory, A. C., Hilbert, J. L., Bartel, D. P., and Crete, P. (2004) Endogenous trans-acting siRNAs regulate the accumulation of *Arabidopsis* mRNAs, *Mol Cell 16*, 69-79.

18. Bartel, D. P. (2004) MicroRNAs: genomics, biogenesis, mechanism, and function, *Cell 116*, 281-297.

19. Mulhbacher, J., St-Pierre, P., and Lafontaine, D. A. (2010) Therapeutic applications of ribozymes and riboswitches, *Curr Opin Pharmacol*.

20. Mulhbacher, J., Brouillette, E., Allard, M., Fortier, L. C., Malouin, F., and Lafontaine, D. A. (2010) Novel riboswitch ligand analogs as selective inhibitors of guanine-related metabolic pathways, *PLoS Pathog 6*, e1000865.

21. Rossbach, M. (2010) Small non-coding RNAs as novel therapeutics, *Curr Mol Med 10*, 361-368.

22. Fire, A., Xu, S., Montgomery, M. K., Kostas, S. A., Driver, S. E., and Mello, C. C. (1998) Potent and specific genetic interference by double-stranded RNA in Caenorhabditis elegans, *Nature 391*, 806-811.

23. Scherr, M., and Eder, M. (2007) Gene silencing by small regulatory RNAs in mammalian cells, *Cell Cycle 6*, 444-449.

24. Palade, G. E. (1955) A small particulate component of the cytoplasm, *J Biophys Biochem Cytol 1*, 59-68.

25. Wilson, D. N., Blaha, G., Connell, S. R., Ivanov, P. V., Jenke, H., Stelzl, U., Teraoka, Y., and Nierhaus, K. H. (2002) Protein synthesis at atomic resolution: mechanistics of translation in the light of highly resolved structures for the ribosome, *Curr Protein Pept Sci 3*, 1-53.

26. Wilson, D. N., and Nierhaus, K. H. (2003) The ribosome through the looking glass, *Angew Chem Int Ed Engl 42*, 3464-3486.

27. Berk, V., Zhang, W., Pai, R. D., and Cate, J. H. (2006) Structural basis for mRNA and tRNA positioning on the ribosome, *Proc Natl Acad Sci U S A 103*, 15830-15834.

28. Zhang, W., Dunkle, J. A., and Cate, J. H. (2009) Structures of the ribosome in intermediate states of ratcheting, *Science 325*, 1014-1017.

29. Cech, T. R. (2000) Structural biology. The ribosome is a ribozyme, *Science 289*, 878-879.

30. Mizushima, S., and Nomura, M. (1970) Assembly mapping of 30S ribosomal proteins from *E. coli*, *Nature 226*, 1214.

31. Sykes, M. T., and Williamson, J. R. (2009) A complex assembly landscape for the 30S ribosomal subunit, *Annu Rev Biophys 38*, 197-215.

32. Nissen, P., Ippolito, J. A., Ban, N., Moore, P. B., and Steitz, T. A. (2001) RNA tertiary interactions in the large ribosomal subunit: the A-minor motif, *Proc Natl Acad Sci U S A 98*, 4899-4903.

33. Holley, R. W., Apgar, J., Everett, G. A., Madison, J. T., Marquisee, M., Merrill, S. H., Penswick, J. R., and Zamir, A. (1965) Structure of a ribonucleic acid, *Science 147*, 1462-1465.

34. Gutell, R. R., Lee, J. C., and Cannone, J. J. (2002) The accuracy of ribosomal RNA comparative structure models, *Curr Opin Struct Biol 12*, 301-310.

35. Woese, C. R., Magrum, L. J., Gupta, R., Siegel, R. B., Stahl, D. A., Kop, J., Crawford, N., Brosius, J., Gutell, R., Hogan, J. J., and Noller, H. F. (1980) Secondary structure model for bacterial 16S ribosomal RNA:

phylogenetic, enzymatic and chemical evidence, *Nucleic Acids Res 8*, 2275-2293.

36. Noller, H. F., Kop, J., Wheaton, V., Brosius, J., Gutell, R. R., Kopylov, A. M., Dohme, F., Herr, W., Stahl, D. A., Gupta, R., and Waese, C. R. (1981) Secondary structure model for 23S ribosomal RNA, *Nucleic Acids Res 9*, 6167-6189.

37. Noller, H. F., and Woese, C. R. (1981) Secondary structure of 16S ribosomal RNA, *Science 212*, 403-411.

38. Samaha, R. R., O'Brien, B., O'Brien, T. W., and Noller, H. F. (1994) Independent in vitro assembly of a ribonucleoprotein particle containing the 3' domain of 16S rRNA, *Proc Natl Acad Sci U S A 91*, 7884-7888.

39. Gutell, R. R., Larsen, N., and Woese, C. R. (1994) Lessons from an evolving rRNA: 16S and 23S rRNA structures from a comparative perspective, *Microbiol Rev 58*, 10-26.

40. Noller, H. F. (2005) RNA structure: reading the ribosome, *Science 309*, 1508-1514.

41. Sargsyan, K., and Lim, C. (2010) Arrangement of 3D structural motifs in ribosomal RNA, *Nucleic Acids Res 38*, 3512-3522.

42. Noller, H. F., Hoffarth, V., and Zimniak, L. (1992) Unusual resistance of peptidyl transferase to protein extraction procedures, *Science 256*, 1416-1419.

43. Monro, R. E. (1967) Catalysis of peptide bond formation by 50 S ribosomal subunits from *Escherichia coli*, *J Mol Biol 26*, 147-151.

44. Kornberg, R. D. (2007) The molecular basis of eukaryotic transcription, *Proc Natl Acad Sci U S A 104*, 12955-12961.

45. Moore, M. J., and Proudfoot, N. J. (2009) Pre-mRNA processing reaches back to transcription and ahead to translation, *Cell 136*, 688-700.

46. Shine, J., and Dalgarno, L. (1974) The 3'-terminal sequence of *Escherichia coli* 16S ribosomal RNA: complementarity to nonsense triplets and ribosome binding sites, *Proc Natl Acad Sci U S A 71*, 1342-1346.

47. Carter, A. P., Clemons, W. M., Jr., Brodersen, D. E., Morgan-Warren, R. J., Hartsch, T., Wimberly, B. T., and Ramakrishnan, V. (2001) Crystal structure of an initiation factor bound to the 30S ribosomal subunit, *Science 291*, 498-501.

48. Ramakrishnan, V. (2002) Ribosome structure and the mechanism of translation, *Cell 108*, 557-572.

49. Schmeing, T. M., and Ramakrishnan, V. (2009) What recent ribosome structures have revealed about the mechanism of translation, *Nature 461*, 1234-1242.

50. Pape, T., Wintermeyer, W., and Rodnina, M. V. (1998) Complete kinetic mechanism of elongation factor Tu-dependent binding of aminoacyl-tRNA to the A site of the E. coli ribosome, *EMBO J 17*, 7490-7497.

51. Pape, T., Wintermeyer, W., and Rodnina, M. (1999) Induced fit in initial selection and proofreading of aminoacyl-tRNA on the ribosome, *EMBO J 18*, 3800-3807.

52. Ogle, J. M., Murphy, F. V., Tarry, M. J., and Ramakrishnan, V. (2002) Selection of tRNA by the ribosome requires a transition from an open to a closed form, *Cell 111*, 721-732.

53. Blaha, G., Stanley, R. E., and Steitz, T. A. (2009) Formation of the first peptide bond: the structure of EF-P bound to the 70S ribosome, *Science 325*, 966-970.

54. Rodnina, M. V., Savelsbergh, A., Katunin, V. I., and Wintermeyer, W. (1997) Hydrolysis of GTP by elongation factor G drives tRNA movement on the ribosome, *Nature 385*, 37-41.

55. Stark, H., Rodnina, M. V., Rinke-Appel, J., Brimacombe, R., Wintermeyer, W., and van Heel, M. (1997) Visualization of elongation factor Tu on the *Escherichia coli* ribosome, *Nature 389*, 403-406.

56. Brown, C. M., and Tate, W. P. (1994) Direct recognition of mRNA stop signals by *Escherichia coli* polypeptide chain release factor two, *J Biol Chem 269*, 33164-33170.

57. Karimi, R., Pavlov, M. Y., Buckingham, R. H., and Ehrenberg, M. (1999) Novel roles for classical factors at the interface between translation termination and initiation, *Mol Cell 3*, 601-609.

58. Kaji, A., Kiel, M. C., Hirokawa, G., Muto, A. R., Inokuchi, Y., and Kaji, H. (2001) The fourth step of protein synthesis: disassembly of the posttermination complex is catalyzed by elongation factor G and ribosome recycling factor, a near-perfect mimic of tRNA, *Cold Spring Harb Symp Quant Biol 66*, 515-529.

59. Kisselev, L. L., and Buckingham, R. H. (2000) Translational termination comes of age, *Trends Biochem Sci 25*, 561-566.

60. Noller, H. F., and Chaires, J. B. (1972) Functional modification of 16S ribosomal RNA by kethoxal, *Proc Natl Acad Sci U S A 69*, 3115-3118.

61. Rosenberger, R. F., and Hilton, J. (1983) The frequency of transcriptional and translational errors at nonsense codons in the lacZ gene of *E. coli*, *Mol Gen Genet 191*, 207-212.

62. Nissen, P., Hansen, J., Ban, N., Moore, P. B., and Steitz, T. A. (2000) The structural basis of ribosome activity in peptide bond synthesis, *Science 289*, 920-930.

63. Thompson, J., Kim, D. F., O'Connor, M., Lieberman, K. R., Bayfield, M. A., Gregory, S. T., Green, R., Noller, H. F., and Dahlberg, A. E. (2001) Analysis of mutations at residues A2451 and G2447 of 23S rRNA in the peptidyltransferase active site of the 50S ribosomal subunit, *Proc Natl Acad Sci U S A 98*, 9002-9007.

64. Muth, G. W., Ortoleva-Donnelly, L., and Strobel, S. A. (2000) A single adenosine with a neutral pKa in the ribosomal peptidyl transferase center, *Science 289*, 947-950.

65. Yassin, A., and Mankin, A. S. (2007) Potential new antibiotic sites in the ribosome revealed by deleterious mutations in RNA of the large ribosomal subunit, *J Biol Chem 282*, 24329-24342.

66. Vila-Sanjurjo, A., and Dahlberg, A. E. (2001) Mutational analysis of the conserved bases C1402 and A1500 in the center of the decoding domain

of *Escherichia coli* 16 S rRNA reveals an important tertiary interaction, *J Mol Biol 308*, 457-463.

67. Franceschi, F. (2007) Back to the future: the ribosome as an antibiotic target, *Future Microbiol 2*, 571-574.

68. Franceschi, F., and Duffy, E. M. (2006) Structure-based drug design meets the ribosome, *Biochem Pharmacol 71*, 1016-1025.

69. Carter, A. P., Clemons, W. M., Brodersen, D. E., Morgan-Warren, R. J., Wimberly, B. T., and Ramakrishnan, V. (2000) Functional insights from the structure of the 30S ribosomal subunit and its interactions with antibiotics, *Nature 407*, 340-348.

70. Fourmy, D., Recht, M. I., Blanchard, S. C., and Puglisi, J. D. (1996) Structure of the A site of *Escherichia coli* 16S ribosomal RNA complexed with an aminoglycoside antibiotic, *Science 274*, 1367-1371.

71. Poehlsgaard, J., and Douthwaite, S. (2005) The bacterial ribosome as a target for antibiotics, *Nat Rev Microbiol 3*, 870-881.

72. Vicens, Q., and Westhof, E. (2003) Crystal structure of geneticin bound to a bacterial 16S ribosomal RNA A site oligonucleotide, *J Mol Biol 326*, 1175-1188.

73. Vicens, Q., and Westhof, E. (2003) RNA as a drug target: the case of aminoglycosides, *Chembiochem 4*, 1018-1023.

74. Borovinskaya, M. A., Shoji, S., Holton, J. M., Fredrick, K., and Cate, J. H. (2007) A steric block in translation caused by the antibiotic spectinomycin, *ACS Chem Biol 2*, 545-552.

75. Yoshizawa, S., Fourmy, D., and Puglisi, J. D. (1998) Structural origins of gentamicin antibiotic action, *EMBO J 17*, 6437-6448.

76. Fourmy, D., Yoshizawa, S., and Puglisi, J. D. (1998) Paromomycin binding induces a local conformational change in the A-site of 16 S rRNA, *J Mol Biol 277*, 333-345.

77. Purohit, P., and Stern, S. (1994) Interactions of a small RNA with antibiotic and RNA ligands of the 30S subunit, *Nature 370*, 659-662.

78. Brodersen, D. E., Clemons, W. M., Jr., Carter, A. P., Morgan-Warren, R. J., Wimberly, B. T., and Ramakrishnan, V. (2000) The structural basis for the action of the antibiotics tetracycline, pactamycin, and hygromycin B on the 30S ribosomal subunit, *Cell 103*, 1143-1154.

79. Ogle, J. M., Brodersen, D. E., Clemons, W. M., Jr., Tarry, M. J., Carter, A. P., and Ramakrishnan, V. (2001) Recognition of cognate transfer RNA by the 30S ribosomal subunit, *Science 292*, 897-902.

80. Pioletti, M., Schlunzen, F., Harms, J., Zarivach, R., Gluhmann, M., Avila, H., Bashan, A., Bartels, H., Auerbach, T., Jacobi, C., Hartsch, T., Yonath, A., and Franceschi, F. (2001) Crystal structures of complexes of the small ribosomal subunit with tetracycline, edeine and IF3, *EMBO J 20*, 1829-1839.

81. Hansen, J. L., Ippolito, J. A., Ban, N., Nissen, P., Moore, P. B., and Steitz, T. A. (2002) The structures of four macrolide antibiotics bound to the large ribosomal subunit, *Mol Cell 10*, 117-128.

82. Schlunzen, F., Zarivach, R., Harms, J., Bashan, A., Tocilj, A., Albrecht, R., Yonath, A., and Franceschi, F. (2001) Structural basis for the interaction of antibiotics with the peptidyl transferase centre in eubacteria, *Nature 413*, 814-821.

83. Hansen, J. L., Moore, P. B., and Steitz, T. A. (2003) Structures of five antibiotics bound at the peptidyl transferase center of the large ribosomal subunit, *J Mol Biol 330*, 1061-1075.

84. Leach, K. L., Swaney, S. M., Colca, J. R., McDonald, W. G., Blinn, J. R., Thomasco, L. M., Gadwood, R. C., Shinabarger, D., Xiong, L., and Mankin, A. S. (2007) The site of action of oxazolidinone antibiotics in living bacteria and in human mitochondria, *Mol Cell 26*, 393-402.

85. Ippolito, J. A., Kanyo, Z. F., Wang, D., Franceschi, F. J., Moore, P. B., Steitz, T. A., and Duffy, E. M. (2008) Crystal structure of the oxazolidinone antibiotic linezolid bound to the 50S ribosomal subunit, *J Med Chem 51*, 3353-3356.

86. Steitz, T. A. (2005) On the structural basis of peptide-bond formation and antibiotic resistance from atomic structures of the large ribosomal subunit, *FEBS Letters 579*, 955-958.

87. Walsh, C. (2000) Molecular mechanisms that confer antibacterial drug resistance, *Nature 406*, 775-781.

88. Levy, S. B. (1992) Active efflux mechanisms for antimicrobial resistance, *Antimicrob Agents Chemother 36*, 695-703.

89. Neu, H. C. (1992) The crisis in antibiotic resistance, *Science 257*, 1064-1073.

90. Wilcox, S. K., Cavey, G. S., and Pearson, J. D. (2001) Single ribosomal protein mutations in antibiotic-resistant bacteria analyzed by mass spectrometry, *Antimicrob Agents Chemother 45*, 3046-3055.

91. Savic, M., Lovric, J., Tomic, T. I., Vasiljevic, B., and Conn, G. L. (2009) Determination of the target nucleosides for members of two families of 16S rRNA methyltransferases that confer resistance to partially overlapping groups of aminoglycoside antibiotics, *Nucleic Acids Res 37*, 5420-5431.

92. Macmaster, R., Zelinskaya, N., Savic, M., Rankin, C. R., and Conn, G. L. (2010) Structural insights into the function of aminoglycoside-resistance A1408 16S rRNA methyltransferases from antibiotic-producing and human pathogenic bacteria, *Nucleic Acids Res*.

93. Thompson, J., Skeggs, P. A., and Cundliffe, E. (1985) Methylation of 16S ribosomal RNA and resistance to the aminoglycoside antibiotics gentamicin and kanamycin determined by DNA from the gentamicin-producer, *Micromonospora purpurea*, *Mol Gen Genet 201*, 168-173.

94. Recht, M. I., Douthwaite, S., Dahlquist, K. D., and Puglisi, J. D. (1999) Effect of mutations in the A site of 16 S rRNA on aminoglycoside antibiotic-ribosome interaction, *J Mol Biol 286*, 33-43.

95. Prammananan, T., Sander, P., Brown, B. A., Frischkorn, K., Onyi, G. O., Zhang, Y., Bottger, E. C., and Wallace, R. J., Jr. (1998) A single 16S

ribosomal RNA substitution is responsible for resistance to amikacin and other 2-deoxystreptamine aminoglycosides in *Mycobacterium abscessus* and *Mycobacterium chelonae*, *J Infect Dis 177*, 1573-1581.

96. Miyaguchi, H., Narita, H., Sakamoto, K., and Yokoyama, S. (1996) An antibiotic-binding motif of an RNA fragment derived from the A-site-related region of *Escherichia coli* 16S rRNA, *Nucleic Acids Res 24*, 3700-3706.

97. Sigmund, C. D., Ettayebi, M., and Morgan, E. A. (1984) Antibiotic resistance mutations in 16S and 23S ribosomal RNA genes of *E. coli*, *Nucleic Acids Res 12*, 4653-4663.

98. Poehlsgaard, J., Pfister, P., Bottger, E. C., and Douthwaite, S. (2005) Molecular mechanisms by which rRNA mutations confer resistance to clindamycin, *Antimicrob Agents Chemother 49*, 1553-1555.

99. Weisblum, B. (1995) Erythromycin resistance by ribosome modification, *Antimicrob Agents Chemother 39*, 577-585.

100. Dinos, G., Wilson, D. N., Teraoka, Y., Szaflarski, W., Fucini, P., Kalpaxis, D., and Nierhaus, K. H. (2004) Dissecting the ribosomal inhibition mechanisms of edeine and pactamycin: the universally conserved residues G693 and C795 regulate P-site RNA binding, *Mol Cell 13*, 113-124.

101. Blaha, G., Gurel, G., Schroeder, S. J., Moore, P. B., and Steitz, T. A. (2008) Mutations outside the anisomycin-binding site can make ribosomes drug-resistant, *J Mol Biol 379*, 505-519.

102. Condon, C., Philips, J., Fu, Z. Y., Squires, C., and Squires, C. L. (1992) Comparison of the expression of the seven ribosomal RNA operons in *Escherichia coli*, *EMBO J 11*, 4175-4185.

103. Laios, E., Waddington, M., Saraiya, A. A., Baker, K. A., O'Connor, E., Pamarathy, D., and Cunningham, P. R. (2004) Combinatorial genetic technology for the development of new anti-infectives, *Arch Pathol Lab Med 128*, 1351-1359.

104. Yonath, A. (2005) Antibiotics targeting ribosomes: resistance, selectivity, synergism and cellular regulation, *Annu Rev Biochem 74*, 649-679.

105. Abeysirigunawardena, S. C., and Chow, C. S. (2008) pH-dependent structural changes of helix 69 from Escherichia coli 23S ribosomal RNA, *RNA 14*, 782-792.

106. Wen, J. D., Lancaster, L., Hodges, C., Zeri, A. C., Yoshimura, S. H., Noller, H. F., Bustamante, C., and Tinoco, I. (2008) Following translation by single ribosomes one codon at a time, *Nature 452*, 598-603.

107. Peattie, D. A., and Gilbert, W. (1980) Chemical probes for higher-order structure in RNA, *Proc Natl Acad Sci U S A 77*, 4679-4682.

108. Ehresmann, C., Baudin, F., Mougel, M., Romby, P., Ebel, J. P., and Ehresmann, B. (1987) Probing the structure of RNAs in solution, *Nucleic Acids Res 15*, 9109-9128.

109. Frank, J., Jr., and Gonzalez, R. L. (2010) Structure and dynamics of a processive Brownian motor: the translating ribosome, *Annu Rev Biochem 79*, 381-412.

110. Frank, J. (2009) Single-particle reconstruction of biological macromolecules in electron microscopy--30 years, *Q Rev Biophys 42*, 139-158.

111. Villa, E., Sengupta, J., Trabuco, L. G., LeBarron, J., Baxter, W. T., Shaikh, T. R., Grassucci, R. A., Nissen, P., Ehrenberg, M., Schulten, K., and Frank, J. (2009) Ribosome-induced changes in elongation factor Tu conformation control GTP hydrolysis, *Proc Natl Acad Sci U S A 106*, 1063-1068.

112. Giege, R., Moras, D., and Thierry, J. C. (1977) Yeast transfer RNAasp: a new high-resolution x-ray diffracting crystal form of a transfer RNA, *J Mol Biol 115*, 91-96.

113. Ban, N., Freeborn, B., Nissen, P., Penczek, P., Grassucci, R. A., Sweet, R., Frank, J., Moore, P. B., and Steitz, T. A. (1998) A 9 A resolution X-ray crystallographic map of the large ribosomal subunit, *Cell 93*, 1105-1115.

114. Ban, N., Nissen, P., Hansen, J., Moore, P. B., and Steitz, T. A. (2000) The complete atomic structure of the large ribosomal subunit at 2.4 A resolution, *Science 289*, 905-920.

115. Wimberly, B. T., Brodersen, D. E., Clemons, W. M., Jr., Morgan-Warren, R. J., Carter, A. P., Vonrhein, C., Hartsch, T., and Ramakrishnan, V. (2000) Structure of the 30S ribosomal subunit, *Nature 407*, 327-339.

116. Schluenzen, F., Tocilj, A., Zarivach, R., Harms, J., Gluehmann, M., Janell, D., Bashan, A., Bartels, H., Agmon, I., Franceschi, F., and Yonath, A.

(2000) Structure of functionally activated small ribosomal subunit at 3.3 angstroms resolution, *Cell 102*, 615-623.

117. Steitz, T. A. (2010) From the structure and function of the ribosome to new antibiotics (Nobel Lecture), *Angew Chem Int Ed Engl 49*, 4381-4398.

118. Rodnina, M. V., and Wintermeyer, W. (2010) The ribosome goes Nobel, *Trends Biochem Sci 35*, 1-5.

119. Borovinskaya, M. A., Pai, R. D., Zhang, W., Schuwirth, B. S., Holton, J. M., Hirokawa, G., Kaji, H., Kaji, A., and Cate, J. H. (2007) Structural basis for aminoglycoside inhibition of bacterial ribosome recycling, *Nat Struct Mol Biol 14*, 727-732.

120. Furtig, B., Richter, C., Wohnert, J., and Schwalbe, H. (2003) NMR spectroscopy of RNA, *Chembiochem 4*, 936-962.

121. Scott, L. G., and Hennig, M. (2008) RNA structure determination by NMR, *Methods Mol Biol 452*, 29-61.

122. Aitken, C. E., Petrov, A., and Puglisi, J. D. (2010) Single ribosome dynamics and the mechanism of translation, *Annu Rev Biophys 39*, 491-513.

123. Sumita, M., Desaulniers, J. P., Chang, Y. C., Chui, H. M., Clos, L., 2nd, and Chow, C. S. (2005) Effects of nucleotide substitution and modification on the stability and structure of helix 69 from 28S rRNA, *RNA 11*, 1420-1429.

124. Brunel, C., and Romby, P. (2000) Probing RNA structure and RNA-ligand complexes with chemical probes, *Methods Enzymol 318*, 3-21.

125. Ziehler, W. A., and Engelke, D. R. (2001) Probing RNA structure with chemical reagents and enzymes, *Curr Protoc Nucleic Acid Chem Chapter 6*, Unit 6 1.

126. Regulski, E. E., and Breaker, R. R. (2008) In-line probing analysis of riboswitches, *Methods Mol Biol 419*, 53-67.

127. Wilkinson, K. A., Merino, E. J., and Weeks, K. M. (2006) Selective 2'-hydroxyl acylation analyzed by primer extension (SHAPE): quantitative RNA structure analysis at single nucleotide resolution, *Nat Protoc 1*, 1610-1616.

128. Wilkinson, K. A., Merino, E. J., and Weeks, K. M. (2005) RNA SHAPE chemistry reveals nonhierarchical interactions dominate equilibrium structural transitions in tRNA(Asp) transcripts, *J Am Chem Soc 127*, 4659-4667.

129. Weeks, K. M. (2010) Advances in RNA structure analysis by chemical probing, *Curr Opin Struct Biol 20*, 295-304.

130. Knapp, G. (1989) Enzymatic approaches to probing of RNA secondary and tertiary structure, *Methods Enzymol 180*, 192-212.

131. Lowman, H. B., and Draper, D. E. (1986) On the recognition of helical RNA by cobra venom V1 nuclease, *J Biol Chem 261*, 5396-5403.

132. Donis-Keller, H., Maxam, A. M., and Gilbert, W. (1977) Mapping adenines, guanines, and pyrimidines in RNA, *Nucleic Acids Res 4*, 2527-2538.

133. Uchida, T., and Egami, F. (1967) Ribonuclease T1 from Taka-Diastase, In *Methods Enzymol* (Lawrence Grossman, K. M., Ed.), pp 228-239, Academic Press.

134. Uchida, T., Arima, T., and Egami, F. (1970) Specificity of RNase U2, *J Biochem 67*, 91-102.

135. Uchida, T., and Egami, F. (1967) The specificity of ribonuclease T2, *J Biochem 61*, 44-53.

136. Sung, S. C., and Laskowski, M., Sr. (1962) A nuclease from mung bean sprouts, *J Biol Chem 237*, 506-511.

137. Goodwin, E. C., and Rottman, F. M. (1992) The use of RNase H and poly(A) junction oligonucleotides in the analysis of in vitro polyadenylation reaction products, *Nucleic Acids Res 20*, 916.

138. Maxam, A. M., and Gilbert, W. (1977) A new method for sequencing DNA, *Proc Natl Acad Sci U S A 74*, 560-564.

139. Chow, C. S., and Barton, J. K. (1992) Recognition of G-U mismatches by tris(4,7-diphenyl-1,10-phenanthroline)rhodium(III), *Biochemistry 31*, 5423-5429.

140. Chow, C. S., Behlen, L. S., Uhlenbeck, O. C., and Barton, J. K. (1992) Recognition of tertiary structure in tRNAs by Rh(phen)2phi3+, a new reagent for RNA structure-function mapping, *Biochemistry 31*, 972-982.

141. Joseph, S., and Noller, H. F. (1996) Mapping the rRNA neighborhood of the acceptor end of tRNA in the ribosome, *EMBO J 15*, 910-916.

142. Adilakshmi, T., Lease, R. A., and Woodson, S. A. (2006) Hydroxyl radical footprinting *in vivo*: mapping macromolecular structures with synchrotron radiation, *Nucleic Acids Res 34*, e64.

143. Peattie, D. A. (1979) Direct chemical method for sequencing RNA, *Proc Natl Acad Sci U S A 76*, 1760-1764.

144. Moazed, D., Van Stolk, B. J., Douthwaite, S., and Noller, H. F. (1986) Interconversion of active and inactive 30 S ribosomal subunits is accompanied by a conformational change in the decoding region of 16 S rRNA, *J Mol Biol 191*, 483-493.

145. Moazed, D., Stern, S., and Noller, H. F. (1986) Rapid chemical probing of conformation in 16 S ribosomal RNA and 30 S ribosomal subunits using primer extension, *J Mol Biol 187*, 399-416.

146. Merryman, C., Moazed, D., Daubresse, G., and Noller, H. F. (1999) Nucleotides in 23S rRNA protected by the association of 30S and 50S ribosomal subunits, *J Mol Biol 285*, 107-113.

147. Merryman, C., Moazed, D., McWhirter, J., and Noller, H. F. (1999) Nucleotides in 16S rRNA protected by the association of 30S and 50S ribosomal subunits, *J Mol Biol 285*, 97-105.

148. Hertzberg, R. P., and Dervan, P. B. (1984) Cleavage of DNA with methidiumpropyl-EDTA-iron(II): reaction conditions and product analyses, *Biochemistry 23*, 3934-3945.

149. Sclavi, B., Woodson, S., Sullivan, M., Chance, M. R., and Brenowitz, M. (1997) Time-resolved synchrotron X-ray "footprinting", a new approach to

the study of nucleic acid structure and function: application to protein-DNA interactions and RNA folding, *J Mol Biol 266*, 144-159.

150. Adilakshmi, T., Bellur, D. L., and Woodson, S. A. (2008) Concurrent nucleation of 16S folding and induced fit in 30S ribosome assembly, *Nature 455*, 1268-1272.

151. Singer, B. (1976) All oxygens in nucleic acids react with carcinogenic ethylating agents, *Nature 264*, 333-339.

152. Climie, S. C., and Friesen, J. D. (1988) *In vivo* and *in vitro* structural analysis of the rplJ mRNA leader of *Escherichia coli*. Protection by bound L10-L7/L12, *J Biol Chem 263*, 15166-15175.

153. Balzer, M., and Wagner, R. (1998) A chemical modification method for the structural analysis of RNA and RNA-protein complexes within living cells, *Anal Biochem 256*, 240-242.

154. Morris, M., Eifel, P. J., Lu, J., Grigsby, P. W., Levenback, C., Stevens, R. E., Rotman, M., Gershenson, D. M., and Mutch, D. G. (1999) Pelvic radiation with concurrent chemotherapy compared with pelvic and para-aortic radiation for high-risk cervical cancer, *N Engl J Med 340*, 1137-1143.

155. Keys, H. M., Bundy, B. N., Stehman, F. B., Muderspach, L. I., Chafe, W. E., Suggs, C. L., 3rd, Walker, J. L., and Gersell, D. (1999) Cisplatin, radiation, and adjuvant hysterectomy compared with radiation and adjuvant hysterectomy for bulky stage IB cervical carcinoma, *N Engl J Med 340*, 1154-1161.

156. Jamieson, E. R., and Lippard, S. J. (1999) Structure, Recognition, and Processing of Cisplatin-DNA Adducts, *Chem Rev 99*, 2467-2498.

157. Bosl, G. J., and Motzer, R. J. (1997) Testicular germ-cell cancer, *N Engl J Med 337*, 242-253.

158. Decatris, M. P., Sundar, S., and O'Byrne, K. J. (2004) Platinum-based chemotherapy in metastatic breast cancer: current status, *Cancer Treat Rev 30*, 53-81.

159. Von Hoff, D. D., Schilsky, R., Reichert, C. M., Reddick, R. L., Rozencweig, M., Young, R. C., and Muggia, F. M. (1979) Toxic effects of cis-dichlorodiammineplatinum(II) in man, *Cancer Treat Rep 63*, 1527-1531.

160. Rosenberg, B., Vancamp, L., and Krigas, T. (1965) Inhibition of cell division in *Escherichia coli* by electrolysis products from a platinum electrode, *Nature 205*, 698-699.

161. Rosenberg, B., VanCamp, L., Trosko, J. E., and Mansour, V. H. (1969) Platinum compounds: a new class of potent antitumour agents, *Nature 222*, 385-386.

162. Hromas, R. A., North, J. A., and Burns, C. P. (1987) Decreased cisplatin uptake by resistant L1210 leukemia cells, *Cancer Lett 36*, 197-201.

163. Wang, D., and Lippard, S. J. (2005) Cellular processing of platinum anticancer drugs, *Nat Rev Drug Discov 4*, 307-320.

164. Pascoe, J. M., and Roberts, J. J. (1974) Interactions between mammalian cell DNA and inorganic platinum compounds. II. Interstrand cross-linking

of isolated and cellular DNA by platinum(IV) compounds, *Biochem Pharmacol 23*, 1345-1357.

165. Akaboshi, M., Kawai, K., Maki, H., Akuta, K., Ujeno, Y., and Miyahara, T. (1992) The number of platinum atoms binding to DNA, RNA and protein molecules of HeLa cells treated with cisplatin at its mean lethal concentration, *Jpn J Cancer Res 83*, 522-526.

166. Jung, Y., and Lippard, S. J. (2007) Direct cellular responses to platinum-induced DNA damage, *Chem Rev 107*, 1387-1407.

167. Hägerlöf, M., Papsai, P., Chow, C. S., and Elmroth, S. K. (2006) More pronounced salt dependence and higher reactivity for platination of the hairpin r(CGCGUUGUUCGCG) compared with d(CGCGTTGTTCGCG), *J Biol Inorg Chem 11*, 974-990.

168. Papsai, P., Aldag, J., Persson, T., and Elmroth, S. K. (2006) Kinetic preference for interaction of cisplatin with the G-C-rich wobble basepair region in both $tRNA^{Ala}$ and Mh^{Ala}, *Dalton Trans*, 3515-3517.

169. Hostetter, A. A., Chapman, E. G., and DeRose, V. J. (2009) Rapid cross-linking of an RNA internal loop by the anticancer drug cisplatin, *J Am Chem Soc 131*, 9250-9257.

170. Chapman, E. G., and DeRose, V. J. (2010) Enzymatic processing of platinated RNAs, *J Am Chem Soc 132*, 1946-1952.

171. Eastman, A. (1986) Reevaluation of interaction of cis-dichloro(ethylenediamine)platinum(II) with DNA, *Biochemistry 25*, 3912-3915.

172. Fichtinger-Schepman, A. M., van der Veer, J. L., den Hartog, J. H., Lohman, P. H., and Reedijk, J. (1985) Adducts of the antitumor drug cis-diamminedichloroplatinum(II) with DNA: formation, identification, and quantitation, *Biochemistry 24*, 707-713.

173. Poklar, N., Pilch, D. S., Lippard, S. J., Redding, E. A., Dunham, S. U., and Breslauer, K. J. (1996) Influence of cisplatin intrastrand crosslinking on the conformation, thermal stability, and energetics of a 20-mer DNA duplex, *Proc Natl Acad Sci U S A 93*, 7606-7611.

174. Cohen, G. L., Bauer, W. R., Barton, J. K., and Lippard, S. J. (1979) Binding of cis- and trans-dichlorodiammineplatinum(II) to DNA: evidence for unwinding and shortening of the double helix, *Science 203*, 1014-1016.

175. Comess, K. M., Burstyn, J. N., Essigmann, J. M., and Lippard, S. J. (1992) Replication inhibition and translesion synthesis on templates containing site-specifically placed cis-diamminedichloroplatinum(II) DNA adducts, *Biochemistry 31*, 3975-3990.

176. Suo, Z., Lippard, S. J., and Johnson, K. A. (1999) Single d(GpG)/cis-diammineplatinum(II) adduct-induced inhibition of DNA polymerization, *Biochemistry 38*, 715-726.

177. Lemaire, M. A., Schwartz, A., Rahmouni, A. R., and Leng, M. (1991) Interstrand cross-links are preferentially formed at the d(GC) sites in the reaction between cis-diamminedichloroplatinum (II) and DNA, *Proc Natl Acad Sci U S A 88*, 1982-1985.

178. Bruhn, S. L., Pil, P. M., Essigmann, J. M., Housman, D. E., and Lippard, S. J. (1992) Isolation and characterization of human cDNA clones encoding a high mobility group box protein that recognizes structural distortions to DNA caused by binding of the anticancer agent cisplatin, *Proc Natl Acad Sci U S A 89*, 2307-2311.

179. Kartalou, M., and Essigmann, J. M. (2001) Recognition of cisplatin adducts by cellular proteins, *Mutat Res 478*, 1-21.

180. Lebwohl, D., and Canetta, R. (1998) Clinical development of platinum complexes in cancer therapy: an historical perspective and an update, *Eur J Cancer 34*, 1522-1534.

181. Fuertes, M. A., Alonso, C., and Perez, J. M. (2003) Biochemical modulation of Cisplatin mechanisms of action: enhancement of antitumor activity and circumvention of drug resistance, *Chem Rev 103*, 645-662.

182. Kelland, L. R. (1993) New platinum antitumor complexes, *Crit Rev Oncol Hematol 15*, 191-219.

183. Reedijk, J. (2009) Platinum anticancer coordination compounds: study of DNA binding inspires new drug design, *Eur J Inorg Chem 2009*, 1303-1312.

184. Gore, M. E., Fryatt, I., Wiltshaw, E., Dawson, T., Robinson, B. A., and Calvert, A. H. (1989) Cisplatin/carboplatin cross-resistance in ovarian cancer, *Br J Cancer 60*, 767-769.

185. Wong, E., and Giandomenico, C. M. (1999) Current status of platinum-based antitumor drugs, *Chem Rev 99*, 2451-2466.

186. Robillard, M. S., Davies, N. P., van der Marel, G. A., van Boom, J. H., Reedijk, J., and Murray, V. (2003) The interaction of peptide-tethered platinum(II) complexes with DNA, *J Inorg Biochem 96*, 331-338.

187. Ziegler, C. J., Sandman, K. E., Liang, C. H., and Lippard, S. J. (1999) Toxicity of platinum(II) amino acid (N,O) complexes parallels their binding to DNA as measured in a new solid phase assay involving a fluorescent HMG1 protein construct readout, *JBIC 4*, 402-411.

188. Altman, J., Wilchek, M., and Warshawsky, A. (1985) Platinum(II) complexes with 2,4-diaminobutyric acid, ornithine, lysine and 4,5-diaminovaleric acid, *Inorganica Chimica Acta 107*, 165-168.

189. Dalla Via, L., Gia, O., Magno, S. M., Dolmella, A., Marton, D., and Di Noto, V. (2006) Synthesis, characterization and biological activity of platinum(II) complexes with l- and d-ornithine ligands, *Inorganica Chimica Acta 359*, 4197-4206.

190. Robillard, M. S., Bacac, M., van den Elst, H., Flamigni, A., van der Marel, G. A., van Boom, J. H., and Reedijk, J. (2003) Automated parallel solid-phase synthesis and anticancer screening of a library of peptide-tethered platinum(II) complexes, *J Comb Chem 5*, 821-825.

191. Eastman, A. (1983) Characterization of the adducts produced in DNA by cis-diamminedichloroplatinum(II) and cis-dichloro(ethylenediamine)platinum(II), *Biochemistry 22*, 3927-3933.

192. Todd, R. C., and Lippard, S. J. (2009) Inhibition of transcription by platinum antitumor compounds, *Metallomics 1*, 280-291.

193. Todd, R. C., and Lippard, S. J. (2010) Structure of duplex DNA containing the cisplatin 1,2-{Pt(NH3)2}2+-d(GpG) cross-link at 1.77 A resolution, *J Inorg Biochem 104*, 902-908.

194. Yang, D., van Boom, S. S., Reedijk, J., van Boom, J. H., and Wang, A. H. (1995) Structure and isomerization of an intrastrand cisplatin-cross-linked octamer DNA duplex by NMR analysis, *Biochemistry 34*, 12912-12920.

195. Fuertes, M. A., Castilla, J., Alonso, C., and Perez, J. M. (2003) Cisplatin biochemical mechanism of action: from cytotoxicity to induction of cell death through interconnections between apoptotic and necrotic pathways, *Curr Med Chem 10*, 257-266.

196. Baik, M. H., Friesner, R. A., and Lippard, S. J. (2003) Theoretical study of cisplatin binding to purine bases: why does cisplatin prefer guanine over adenine?, *J Am Chem Soc 125*, 14082-14092.

197. Mantri, Y., Lippard, S. J., and Baik, M. H. (2007) Bifunctional binding of cisplatin to DNA: why does cisplatin form 1,2-intrastrand cross-links with AG but not with GA?, *J Am Chem Soc 129*, 5023-5030.

198. Parker, R., and Song, H. (2004) The enzymes and control of eukaryotic mRNA turnover, *Nat Struct Mol Biol 11*, 121-127.

199. Doma, M. K., and Parker, R. (2007) RNA quality control in eukaryotes, *Cell 131*, 660-668.

200. Pascoe, J. M., and Roberts, J. J. (1974) Interactions between mammalian cell DNA and inorganic platinum compounds. I. DNA interstrand cross-

linking and cytotoxic properties of platinum(II) compounds, *Biochem Pharmacol 23*, 1359-1365.

201. Rosenberg, J., and Sato, P. (1988) Messenger RNA loses the ability to direct in vitro peptide synthesis following incubation with cisplatin, *Mol Pharmacol 33*, 611-616.

202. Schmittgen, T. D., Ju, J. F., Danenberg, K. D., and Danenberg, P. V. (2003) Inhibition of pre-mRNA splicing by cisplatin and platinum analogs, *Int J Oncol 23*, 785-789.

203. Danenberg, P. V., Shea, L. C., Danenberg, K. D., and Horikoshi, T. (1991) Inactivation of Tetrahymena rRNA self-splicing by cis-platin proceeds through dissociable complexes, *Nucleic Acids Res 19*, 3123-3128.

204. Rijal, K., and Chow, C. S. (2009) A new role for cisplatin: probing ribosomal RNA structure, *Chem Commun (Camb)*, 107-109.

205. Hagerlof, M., Papsai, P., Chow, C. S., and Elmroth, S. K. (2006) More pronounced salt dependence and higher reactivity for platination of the hairpin r(CGCGUUGUUCGCG) compared with d(CGCGTTGTTCGCG), *J Biol Inorg Chem 11*, 974-990.

206. van Garderen, C. J., and van Houte, L. P. (1994) The solution structure of a DNA duplex containing the cis-Pt(NH3)2[d(-GTG-)-N7(G),N7(G)] adduct, as determined with high-field NMR and molecular mechanics/dynamics, *Eur J Biochem 225*, 1169-1179.

207. Sykfont, A., Ericson, A., and Elmroth, S. K. C. (2001) Non-uniform rate for platination of guanine-N7 located in short DNA oligomers, *Chem Commun*, 1190-1191.

208. Rhodes, D., Piper, P. W., and Clark, B. F. (1974) Location of a platinum binding site in the structure of yeast phenylalanine transfer RNA, *J Mol Biol 89*, 469-475.

209. Dewan, J. C. (1984) Binding of the antitumor drug cis-diamminedichloroplatinum to crystalline tRNAPhe at 6 .A. resolution, *J Am Chem Soc 106*, 7239-7244.

210. Pichorner, H., Lickl, E., Tuma, K., Alth, G., Praznik, W., and Ebermann, R. (1993) Effects of cis-platin on t-RNA of Saccharomyces cerevisiae, *Biosci Biotechnol Biochem 57*, 1198-1199.

211. Chow, C. S., Cunningham, P. R., Lee, K., Meroueh, M., SantaLucia, J., Jr., and Varma, S. (2002) Photoinduced cleavage by a rhodium complex at G.U mismatches and exposed guanines in large and small RNAs, *Biochimie 84*, 859-868.

212. Kieltyka, J. W., and Chow, C. S. (2006) Probing RNA hairpins with cobalt(III)hexammine and electrospray ionization mass spectrometry, *J Am Soc Mass Spectrom 17*, 1376-1382.

213. Lim, M. H., Lau, I. H., and Barton, J. K. (2007) DNA strand cleavage near a CC mismatch directed by a metalloinsertor, *Inorg Chem 46*, 9528-9530.

214. Spedding, G. (1990) *Ribosomes and protein synthesis "A practical approach"*, Oxford University Press.

215. Todd, R. C., Lovejoy, K. S., and Lippard, S. J. (2007) Understanding the effect of carbonate ion on cisplatin binding to DNA, *J Am Chem Soc 129*, 6370-6371.

216. Motorin, Y., Muller, S., Behm-Ansmant, I., and Branlant, C. (2007) Identification of modified residues in RNAs by reverse transcription-based methods, *Methods Enzymol 425*, 21-53.

217. Fasman, G. D. (1976) *Handbook of biochemistry and molecular biology* 3rd ed., CRC Press.

218. Sykfont Snygg, A., Brindell, M., Stochel, G., and Elmroth, S. K. C. (2005) A combination of access to preassociation sites and local accumulation tendency in the direct vicinity of G-N7 controls the rate of platination of single-stranded DNA, *Dalton Trans*, 1221-1227.

219. McClain, W. H., and Foss, K. (1988) Changing the identity of a tRNA by introducing a G-U wobble pair near the 3' acceptor end, *Science 240*, 793-796.

220. Hou, Y. M., and Schimmel, P. (1988) A simple structural feature is a major determinant of the identity of a transfer RNA, *Nature 333*, 140-145.

221. White, S. A., and Li, H. (1996) Yeast ribosomal protein L32 recognizes an RNA G:U juxtaposition, *RNA 2*, 226-234.

222. Schuwirth, B. S., Borovinskaya, M. A., Hau, C. W., Zhang, W., Vila-Sanjurjo, A., Holton, J. M., and Cate, J. H. (2005) Structures of the bacterial ribosome at 3.5 A resolution, *Science 310*, 827-834.

223. Chow, C. S., and Bogdan, F. M. (1997) A structural basis for RNA-Ligand interactions, *Chem Rev 97*, 1489-1514.

224. Zou, Y., Van Houten, B., and Farrell, N. (1994) Sequence specificity of DNA-DNA interstrand cross-link formation by cisplatin and dinuclear platinum complexes, *Biochemistry 33*, 5404-5410.

225. Snygg, A. S., Brindell, M., Stochel, G., and Elmroth, S. K. (2005) A combination of access to preassociation sites and local accumulation tendency in the direct vicinity of G-N7 controls the rate of platination of single-stranded DNA, *Dalton Trans*, 1221-1227.

226. Hermann, T., and Westhof, E. (1998) Exploration of metal ion binding sites in RNA folds by Brownian-dynamics simulations, *Structure 6*, 1303-1314.

227. Riley, C. M., Sternson, L. A., Repta, A. J., and Slyter, S. A. (1983) Monitoring the reactions of cisplatin with nucleotides and methionine by reversed-phase high-performance liquid chromatography using cationic and anionic pairing ions, *Anal Biochem 130*, 203-214.

228. Davies, M. S., Cox, J. W., Berners-Price, S. J., Barklage, W., Qu, Y., and Farrell, N. (2000) Equilibrium and kinetic studies of the aquation of the dinuclear platinum complex [[trans-$PtCl(NH_3)_2$]2(mu-$NH_2(CH_2)_6NH_2$)]$^{2+}$: pKa determinations of aqua ligands via [1H,15N] NMR spectroscopy, *Inorg Chem 39*, 1710-1715.

229. Bancroft, D. P., Lepre, C. A., and Lippard, S. J. (1990) Platinum-195 NMR kinetic and mechanistic studies of cis- and trans-

diamminedichloroplatinum(II) binding to DNA, *J Am Chem Soc 112*, 6860-6871.

230. Muralikrishna, P., and Wickstrom, E. (1989) *Escherichia coli* initiation factor 3 protein binding to 30S ribosomal subunits alters the accessibility of nucleotides within the conserved central region of 16S rRNA, *Biochemistry 28*, 7505-7510.

231. Tapprich, W. E., and Hill, W. E. (1986) Involvement of bases 787-795 of *Escherichia coli* 16S ribosomal RNA in ribosomal subunit association, *Proc Natl Acad Sci U S A 83*, 556-560.

232. Doring, T., Mitchell, P., Osswald, M., Bochkariov, D., and Brimacombe, R. (1994) The decoding region of 16S RNA; a cross-linking study of the ribosomal A, P and E sites using tRNA derivatized at position 32 in the anticodon loop, *EMBO J 13*, 2677-2685.

233. Woodson, S. A. (2005) Metal ions and RNA folding: a highly charged topic with a dynamic future, *Curr Opin Chem Biol 9*, 104-109.

234. Moazed, D., and Noller, H. F. (1987) Chloramphenicol, erythromycin, carbomycin and vernamycin B protect overlapping sites in the peptidyl transferase region of 23S ribosomal RNA, *Biochimie 69*, 879-884.

235. Moazed, D., and Noller, H. F. (1987) Interaction of antibiotics with functional sites in 16S ribosomal RNA, *Nature 327*, 389-394.

236. David-Eden, H., Mankin, A. S., and Mandel-Gutfreund, Y. (2010) Structural signatures of antibiotic binding sites on the ribosome, *Nucleic Acids Res 38*, 5982-5994.

237. Jenner, L. B., Demeshkina, N., Yusupova, G., and Yusupov, M. (2010) Structural aspects of messenger RNA reading frame maintenance by the ribosome, *Nat Struct Mol Biol 17*, 555-560.

238. Korostelev, A., Trakhanov, S., Laurberg, M., and Noller, H. F. (2006) Crystal structure of a 70S ribosome-tRNA complex reveals functional interactions and rearrangements, *Cell 126*, 1065-1077.

239. Balzer, M., and Wagner, R. (1998) Mutations in the leader region of ribosomal RNA operons cause structurally defective 30 S ribosomes as revealed by *in vivo* structural probing, *J Mol Biol 276*, 547-557.

240. Lindell, M., Romby, P., and Wagner, E. G. (2002) Lead(II) as a probe for investigating RNA structure *in vivo*, *RNA 8*, 534-541.

241. Spedding, G. (1990) *Ribosomes and protein synthesis "A practical approcah"*, Oxford University Press.

242. Nuyts, S., Van Mellaert, L., Lambin, P., and Anne, J. (2001) Efficient isolation of total RNA from Clostridium without DNA contamination, *J Microbiol Methods 44*, 235-238.

243. Nilsson, M., Wahlund, K.-G., and Bülow, L. (1998) Monitoring of Ribosomes and Subunits in *Escherichia coli* During Production of Glucose Isomerase Using Flow Field-Flow Fractionation, *Biotechnol Tech 12*, 477-480.

244. Cannone, J. J., Subramanian, S., Schnare, M. N., Collett, J. R., D'Souza, L. M., Du, Y., Feng, B., Lin, N., Madabusi, L. V., Muller, K. M., Pande, N., Shang, Z., Yu, N., and Gutell, R. R. (2002) The comparative RNA web

(CRW) site: an online database of comparative sequence and structure information for ribosomal, intron, and other RNAs, *BMC Bioinformatics 3*, 2.

245. Selmer, M., Dunham, C. M., Murphy, F. V. t., Weixlbaumer, A., Petry, S., Kelley, A. C., Weir, J. R., and Ramakrishnan, V. (2006) Structure of the 70S ribosome complexed with mRNA and tRNA, *Science 313*, 1935-1942.

246. Brodersen, D. E., Clemons, W. M., Jr., Carter, A. P., Wimberly, B. T., and Ramakrishnan, V. (2002) Crystal structure of the 30 S ribosomal subunit from Thermus thermophilus: structure of the proteins and their interactions with 16 S RNA, *J Mol Biol 316*, 725-768.

247. Lee, K., Varma, S., SantaLucia, J., Jr., and Cunningham, P. R. (1997) *In vivo* determination of RNA structure-function relationships: analysis of the 790 loop in ribosomal RNA, *J Mol Biol 269*, 732-743.

248. Moazed, D., Samaha, R. R., Gualerzi, C., and Noller, H. F. (1995) Specific protection of 16 S rRNA by translational initiation factors, *J Mol Biol 248*, 207-210.

249. Moazed, D., and Noller, H. F. (1986) Transfer RNA shields specific nucleotides in 16S ribosomal RNA from attack by chemical probes, *Cell 47*, 985-994.

250. Muller, R., Garrett, R. A., and Noller, H. F. (1979) The structure of the RNA binding site of ribosomal proteins S8 and S15, *J Biol Chem 254*, 3873-3878.

251. Simonsen, K. B., Ayida, B. K., Vourloumis, D., Takahashi, M., Winters, G. C., Barluenga, S., Qamar, S., Shandrick, S., Zhao, Q., and Hermann, T. (2002) Novel paromamine derivatives exploring shallow-groove recognition of ribosomal-decoding-site RNA, *Chembiochem 3*, 1223-1228.

252. Vourloumis, D., Winters, G. C., Simonsen, K. B., Takahashi, M., Ayida, B. K., Shandrick, S., Zhao, Q., Han, Q., and Hermann, T. (2005) Aminoglycoside-hybrid ligands targeting the ribosomal decoding site, *Chembiochem 6*, 58-65.

253. Morosyuk, S. V., Cunningham, P. R., and SantaLucia, J., Jr. (2001) Structure and function of the conserved 690 hairpin in *Escherichia coli* 16 S ribosomal RNA. II. NMR solution structure, *J Mol Biol 307*, 197-211.

254. Llano-Sotelo, B., Klepacki, D., and Mankin, A. S. (2009) Selection of small peptides, inhibitors of translation, *J Mol Biol 391*, 813-819.

255. Tapprich, W. E., Goss, D. J., and Dahlberg, A. E. (1989) Mutation at position 791 in *Escherichia coli* 16S ribosomal RNA affects processes involved in the initiation of protein synthesis, *Proc Natl Acad Sci U S A 86*, 4927-4931.

256. Lancaster, L., and Noller, H. F. (2005) Involvement of 16S rRNA nucleotides G1338 and A1339 in discrimination of initiator tRNA, *Mol Cell 20*, 623-632.

257. Santer, M., and Shane, S. (1977) Area of 16S ribonucleic acid at or near the interface between 30S and 50S ribosomes of *Escherichia coli*, *J Bacteriol 130*, 900-910.

258. Mankin, A. S. (1997) Pactamycin resistance mutations in functional sites of 16 S rRNA, *J Mol Biol 274*, 8-15.

259. Cate, J. H., Yusupov, M. M., Yusupova, G. Z., Earnest, T. N., and Noller, H. F. (1999) X-ray crystal structures of 70S ribosome functional complexes, *Science 285*, 2095-2104.

260. Yonath, A. (2002) The search and its outcome: high-resolution structures of ribosomal particles from mesophilic, thermophilic, and halophilic bacteria at various functional states, *Annu Rev Biophys Biomol Struct 31*, 257-273.

261. Ramakrishnan, V. (2010) Unraveling the structure of the ribosome (Nobel Lecture), *Angew Chem Int Ed Engl 49*, 4355-4380.

262. Gootz, T. D. (2010) The global problem of antibiotic resistance, *Crit Rev Immunol 30*, 79-93.

263. Boulikas T, P. A., Bellis E, and Christofis P (2007) Designing platinum compounds in cancer: structures and mechanisms, *Cancer Ther 5*, 537-583.

264. Ishida, S., Lee, J., Thiele, D. J., and Herskowitz, I. (2002) Uptake of the anticancer drug cisplatin mediated by the copper transporter Ctr1 in yeast and mammals, *Proc Natl Acad Sci U S A 99*, 14298-14302.

265. Pitts, A. E., Van Loon, J. C., and Beamish, F. E. (1970) The determination of platinum by atomic absorption spectroscopy, *Analytica Chimica Acta 50*, 195-199.

266. Chappuy, M., Caudron, E., Bellanger, A., and Pradeau, D. (2010) Determination of platinum traces contamination by graphite furnace atomic absorption spectrometry after preconcentration by cloud point extraction, *J Hazard Mater 176*, 207-212.

267. Iannitti-Tito, P., Weimann, A., Wickham, G., and Sheil, M. M. (2000) Structural analysis of drug-DNA adducts by tandem mass spectrometry, *Analyst 125*, 627-633.

268. Kartalou, M., and Essigmann, J. M. (2001) Mechanisms of resistance to cisplatin, *Mutat Res 478*, 23-43.

269. Weiss, R. B., and Christian, M. C. (1993) New cisplatin analogues in development. A review, *Drugs 46*, 360-377.

270. Perez, J. M., Kelland, L. R., Montero, E. I., Boxall, F. E., Fuertes, M. A., Alonso, C., and Navarro-Ranninger, C. (2003) Antitumor and cellular pharmacological properties of a novel platinum(IV) complex: trans-[PtCl(2)(OH)(2)(dimethylamine) (isopropylamine)], *Mol Pharmacol 63*, 933-944.

271. Temple, M. D., McFadyen, W. D., Holmes, R. J., Denny, W. A., and Murray, V. (2000) Interaction of Cisplatin and DNA-Targeted 9-Aminoacridine Platinum Complexes with DNA†, *Biochemistry 39*, 5593-5599.

272. Temple, M. D., McFadyen, W. D., Holmes, R. J., Denny, W. A., and Murray, V. (2000) Interaction of cisplatin and DNA-targeted 9-

aminoacridine platinum complexes with DNA, *Biochemistry 39*, 5593-5599.

273. Temple, M. D., Recabarren, P., McFadyen, W. D., Holmes, R. J., Denny, W. A., and Murray, V. (2002) The interaction of DNA-targeted 9-aminoacridine-4-carboxamide platinum complexes with DNA in intact human cells, *Biochim Biophys Acta 1574*, 223-230.

274. Sandman, K. E., Fuhrmann, P., and Lippard, S. J. (1998) A mechanism-based, solution-phase method for screening combinatorial mixtures of potential platinum anticancer drugs, *JBIC 3*, 74-80.

275. Marciniak, R. A., Calnan, B. J., Frankel, A. D., and Sharp, P. A. (1990) HIV-1 Tat protein trans-activates transcription *in vitro*, *Cell 63*, 791-802.

276. Weeks, K. M., and Crothers, D. M. (1991) RNA recognition by Tat-derived peptides: interaction in the major groove?, *Cell 66*, 577-588.

277. Loskotova, H., and Brabec, V. (1999) DNA interactions of cisplatin tethered to the DNA minor groove binder distamycin, *Eur J Biochem 266*, 392-402.

278. Guddneppanavar, R., and Bierbach, U. (2007) Adenine-N3 in the DNA minor groove - an emerging target for platinum containing anticancer pharmacophores, *Anticancer Agents Med Chem 7*, 125-138.

279. Denny, W. A. (2001) DNA minor groove alkylating agents, *Curr Med Chem 8*, 533-544.

280. Armitage, J. O., and Weisenburger, D. D. (1998) New approach to classifying non-Hodgkin's lymphomas: clinical features of the major

histologic subtypes. Non-Hodgkin's Lymphoma Classification Project, *J Clin Oncol 16*, 2780-2795.

281. Cheson, B. D., and Leonard, J. P. (2008) Monoclonal antibody therapy for B-cell non-Hodgkin's lymphoma, *N Engl J Med 359*, 613-626.

282. http://www.cancer.gov/cancertopics/types/non-hodgkin.

283. Klapproth, K., and Wirth, T. (2010) Advances in the understanding of MYC-induced lymphomagenesis, *Br J Haematol 149*, 484-497.

284. Dang, C. V., O'Donnell, K. A., Zeller, K. I., Nguyen, T., Osthus, R. C., and Li, F. (2006) The c-Myc target gene network, *Semin Cancer Biol 16*, 253-264.

285. Cole, M. D. (1986) The myc oncogene: its role in transformation and differentiation, *Annu Rev Genet 20*, 361-384.

286. Hecht, J. L., and Aster, J. C. (2000) Molecular biology of Burkitt's lymphoma, *J Clin Oncol 18*, 3707-3721.

287. Dang, C. V. (1999) c-Myc target genes involved in cell growth, apoptosis, and metabolism, *Mol Cell Biol 19*, 1-11.

288. Lee, J. T., Innes, D. J., Jr., and Williams, M. E. (1989) Sequential bcl-2 and c-myc oncogene rearrangements associated with the clinical transformation of non-Hodgkin's lymphoma, *J Clin Invest 84*, 1454-1459.

289. Sharp, P. A. (2001) RNA interference--2001, *Genes Dev 15*, 485-490.

290. Elbashir, S. M., Harborth, J., Lendeckel, W., Yalcin, A., Weber, K., and Tuschl, T. (2001) Duplexes of 21-nucleotide RNAs mediate RNA interference in cultured mammalian cells, *Nature 411*, 494-498.

291. Bernstein, E., Caudy, A. A., Hammond, S. M., and Hannon, G. J. (2001) Role for a bidentate ribonuclease in the initiation step of RNA interference, *Nature 409*, 363-366.

292. Whitehead, K. A., Langer, R., and Anderson, D. G. (2009) Knocking down barriers: advances in siRNA delivery, *Nat Rev Drug Discov 8*, 129-138.

293. Rand, T. A., Ginalski, K., Grishin, N. V., and Wang, X. (2004) Biochemical identification of Argonaute 2 as the sole protein required for RNA-induced silencing complex activity, *Proc Natl Acad Sci U S A 101*, 14385-14389.

294. Matranga, C., Tomari, Y., Shin, C., Bartel, D. P., and Zamore, P. D. (2005) Passenger-strand cleavage facilitates assembly of siRNA into Ago2-containing RNAi enzyme complexes, *Cell 123*, 607-620.

295. Ameres, S. L., Martinez, J., and Schroeder, R. (2007) Molecular basis for target RNA recognition and cleavage by human RISC, *Cell 130*, 101-112.

296. Bartlett, D. W., and Davis, M. E. (2006) Insights into the kinetics of siRNA-mediated gene silencing from live-cell and live-animal bioluminescent imaging, *Nucleic Acids Res 34*, 322-333.

297. Sato, Y., Murase, K., Kato, J., Kobune, M., Sato, T., Kawano, Y., Takimoto, R., Takada, K., Miyanishi, K., Matsunaga, T., Takayama, T., and Niitsu, Y. (2008) Resolution of liver cirrhosis using vitamin A-coupled liposomes to deliver siRNA against a collagen-specific chaperone, *Nat Biotechnol 26*, 431-442.

298. Song, E., Lee, S. K., Wang, J., Ince, N., Ouyang, N., Min, J., Chen, J., Shankar, P., and Lieberman, J. (2003) RNA interference targeting Fas protects mice from fulminant hepatitis, *Nat Med 9*, 347-351.

299. Niu, X. Y., Peng, Z. L., Duan, W. Q., Wang, H., and Wang, P. (2006) Inhibition of HPV 16 E6 oncogene expression by RNA interference *in vitro* and *in vivo*, *Int J Gynecol Cancer 16*, 743-751.

300. Halder, J., Kamat, A. A., Landen, C. N., Jr., Han, L. Y., Lutgendorf, S. K., Lin, Y. G., Merritt, W. M., Jennings, N. B., Chavez-Reyes, A., Coleman, R. L., Gershenson, D. M., Schmandt, R., Cole, S. W., Lopez-Berestein, G., and Sood, A. K. (2006) Focal adhesion kinase targeting using *in vivo* short interfering RNA delivery in neutral liposomes for ovarian carcinoma therapy, *Clin Cancer Res 12*, 4916-4924.

301. Takeshita, F., Minakuchi, Y., Nagahara, S., Honma, K., Sasaki, H., Hirai, K., Teratani, T., Namatame, N., Yamamoto, Y., Hanai, K., Kato, T., Sano, A., and Ochiya, T. (2005) Efficient delivery of small interfering RNA to bone-metastatic tumors by using atelocollagen *in vivo*, *Proc Natl Acad Sci U S A 102*, 12177-12182.

302. Bumcrot, D., Manoharan, M., Koteliansky, V., and Sah, D. W. (2006) RNAi therapeutics: a potential new class of pharmaceutical drugs, *Nat Chem Biol 2*, 711-719.

303. Zimmermann, T. S., Lee, A. C., Akinc, A., Bramlage, B., Bumcrot, D., Fedoruk, M. N., Harborth, J., Heyes, J. A., Jeffs, L. B., John, M., Judge, A. D., Lam, K., McClintock, K., Nechev, L. V., Palmer, L. R., Racie, T., Rohl,

I., Seiffert, S., Shanmugam, S., Sood, V., Soutschek, J., Toudjarska, I., Wheat, A. J., Yaworski, E., Zedalis, W., Koteliansky, V., Manoharan, M., Vornlocher, H. P., and MacLachlan, I. (2006) RNAi-mediated gene silencing in non-human primates, *Nature 441*, 111-114.

304. Torchilin, V. P. (2005) Recent advances with liposomes as pharmaceutical carriers, *Nat Rev Drug Discov 4*, 145-160.

305. Putnam, D. (2006) Polymers for gene delivery across length scales, *Nat Mater 5*, 439-451.

306. MacLachlan, I. (2008) Liposomal formulations for nucleic acid delivery, In *Antisense Drug Technologies* (Crooke, S. T., Ed.) second ed., CRC press

307. Bangham, A. D. (1972) Lipid bilayers and biomembranes, *Annu Rev Biochem 41*, 753-776.

308. Hamdy, N., Goustin, A. S., Desaulniers, J. P., Li, M., Chow, C. S., and Al-Katib, A. (2005) Sheep red blood cells armed with anti-CD20 single-chain variable fragments (scFvs) fused to a glycosylphosphatidylinositol (GPI) anchor: a strategy to target CD20-positive tumor cells, *J Immunol Methods 297*, 109-124.

309. Samad, A., Sultana, Y., and Aqil, M. (2007) Liposomal drug delivery systems: an update review, *Curr Drug Deliv 4*, 297-305.

310. Mayer, L. D., Bally, M. B., Hope, M. J., and Cullis, P. R. (1986) Techniques for encapsulating bioactive agents into liposomes, *Chem Phys Lipids 40*, 333-345.

311. Hernandez, J., Estelrich, J., and Pouplana, R. (1987) Determination of the encapsulation efficiency in liposomes obtained by the 'extruder method', *J Microencapsul 4*, 315-320.

312. Immordino, M. L., Dosio, F., and Cattel, L. (2006) Stealth liposomes: review of the basic science, rationale, and clinical applications, existing and potential, *Int J Nanomedicine 1*, 297-315.

313. Sanguino, A., Lopez-Berestein, G., and Sood, A. K. (2008) Strategies for *in vivo* siRNA delivery in cancer, *Mini Rev Med Chem 8*, 248-255.

314. Mohammad, R. M., Mohamed, A. N., Smith, M. R., Jawadi, N. S., and al-Katib, A. (1993) A unique EBV-negative low-grade lymphoma line (WSU-FSCCL) exhibiting both t(14;18) and t(8;11), *Cancer Genet Cytogenet 70*, 62-67.

315. Ujjani, C., and Cheson, B. D. (2010) Monoclonal antibodies in advanced B-cell lymphomas, *Oncology (Williston Park) 24*, 156-166.

316. Press, O. W., Appelbaum, F., Ledbetter, J. A., Martin, P. J., Zarling, J., Kidd, P., and Thomas, E. D. (1987) Monoclonal antibody 1F5 (anti-CD20) serotherapy of human B cell lymphomas, *Blood 69*, 584-591.

317. Bennett, C. F., and Swayze, E. E. (2010) RNA targeting therapeutics: molecular mechanisms of antisense oligonucleotides as a therapeutic platform, *Annu Rev Pharmacol Toxicol 50*, 259-293.

318. Jackson, A. L., Burchard, J., Leake, D., Reynolds, A., Schelter, J., Guo, J., Johnson, J. M., Lim, L., Karpilow, J., Nichols, K., Marshall, W., Khvorova,

A., and Linsley, P. S. (2006) Position-specific chemical modification of siRNAs reduces "off-target" transcript silencing, *RNA 12*, 1197-1205.

319. Ui-Tei, K., Naito, Y., Takahashi, F., Haraguchi, T., Ohki-Hamazaki, H., Juni, A., Ueda, R., and Saigo, K. (2004) Guidelines for the selection of highly effective siRNA sequences for mammalian and chick RNA interference, *Nucleic Acids Res 32*, 936-948.

320. Desaulniers, J. P. (2005) Exploring nucleic acid modifications in RNA hairpins and antisense oligonucleotides, In *Chemistry*, Wayne State University Detroit

321. Zelphati, O., Imbach, J. L., Signoret, N., Zon, G., Rayner, B., and Leserman, L. (1994) Antisense oligonucleotides in solution or encapsulated in immunoliposomes inhibit replication of HIV-1 by several different mechanisms, *Nucleic Acids Res 22*, 4307-4314.

ABSTRACT

EXPLORING POTENTIAL DRUG TARGET SITES IN THE RIBOSOME USING CISPLATIN AND ITS ANALOGUES

by

KESHAB RIJAL

May 2011

Advisor : Prof. Christine S. Chow

Major : Chemistry

Degree : Doctor of Philosophy

Cis-diamminodichloridoplatinum (II), cisplatin, is an antitumor drug that has been used to treat several types of cancers. The reaction of cisplatin with DNA has been studied and discussed extensively in the literature; however, the effects of cisplatin on RNA function are poorly understood. In this thesis, two aspects of cisplatin, its preferred sites of interaction with RNA and its use as a chemical probe to gain accessibility information, were explored.

To understand the site-selectivity of cisplatin with RNA, model RNA constructs and full-length 16S rRNA were employed. The binding studies revealed a cisplatin preference for guanosine-rich sequences. Primer extensions in 16S rRNA and MALDI-TOF in model constructs were used to locate the binding sites of cisplatin. HPLC and LC-MS were useful to determine the types and ratios of various adducts formed. Cisplatin and its analogues were employed to probe the accessibility of nucleotides on 16S rRNA, 30S subunits and 70S ribosomes in *vitro* as well as *in vivo*. This study revealed that many functionally

important sites, such as helix 18, 24, 27, and 34 are accessible to the aquated platinum complex. Thus, these accessible sites can potentially be utilized as a new target sites in the design of structure-based antibiotics. When charge and size of the complex were changed, the binding preference was altered. In addition to the expected consecutive Gs, cisplatin analogues preferentially targeted AG sites on loop or bulge regions. Thus, several new complexes could be synthesized and utilized to gain more information about drug accessibility on the ribosome.

The last part of the research focused on the application of siRNA to target non-Hodgkin's lymphoma (NHL). Small interfering RNAs were designed to downregulate the c-Myc expression in NHL cells. Stabilities of designed siRNAs in media and their incorporation into liposomes were studied. Complexes of siRNA, liposomes, and antibody fragments (scFv) could be utilized in future applications to target specifically the c-Myc expression in NHL cells.

Overall, this thesis work explored cisplatin binding to RNA and a number of possible new antibiotic target sites on the ribosome were identified. In the long term, further studies with fully functional ribosomes and comparisons with other organisms will have a greater impact on identifying novel drug target sites in pathogenic bacteria.

AUTOBIOGRAPHICAL STATEMENT

KESHAB RIJAL

ADVISOR: Prof. Christine S. Chow

THESIS TITLE: EXPLORING POTENTIAL DRUG TARGET SITES IN THE RIBOSOME USING CISPLATIN AND ITS ANALOGUES

EDUCATION

- **Ph.D; Biological Chemistry**, 2011, Wayne State University, MI, USA
- **M. S; Organic Chemistry**, 1998, Tribhuvan University, Nepal
- **B. S; Chemistry,** 1996, Tribhuvan University, Nepal

PUBLICATION:

1. **Keshab Rijal** and Christine S. Chow; A New Role for Cisplatin: Probing Ribosomal RNA Structure. *Chem. Commun*. 2009, 107-109.
2. **Keshab Rijal** and Christine S. Chow; Exploring Potential Drug Target Sites in the Ribosome with Cisplatin. Manuscript in preparation
3. **Keshab Rijal** and Christine S. Chow; Probing Ribosomal RNA with Analogues of Cisplatin. Manuscript in preparation
4. **Keshab Rijal,** Christopher Lajeunesse and Christine S. Chow; Cisplatin Binding Study and Adducts Characterization in 790 Hairpin of 16S Ribosomal RNA. Manuscript in preparation